

AD _____

COOPERATIVE AGREEMENT NUMBER DAMD17-93-V-3018

TITLE: Georgetown Institute for Cognitive and Computational
Sciences

PRINCIPAL INVESTIGATOR: Robert S. Ledley, D.D.S.

CONTRACTING ORGANIZATION: National Biomedical Research Foundation
Washington, DC 20007

REPORT DATE: December 1997

TYPE OF REPORT: Annual

PREPARED FOR: Commander
U.S. Army Medical Research and Materiel Command
Fort Detrick, Maryland 21702-5012

DISTRIBUTION STATEMENT: Approved for public release;
distribution unlimited

The views, opinions and/or findings contained in this report are those of the author(s) and should not be construed as an official Department of the Army position, policy or decision unless so designated by other documentation.

DTIC QUALITY INSPECTED 3

19980210 107

REPORT DOCUMENTATION PAGE

Form Approved
OMB No. 0704-0188

Public reporting burden for this collection of information is estimated to average 1 hour per response, including the time for reviewing instructions, searching existing data sources, gathering and maintaining the data needed, and completing and reviewing the collection of information. Send comments regarding this burden estimate or any other aspect of this collection of information, including suggestions for reducing this burden, to Washington Headquarters Services, Directorate for Information Operations and Reports, 1215 Jefferson Davis Highway, Suite 1204, Arlington, VA 22202-4302, and to the Office of Management and Budget, Paperwork Reduction Project (0704-0188), Washington, DC 20503.

1. AGENCY USE ONLY (Leave blank)		2. REPORT DATE December 1997	3. REPORT TYPE AND DATES COVERED Annual (30 Sep 96 - 15 Nov 97)	
4. TITLE AND SUBTITLE Georgetown Institute for Cognitive and Computational Sciences			5. FUNDING NUMBERS DAMD17-93-V-3018	
6. AUTHOR(S) Ledley, Robert S., D.D.S.				
7. PERFORMING ORGANIZATION NAME(S) AND ADDRESS(ES) National Biomedical Research Foundation Washington, DC 20007			8. PERFORMING ORGANIZATION REPORT NUMBER	
9. SPONSORING / MONITORING AGENCY NAME(S) AND ADDRESS(ES) U.S. Army Medical Research Command Fort Detrick, Maryland 21702-5012			10. SPONSORING / MONITORING AGENCY REPORT NUMBER	
11. SUPPLEMENTARY NOTES				
12a. DISTRIBUTION / AVAILABILITY STATEMENT Approved for public release; distribution unlimited			12b. DISTRIBUTION CODE	
13. ABSTRACT (Maximum 200 words) <p>GICCS faculty has begun a major initiative to elucidate the complex mechanisms of higher auditory processing. Species with specialized hearing, such as bats, are used as models for complex sound processing and compared to those using cats and primates, which also use acoustic signals as a primary means of communication. Parallel research in humans using functional brain imaging and cognitive psychology examine how the human brain deals with complex sounds, particularly those relating to speech. These studies address not only normal language processing but also examine disorders of speech/language, including developmental and acquired dyslexias.</p> <p>Understanding and modifying brain plasticity represents another major research area. Investigators use tools from cellular/molecular neurobiology and from systems neuroscience, to study plasticity after acute or chronic brain injury as well as after early vision or hearing loss. This includes development of novel pharmacological strategies to limit brain damage and to enhance cognitive function after injury or neurodegeneration. Brain magnetic resonance techniques (including functional imaging) are also used. Sophisticated computational methods are used to model sensory processing based upon experimental studies. Predictions based upon mathematical modeling are evaluated in subsequent laboratory experiments.</p>				
14. SUBJECT TERMS Neuroscience, Cognitive neuroscience, Visual Functions, Compensatory Plasticity, fMRI experiments, Dyslexia, Alzheimer's Disease, Amnesia, Language, Auditory Communication, Injury, Cortical Auditory Mechanisms, Allergic Encephalomyelitis			15. NUMBER OF PAGES 151	
			16. PRICE CODE	
17. SECURITY CLASSIFICATION OF REPORT Unclassified	18. SECURITY CLASSIFICATION OF THIS PAGE Unclassified	19. SECURITY CLASSIFICATION OF ABSTRACT Unclassified	20. LIMITATION OF ABSTRACT Unlimited	

FOREWORD

Opinions, interpretations, conclusions and recommendations are those of the author and are not necessarily endorsed by the U.S. Army.

n/a Where copyrighted material is quoted, permission has been obtained to use such material.

n/a Where material from documents designated for limited distribution is quoted, permission has been obtained to use the material.

x Citations of commercial organizations and trade names in this report do not constitute an official Department of Army endorsement or approval of the products or services of these organizations.

x In conducting research using animals, the investigator(s) adhered to the "Guide for the Care and Use of Laboratory Animals," prepared by the Committee on Care and Use of Laboratory Animals of the Institute of Laboratory Resources, National Research Council (NIH Publication No. 86-23; Revised 1985).

x For the protection of human subjects, the investigator(s) adhered to policies of applicable Federal Law 45 CFR 46.

n/a In conducting research utilizing recombinant DNA technology, the investigator(s) adhered to current guidelines promulgated by the National Institutes of Health.

n/a In the conduct of research utilizing recombinant DNA, the investigator(s) adhered to the NIH Guidelines for Research Involving Recombinant DNA Molecules.

x In the conduct of research involving hazardous organisms, the investigator(s) adhered to the CDC-NIH Guide for Biosafety in Microbiological and Biomedical Laboratories.

Robert S. Tedley 12/17/97
PI - Signature Date

Cooperative Agreement No. DAMD17-93-V-3018

TABLE OF CONTENTS

Introduction.....	3
Human Cognitive Neuroscience.....	4
Dr. Daphne Bavelier	4
Dr. Guinevere Eden.....	12
Dr. Rhonda Friedman	20
Dr. Michael Ullman.....	28
Animal Cognitive Neuroscience.....	34
Dr. Jagmeet Kanwal	34
Dr. James Pekar.....	44
Dr. Josef Rauschecker.....	51
Dr. Jian-Young Wu.....	59
Computational Neuroscience	71
Dr. Geoffrey Goodhill.....	71
Dr. Alexandre Pouget.....	76
Drug Discovery and Design.....	83
Dr. Alan Kozikowski.....	83
Dr. Shaomeng Wang	91
Molecular Neurobiology and Plasticity.....	99
Dr. René Etcheberrigaray	99
Dr. Alan Faden	108
Dr. Sheridan Swope	117
Other GICCS Sponsored Research	123
Faculty publications during the past year	140

INTRODUCTION

The Georgetown Institute for Cognitive and Computational Sciences (GICCS) is a neuroscience research institute whose mission is to understand higher cognitive function through interactive collaborative efforts among scientists using multidisciplinary investigative strategies. Its major focus areas are: higher auditory processing and language; brain injury and plasticity; computational neuroscience; and drug discovery.

GICCS faculty are working to elucidate the complex mechanisms of higher auditory processing. Species with specialized hearing, such as bats, are used as models for complex sound processing and compared to those using cats and primates, which also use acoustic signals as a primary means of communication. Parallel research in humans using functional brain imaging and cognitive psychology examine how the human brain deals with complex sounds, particularly those relating to speech. These studies address not only normal language processing but also examine disorders of speech/language, including developmental and acquired dyslexias. One goal is to develop treatments for these disorders through specialized training.

Understanding and modifying brain plasticity represents another major research area. Investigators use tools from cellular/molecular neurobiology and from systems neuroscience to study plasticity after acute or chronic brain injury as well as after early vision or hearing loss. This includes development of novel pharmacological strategies to limit brain damage and to enhance cognitive function after injury or neurodegeneration. Brain magnetic resonance techniques (including functional imaging) are also used, employing a high field (7T) animal research magnet as well as a human 1.5T magnet, to clarify mechanisms of tissue damage and plasticity and the response to targeted treatments. In addition to advanced brain imaging, computational neuroscience is an important experimental area that serves to integrate these multidisciplinary research efforts. Sophisticated computational methods are used to model sensory processing based upon experimental studies. Predictions based upon mathematical modeling are evaluated in subsequent laboratory experiments.

Together, the goal of this diverse but complementary research team is to better understand cognitive processes in order to address important clinical problems including deafness, language disorders, traumatic and ischemic brain injury, and Alzheimer's Disease.

During the past fiscal year the development of all the research laboratories has been completed — including instrumentation and staff recruitment. Faculty include three at the professorial level, 1 associate professor, 12 assistant professors, 7 research associates, and 1 research instructor. A total of 24 postdoctoral fellows and 17 research technicians have also been recruited to date. The faculty are divided into 5 sections: cognitive neuroscience (human); cognitive neuroscience (animal); computational neuroscience; drug discovery and design; and molecular neurobiology and plasticity. There are numerous collaborative connections within and across these sections. For example, all members of the human cognitive group and several members of the animal cognitive group share a common interest in the use of magnetic resonance imaging technology to address fundamental questions. Magnetic resonance technology also links the animal cognitive group with the group in molecular biology and plasticity. The drug development and design group has extensive collaborations both within the Institute as well as involving other departments at the Medical Center. Additional projects have been funded through the Institute with other neuroscience faculty in areas of complementary interest. Research developments during the past year are divided into 6 parts, one relating to each institute section and one relating to collaborative projects within Georgetown University Medical Center.

HUMAN COGNITIVE NEUROSCIENCE: There are four faculty members who are grouped into this area. Dr. Bavelier examines neural bases of visual cognition. Dr. Eden uses functional neuroimaging to study the pathophysiology of developmental dyslexia. Dr. Friedman examines the neuropsychology of language. Dr. Ullman investigates neural bases of language and memory. In addition, Drs. Pekar and Rauschecker conduct research projects in Human Cognitive Neuroscience using fMRI.

DAPHNE BAVELIER, Ph.D.

Dr. Bavelier's research focuses on visual scene analysis and its underlying neural bases in humans. Behavioral techniques are used to characterize the processing stages of visual analysis, and imaging techniques (event related potentials (ERP) and functional magnetic resonance imaging (fMRI)) to investigate their neural implementation. With the support of the Otolaryngology department at Georgetown, a vision laboratory which also includes ERP has been set up. In collaboration with Dr. Liu, an assistant professor at Georgetown expert in fMRI, a series of fMRI experiments have also been developed. Two independent but complementary lines of research have been supported by Institutional funds.

Project 1: Visual Functions in Normal Human Adults

The visual scenes we see are not given in the image at the eyes. The human visual system constructs them so that the different objects in the scene are separated from the background and recognized (Treisman, 1992). A striking example of this are patients who are unable to recognize objects in the face of preserved color and motion vision (a syndrome called visual agnosia). Our broad goals are to understand how the objects we see become available for awareness (Bavelier, 1994; Bavelier, In Press).

Our present line of research focuses on the relationships between objects and their parts during the construction of visual short term memories. While objects and their spatial/temporal relationships provide a powerful first index into one's visual memory for scenes, parts and their spatial/temporal relationships provide a powerful first index into one's visual memory for shapes. This has led a number of authors to propose that similar processes are at play when constructing a scene from objects or an object from parts. We have been assessing this claim. This work will be presented at the Psychonomics Society in November, 1997.

Project 2: Compensatory Plasticity In Visual Functions

Our broad goals are to characterize the role of altered sensory and language experience on the cerebral organization of visual functions by studying deaf individuals who acquire at birth American Sign Language, a visuo-spatial language. To separately assess the effects of deafness and ASL acquisition, we also study hearing individuals who are born to deaf parents and native signers.

The working hypothesis is that there is considerable variability in the degree to which different visual functions are modified by early experience. We will test the hypothesis that experience-dependent changes are (i) functionally specialized, i.e. they affect only certain aspects of visual processing such as visual attention, and (ii) limited to specific critical periods, i.e. the amount of compensatory plasticity observed in congenitally deaf individuals is expected to be greater than that observed in later deafened individuals.

Project 2A: Cerebral Organization for Visual Attention

While there is anecdotal evidence that the deaf 'see' better than the hearing, evidence supporting this claim is limited and controversial. Interestingly, most investigations have focused on the assessment of psychophysical thresholds neglecting higher visual functions such as visual attention/selection or object tracking. Since coming to Georgetown, we have directed our efforts to test the hypothesis that some aspects of these functions will be enhanced in congenitally deaf individuals.

Behavioral Experiments:

We have been programming a number of behavioral experiments to assess compensatory plasticity in higher visual functions. Previous work on the resolution of visual attention in human has shown higher resolution in the lower visual field than the upper visual field (He et al., 1997). These experiments will be replicated in deaf individuals to assess the resolution of visual attention after congenital deafness. We predict a higher resolution for congenitally deaf individuals than for later deafened individuals or hearing individuals. Two of the experiments we have been designing are described below.

Experiment 1: Visual Tracking

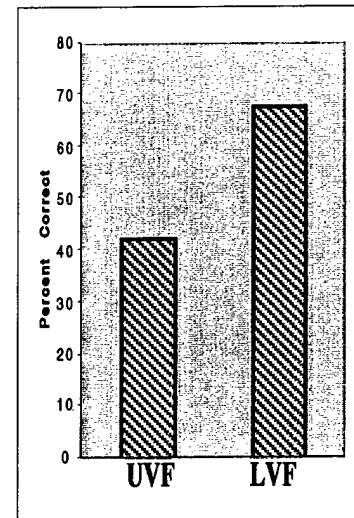
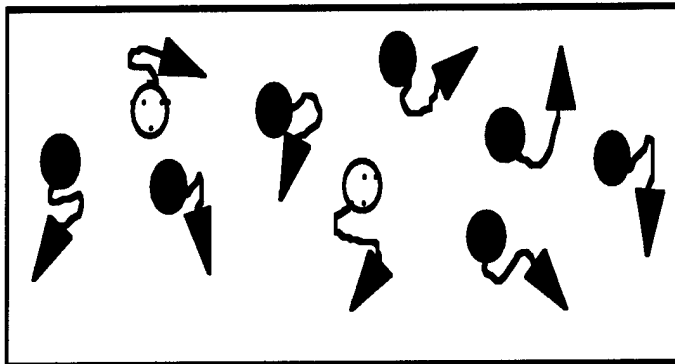


Figure 1. Attentional tracking task and accuracy data for normally hearing subjects in upper and lower visual fields. (A) Subjects fixated 10 degrees above or below the center of a rectangle area in which nine green moving balls were presented. At the beginning of each trial, two of the balls were changed to red for 1 sec and then turned back to green. The subjects' task was to keep track of those two balls while keeping their gaze steady on the fixation cross. After 5 sec, all nine balls stopped moving and observers indicated which two balls were the ones that had turned red at the beginning. (B) Subjects performed better in the lower visual field (LVF) than the upper visual field (UVF). Adapted from He et al. (1996)

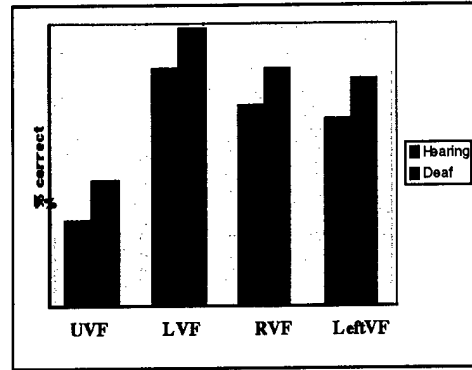


Figure 2. Attentional Tracking Experiment: Predicted accuracy data for congenitally deaf and normally hearing subjects in the upper, lower, right and left visual fields. We predict an increase in performance for deaf as compared to hearing for all visual fields.

Experiment 2: Attentional Capture

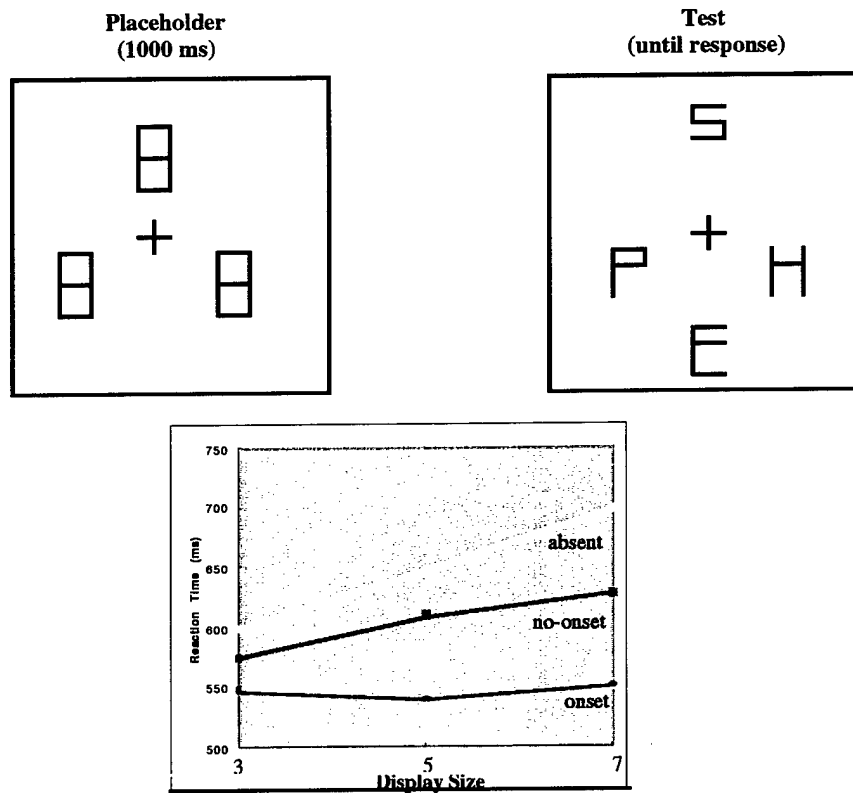


Figure 3. Abrupt onset stimuli attract attention in hearing individual. (A) Subjects viewed first a frame with place holders and then a frame with letters. They were to determine whether a pre-specified letter was present in the array. (B) If the target letter appeared at the same location as place holders, subjects' detection time increased with the number of letters in the display ($n=4$ in the example displayed). However, display size did not affect performance when the target letter appears at a new location (creating an abrupt onset).

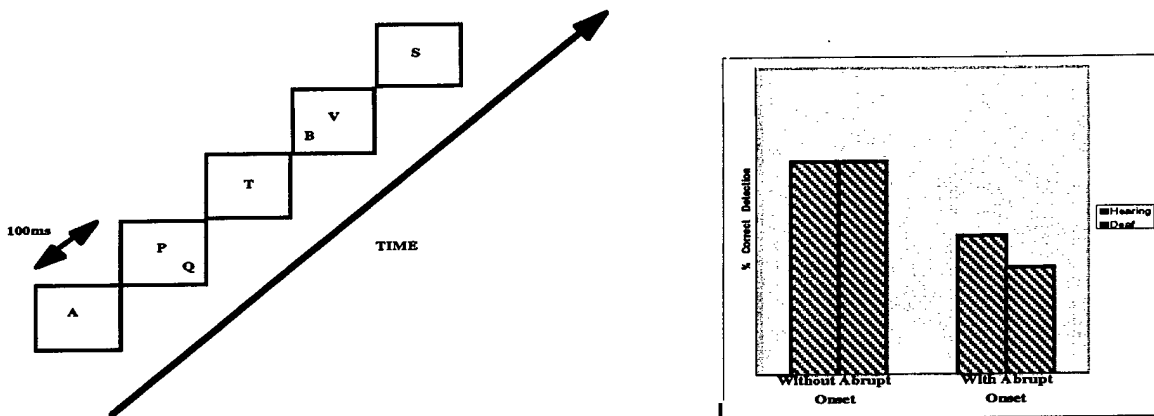


Figure 4. Predicted sensitivity to abrupt onset in deaf and hearing individuals. (A) Subjects will be asked to monitor the shape of the letter presented at the center of the screen (press the key when a V is presented) while ignoring letters flashed in the periphery. (B) We predict that abrupt onsets will be more disruptive for deaf than hearing individuals. Thus, on trials with abrupt onset, we expect a lower performance from deaf individuals.

fMRI Experiments:

Preliminary data collected at NIH suggested that areas that normally subserve auditory functions get recruited into visual processing in congenitally deaf individuals. We have been carrying a systematic investigation of this hypothesis. We are using the newly acquired SIEMENS magnet to assess the cortical organization for motion processing in congenitally deaf subjects.

Subjects: We have run 14 congenitally deaf subjects (from Gallaudet University), 2 hearing native signers and 5 hearing monolingual subjects.

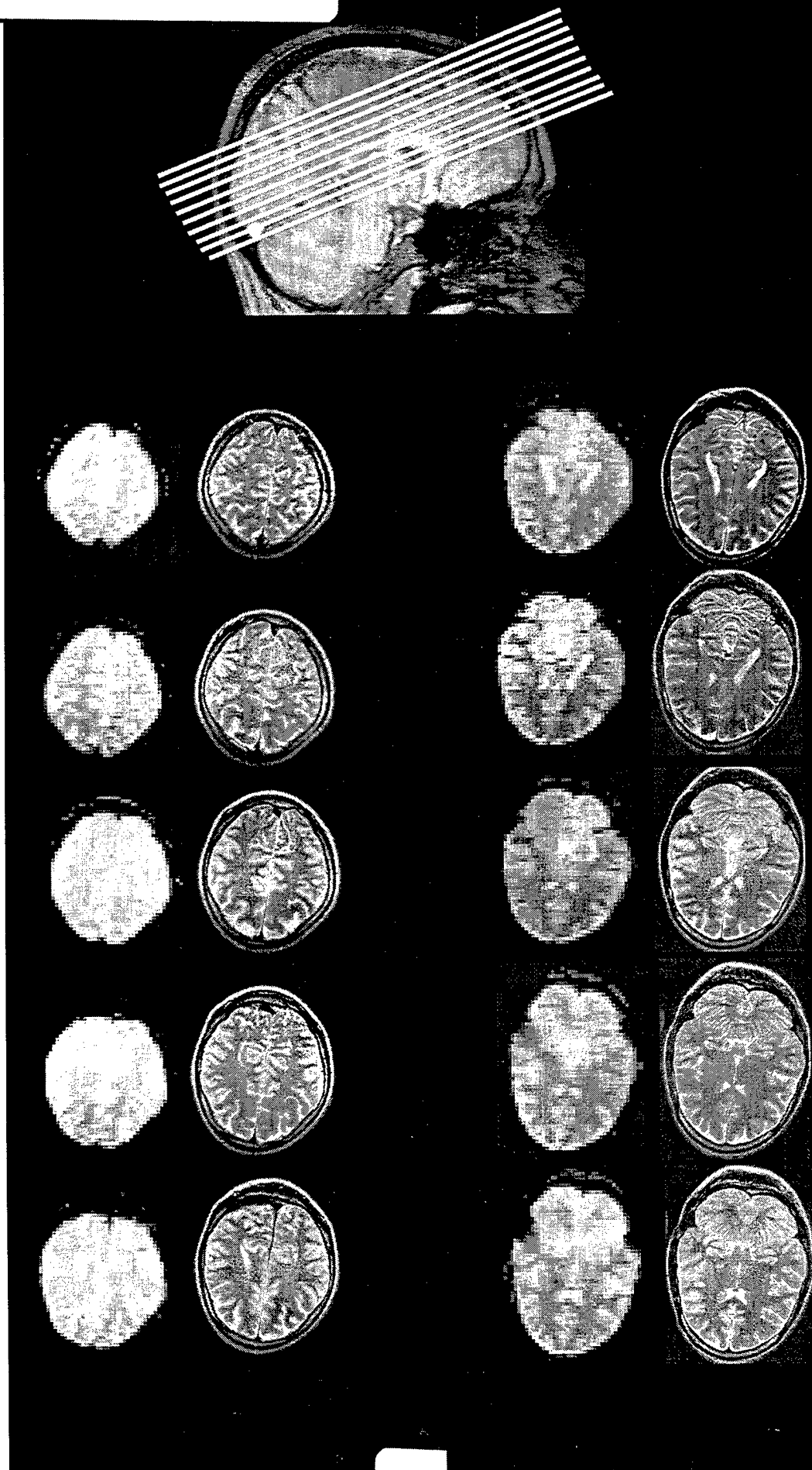
Material and Procedure: Computer-generated flow fields were downloaded on a videotape, and displayed to the subject through an LCD projector. Subjects were lying on a patient bed viewing a translucent screen at their feet through the means of a mirror. In a first condition, subjects viewed passively an alternation of radially-moving dots and of static random dots. Attention was then manipulated by asking subjects to detect either luminance changes or velocity changes. To assess whether plastic changes are larger in the periphery than the fovea, for some conditions changes occurred only in the periphery while for others they occurred only in the fovea.

MR Parameters: Spin-echo-2D echo-planar images (TE=40 ms, Flip angle=90 degree) were obtained using a 1.5 SIEMENS Vision MR system fitted with a removable head receive/transmitter coil (Figure 5). Twenty tilted axial slices were collected during each TR of 4 sec with an in plane resolution of 3.5x3.5 and slice thickness of 5 mm. Each experimental run consisted of 64 images per slice.

Data Analysis: Behavior: Subjects accurately detected the changes in luminance or velocity indicating that they paid attention to the stimuli.

fMRI: Data analysis is proceeding using the SPM software in close collaboration with Chloe Hutton, who is part of the team developing SPM at the Functional Imaging Laboratory in London.

Bavelier - Figure 5
legend to follow



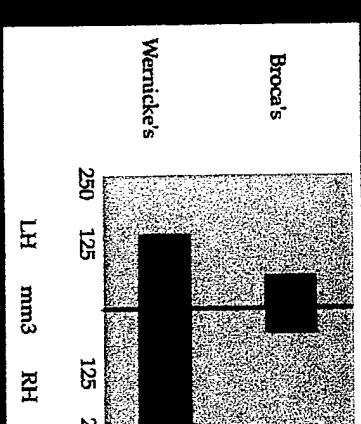
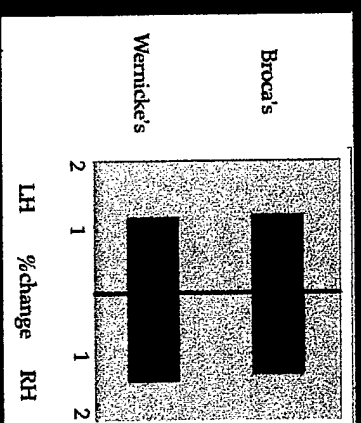
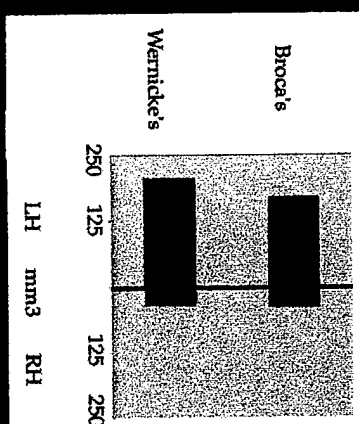
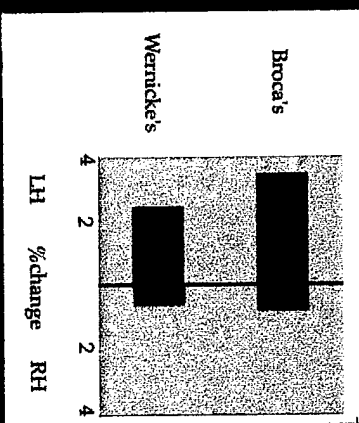


Figure 5.

Images collected on a deaf individual with the 1.5T Vision Siemens Magnet. Slice selection is shown above a subset of the twenty titled axial slices. Functional images are displayed side by side with their corresponding structural images.

Figure 6.

Summary of the pattern of activation in native speakers of English and native signers of American Sign Language in the classical language areas of Broca's and Wernicke's.

Project 2B. Cerebral Organization for Visuo-Manual Languages such as American Sign Language

We have employed fMRI to compare the brain regions active during sentence processing in English and in ASL. We report that classical language areas within the left hemisphere are recruited by both English and ASL (Figure 6; Bavelier et al., 1997; Neville et al., in press). This suggests a bias of the left hemisphere to process natural languages independently of the modality through which language is perceived. Furthermore, in contrast to English, ASL strongly recruited right hemisphere structures. This was true irrespective of whether the native signers were deaf or hearing. Thus, language modality appears to affect the cortical organization for language. These results show that the processing of fast acoustic transitions is not necessary for recruitment of the left hemisphere structures in the language system (Tallal et al., 1993). In contrast, the left hemisphere invariance across languages is consistent with the view that grammatical recoding drives the left hemisphere specialization for language (Neville, 1995). The finding of a different right hemisphere recruitment for English and ASL raises the possibility that some aspects of language processing can also drive a right hemisphere specialization for language. In collaboration with David Corina at the U of Washington, we are constructing ASL material to perform a finer assessment of the functional role of right hemisphere structures during ASL processing. These studies are scheduled to be carried on the SIEMENS magnet at Georgetown University in February, 1998.

References

- Bavelier, D. Repetition Blindness between visually different items: the case of pictures and words. *Cognition*, 51, 199-236, 1994.
- Bavelier, D. (In Press) Role and Nature of Object Representations in Perceiving and Acting. In Coltheart, V. (Ed), Boston: MIT Press. Invited book chapter.
- Bavelier, D., Deruelle, C. & Proksch, J. Consistency Effects: The positive and the negative of it. Submitted.
- Treisman, A.M. Perceiving and Re-perceiving Objects. Berkeley: University of California, 1992.
- Jonides, J. and Yantis, S. Uniqueness of Abrupt Onset in Capturing Attention. *Perception and Psychophysics*, 43, 346-354, 1988.
- He, S., Cavanagh, P., & Intriligator, J. Attentional Resolution and the locus of visual awareness. *Nature*, 383, 334-337, 1996.
- Neville, H.J., & Bavelier, D. (1997) Variability of developmental plasticity within sensory and language systems: Behavioral, ERP and fMRI studies. D. Hann, L. Huffman, I.I. Lederhendler, & D. Meinecke (Eds.) *Proceedings of the Conference for Advancing Research on Developmental Plasticity*.
- SPM (Statistical Parametric Method). The Functional Imaging Laboratory, Institute of Neurology, Wellcome Department, London, England, 1996.
- Yantis, S. Attentional Capture in Vision. In A.F. Kramer, Coles, M.G.H, and Logan, G.D (Eds), *Converging Operations in the Study of Visual Selective Attention* (pp. 45-76). Washington: American Psychological Association, 1996..

- Bavelier, D., Corina, D., Jezzard, P., Padmanabhan, S., Clark, V. P., Karni, A., Prinster, A., Braun, A., Lalwani, A., Rauschecker, J., Turner, R. & Neville, H. Sentences Reading: a functional MRI study at 4T. *Journal of Cognitive Neuroscience*, 9 (5), 664-686. 1997.
- Neville, H. J. (1995). In Gazzaniga, M.S. (Ed), *The Cognitive Neurosciences*, 219-231. Cambridge: MIT Press.
- Neville, H., Bavelier, D., Corina, D., Rauschecker, J., Karni, A., Lalwani, A., Braun, A., Clark, V. P., Jezzard, P., & Turner, R. (In Press). Cerebral Organization for Language in Deaf and Hearing Subjects: Biological Constraints and Effects of Experience. *Proceedings of the National Academy of Science*.
- Tallal, P., Miller, S., & Fitch, R. H. Ann. N.Y. Acad. Sci. 482, 27-47, 1993.

GUINEVERE EDEN, D.PHIL.

Dr. Eden's laboratory uses behavioral testing and functional magnetic resonance imaging (fMRI) to characterize disorders in sensory processing in individuals with developmental dyslexia. These studies include examinations of rapid visual and auditory processing as well as phonological awareness. Although these processes have been previously shown to be impaired in dyslexics, the nature of their shared contribution and questions concerning a common neocortical etiology are being investigated for the first time.

The clinical manifestations of developmental dyslexia are varied. In addition to their reading difficulties, individuals with developmental dyslexia exhibit impairments in their ability to process the phonological features of written or spoken language. We (Eden, Stein, Wood & Wood, 1994; Eden, Stein, Wood & Wood, 1995; Eden, Stein, Wood & Wood, 1995; Eden et al., 1996) and others (Lovegrove, 1993; Lovegrove & Brown, 1978; Lovegrove, Heddle & Slaghuis, 1980; Lovegrove, Pepper, Martin, Mackenzie & MacNicol, 1982) have demonstrated that these individuals are also impaired on a number of visual tasks, involving visuomotor, visuospatial and visual motion processing. These results suggest that the pathophysiology of dyslexia is more complex than originally thought, extending beyond the classically defined brain language areas. We are currently investigating the existence of a deficit in sensory information processing in dyslexia that is common to multiple sensory modalities. Our approach is to perform analogous behavioral and functional studies in the (1) visual and (2) auditory system and to relate them to (3) phonological awareness skills in dyslexics and controls. The results will further delineate the relationship between psychophysical performance and neuronal processing mechanisms in dyslexia and may suggest new strategies for remediation.

Project 1: Developmental Dyslexia and the Visual System Background

Unlike language research, studies of human visual processing have had the benefit of a more detailed understanding of the anatomy and physiology of the visual system gained from experiments with non-human primates. From these studies, schemes for regional functional specialization of the visual cortical pathways have been described. Notable among these is a dichotomy based on relative selectivity of particular cortical areas for processing color and form versus motion as depicted in Figure 1. Functional neuroimaging utilizing positron emission tomography (PET) and functional magnetic resonance imaging (fMRI) have identified a specific motion sensitive area, V5/MT, thought to be dominated by input from the magnocellular stream. These channels can be distinguished by their spatial frequency preference, their temporal properties and their contrast sensitivity. Both contrast sensitivity and visible persistence has been shown to be varied in reading disabled children, indicating that these children have disturbances in the magnocellular or transient system, which mediates global form, movement, and temporal resolution (Lovegrove, 1993; Lovegrove & Brown, 1978; Lovegrove et al., 1980; Lovegrove et al., 1982).

We investigated such a motion processing deficit in the visual system of dyslexics (Eden et al., 1996) and found passive perception of visual motion in dyslexics failed to produce any detectable task-related functional activation in area V5/MT (part of the magnocellular system). In contrast, all control subjects had a robust response in the same region. We concluded that dyslexics suffer from abnormalities of the fast visual processing pathway (magnocellular), whilst the slower form processing system (parvocellular) was unaffected. This profound physiological abnormality was accompanied by a relatively subtle behavioral deficit in visual motion detection. This finding of an V5/MT deficiency in dyslexia has recently been replicated in an fMRI study that showed activity in this area to be directly correlated with reading skill (Demb, Boynton & Heeger, in press).

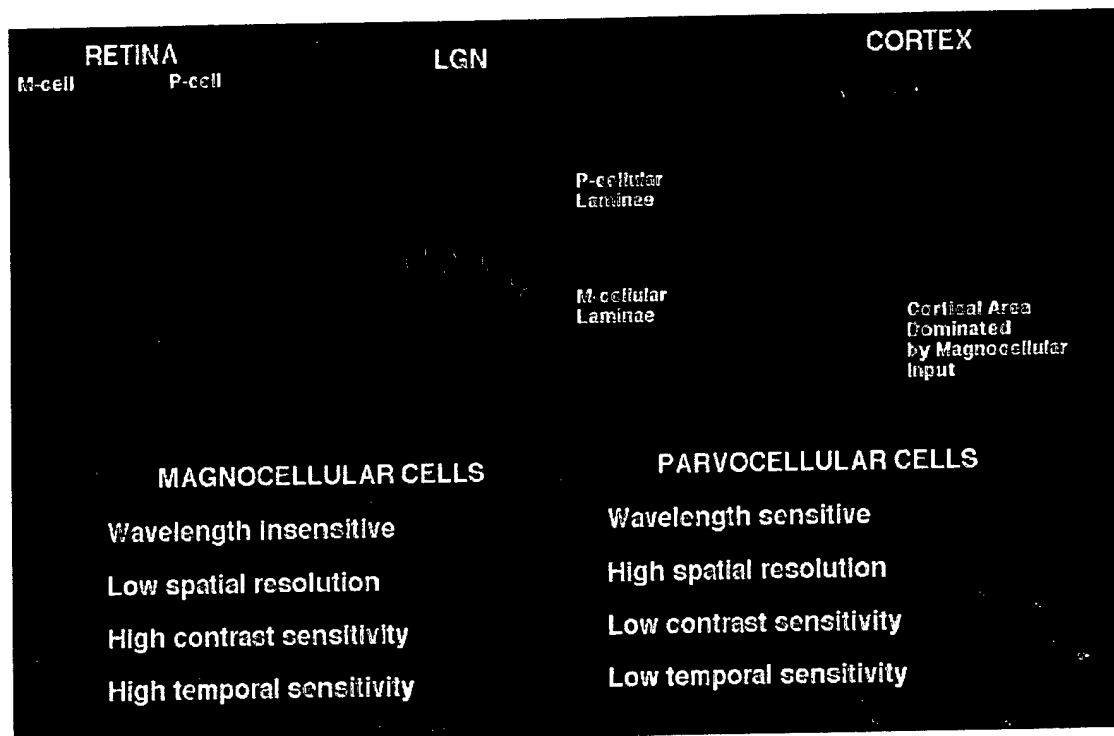


Figure 1: Functional Specialization of the Primate Visual System

In our current studies we are employing a different motion stimulus, that is optimized to activate area V5/MT and less likely to introduce eye movements. Coherent motion of random dot fields has now been replaced by radial movements of dots (Figure 2). Stimulus parameters can be changed to adjust speed, luminance and dot size. This stimulus has been generated in our laboratory using Microsoft Visual Basic. This strategy is also suitable for auditory stimulus generation allowing us to easily perform experiments in the same session across sensory modalities, inside and outside of the scanner.

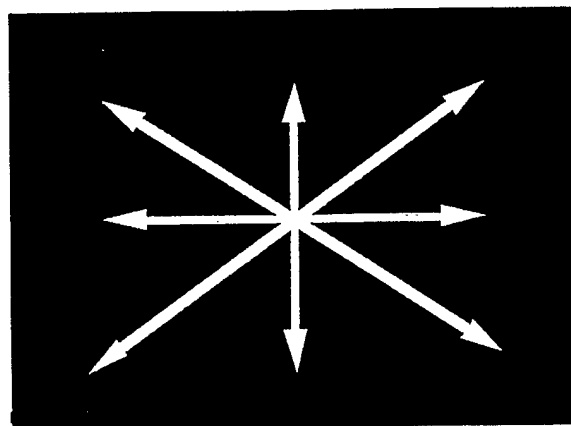


Figure 2: New radial motion stimulus for activation of motion sensitive cortical areas.

Future Directions

We will be studying visual motion processing in dyslexics and controls to address two questions:

(1) Is attention used to compensate for visual motion processing deficits in dyslexia?

Behavioral compensation is an important mechanism by which individuals demonstrate recovery after brain injury of various kinds. The aim is to examine the attentional modulation of visual motion processing in dyslexia. These experiments examine whether it is possible for dyslexics to compensate for faulty visual motion processing with increased attention. If this is the case, then attentional modulation may explain the relatively minor behavioral motion detection abnormality. We will examine the effects of attending to visual motion in individuals with dyslexia. If the behavioral compensation hypothesis is correct, dyslexics should show a large attention-related modulation of activation in relation to visual motion (and the same could be true in analogous studies of audition).

(2) Is activity in area V5/MT different in dyslexics and controls during a visual velocity judgment task?

Replacing passive viewing with having subjects perform an active velocity discrimination task will allow us to study active visual motion viewing. This task will be developed to make it suitable for behavioral testing outside of the scanner in children and adults, and designed as to construct analogous auditory velocity judgment tasks.

Project 2: Developmental Dyslexia and the Auditory System Background

We have previously described a visual deficit in dyslexia is associated with abnormal processing in a subsystem specialized for rapid visual information processing. It has been argued that analogous problems may exist in the auditory system and may have a direct effect on phonological processing in dyslexics (Tallal, 1980; Tallal, Miller & Fitch, 1993; Wright et al., 1997; Tallal et al., 1996). Although this theory is still controversial (Studdert-Kennedy & Mody, 1995), it is clear that the ability to read requires rapid processing and that dyslexia involves disorders of rapid or automatized visual naming speed (Denckla & Rudel, 1976; Wolf & Goodglass, 1986).

We are currently extending these recent fMRI studies demonstrating differences in functional activity of brains of dyslexics to include the auditory system and to relate them to mechanisms underlying phonological processing. Our studies are based on a previous investigation demonstrating that adult dyslexics are poorer at perceiving illusionary auditory motion (Hari & Kiesila, 1996). Illusionary motion is generated by presenting tone clicks with an interaural delay, resulting in the illusion of a moving sound source. We are currently developing software to generate the same stimuli to be used for behavioral assessment and for auditory motion presentation inside of the scanner.

Future Directions

(1) Does the motion processing deficit in dyslexia involve both vision and audition?

Dyslexics may exhibit difficulties in detecting and processing motion in sensory modalities other than vision. The aim of these experiments is to search for the physiological motion processing mechanisms common to vision and audition. Normal and dyslexic subjects will perform motion discrimination tasks while attending to visual or auditory motion and their performance will be analyzed for group and task effects. Task-related signal change will be

contrasted in the two groups using functional magnetic resonance imaging (fMRI). We will examine the degree to which these physiological changes correlate with the observed behavioral deficits. Comparison of results across modalities will reveal to what degree dyslexics exhibit functional deficits common to vision and audition, and may suggest the neuroanatomical localization of a common neural substrate.

Project 3: Developmental Dyslexia and Phonological Awareness Background

The most widely accepted current explanation for dyslexic's reading difficulties involves abnormal phonological processing. The term "phonological awareness" has been used as an umbrella term for the skill of manipulation and segmentation of the constituent sounds of words (Stanovich, 1988). Phonological awareness was first described by Bruce (Bruce, 1964), who asked children to repeat the words after a particular sound had been taken away. Since then a large body of evidence has shown that certain phonological abilities can predict reading acquisition (Goswami, 1990; Snowling, 1991; Stanovich, 1988b). The neuronal mechanisms that subserve the type of rapid phonological retrieval and phonological segmentation impaired in dyslexia are not yet clearly defined. Some of the differences observed in dyslexics during previous functional neuroimaging studies are difficult to interpret due to our incomplete understanding of "normal" language processing. With advancements in neuroimaging technology, it is now possible to study an individual subject's performance during a wider variety of tasks than was previously possible due to radiation dosimetry limits. As a result, an effort has begun in our laboratory to systematically study individuals with normal cognitive development to understand the functional organization of the brain for language. These efforts will allow a deeper understanding of the effects of developmental dyslexia on a range of sensory and phonologically related skills.

Our initial step is to assess the feasibility of having subjects articulate in the scanner. PET studies of overt and covert reading have shown that areas engaged when reading words aloud compared to silent reading suggest an additional cognitive network other than just motor cortex. Because reading aloud is the measure on which the classification of developmental dyslexia is made, this is an important issue. The degree of head motion resulting from articulation versus silent reading is currently being assessed. Experiments to study phonological processing will be designed taking the results from this study into account.

Future Directions

(1) How are the visual and auditory deficits related to language processing deficits in dyslexia?

We will examine the abilities in individuals with and without dyslexia using phonological and rapid naming tests. Differences between dyslexic and control group maps of task-related brain activity will allow neuroanatomical localization of the areas affected by dyslexia. Most importantly, this experiment will reveal the anatomical and functional characteristics of brain areas subserving phonological and rapid naming abilities in relation to those areas subserving visual and auditory temporal processing. The areas altered in dyslexia are predicted to be those engaged during both phonological and rapid temporal task. Co-localization of these two apparently disparate brain functions may explain the co-occurrence of reading disability and sensory abnormalities in dyslexia.

Project 4: Auditory and Visual Duration Judgment

Another way of testing the integrity of temporal information processing of the visual and auditory system is measuring the ability of subjects to judge the duration of a tone or a visual display. Such a task requires accurate sensory information processing to allow for accurate judgment in the millisecond range.

Subjects listened to a tone or saw a dot presented on a screen. This presentation was followed by a second tone or dot, depending on the modality measured, and the task was to make a decision whether the second presentation was longer or shorter than the first. We performed two studies.

In the first study we applied this measure to a group of children that were undergoing intervention procedures at the National Speech Therapy Center, Bethesda, MD. The data were collected by Courtney Dorn, an undergraduate student from Vanderbilt University working in the laboratory during the summer. Twelve children (mean age=8.5) were enrolled in the summer session of the Fast Forward Program. This program is thought to improve rapid auditory processing skills as well as receptive language skills in children with learning disabilities (Tallal et al., 1996). We hypothesized that if the program was able to improve auditory skills by elevating the auditory temporal resolution in these children, this would be reflected in an improvement in detecting a short duration difference in two sequentially presented tones. This ability was measured initially during the same week the intervention with Fast Forward was initiated and every two weeks thereafter until the 6th week, by which time most children had completed the course of the program. An analogous task was performed in the visual domain, and it was predicted that no change would be observed in visual performance, as only audition was targeted by the program. Should both sensory modalities improve, the results would suggest the improvement brought about by a more general mechanism, such as attention.

In the second experiment auditory and visual duration judgments were studied in a group of 16 adults in order to understand the differences and the effect of learning on this task. These data were collected by John Agnew, a graduate student from the Interdisciplinary Neuroscience Program. Subjects were asked to perform the task over two days to study the effect of learning. We also investigated the effect on performance by varying the duration of the first stimulus. The results have implications not only on the interpretation of the data from the learning disabled children, but aid us in the design of fMRI studies where the choice of duration and learning have important implications.

The results are depicted in Figure 3 for the adults. Not surprisingly there was a significant effect for sensory modality, confirming better temporal resolution in the auditory system compared to the visual system. There was an effect for training, demonstrated by a significant influence of learning for day one versus day two ($p < .05$). Performance is profoundly affected by the time duration of the first stimulus, with performance levels being worse if the first stimulus is longer ($p < .0001$). The results for the children are depicted in Figure 4. There was no observation of improvement in the performance of visual or auditory judgment in the group when comparing pre and post treatment. Three of the children were too young to perform the test above chance, however the others were able to complete the experiments. The lack of improvement suggests no measurable change in the ability to process rapid auditory stimuli. However, further studies are required.

Future Directions

(1) What are the cortical areas engaged during visual and auditory temporal judgment and how do they differ in individuals with developmental dyslexia?

These pilot data will be used to design fMRI experiment to study temporal duration judgment in adults with and without dyslexia. We predict that we will find areas common to auditory and visual duration judgment and expect to find poorer performance in individuals with dyslexia. As previous PET studies have found that the right inferior parietal cortex is one of the areas subserving visual duration judgment and because this cortical area receives projections from the magnocellular system known to be defective in dyslexia, this area is expected to differ between the groups.

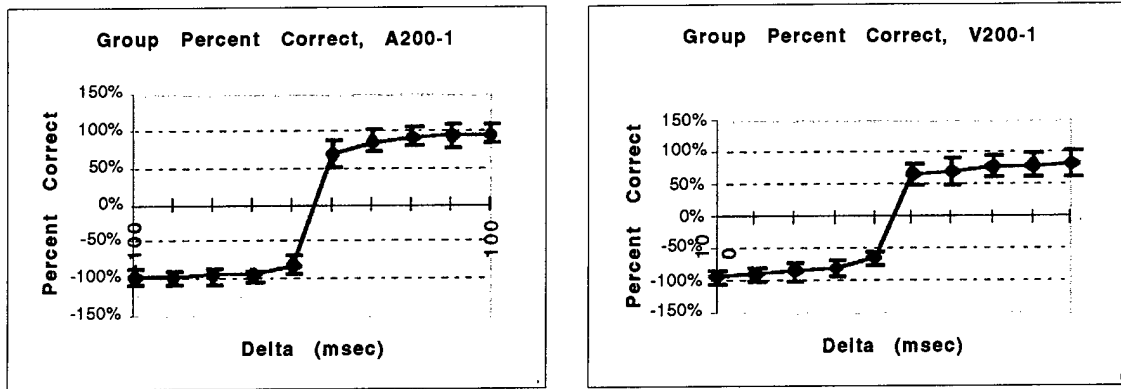


Figure 3a: Adult group performance across a range of duration differences for auditory and visual judgment with an initial stimulus of 200msec.

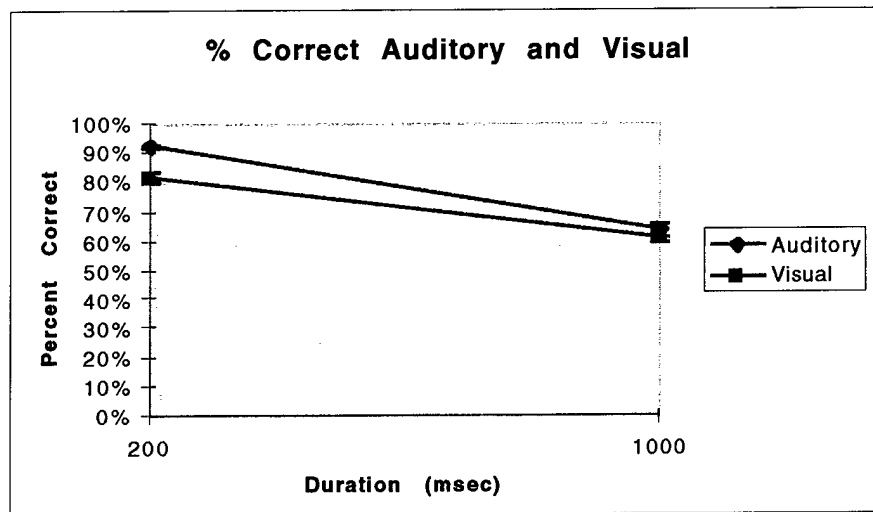


Figure 3b: Adult group performance on auditory and visual duration judgment at long and short presentation durations.

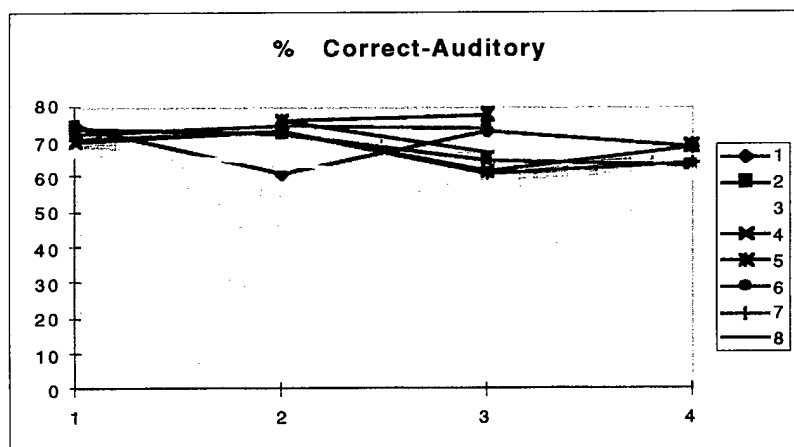


Figure 4a: Performance on auditory duration judgment for eight children sampled at four two week intervals during intervention.

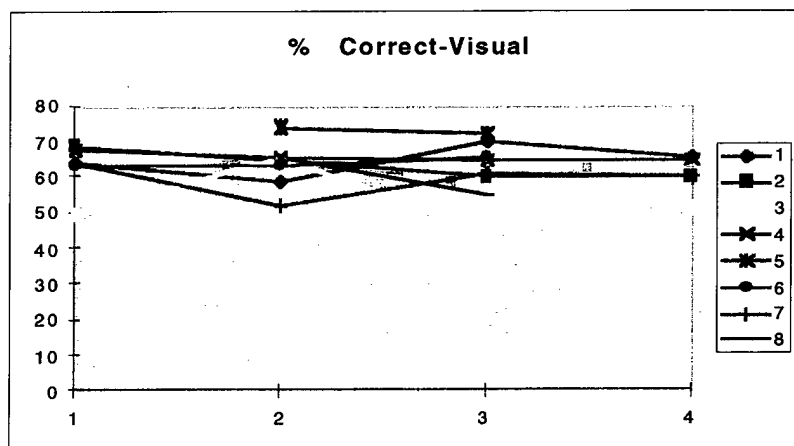


Figure 4b: Performance on visual duration judgment sampled for eight children at four two week intervals during intervention.

Summary

Integration of the resulting behavioral, anatomical and physiological information into structure/function correlations is a principal goal of our research program. Using these techniques we will examine the degree to which these physiological changes correlate with the observed behavioral deficits. Comparison of results across modalities will reveal to what degree dyslexics exhibit functional deficits common to vision and audition, and may suggest the neuroanatomical localization of a common neural substrate. The results of these experiments will provide new information concerning the neural substrates responsible for the visual, auditory and phonological abnormalities characteristic of developmental dyslexia. Moreover, the laboratory is interested in the development of new diagnostic tools that may allow earlier and more accurate identification of individuals with developmental language disorders.

Preliminary Data From The Georgetown Siemens Vision System

The Institute has recently installed a 1.5T Siemens Magnetom Vision system capable of acquiring multislice echo-planar imaging data. Until recently the system had been undergoing acceptance testing and is now fully operational. We present preliminary data from this system: subjects executed a simple motor task while lying supine with eyes closed. Individuals were scanned while performing a self-paced finger opposition task with the dominant hand at a rate of 2 finger oppositions per second alternating with periods of rest. Echo-planar images (EPI) were acquired with the following parameters: 26 msec TE, 5 sec TR, 64x64 matrix, 24 slices with 4 mm thickness, 3.75 mm in-plane resolution, resulting in approximately cubic 4 mm voxels. Epochs of finger movement or rest lasted 60 seconds each with task alternation every 60 seconds. There were a total of 7 epochs per experimental run and each run began with the rest condition. The image data was corrected for head motion, global intensity variations and local intensity variations prior to statistical analysis. Figure 5 depicts areas of significant signal change after calculation of the t-statistic contrasting movement and rest conditions. Areas of statistically significant change are displayed ($p < 0.00001$) on an averaged axial echoplanar image. This statistical map reveals task related changes in primary motor cortex, primary somatosensory cortex, premotor cortex, supplementary motor area, cingulate motor area, thalamus and anterior cerebellum. The magnitude and statistical significance of these changes is similar to those obtained in our previous visual studies using other imaging systems (Eden et al., 1996; Zeffiro, Eden, Woods & vanMeter, 1997).

Subject Recruitment

(1) Normal volunteers have been recruited by advertising around the Georgetown University Campus. After a detailed telephone screening, each subject's information is held in a protected data base and the subjects are called for participation in experiments. (2) We have recently engaged in a collaborative effort with the Lab School of Washington to study young adults and children with learning disabilities. These individuals have already undergone extensive neuropsychological testing as part of a routine school-wide assessment. We are initiating studies to measure sensory processing behaviorally in these children at the Lab School. Another source of children with learning disabilities is provided by the National Speech Therapy Center in Bethesda, MD. Children at this site are undergoing remedial training in order to try to alleviate their attentional and reading problems.

The Interdisciplinary Dyslexia Research Program

This program is funded by the Georgetown University President's Interdisciplinary Program. The aim is to integrate individuals from the Department of Psychology (Dr. D. Howard), Pediatrics (Dr. J. Rumsey) and GICCS (Dr. G. Eden) to be involved in the studies of developmental dyslexia and share students who wish to learn about sensory processing, developmental dyslexia and functional neuroimaging. Funds provided are to support the establishment of a database to allow compilation of neuropsychological testing that has been carried out on children with learning disabilities. We are currently constructing this database and exploring the possibility of recruiting subjects from this site.

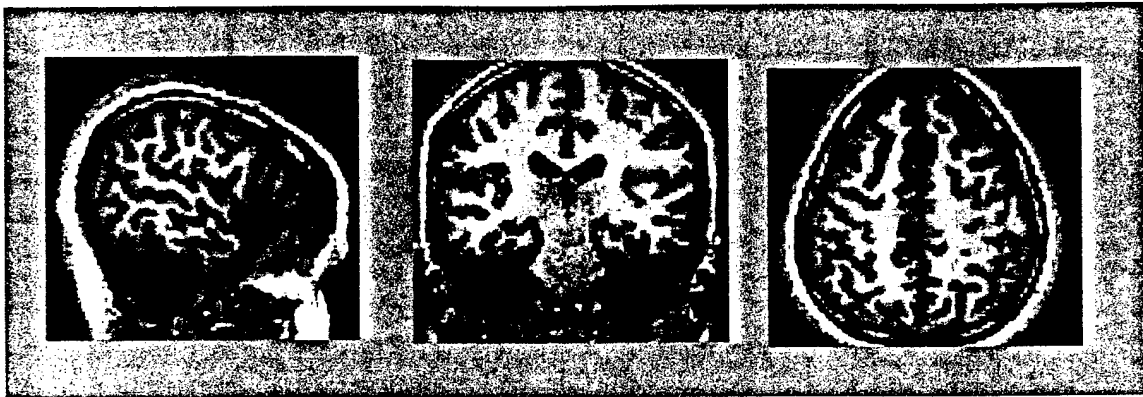


Figure 5: Cortical Signal Changes During Finger Opposition Viewed on Sagittal, Coronal, and Axial Sections of the Brain.

DR. RHONDA B. FRIEDMAN, Ph.D.

Dr. Friedman's research encompasses three major projects: (1) Written language processing in Alzheimer's Disease and related disorders; (2) Cognitively-based treatments of acquired dyslexias; and (3) Evaluating cognitive neuropsychological models of language recovery with fMRI.

Project 1: Written Language Processing in Alzheimer's Disease and Related Disorders

Study 1: Patterns of Lexical and Semantic Associative Priming in AD

This past year saw completion of this study, whose design and initial results were described in last year's report. The final results did not differ from the initial results, and are consistent with the view that at least part of the semantic deficit in AD is caused by a disruption of semantic knowledge that affects relationships among basic level concepts.

Study 2: Orthographic Processing in Patients with Semantic Impairments

It has been suggested that lexical orthographic processing becomes impaired relatively early in Alzheimer's Disease, and this impairment has been said to be a consequence of the semantic processing deficit that typically occurs early in the disease. This claim is based on the notion that semantic knowledge is necessary to reinforce the integrity of the representations of orthographic whole word patterns. In a study completed this past year, we tested this hypothesis by examining the spelling of a mentally retarded child, LA, with hyperlexia who demonstrates profound semantic impairments, much like those seen in AD. We reasoned that if semantic knowledge is necessary to bind together orthographic codes for words with irregular spellings, then LA should have great difficulties learning and recalling spellings for irregular words whose meanings he does not know.

Two matched lists of low frequency picturable nouns with irregular spelling-to-sound correspondences were generated. When first tested for spelling to dictation, LA performed equally poorly on both lists (44% correct). Following a multiple baseline design, LA was trained to spell the words on List A but not List B. Six weeks after the training, LA's ability to spell the words was assessed. He spelled 75% of the trained words (List A) correctly, but only 44% of the untrained (List B) words, indicating that he had learned and retained the spellings of the words that he had been taught. LA was then trained on the List B words. Additionally, LA was given a word-picture matching task on two occasions (match the word to one of four pictures) to assess his knowledge of the meanings of the trained words: after the training of the List A words, and after at the time of the final testing. LA chose the correct picture on 69% and 59% of the trials, respectively. Only 23% of his total errors consisted of the semantically-related foil.

For the following analysis, a word was considered to be "known" by LA if its picture was correctly chosen on both tests. Using this criterion, 44% of the words were "unknown" by LA. Table 1 presents LA's spelling, pre- and post-training, for the words that were known and unknown. Before training, LA spelled known words significantly better than unknown words ($c^2 = 4.89$; $p < .05$). Three weeks after training, however, there was no significant advantage for spelling known versus unknown words ($c^2 = .003$; $p = .90$). Without learning the meanings of the words, LA acquired and retained new orthographic patterns for words without apparent semantic representation. These results are consistent with the view that semantic influence is not required for orthographic processing.

Table 1: Percentage of words spelled correctly by LA

	before training	after training
semantically known words	67	88
semantically unknown words	14	71

Study 3: Nonword Spelling in Patients with Probable AD

Writing often becomes impaired early in the course of AD, but the reasons for this impairment are not well understood. The goal of the current study was to investigate the cognitive processes underlying the spelling disorders observed in patients with AD. Participants were 23 patients with probable AD and 27 healthy age and education matched controls. To focus on phonological processing, three sets of single syllable pseudowords (PWs) were presented for writing to dictation: 1) "Regular PWs" were composed of familiar phoneme sequences that had a single possible spelling (e.g. /plunt/); 2) "Ambiguous PWs" were composed of familiar phoneme sequences that had more than one possible spelling (e.g., /pred/); 3) "Unusual PWs" contained pronounceable phoneme sequences that do not occur in English words (e.g., /fwΛg/).

The results are shown in Table 2. A 2 X 2 ANOVA revealed a main effect of PW type (regular and ambiguous PW were spelled better than unusual PWs), and a main effect of group (control subjects were better spellers than AD patients). However, there was no group X PW type interaction; that is, the AD patients showed the same pattern of performance as the control subjects. In addition, in all twelve of the of the ambiguous spelling patterns that were sampled, AD patients did not differ from controls in terms of the most preferred spelling pattern. (For example, for the stimulus /plon/, both groups preferred the spelling plone to ploan. Finally, although AD patients made many more errors than control subjects, the groups did not differ in the distribution of different error types across PW conditions.

Table 2: Percentage of pseudowords spelled correctly

	Normal Controls	AD Patients
Regular PWs	85	52
Ambiguous PWs	88	53
Unusual PWs	19	19

These results suggest that phonological processes underlying spelling operate in a relatively normal fashion in AD patients even at moderate-severe levels of dementia. The decline in response accuracy on cognitively demanding writing tasks in patients with more advance dementia, then, is most likely due to nonlinguistic and peripheral cognitive impairments, rather than a disturbance within language specific cognitive processes.

Project 2: Cognitively-Based Treatments of Acquired Dyslexias

The purpose of this project is the development of a set of therapy programs that are shown to be effective in the treatment of acquired disorders of reading (acquired dyslexias, also known as alexias.). This goal is achieved through the development, implementation, and evaluation of several experimental therapies, each targeted for a specific type of reading deficit, based upon a cognitive neuropsychological model of reading. The data obtained from this study are also used to improve our models of normal reading, which may lead to more effective methods of teaching reading to both normal and developmentally dyslexic children.

Patients with acquired reading disorders following stroke are referred to our project by neurologists or speech pathologists for further evaluation. The patient's reading and other cognitive skills are assessed using a battery of screening tests that we have developed over the past several years. Based upon the results of these tests, the patient's alexic disorder is characterized. Patients whose deficits are

among those that are the focus of this project are assigned to one of the treatment programs devised specifically for that type of deficit. For many, the question of bypassing an impaired system vs. remediating the disturbance is addressed. When feasible, factors that might predict the success of a particular treatment for a particular patient are examined. The overall structure of the study consisted of single case studies, replicated over several patients, each employing a multiple baseline design. The following results have been obtained over the past year.

Study 1. Pure Alexia

A. Semantic Treatment. The theoretical basis for this therapy was the suggestion in the literature that some information is passed on to the semantic system when pure alexic patients view words that they fail to identify. The task here, then, focuses on semantics: the patients say "yes" if a rapidly presented word belongs to a given category or "no" if it does not belong.

Replicating previous results, a new subject, SV, successfully learned to categorize the trained words. There was some generalization to untrained words. However, length effects remained, and no part of speech effect emerged, contrary to what was expected for semantic reading. As before, it appeared that whatever was being learned might not be a semantic reading strategy. To pursue this further, the task was switched to oral reading, i.e. the patient simply read each rapidly presented word aloud. SV was successful with the oral reading task (Figure 1). In order to further replicate these results, new subject FR has been evaluated and has just begun this therapy.

To further rule out reading via semantics as the reason for the patients' improvement in reading trained words, pseudowords, which have no semantic value, were substituted for the nouns in the oral reading task. Again, replicating prior results, SV improved her reading of the trained pseudowords, but could not learn them to criterion (90% correct) (See Figure 1).

The results obtained this year for SV, in conjunction with those obtained in the previous year, demonstrate that for some patients with pure alexia, improvement may be effected by reteaching the patient to rapidly recognize words that had been known previously, but can no longer be recognized rapidly. This type of relearning does not appear to generalize to items that are not taught.

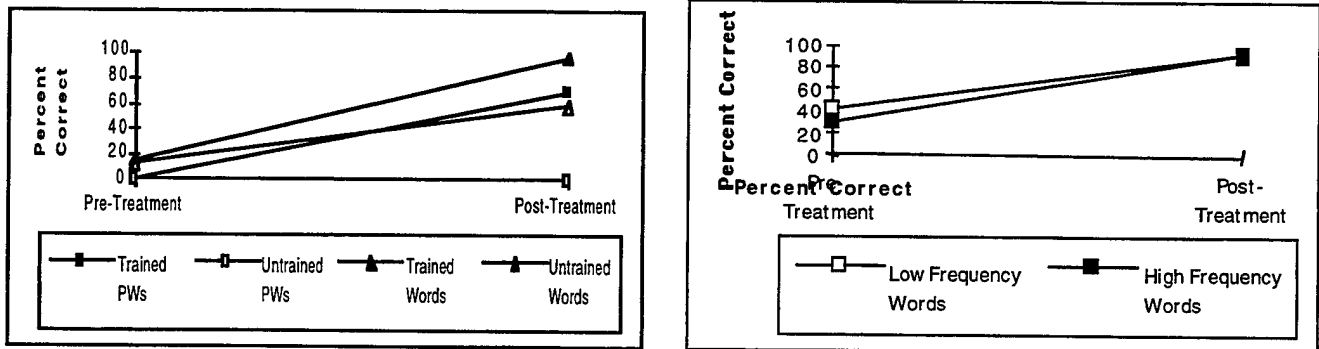


Figure 1: Subject SV's accuracy in reading trained and untrained words and nonwords, before and after rapidly-presented word reading treatment.

Figure 2: Subject SV's accuracy in reading trained words with a high or low frequency of occurrence, before and after rapidly-presented word reading treatment.

To determine if the superior learning of real words compared to pseudowords can be attributed to the familiarity of real words, a new set of stimuli were constructed. This set consisted of words with either a high or a low frequency of occurrence. We predicted that if familiarity enabled the reading of words to be relearned more easily, then reading of words with a high frequency of occurrence would be learned faster than that of words with a low frequency of occurrence. For subject SV, there was no difference in learning between the two sets of words (See figure 2). Due to SV's extraordinary vocabulary, the words with a low frequency of occurrence may actually have been quite familiar to her, thereby blurring our distinction between the two sets of words. Replication with other subjects, therefore, is needed before any conclusions may be drawn concerning these results.

B. Hybrid Treatment. Hybrid treatment combines the successful elements of the two pure alexia approaches we are examining, rapid word presentation and speeded letter-by-letter reading (described in previous annual report). The patient is trained to (1) rapidly recognize a set of the most frequently occurring words, (2) quickly read less frequently occurring words in letter-by-letter fashion, and finally (3) combine both strategies when reading sentences. Patient FT is currently in the second phase of this treatment.

In the first phase of treatment, FT successfully learned to read the sight words (See Figure 3). These 240 words were trained sequentially in sets of 40. Performance on initially trained sets was maintained during training on subsequent sets. When words were tested in sets of 80, however, performance dropped to 86%. After treatment in sets of 80 words, performance rose to 93%. When all 240 words were tested together, performance dropped back to 85%. After training all 240 words together, performance again rose to 91% correct. These results indicate that training in larger contexts is a necessary treatment step.

Following the sight word treatment, FT's reading of sentences composed entirely of the trained sight words became considerably faster, from 9.4 to 7.7 seconds per sentence, without any loss in accuracy. Her speed of reading sentences composed of a combination of trained sight words and untrained words, however, did not noticeably change (from 10.2 to 9.8 seconds per sentence). These data indicate that the sight word treatment effect transferred to speed of sentence reading of the trained words, but not of the untrained words, as we predicted.

In the second phase of treatment, no measurable change in FT's mean response time for naming letters in isolation was observed (0.7 to 0.6 seconds/letter). She has, however, increased her letter-by-letter reading time for words of 3 to 5 letters in length; See Figure 4). She will be trained on longer words next.

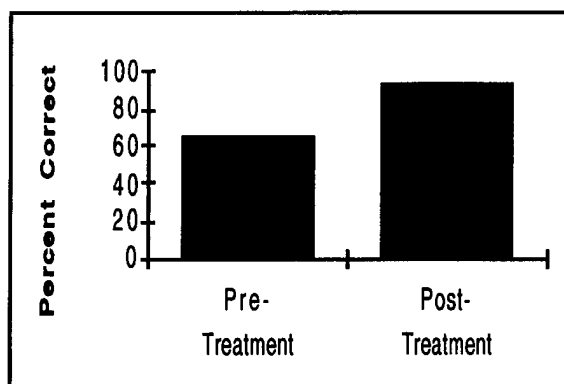


Figure 3. Subject FT's accuracy reading the hybrid sight words, before and after rapidly- presented word reading treatment.

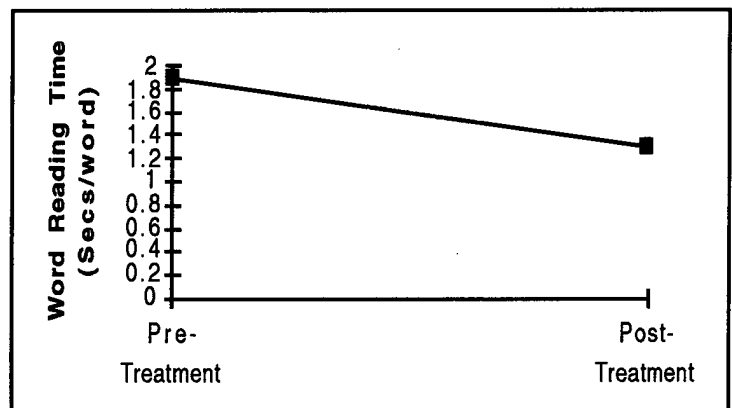


Figure 4. Subject FT's mean time to read short words, before and after letter-by-letter word reading treatment.

Study 2: Phonological/Deep Alexia

Patients with this type of alexia cannot read via a system of assembled phonology (letter - sound conversion). Thus unfamiliar words and pronounceable nonwords are read poorly relative to real familiar words.

A. Bigraph-Phoneme Conversion Treatment. This therapy is predicated on the premise that grapheme-phoneme conversion is not the most natural way to translate letters into sounds. Our treatment uses the bigraph syllable, which is a more natural and psychologically real unit of language. In this treatment, patients are trained to pronounce syllables by pairing them with key words (e.g. li - lips), and then to sound out words by combining these syllables. The success of this treatment with two subjects to date confirms our prediction. Furthermore, both patients demonstrated considerable generalization to words that were untrained but composed of trained bigraphs (See Figures 5-6).

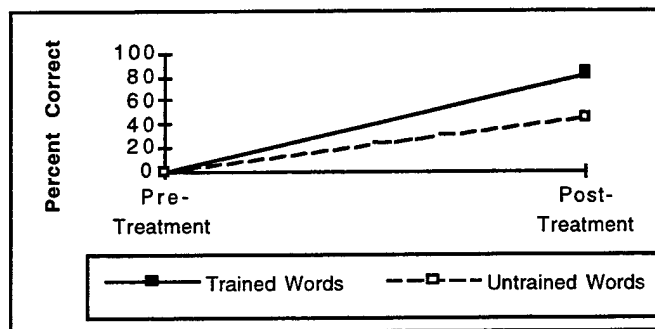


Figure 5. Subject LR's accuracy in reading trained and untrained words, before and after bigraph syllable treatment; Sets 2 and 3 Words

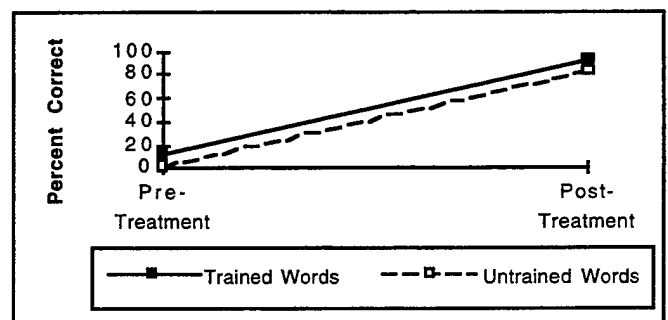


Figure 6. Subject KT's accuracy in reading trained and untrained words, before and after bigraph syllable treatment; Sets 2 and 3 Words

After training was completed on all 3 sets, when all stimuli were tested together, we discovered that LR and KT were no longer performing as well on previously trained items. We set up a new treatment phase in which all bigraphs were trained simultaneously. After combined training of all bigraphs, LR again achieved criterion level performance on the bigraphs, and this resulted in improved word reading as well (See Figure 7). KT has just initiated this combined treatment.

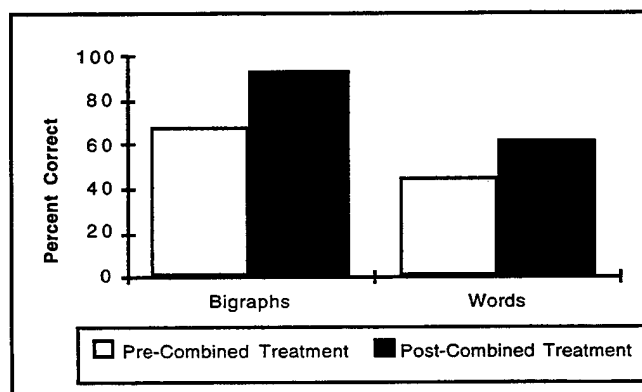


Figure 7. Subject LR's accuracy in pronouncing trained bigraphs and words (composed of trained bigraphs), before and after combined bigraph syllable treatment (words were not yet trained in the combined format).

B. Phonological Neighborhood Treatment. This therapy derives from connectionist models of word reading, which hold that the ability to read unfamiliar words is related to the strengths of the connections between the orthographic and phonologic units of which they are composed. These strengths are related to the number of times that words containing those connections have been read, i.e. the number of times that the orthography has been paired with the phonology. In the therapy, the oral reading of two groups of orthographically similar words are trained to criterion. One group is similar in its initial unit (e.g. came, case, cape), while the other is similar in its final unit (e.g. bake, make, lake). The patient is tested on his/her ability to read a target word composed of the two trained orthographic units (e.g. cake). As controls, words containing one trained and one untrained unit and words containing no trained units were also tested. The models predict that the repeated pairing of each of these written words with their pronunciations should strengthen all of the component orthography to phonology connections needed to orally read the target word.

GR's reading of words composed of two trained units improved from 18% to 87% correct. Reading of control words that contained one of the two trained units improved from 32% to 79% correct. Control words which did not contain any trained units improved from 18% to 60% correct. These results suggest that there was a positive effect of training in addition to the effect of repeated exposure of the words. The data also support our hypothesis that orthography to phonology connection strengths can be reestablished in an implicit processing task.

C. Semantic Mediation Treatment. While the previous therapy concentrated on "restoring" the damaged route to reading, this therapy takes the "re-organization" approach. It attempts to use the semantic route to circumvent the problems in the phonological reading route. This treatment pairs difficult words low in semantic value (functors and verbs), which are difficult for these patients to read, with homophones (words that are pronounced the same) or near homophones (e.g. in and inn, me and meat) that have high semantic value. The word pairs are trained via flashcards; the front contains the written target word and the back contains the written homophone along with its picture. Three sets of targets were trained sequentially.

Both subjects DN and HN improved their reading of the target words (See Table 3). These results support the hypothesis that semantic route reading may be invoked to re-organize impaired phonologic route reading.

Table 3. *DN's and HN's reading of target words before and after pairing with homophones.*

Subject	Pre-Treatment	Post-Treatment
DN	10%	82%
HN	0%	92%

As with the bigraph treatment, we found that when all stimuli were tested together at the end of treatment, patient HN had not maintained as high a level of performance on previously trained items (sets 1 and 2). Again, we added a final treatment phase in which all stimuli were trained together. After combined treatment of all stimuli, HN again achieved criterion level performance (See Figure 8).

During the past year, this issue of decreased performance on previously trained items has appeared in three of our treatments: hybrid sight words, bigraphs, and semantic mediation. All the patients that have completed combined treatments were successful in regaining criterion level performance in the combined context. We are currently exploring mechanisms to which the decreased maintenance can be attributed.

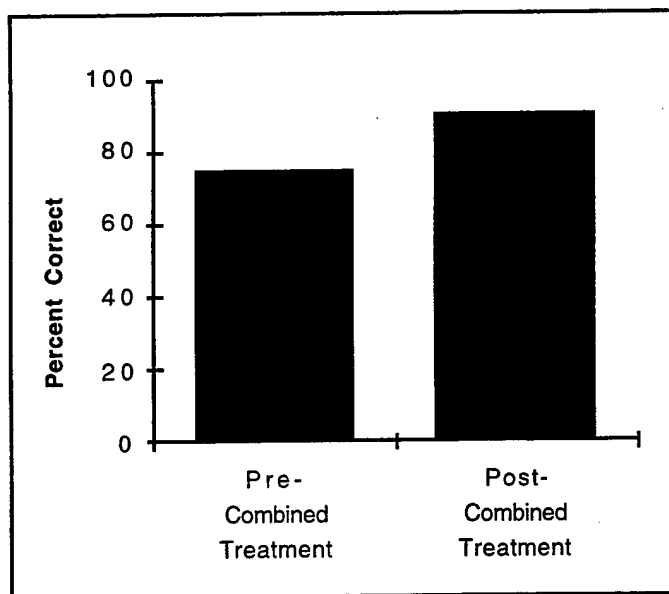


Figure 8. Subject HN's accuracy in reading target words, before and after combined treatment.

Project 3: Evaluating Neuropsychological Models of Language Recovery with fMRI

Functional MRI studies are currently underway to (1) determine the potential usefulness of the technique of fMRI in predicting the outcomes of various treatments for certain types of language and reading disorders; (2) elucidate the mechanisms of recovery from aphasic and alexic symptoms; and (3) provide data that will help refine current neuropsychological models of language and reading. Functional MRI scans of the brains of alexic patients will be obtained while the patients perform various reading tasks. These scans will be compared to those of normal controls to identify the source of the reading deficit.

Several different experimental designs have been used over the past year in an attempt to identify areas of the brain involved in phonological processing during reading tasks. Various types of stimuli were presented to subjects through a pair of goggles specifically designed for use in the MR machine. To date, we have used only normal control subjects in our studies. All of the paradigms we have implemented consist of an ABAB alternating task design.

Study 1: Alternating Letter Strings and Pseudowords

In this study, subjects were told to simply look at alternating blocks of non-pronounceable letter strings (e.g. lxxpt) and blocks of pseudowords (e.g. blink). It was expected that both conditions would produce activation associated with visual processing of letters. In addition, it was expected that there would be activation in the pseudoword (PW) condition that is not seen in the letter string condition, reflecting two components of reading that are involved in reading PWs: recognition of orthographic regularity, and determination of pronunciation. Based on previous results in the literature, we expected such processing to occur automatically upon viewing PWs. Subtraction of the letter string blocks from the pseudoword blocks should show activation in areas of the brain involved in one or both of these processes. Data was collected from five subjects using this paradigm, and as expected, both conditions produced activation in the occipital area due to visual processing. However, no significant differences in activation were found between the letter string and pseudoword blocks.

The stimuli used in this study were pairs of real words. The word pairs varied along two dimensions: 1) the words either rhymed or did not rhyme 2) the words were either printed in the same case (both upper or both lower) or in different case (one upper, one lower). Each run consisted of a block of one 36-second block of rhyme judgments and one 36-second block of case judgments. Each of those blocks was preceded by a block consisting of a flashing fixation letter (C prior to the case judgment block; R prior to the rhyme judgment block). The rhyme judgment task was expected to engage phonological processing, while the case judgment task served as a control for the visual complexity and familiarity of the word pairs.

Five normal subjects were tested using this paradigm, and three of them showed activation in the left frontal lobe during the rhyme judgment task that was not seen during the case judgment task (See Figure 9). These results are similar to other reports of frontal activation for phonological tasks, reported in the literature. We are currently in the process of refining the protocol in order to better delineate the areas of the brain involved in reading. We will then begin studies involving patients with acquired alexia.

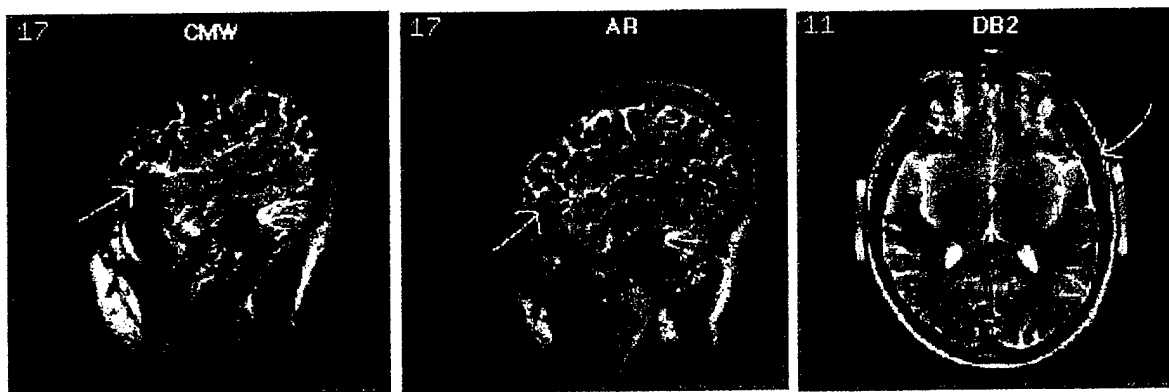


Figure 9. Rhyme judgment minus case judgment activations for 3 normal subjects.

MICHAEL ULLMAN, Ph.D.

The long-term objective of the Ullman laboratory research is to understand the brain bases of the two capacities which give language its vast expressive power: (1) the *mental lexicon*, containing a memorized list of words, each an arbitrary sound-meaning pairing; and (2) the *mental grammar*, containing rules which productively combine words into an infinite number of predictably structured larger words, phrases, and sentences.

These two capacities have been explained by two competing theories. "Dual-system" theories posit distinct brain structures dedicated to each of the two capacities, with lexical memory linked to temporal cortex, and a grammar-specific component linked to frontal cortex. Double dissociations between lexical and grammatical processing from neurological and neuroimaging studies support the dual system view. However, imperfections in these dissociations, and the advent of connectionist models, have fueled support for "single-system" theories. These posit that the two capacities are subserved by a single general-purpose computational system with broad anatomical distribution.

Although dual-system theories usually assume components dedicated ("domain-specific") to language, and single-system theories usually assume general-purpose ("domain-general") circuitry, the dual-system/single-system issue is logically distinct from the domain-specific/domain-general issue. We have been investigating both issues, and have posited that dual but domain-general systems subserve the lexicon and the grammar.

To distinguish between the dual and single system views, we have been investigating the brain bases of the grammatical transformation of words. *Irregular* and *regular* transformations allow lexicon and grammar to be contrasted, while other factors are held constant. For example, in English past tense, irregular transformations are unpredictable (e.g., *cling-clung*, *bring-brought*) and unproductive (new irregulars rarely enter the language), whereas regular transformations are predictable (verb + *-ed*) and apply productively to new words (*fax-faxed*). A dual system view links irregulars (lexicon) to temporal cortex, and regulars (grammar) to frontal cortex.

To address the domain-specific/domain-general controversy, we have proposed a new theory, which supports the lexicon/grammar distinction, but extends it to two well-studied brain systems that cut across domains such as vision and language: We posit that lexical memory is part of the temporal lobe declarative memory system for the learning and storage of facts and events, whereas grammatical rules are processed by the frontal/basal-ganglia procedural memory system for learning and processing motor, perceptual, and cognitive skills.

Double dissociations between irregulars and regulars in our studies of patients with impairments of either declarative or procedural memory support this theory, and suggest that the basal ganglia's well-studied role in motor activity extends to grammatical rule use (Ullman et al., 1997; Ullman, in press). Specifically, we asked brain-damaged patients to produce the past tense of regular verbs like "walk" and made-up verbs like "wug" (both of which should require a rule), and of irregular verbs like "think" (which should require memory lookup). We found that patients with damage to brain structures underlying declarative memory (patients with a stroke in left temporal cortex as well as patients with Alzheimer's disease, who have a degenerative disease primarily afflicting the temporal lobes) were worse at producing past tense forms for irregular verbs than for regular or novel verbs. In contrast, patients with damage to brain structures underlying the procedural system (patients with a stroke in left frontal cortex as well as patients with Parkinson's disease, who have a degenerative disease of the basal ganglia) showed the opposite pattern: They were worse producing forms like "walked" and "wugged" than forms like "thought." Unlike patients with Parkinson's disease, whose basal ganglia damage resulted in suppressed movements (trouble starting and carrying out movements) and suppressed rule use ("Yesterday I walk into town"), the different type of basal ganglia damage in patients with Huntington's disease which leads to unsuppressible movements (irrepressible dance-like movements called chorea) also led unsuppressible rule use ("Yesterday I walkeded into town, and dugged a hole").

In the year since I joined the faculty of GICCS, my lab has been working on four new projects, each of which is aimed at confirming, generalizing, or extending the findings described above.

Project 1: Lexical Memory in Amnesia: A Role for Medial Temporal Structures in Language

In the declarative memory system, the hippocampus and other medial temporal lobe structures are thought to underlie the acquisition of new knowledge, whereas the eventual storage of this knowledge is thought to be no longer dependent upon these structures, but rather on neocortex. Thus patients with damage limited to medial temporal lobe structures are impaired at acquiring new facts and events, but generally spared at remembering facts and events learned years before their injury. If word memory is part of declarative memory, such "amnesic" patients should therefore also be spared at remembering words learned in childhood, such as irregular past tense forms.

To investigate this prediction, we have been collaborating with Suzanne Corkin of MIT to test the amnesic patient H.M., whose bilateral medial temporal lobe lesion spared most of his neocortex. H.M. is a well-studied amnesic subject who at age 27 underwent bilateral excision of the hippocampus and other medial temporal lobe structures for the relief of intractable epilepsy. Afterwards, intensive study of his behavior by Brenda Milner, Corkin, and their colleagues revealed that he was no longer able to learn new facts, events, or words. In contrast, his memory for facts and events occurring substantially *before* the operation was largely spared (Corkin, 1984).

We tested H.M. as well as 10 normal adults who were matched to H.M. in age and education level. All subjects were given the past tense task previously given to the aphasic, Alzheimer's, Parkinson's, and Huntington's patients, as described above: Twenty irregular and 20 regular verbs in a past tense production task ("Every day I dig a hole. Yesterday I _____ a hole"), and 9 irregular and 9 regular nouns in a plural production task ("Here is one mouse. Here are three _____").

To our surprise, H.M. was significantly worse at producing past tense forms for irregular verbs (81% correct) than regular verbs (100% correct). His errors on irregular verbs were incorrect irregularizations such as "swing-swang" and "cling-clang." In contrast, the age- and education-matched normal adult subjects were about equally good at producing past tense forms for irregular and regular verbs (95% vs. 98% correct). H.M. was also worse at producing irregular plurals (44% correct) than regular plurals (100% correct). All of his errors for irregular plurals were "over-regularizations" like "gooses" or "tooths," in which he incorrectly added an "-s" suffix. In summary, H.M. had difficulty producing irregular past tense and plural forms, but was perfect at producing regular past tense and plural forms (Ullman & Corkin, 1997).

This evidence suggests that H.M. has a deficit of word memory, but not of processing rules of grammar. This in turn suggests that, contrary to our and others' expectations, medial temporal lobe structures may play a role in the memory for established declarative knowledge, at least for the knowledge of words. Because H.M.'s lesion is largely restricted to the hippocampus and other medial temporal lobe structures underlying declarative memory, the results also provide further support for the hypothesis that word memory is part of declarative memory.

The results must nonetheless be viewed with caution. They come from testing only one amnesic subject on only two tasks requiring word memory lookup. Moreover, H.M. has marked atrophy of the cerebellum, which might also affect his language. Thus the results suggest that other amnesic subjects should be tested on these tasks as well as other tasks probing established memories of words, facts, and events.

Current Directions

We are currently following up on this result by testing additional medial temporal lobe amnesic subjects on the same and additional tasks, in a collaboration with Larry Squire of the

University of California at San Diego. One patient has thus far been tested; as predicted, he had greater difficulty producing irregular than regular past tense and plural forms, producing over-regularizations instead of the correct irregular form.

Project 2: The Role of the Cerebellum in Language

The cerebellum has long been thought to have a role in movement. However, recent evidence from studies of patients with cerebellar lesions and from functional brain imaging studies have implicated the cerebellum in cognition (see Schmahmann, 1996). We have been investigating whether the cerebellum has a role in language, and in particular, whether it may play different roles in lexical memory and grammatical processing.

In a collaboration with Jeremy Schmahmann of the Massachusetts General Hospital (MGH) and Harvard Medical School and Hilary Bromberg of Harvard University, we have tested 13 patients with cerebellar lesions or degeneration, as well as age- and education-matched control subjects. All subjects were given the past tense task described above: Twenty irregular and 20 regular verbs in a past tense production task ("Every day I dig a hole. Yesterday I _____ a hole"), and 9 irregular and 9 regular nouns in a plural production task ("Here is one mouse. Here are three _____").

Five of the 13 cerebellar subjects were more impaired than their control subjects at producing either regular or irregular past tense and plural forms. Intriguingly, these 5 subjects did not all show the same pattern of impairment on the tasks. Two were selectively impaired at producing irregulars, 2 at producing regulars, and 1 showed difficulties producing both types of past tense forms. We are currently investigating whether these patterns vary in a reliable manner with the patients' lesion sites.

Project 3: Functional Magnetic Resonance Imaging of language

We have also been investigating the brain bases of lexicon and grammar with functional brain imaging. In a collaboration with Robert Savoy and Kathleen O'Craven of the Massachusetts General Hospital and Harvard University, we have carried out a functional magnetic resonance imaging (fMRI) study of English irregular and regular past tense production (Ullman, Bergida, & O'Craven, 1997).

Five healthy right-handed men were shown the stems of irregular verbs (*sleep*) and non-rhyming regular verbs (*slip*) on a screen, and were asked to silently produce their past tense forms. Twenty seconds of regulars (10 verbs) were followed by 20 seconds of fixation, 20 seconds of irregulars (10 verbs), and 20 seconds of fixation. This sequence was repeated for 80 irregular and 80 regular verbs. Functional scans were obtained using an Asymmetric Spin Echo pulse sequence with a TR of 2 seconds. We examined 12 axial oblique slices spanning the frontal, temporal, and occipital lobes, and the cerebellum. All functional data were motion-corrected using a modification of the AIR algorithm. Functional data from each subject were then transformed into Talairach space. Signed Kolmogorov-Smirnov statistics were calculated for three comparisons: Regular vs. Fixation, Irregular vs. Fixation, and Irregular vs. Regular. In addition to examining the data from each individual subject, the Talairach transformations allowed us to combine the data from all five subjects.

The 5 subjects showed similar patterns of activation. We found overlapping as well as distinct patterns of brain activation for the irregular and regular conditions. All activation changes were confirmed with time-course analyses (Figure 1). Compared to fixation, both the irregular and regular conditions yielded activation increases in inferior frontal regions (including Broca's area), and in the basal ganglia (in the caudate nucleus). This suggests that these regions may subserve a function common to both past tense types, such as the computation of the grammatical tense feature

(Jaeger et al., 1996). Alternatively, the data is consistent with distinct frontal/basal-ganglia functions for the two past tense types, such as grammatical rule processing for regulars, and search or retrieval of stored words for irregulars (Buckner & Petersen, 1996; Ullman, in press).

Left temporal and temporo-parietal regions were associated with an activation decrease for irregulars, but not for regulars (Figure 1, left graph). In contrast, a left prefrontal region was associated with an activation increase for irregulars, but a decrease for regulars (Figure 1, right graph). Interestingly, the activation increase in left prefrontal cortex, and decrease in superior temporal cortex associated with irregulars, but not regulars, was also observed during a verbal fluency task (generating words in a category) by Wise et al. (1991). While the specific causes of these activation changes remain to be investigated, the double dissociations suggest that irregulars and regulars have distinct neural underpinnings linked to temporal and frontal regions. It is also of interest that the patterns of activation reported for a recent PET study of German regular and irregular past tense processing (Indefrey et al., 1997) are similar to those found in this study, and therefore may also in part be explained by activation decreases.

Current Directions

We have tested 4 additional subjects, all women, and are currently examining whether their patterns differ from those of the 5 male subjects. We have also run several subjects on a version of the task in which regular and irregular verbs are presented in a randomized rather than a blocked sequence. We have acquired images after each verb, thus treating each verb as a distinct trial. Such “single-trial fMRI” (also termed “event-related fMRI”) is a promising new technique which may allow us to observe the time course for each linguistic event. The technique avoids the problems inherent in presenting blocks of stimuli of the same condition.

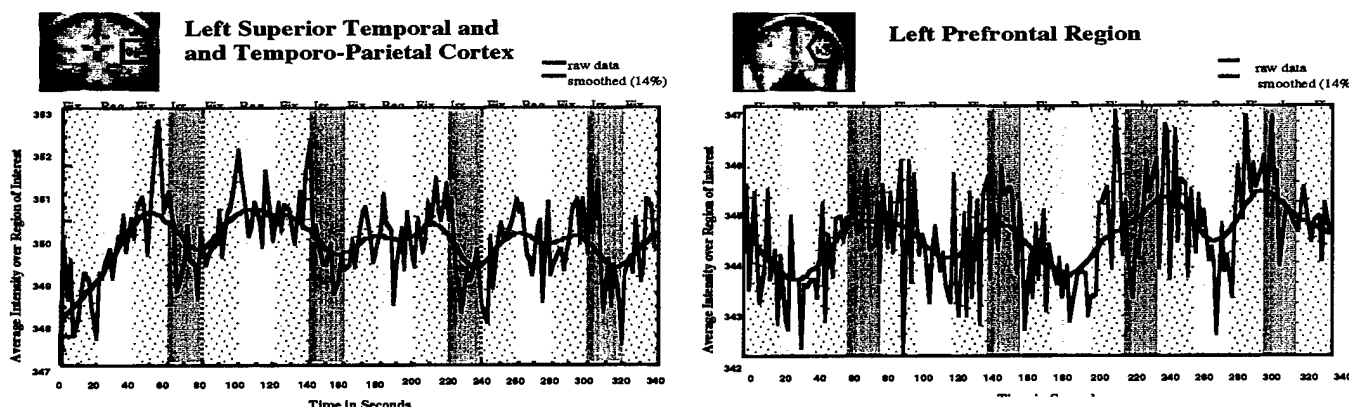


Figure 1: Time course data from our fMRI study of the production of regular and irregular past tense forms. Graph on left shows an activation decrease for irregulars, but not for regulars, in left temporal cortex. Graph on right shows an activation increase for irregulars, but decrease for regulars, in left prefrontal cortex.

Project 4: Sex Differences: Neuropsychological Evidence

Examination of the findings described in the Background section (see above) separately for men and women led to the hypothesis that men and women may show a different pattern of reliance on declarative and procedural memory for the computation of irregular and regular past tense forms. We have followed up on this preliminary data with an investigation of the regular and irregular past tense production in patients with Alzheimer’s disease (AD), Parkinson’s disease (PD), and normal control subjects.

Six male and 13 female AD patients, 21 male and 13 female PD patients, and 6 male and 10 female age- and education-matched control subjects were given the past tense production task described above, and an object naming task.

Men showed the predicted memory/rule dichotomy: For men, in all three subject groups (AD, PD, control), errors at object naming (a lexical memory measure) correlated with production errors of irregular (*dug*) but not regular or novel (*looked, plagged*) past tense forms (Figure 2). Moreover, among the PD subjects, hypokinesia (from degeneration of the basal ganglia, in the procedural system) correlated with errors in the production of regular but not irregular past tense forms (Figure 3). Women appear to rely on memory for the production of both past tense types: For women, in all three subject groups, object naming errors correlated with production errors of irregular and regular past tense forms (Figure 2). Among the PD subjects, hypokinesia did not correlate with errors of either regular or irregular pasts (Figure 3).

These findings suggest that men may memorize irregular past tenses and other lexicalized forms in declarative memory, but rely on the procedural system's basal ganglia to rule-produce grammatical forms like regular past tenses. In contrast, women may tend to memorize both types of forms. In general, men may rely more on the procedural system than women, while women rely more on declarative memory than men (Ullman & Yee, 1997).

Current Directions

We are currently developing a new sequence of tests which will be given to AD, PD, and other patient groups, and to control subjects, to further investigate these hypotheses.

Men

	Normal Adults		Alzheimer's Patients		Parkinson's Patients	
	r	p	r	p	r	p
Irregulars	.85	<.05	.74	<.05	.39	<.05
Regulars	-.70	ns	.04	ns	.13	ns
Novel Regulars	-.15	ns	.15	ns	.19	ns

Women

	Normal Adults		Alzheimer's Patients		Parkinson's Patients	
	r	p	r	p	r	p
Irregulars	.60	<.05	.61	<.05	.51	<.05
Regulars	.56	<.05	.48	<.05	.63	<.05
Novel Regulars	.06	ns	.51	ns	.14	ns

Figure 2: Correlations between errors at object naming (a measure of lexical memory) and at producing past tense forms; for men (top table) and women (bottom table).

Men

	Parkinson's Patients	
	r	p
Irregulars	.08	ns
Regulars	-.71	<.001
Novel Regulars	-.66	<.001

Women

	Parkinson's Patients	
	r	p
Irregulars	.07	ns
Regulars	.29	ns
Novel Regulars	-.04	ns

Figure 3: Correlations between level of hypokinesia (which reflects the degree of basal ganglia degeneration) and errors producing past tense forms for men (top table) and women (bottom table).

References

- Buckner, R. L., & Peterson, S. E. What does neuroimaging tell us about the role of prefrontal cortex in memory retrieval? *Seminars in the Neurosciences*, 8, 47-55, 1996.
- Corkin, S. Lasting consequences of bilateral medial temporal lobectomy: Clinical course and experimental findings in H. M. *Seminars in Neurology*, 4(2), 249-259, 1984..
- Indefrey, P., Brown, C., Hagoort, P., Herzog, H., Sach, M., & Seitz, R. J. A PET study of cerebral activation patterns induced by verb inflection. *NeuroImage*, 5(4), S548, 1997.
- Jaeger, J. J., Lockwood, A. H., Kemmerer, D. L., Van Valin, J., Robert D., Murphy, B. W., & Khalak, H. G. A PET study of English verb morphology. *Language*, 2(3), 451-497, 1996.
- Schmahmann, J. D. From movement to thought: Anatomic substrates of the cerebellar contribution to cognitive science. *Human Brain Mapping*, 4, 174-198, 1996.
- Shimamura, A. P. Memory and Frontal Lobe Function. In M. S. Gazzaniga (Ed.), *The Cognitive Neurosciences* (pp. 803-813). Cambridge, MA: MIT Press, 1995.
- Ullman, M. Evidence that lexical memory is part of the temporal lobe declarative memory, and that grammatical rules are processed by the frontal/basal-ganglia procedural system. *Brain and Language* (in press).
- Ullman, M., Corkin, S., Coppola, M., Hickok, G., Growdon, J. H., Koroshetz, W. J., & Pinker, S. A Neural Dissociation within Language: Evidence that the mental dictionary is part of declarative memory, and that grammatical rules are processed by the procedural system. *Journal of Cognitive Neuroscience*, 9(2), 266-276, 1997a.
- Ullman, M. T., Bergida, R., & O'Craven, K. *Distinct fMRI activation patterns for regular and irregular past tense*. Paper presented at the Functional Mapping of the Human Brain, Copenhagen, Denmark, 1997b.
- Ullman, M. T., & Corkin, S. *Lexical memory is part of declarative memory: H.M. is worse at irregular than regular past tense and plural formation*. Paper presented at the Society for Neuroscience, New Orleans, LA., 1997c.
- Ullman, M. T., & Yee, E. *Sex Differences in Language: Evidence that men and women rely on different brain systems for past tense production*. Paper presented at the Cognitive Neuroscience Society, Boston, MA., 1997.

ANIMAL COGNITIVE NEUROSCIENCE: There are four faculty members who are grouped into this area. Dr. Kanwal investigates the processing of communication sounds and modeling of a neural network for multidimensional analysis of speech sounds and pattern recognition. Dr. Pekar utilizes magnetic resonance imaging (MRI) to evaluate brain structure, physiology, and function. Dr. Rauschecker examines the functional organization and plasticity of the cerebral cortex with an emphasis on the auditory cortex and multi-modal processing using single-neuron microelectrode recording, optical recording, and functional MRI. Dr. Wu studies large-scale neuronal events and distributed processes in the CNS.

JAGMEET S. KANWAL, Ph.D.

The major goal of Dr. Kanwal's research is to elucidate normal auditory processes involved in the coding/decoding and perception of communication sounds. The dogma challenged by his research is that animal studies can teach us little, if anything, about two of the most highly specialized functions of the human CNS, namely, perception of speech and music - two related facets of human cognition that make us unique from all other animals. It appears, however, that to really understand the neural mechanisms and neurophysiological principles underlying speech-sound perception one must study its minimal analogs present in an animal CNS. This has led to significant progress in the last decade, in our understanding of early auditory processing that underlies speech production as well as perception in humans. Similarly, basic phenomena such as perception of the "missing fundamental" that can be equated to certain aspects of music perception have been recently demonstrated at the psychophysical and neurobiological levels in bats and primates, respectively.

Dr. Kanwal's research uses multiple approaches to investigate auditory processing within higher levels of the CNS in auditorily specialized animals, such as bats. These approaches include single cell electrophysiology, evoked potentials and ERPs and functional MRI as well as behavioral techniques. A quantitative methodology incorporating advanced statistical analyses is stressed. During the last year, a major effort of setting up the electrophysiology laboratory has come to fruition together with significant progress being made in starting several independent research projects. Efforts are also underway to set up a core histology/imaging facility that will open up new avenues of research. Results obtained from five ongoing/completed research projects, supported in part by the Institute are briefly described below:

Project 1: Auditory Communication in Bats: acoustics, behavior and neurophysiology

Mustached bats depend largely on their auditory systems to survive in their ecological niche just as humans are uniquely equipped for survival by their ability to communicate acoustically. The significance of the single development of "speech" in humans is especially clear when one considers human evolutionary history. For several reasons, the auditory system of bats is an excellent model to study neural mechanisms that may underlie processing of communication sounds in mammals, including speech sounds in humans. For example, recent studies suggest that the bat's cortex shows hemispheric asymmetry for processing communication sounds. In addition, the presence of combination-sensitive neurons and multidimensional representational schemes for processing complex syllables in the auditory cortex may be applicable to speech sound processing as well. Not surprisingly, the field of communication sound processing is re-emerging as an actively growing field as it attempts to understand the neural basis of speech perception and its commonalties with the audio-vocal system of mammals at the single neuron level. Bats are useful models also because they employ a complex repertoire of sounds for acoustic communication rivaling that of the most vocal primate species. Even though the auditory system of microchiropteran bats is the best studied among mammals, previous neurophysiological studies on audition in bats have mostly focused on their echolocation behavior.

Project 1A: Acoustic communication behavior in mustached bats.

This study was begun at Washington University in St. Louis and is being continued at Georgetown University. Significant progress on this project was made by an MD/PhD student, Nicole Dietz, during a summer rotation in Dr. Kanwal's laboratory.

The species of mustached bats used, *Pteronotus parnellii*, were collected from a cave in Puerto Rico. These microchiropteran adult bats were preserved in a flight room at 28° to 30° C and with humidity at 55%. In addition to the elevated temperature, the natural roosting site of the bats was also mimicked by hanging two large inverted clay-lined pots in which the bats could hang. Their food consisted of live meal worms and water which was provided to them during feeding times. To receive and record the sounds emitted by the bats, a broad-band QMC; S-200 microphone (appendix; calibration curve) was placed about three feet from a nylon mesh cage and was also connected to a RACAL V-Stor tape recorder (Fig. 1). For analysis, the sounds recorded on the tape recorder were heard at one-half to one-sixteenth the speed at which they were recorded. To monitor the vocal sounds produced by the bat, a bat detector with a speaker was also connected to the microphone to convert the high frequency sounds emitted by the bats to frequencies audible by the human ear. To reduce excess noise that might interfere with the identification of the sounds, sound frequencies below 5 kHz and above 100 kHz were filtered out using a filter with a 80 dB/octave slope before recording. The frequency setting of this band pass filter matched that of communication calls which range from 7 kHz to 100 kHz (120 kHz for biosonar). The frequencies allowed to pass were amplified by a 20 dB Hewlett Packard 465A amplifier to increase their amplitude on the oscilloscope and clarify their audibility). A 2 channel Tektronix 2211 digital storage oscilloscope was used to monitor the amplitude of the signals produced by the bats and also the quality of the recordings. To hear the vocal responses of the bats, a mini-speaker was connected to an audio amplifier. An infrared low-light intensity sensitive video camera along with infra-red light emitting diodes was placed inside the sound proof room approximately one foot from the bat cage and directed at the bats. It was then connected to a Panasonic VHS videocassette recorder, which was connected to a monitor for video analysis and recording. This videocassette recorder allowed the visual recordings to be analyzed at various slow motion speeds or at one frame at a time. This was very useful as many behaviors were completed within a few milliseconds. The experiments were run at various times in the late afternoon and early to late evening because many bats, such as the Trinidad bats and most likely this species as well, are most active around 6:00p.m. (Bradbury and Emmons 1974)

Stereotypic Behavior Patterns

When bats were observed in their semi-natural environment, there were several instances of communication calls. It was very difficult, however, to determine which bat was actually emitting the call or calls. Like other gregarious bats, mustached bats have a basic instinct to cluster by making contact back to back. Since the bats collectively form tight clusters, called colonies, and exhibit very rapid movements and complex behaviors, it was difficult to follow the behavior of one particular bat in a highly populated colony. In the three-bat arrangement, this instinctive behavior was more clearly observed when two bats hung together leading to the exclusion of the third bat, regardless of its sex. While two bats hang together, the third bat would attempt to take the place of one of the other bats. In this process, several stereotypic behaviors such as crouching and wing-flicking were observed.

Since mustached bats live in absolute darkness, it is odd that they still exhibit stereotypic behaviors that usually have significance as visual displays. These include boxing, or hitting between two bats, flicking of wings, crouching, and wing flapping. For the purposes of this study, these characteristic behaviors are described below.

"Crouching" is the bending, or stooping, over of the bat's body so as to bring its head near its feet. "Boxing" is described as the hitting or fighting between two or more bats with the joint of the wing. This action is performed using either one wing or both wings. "Wing-flicking" is the rapid movement, or quick sharp motion of a wing back and forth. "Wing-flapping" is similar to wing flicking

except the wings are three-fourths open, or spread out. These behaviors were observed in 4 different situations for 5 minute intervals (Table 1).

Communication sounds were emitted by both sexes in all cases. According to the table, crouching was increasingly less common with more bats. However, the reverse is true for wing flapping. Wing flicking and boxing did not show any relationship to the number of bats. The type of calls emitted means that that call was specifically heard for that stereotypic behavior. However, this does not mean that other calls could not be emitted or that these calls are only emitted during these behaviors.

Conclusions

Different types of calls are associated with different behaviors in bats. These data are promising for planning additional studies to investigate the rate and level of information flow during acoustic communication in mustached bats.

Stereotypic Behaviors	3 Bats	4 Bats	11 Bats	Colony	Frequency per 5 minute interval	Vocal Response	Types of Calls
Crouching	19	6	4	1	.26	?	
Boxing	4	2	3	14	.2	yes	SFM, RFM
Wing Flicking	7	2	8	20	.32	yes	SFM, BBNB
Wing Flapping	0	0	2	25	.23	?	

Table 1. The table shows the number of the 4 stereotypic behaviors in 4 different bat arrangements and their frequency relative to the total number of stereotypic behaviors counted. The communication calls, if observed to be related to the behavior, are also listed. The ? means that it was unclear if the calls heard were specifically associated with the corresponding stereotypic behavior.

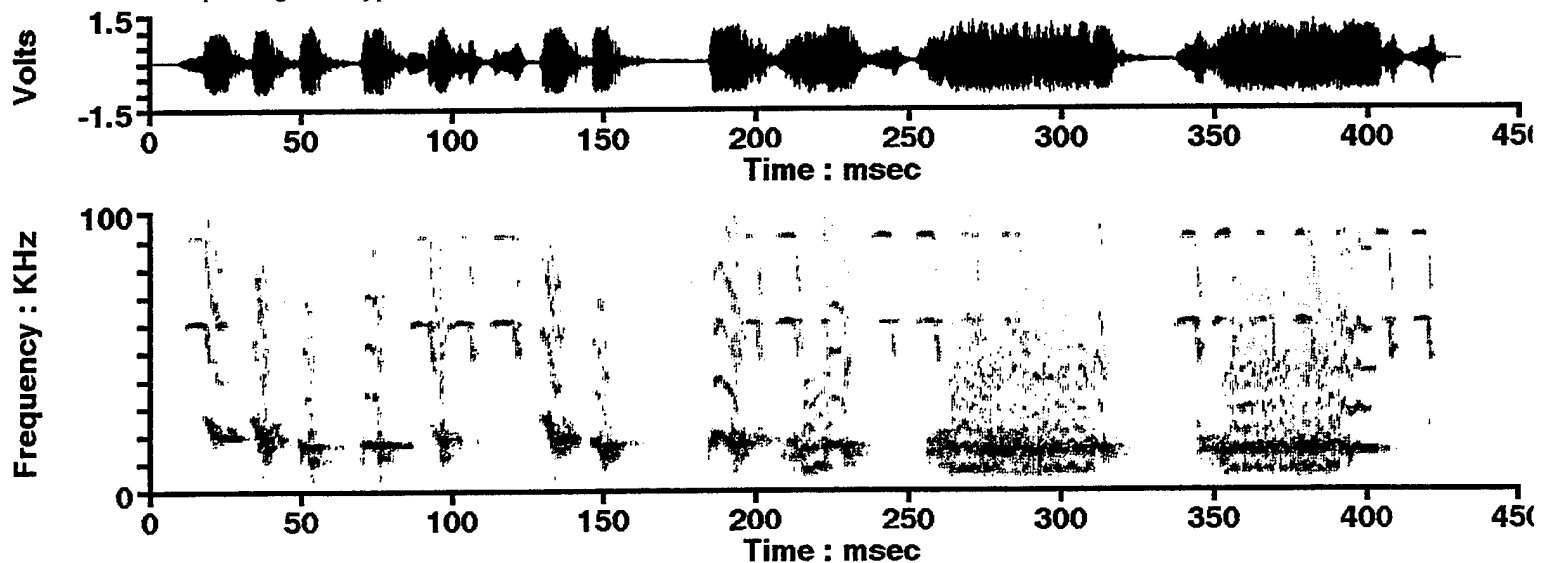


Figure 1. Amplitude oscillograms and frequency-time spectrograms of a stream of complex communication sounds emitted by one mustached bat during an aggressive encounter. A second bat is emitting stereotypic echolocation sounds indicated by a constant frequency component followed by a downward sweeping FM.

Project 1B: Processing of syntactic information in the FM-FM area of the auditory cortex

Data for this project were acquired at Washington University in St. Louis although data analysis and writing was primarily carried out at the University of Ulm, Ulm, Germany and at Georgetown University. This project has been completed and the results have been accepted for publication in the "Proceedings of the National Academy of Sciences".

Details of the surgical and chronic recording techniques have been described elsewhere. During the 4-8 hour recording session the awake bat was continuously monitored via video for signs of discomfort or distress. Extracellular recordings were obtained from the FM-FM cortical area of mustached bats ($n = 5$) using custom-made lacquer-coated tungsten microelectrodes (tip diameter: 4-8 μm). Single-units were isolated with a level and time window discriminator (BAK Electronics) on the basis of spike height and slope of the waveform. The composite calls used as stimuli were digitized, manipulated and played back using an A/D-D/A-converter board (Data Translation, DT2821G; 250 kHz sample rate) and SIGNAL software. Acoustic signals mimicking the FM components of the bats' echolocation sound ("pulse") and "echo" were generated with conventional analog equipment.

Upon isolation of a single unit, the FM1-FM n subtype (i.e. FM1-FM2, FM2-FM3 or FM1-FM4) and best pulse-echo delay (BD) of the neuron were determined. The neuron's responses to the most effective biosonar pulse-echo pair were further quantified by PSTHs (PSTH = peristimulus-time histogram) from a computer. We sequentially presented the 10 digitally-stored and energy-matched (on the basis of root-mean-square values) natural composites (Fig. 2) at a rate of 1/s. This composite series was played 10 times at each stimulus level (50, 60, 70, 80, and 90 dB SPL) and the neuron's response to each of the composites was measured as the number of spikes minus spontaneous activity in a 20-ms window around the peak response. The "best composite" was determined by summing the neuron's responses over five stimulus levels. Subsequent testing of the neuron's response selectivities was carried out using the best composite at its best amplitude. Depending on the particular best composite and/or the duration of the neuronal response, spike numbers (spontaneous activity subtracted) were measured using either a 100 or 200-ms time window. The best composite (AB) and its individual syllables (A and B) were presented separately (200 trials each, repetition rate = 1/s) to determine the neuron's response ratio in percent, i.e., the response to the original composite divided by the sum of the responses to the individual parts and the quotient multiplied by 100. To examine the effect of temporal order on the neuron's response selectivity, the original composite was played backwards, reversed in order (BA), and/or a silent period was inserted between the two syllables of the composite. The responses to these manipulations were compared to the neuron's response to the original composite. Also, interactions between spectral components of composites were studied by filtering the syllables. Filtered syllables were presented both separately (A or B) and re-combined (AB) to determine the neuron's response ratio.

Syntax denotes a rule system that allows one to predict the sequencing of communication signals. Despite its significance for both, human speech processing and animal acoustic communication, the representation of syntactic structure in the mammalian brain has not been studied electrophysiologically at the single-unit level. In the search for a neuronal correlate for syntax we used playback of natural and temporally destructured complex species-specific communication calls - so-called composites - while recording extracellularly from neurons in a physiologically well-defined area (the FM-FM area) of the mustached bat's auditory cortex. Even-though this area is known to be involved in the processing of target distance information for echolocation, we found that units in the FM-FM area were highly responsive to composites. Further, responses of about 50% of all neurons studied were strongly affected by manipulation in the time-domain of the natural composite structure (e.g. by introducing silent intervals within a composite). The finding that a substantial fraction of FM-FM area neurons showed either facilitative or suppressive inter-syllable interactions during composite communication call processing lends support to the hypothesis that syntax processing in mammals occurs at least at the single level of the non-primary auditory cortex.

Table 1. Summary of the temporal combination sensitivity of FM-FM neuron subtypes (FM_1 - FM_n) for composite calls

Response type	FM_1 - FM_2	FM_1 - FM_3	FM_1 - FM_4	ΣFM_1 - FM_n
Facilitation	8%	42%	11%	21%
Suppression	31%	19%	40%	30%
No change	56%	14%	37%	36%
No response	6%	25%	11%	14%
n =	36	36	35	107

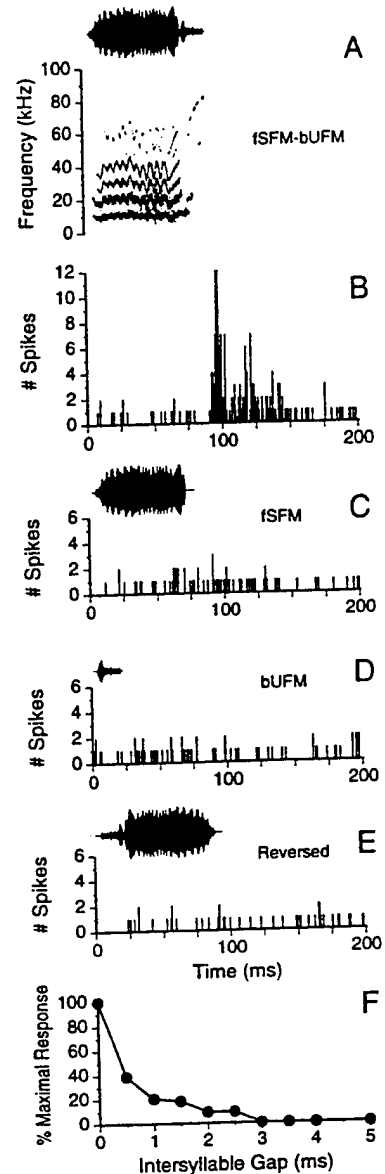
Figure 1. A Oscillogram and sonagram of composite #5 (fSFM-bUFM), the best composite for unit #102 (FM_1 - FM_3 , BD = 8.1 ms). B PSTH shows unit's robust response to the original composite (fSFM-bUFM; response ratio = 1108%). C unit almost failed to respond to the first syllable (fSFM). D Unit nearly failed to respond to the second syllable (bUFM). E No response to playback of the reversed composite. F Unit's response decreased dramatically and eventually ceased when a silent period ≥ 0.5 ms was inserted between the two components of composite #5.

Conclusions

In the mustached bat, a heterogeneous set of neurons responsive to composite communication calls is embedded in a mapped representation of echolocation pulse-echo delays. This heterogeneity is evident only when different types of species-specific communication calls are used as experimental acoustic stimuli. Results from this experiment provide some of the first evidence for processing of syntax in communication sounds at the single cell level within the mammalian auditory cortex.

Project IC: Functional MRI of the auditory cortex in mustached bats

Dr. Kanwal's laboratory in collaboration with Dr. Pekar's NMR laboratory has succeeded in imaging the brain of unanesthetized bats. This is the first example of obtaining high resolution structural MR images from an awake animal. The images obtained from these studies are presented on the following pages. Figure 1 is a sagittal view of the bat's brain showing the location of the structural images of coronal slices shown in Figures 2 to 4. Inset shows a diagrammatic view of the mustached bat's forebrain with different auditory cortical areas. Figure 5 is a FFT analysis to show that sounds



produced by the magnet during imaging have predominant frequencies below the hearing range of bats. All of these images were obtained with a modified Fluorine surface coil provided by Bruker. The coil was tuned to 300 MHz for proton imaging.

Conclusions

From our results obtained thus far we have shown that it is possible to obtain both structural and functional NMR images from unanesthetized animals. This is critical for studies on the neurobiological basis of cognition where cortical activation is necessary. We are now poised to obtain useful new data by presenting various kinds of auditory stimuli.

Abbreviations: Ac, auditory cortex; Cb, cerebellum; FAC, frontal auditory cortex; IC, inferior colliculus; Sp, Spinal cord.

Project 2 : Music perception in humans: acoustics, psychophysics and neurophysiology.

Early psychophysical studies on music perception in Dr. Kanwal's laboratory have yielded interesting data (Stoltz et al., 1997). This independent though related line of research is being pursued in parallel with other studies. Music is the combination of complex and pleasant vocal/instrumental sounds or tones consisting of rhythm, melody and harmony. Music can facilitate all biological drives and motivation and generate states of relaxation and ecstasy which play an important role in creating a sense of well being (Machlis, 1984). The underlying neural basis of these effects, however, is largely unexplored.

Music perception requires integrity of sensory-motor mechanisms for audition, speech and language processes. This includes involvement of fronto-parietal-temporal association cortical regions, and limbic system-hypothalamic brainstem areas. These areas participate in the genesis of responses like serenity and ecstasy and are involved in visceral, autonomic, endocrine and behavioral activities as well. In addition, recent imaging studies show that the auditory cortex and inferior colliculus, two important auditory structures, show the highest amounts of activity based on blood flow and oxygen utilization data (Sakurada et al., 1978; Sokoloff, 1981). Our EEG studies will be done in consultation with Dr. Plotkin in the Dept. of Neurology and for equipment usage we hope to collaborate with either Dr. Kay (Neuroscan) also in the Dept. of Neurology or Dr. Bavalier, another faculty member of the Institute.

The long-term goal is to initiate a series of studies that will revitalize research in the area of music perception and provide us with a new understanding of some of its neurophysiological effects. The time is ripe to take a fresh look at this complex cognitive ability of humans. The development of new non-invasive technologies for computerized digitization and analysis of sounds, high resolution EEG, and functional MRI allow one to identify and study many transient acoustical and neural events for the first time. As a spin-off, some of these events may also turn out to be important markers for early detection of cognitive deficits resulting from neurological trauma and disorders such as Alzheimer's disease.

Project 2A: Effect of music presentation on a tactile pattern matching task in humans.

Music is known to improve motor performance in humans (Furman, 1996) but the neural basis of its impact on cognition and sensorimotor performance is unclear. As a first step towards delineating the effect of musical versus non-musical sounds on sensorimotor performance, we presented three types of sound stimuli - music, white noise, and speech separately to each ear. Sixteen subjects were asked to examine four Braille characters with an index finger and indicate the position of the two identical ones in a line (Kennison and McFarland, 1989). Each trial consisted of 10 lines. Each presentation lasted for 5 minutes, and trials were administered approximately 2 minutes after onset of the sound presented and lasted for up to 3 minutes. Post-presentation trials were also conducted during a silent period after each presentation. Performance scores were based on the number of correct matches per trial. Latency was

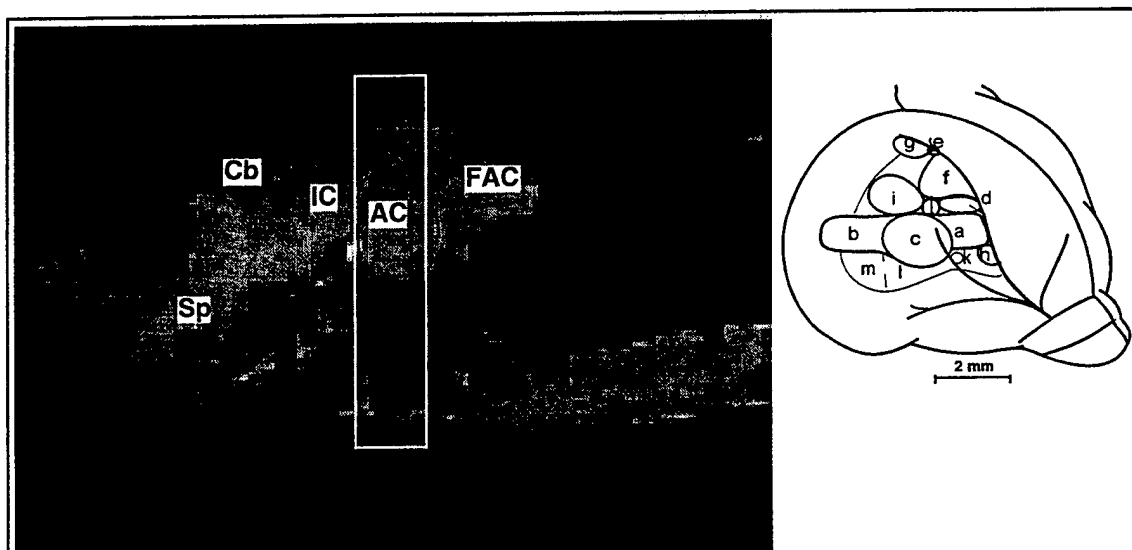


Figure 1. Sagittal view of the bat's head (Gradient Echo, TE=5 ms)

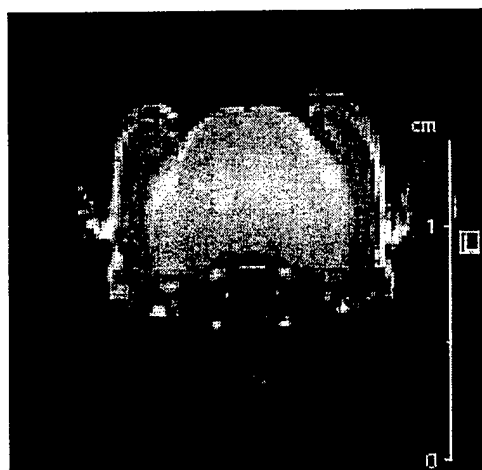


Figure 2. (Spin Echo, TE=10 ms)

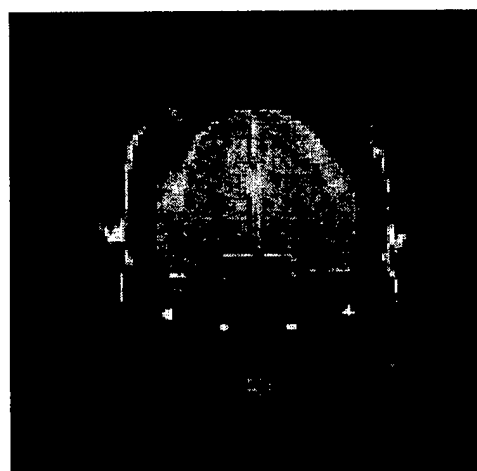


Figure 3. (Spin Echo, TE=40 ms)

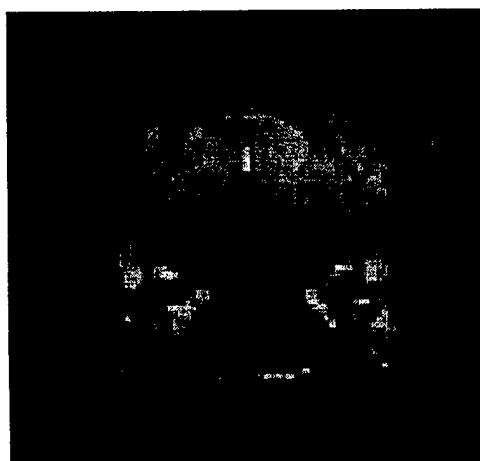


Figure 4. (Gradient Echo, TE=5 ms)

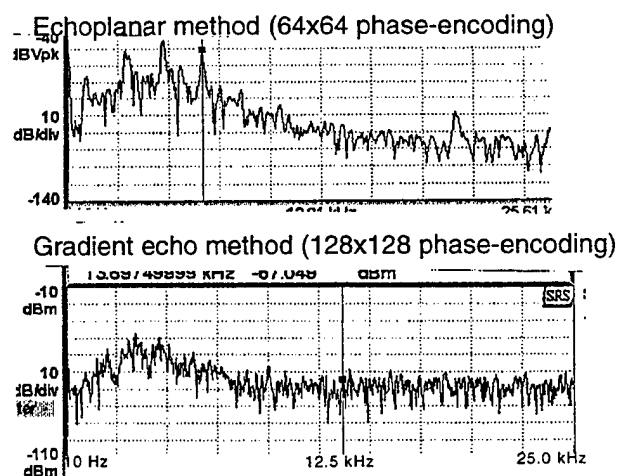


Figure 5. FFT analysis of MRI acoustic noise

based on the time taken to complete a single trial within the allocated time. All scores were normalized with performance/latency scores for an initial trial during silence. Results showed a 40% to 60% increase in the average performance levels for pattern matching for trials conducted during and post sound presentation (see figures 1 to 3). Performance scores on post-presentation trials were up to 15% better than performance scores for trials during sound presentation regardless of the nature of the sound. For music and noise, this affect is due mainly to the presentation of sound to the ear ipsilateral to the hand performing the task. Both music and speech showed a lateralized effect on performance levels during sound presentation. Presentation of music to the side contralateral to the hand performing the task resulted in improved performance, whereas for speech the ipsilateral side was more effective.

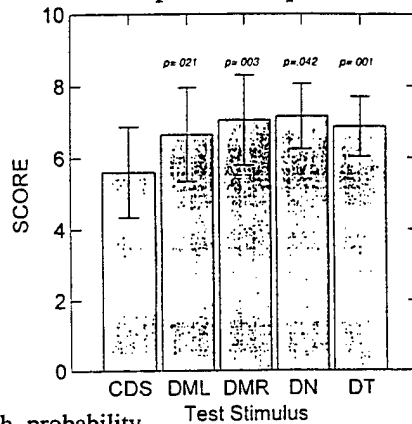
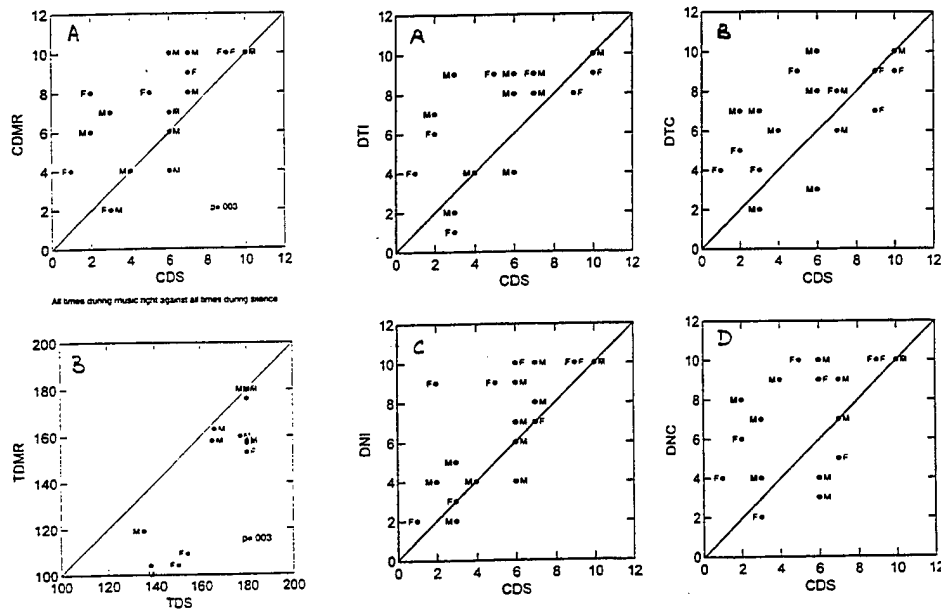


Figure 1. Score of different stimuli with probability values compared to that for silence.



Abbreviations: CDS, correct scores during silence; DML, during music presented on left side; DMR, during music presented on right side; DT, while listening to a speech (talking); DN, while listening to noise presented to both ears; TDS, time to complete test during silence; TDMR, time taken to complete test while listening to music presented at the right year.

Conclusions

These results suggest that auditory processing primes nonauditory neural circuits involved in a pattern matching task and this improvement continues beyond the period of sound exposure. It also appears that monaural presentation of music is sufficient to improve performance on a tactile pattern matching task in humans.

Project 2B: Effect of imagined and presented music on P300 evoked response in humans

The effect of music was studied on the P 300 auditory evoked response in 2 normal healthy young (age 21 years) volunteers. In 10 sessions lasting from 2-3 hours, 64 recordings were made. A basal pattern was established in 41 responses during silence. This was followed by responses to an imagined silent singing of a favorite melody of the subject in 11 recordings and listening to a tape of a preferred song, each for five minutes, preceding the recording of the evoked response, in 12 recordings of P300.

Long Latency P300 ACER

The equipment used was Nicolet P 300 Cognitive Response software on Nicolet Spirit recorder of Nicolet Spirit Instrument Corporation and an auditory transducer TIP-300 tubal insert phone. Two distinguishable tones were presented in random sequence (the "odd-ball" paradigm), using TIP-300 tubal insert phone. The frequent tone (500 Hz) was presented 80% of the time interspersed with a rare tone (2 kHz) 20% of the time. The tone bursts triggered an averager. The plateau portion of signal was 20 Hz. Two channels of the recorder were used for obtaining P300 responses. Trace 1 of each channel recorded averaged responses to frequent tone stimuli and trace 2 recorded the averaged responses to rare stimuli. The subjects were asked to silently count and concentrate on the rare tone stimuli, while sitting comfortably on a reclining chair with the head resting on a pillow, in a partially dark room, with the eyes closed. Responses to a total of 300 stimuli were averaged (both frequent and rare stimuli included). The averaged long latency responses to 249 frequent stimuli are shown in overlapped trace 5-7 of figure 1. The overlapped traces 6 and 8 depict averaged 51 recordings of P300 produced by rare tones interspersed between the frequent stimuli. The playing of music and imagined singing of a favorite melody produced an average decrease of 60 ms in the latency of long latency cognitive evoked responses (see table below). The reduction in the P300 responses may be indicative of facilitation of cognitive neural processes of auditory signals by music.

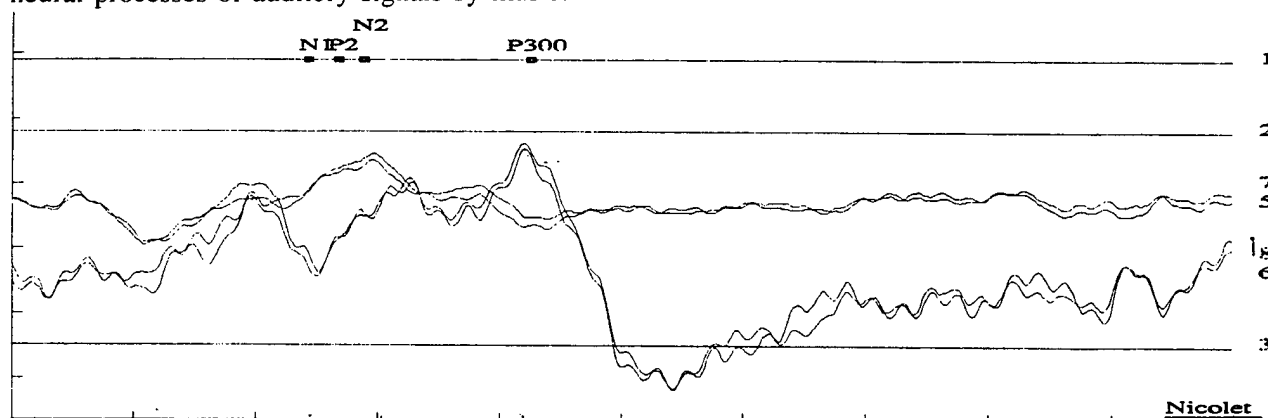


Figure 1. Traces 5 and 7 show the N1 P2 recording of averaged responses to 249 frequent tone stimuli delivered to left ear of 21 Yr. old male subject, JE, obtained from Cz-A2 leads with Fpz as a common electrode. The P 300 in this record (traces 6 and 8) had a latency of 318 msec. The time calibration on the ordinate is 75 msec/div.

Evoked response wave	N1	P2	N2	P300
Normal latency in msec.	111.6	188.4	265.2	357.4
Shift in msec. from normal (Mean \pm S.D.) * = decrease				
Thinking of melody	1.12 \pm 11.1	1.4 \pm 25.1	17.4 \pm 45.5	*21.2 \pm 18.2
Listening to music	1.6 \pm 39.6	*18.5 \pm 32.8	*47.6 \pm 41.7	*59 \pm 35.2

Conclusions

We conclude that P300 is a good neurophysiological indicator of changes in auditory cognitive processes associated with both real and imagined music perception. We hope that it will be possible to use this as a temporal marker during simultaneous studies of fMRI and evoked potentials to localize brain areas associated with music perception.

Future Directions

Data obtained from the above described studies on communication sound processing will allow Dr. Kanwal's group to explore novel mechanisms and formulate new principles of auditory processing, especially at the cortical level. New methods to be developed over the next 2 to 3 years include telemetry and multi-site single unit recording from awake bats and, in collaboration with Dr. Wu, optical imaging of cortical activity. For human studies, we will develop fMRI protocols for examining speech and music processing that will be based on principles of communication sound processing learnt from animal studies. This together with similar studies on other species will provide a test for the generality of the principles formulated. The long-term goal is to elucidate both similarities and differences in communicative auditory processing among animals and humans.

Selected References

- Bhaskar, P. A. (1994) Effect of music on the human brain alpha rhythm. *J. Assoc. Physicians India*. 42(4),319-323,.
- Cheng, M. and Peng, J. (1997) Reciprocal talk between the auditory thalamus and the hypothalamus: an antidromic study. *Neuroreport* 8:653-657P.
- Chomsky, N. (1957) *Syntactic structures* (Mouton, The Hague).
- Ehret, G. & Haack, B. (1981) *Naturwissenschaften* 68, 208-209.
- Esser, K-H., Condon, C.J., Suga, N., and Kanwal, J.S. (1997) Syntax processing by auditory cortical neurons in the FM-FM area of the mustached bat, *Pteronotus parnellii*. *PNAS*, in press.
- Kamada K, Saguer M, Möller M, Wicklow K, Kartenhäuser M, Kober H, Vieth J. Functional and Metabolic Analysis of Cerebral Ischemia using MEG and Proton MR Spectroscopy. *Annals of Neurology* (in press).
- Kamada K, Möller M, Saguer M, Kassubek J, Kaltenhäuser M, Kober H, Überall M, Lauffer H, Wenzel D, Vieth J. Localization Analysis of Neuronal Activities in Benign Rolandic Epilepsy using Magnetoencephalography. *J Neurol Sci* (in press).
- Kamada K, Houkin K, Iwasaki Y, Abe H, Kashiwaba T. Metabolic and neurological patterns in chronic cerebral infarction: a single-voxel ¹H-MR spectroscopy study. *Neuroradiology* 39: 560-565, 1997.
- Kamada K, Houkin K, Hida K, Matsuzawa H, Iwasaki Y, Abe H, Nakada T: Localized proton spectroscopy of focal brain pathology in humans: Significant effects of edema on spin-spin relaxation time. *Magn Reson Med* 31:537-540, 1994.
- Kanwal, J.S., Matsumura, S., Ohlemiller, K., and Suga, N. (1994) "Analysis of acoustic elements and syntax in communication sounds emitted by mustached bats." *J. Acoust. Soc. Am.*, 96 :1229-1254
- Kanwal, J.S. (1997) Charting Speech with Bats but not Maps. *Brain Behav. Sci.* (in press).
- Kanwal, J.S., and Suga, N. (1997) Excitatory, facilitatory and inhibitory frequency tuning of combination-sensitive neurons in the auditory cortex of the mustached bat. *J. Neurophysiol.* (in press).
- Kanwal, J.S., and Finger, T.E. (1997) Parallel medullary gustatospinal pathways in a catfish: possible neural substrates for taste-mediated food search. *J. Neurosci.* (in press).
- Kennison, R.F. and McFarland, R.A. (1989) Music affects learning of a Braille-like task by sighted subjects. *Percept. Mot. Skills* 69:923-929
- Ohlemiller, K.K., Kanwal, J.S., and Suga, N. (1996) Temporal facilitation for call processing in the FM-FM and CF/CF areas of the auditory cortex of the mustached bat. *Neuroreport* 7:1749-1755.
- Peng, J. and Yang C. (1995) Effects of the neurotransmitters and amino acids on the electric activities of the PPN: POA/AHA and LH release from the hypophysis. *J. Neuroscience (China)* 6:186-194.
- Stoltz, B., Chhina, G.S. and Kanwal, J.S. (1997) Monaural presentation of music improves performance on a tactile pattern matching task in humans. *Soc. for Neuroscience Abstr.*

JAMES J. PEKAR, Ph.D.

The Neurobiological Magnetic Resonance Laboratory, dedicated to the application of nuclear magnetic resonance to the study of brain anatomy, physiology, and function, made considerable progress in its second year, both in the development of advanced biomedical engineering technology for brain imaging, and in the application of this technology to questions in neurobiology.

Functional MRI of the brain reveals brain regions subserving a variety of tasks, using deoxyhemoglobin as an endogenous MRI contrast agent reporting on hyperemia concomitant to neural activation. One key to the success of human fMRI is the ability to perform longitudinal studies within the same individual. Such serial studies allow for evaluation of test-retest robustness, as well as investigation of plastic processes including development, learning, and the effects of therapy and therapeutics in cases of pathology. However, while serial studies are of crucial importance to human fMRI, they have not yet been applied to animal models: The application of functional MRI to animal models has generally been performed using acute animal preparations, which rule out studies lasting longer than a single MRI examination. In contrast, we have pioneered the use of non-acute animal preparations for fMRI studies: We are using non-acute animal preparations to pursue functional MRI studies of somatosensory stimulation in rats, visual stimulation in cats, and auditory stimulation in bats.

Development of Laboratory

The greatest challenge of the last year was that our primary resource, our seven Tesla superconducting magnet, was flawed: A poor superconducting join resulted in a magnetic field which, rather than being stable over time, drifted down at a rate of one Hz per minute, which made many studies impossible. We shipped the magnet back to its maker, Bruker Instruments, Inc., of Germany, who repaired it. While the repair was free, as the system was under warranty, we suffered four months of "downtime" due to absence of the magnet.

Our goal remains the development of a develop a state-of-the-art facility for magnetic resonance imaging of brain structure, physiology, and function, with outstanding spatial and temporal resolution. Following repair of our magnet, our laboratory is fully operational. Recent progress includes development of pulse sequences for rapid three-dimensional imaging, as well as software for homogeneity optimization via field-mapping; this last project was conducted in collaboration with Dr. Peter Jezzard of the National Institutes of Health.

Radio-frequency hardware is essential for high-sensitivity imaging. We have contracted for custom-built quadrature head coils, sized for mice and rats, from a contractor who excels in this area; delivery of this new hardware is expected in September of 1997.

The addition of five Silicon Graphics "O2" workstations to the laboratory computer network, together with discounted purchase of five additional licenses of "ParaVision" NMR software from Bruker Instruments, gives all lab personnel the ability to process and visualize data from their own "desktops."

We also are developing a "physiological infrastructure" for MRI in live subjects; this project has three goals: (1) To apply biomedical engineering principles to develop apparatus for the monitoring of physiological parameters (e.g., temperature, respiration, electrocardiogram) during MRI scanning; (2) To develop means of providing multimodal sensory stimulation to animals while they are in the seven Tesla magnet; (3) To synchronize MRI acquisitions and sensory stimuli to the subject's respiration.

We have successfully implemented non-invasive monitoring of temperature, respiration, electrocardiogram, and expired CO₂. We are using a LabView (National Instruments, Austin, TX) system sampling to monitor and record these data, and to derive “triggers” for our MR scanner and stimulation devices.

Temperature is monitored using a fluoroptic thermometer (Luxtron Instruments, Inc.); ECG leads (pin type, Grass Instruments, Astro-Med, Inc., West Warwick, RI) were placed in three positions (forepaws and left rear leg); a small coil (36 gauge, approx. 40 turns, 2 cm dia.) was taped to the animal’s abdomen to provide a respiratory signal from the moving abdomen (this takes advantage of the fact that a coil moving through an inhomogeneous magnetic field induces a current in the wire).

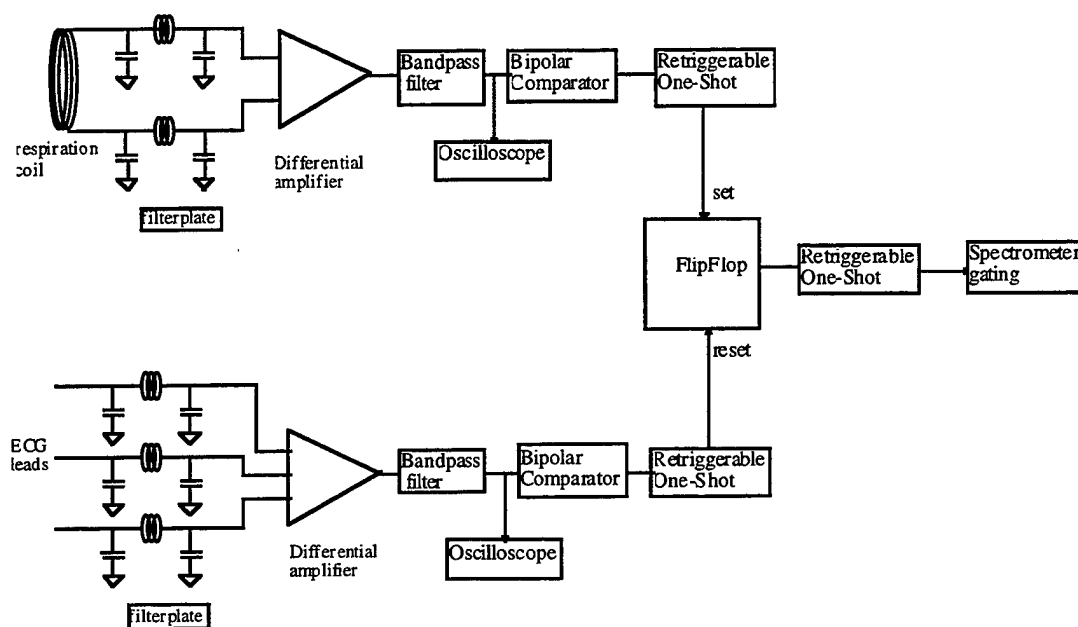


Figure 1. Circuit for combined cardiac and respiratory triggering.

Signals are processed (as shown in Figure 1) (Coulbourn Instruments, Allentown, PA) with bioamplifiers and bandpass filters. Gain and filter bandwidth may be manually adjusted to obtain a reasonably clean signal. At this point, the signals may be tapped off and sent to an oscilloscope for monitoring. For combined respiratory and cardiac gating, the respiration trigger is sent through a one-shot, then into the “set” input of a flip/flop. The ECG trigger is also sent through a one-shot, then into the “reset” input of the flip/flop. The output is then sent to a third one-shot and on to the spectrometer trigger. In this manner, overall triggering first waits for a respiratory signal (about once per second for a rat), then waits for the next ECG trigger (about 6 times per second for a rat).

Using these methods, images may be obtained which combine remarkably high spatial resolution with freedom from motion-induced artifacts. A sample image is shown in Figure 2, which depicts a horizontal plane in the head of a freely-breathing rat. The in-plane resolution is 74 microns.

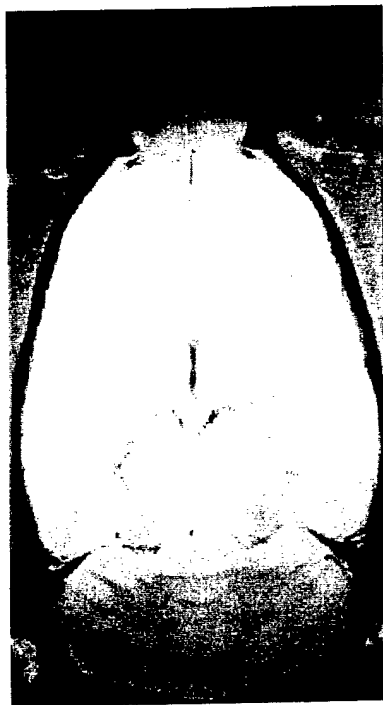


Figure 2. Axial image of rat.

Our physiological monitoring setup not only allows us to continuously evaluate the physiological state of the animal, but also enables us to gate the spectrometer to the animal's natural respiratory and cardiac cycles. We see very little motional artifacts in the high resolution images which have been gated to the animal's respiration. Careful choice of delay times enables us to observe substantial structural details. Information on the location of the microvasculature may provide valuable insight into the understanding of functional MRI data.

Because these techniques are minimally invasive, the amount of stress placed on the animal is greatly reduced. This allows repeated scanning of the animal on separate days, enabling the possibility of serial studies to study phenomena such as experience dependent plasticity, or the timecourse of CNS injury.

Project 1: Functional Brain Mapping

This area of our research activities uses magnetic resonance imaging as a non-invasive probe for brain function, by exploiting deoxyhemoglobin as an endogenous contrast agent. We desire to use MRI to study cortical representations of a variety sensory modalities, and to study plasticity of these cortical representations. Our collaborators include Prof. Josef Rauschecker of GICCS, and Dr. Biao Tian of his laboratory; Prof. Jag Kanwal of GICCS, and Dr. Kyousuke Kamada of his laboratory; Prof. Jian-Young Wu of GICCS; Prof. Guoying Liu of GICCS; Dr. Dov Malonek of the Weitzmann Institute; and Dr. Peter Jezzard of the National Institutes of Health.

Project 1a: Visual Cortex

Our goals were: (1) To map the hierarchical cortical representations of visual stimuli using functional magnetic resonance imaging in cats; (2) to compare these maps with maps from intrinsic optical imaging; (3) to use the non-invasive functional MRI mapping to study developmental plasticity in the visual cortex. These studies were performed in collaboration with the laboratory of Dr. Josef Rauschecker.

Figures 3 and 4 show sagittal and coronal images of the brain of a kitten, respectively. Figure 5 shows a single-pixel brain MRI time course well-correlated to visual stimulation presented via rear-projection video screen. This time course demonstrates that we are now obtaining MR data which reports on neural activity induced by our sensory stimuli. Studies using a variety of visual stimuli in order to yield maps of hierarchical cortical representations are now being planned.

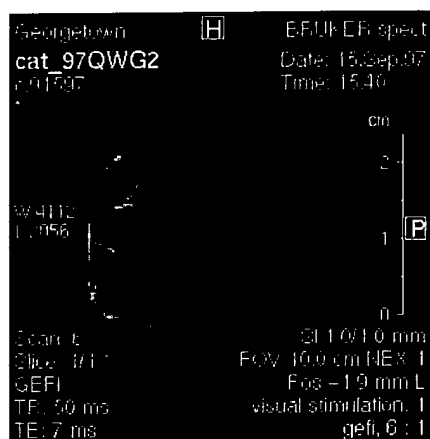


Figure 3. Sagittal image of cat.

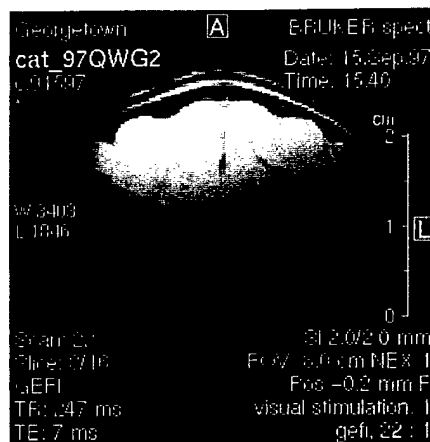
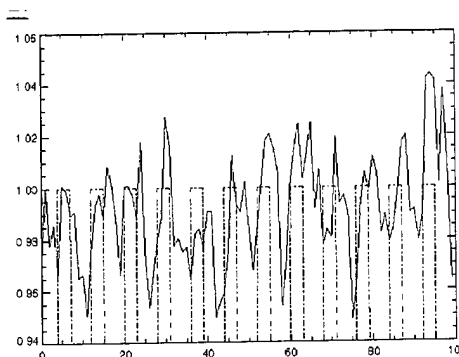


Figure 4. Coronal image of cat.

Figure 5. Functional MRI time course from single pixel in brain of a cat subjected to intermittent visual stimulation during MRI scanning. Dashed line shows visual stimuli; solid line shows MRI pixel intensity.



Project 1b: Auditory Cortex

Our goals were: (1) To map the auditory cortex of *pteronotus parnellii* (the "mustached bat") using functional magnetic resonance imaging; (2) to compare these maps with data from single-unit electrophysiological recordings; (3) to use the non-invasive functional MRI mapping to address a variety of neurobiological questions about auditory processing in the bat. These studies were performed in collaboration with the laboratory of Dr. Jag Kanwal.

There are two special characteristics of *pteronotus parnellii* which make it an exciting candidate for functional brain mapping using magnetic resonance imaging: Firstly, sedation is not necessary in these animals, as they are in general not stressed by immobilization. Hence, functional MRI of awake alert animals is possible. Secondly, as these animal's hearing starts at about seven kilohertz, they are essentially "deaf" to the loud one kilohertz sounds made by the MRI scanner during echo planar imaging. Both of these characteristics are unique.

Figure 6 shows a coronal image of the head of a bat. Functional studies, using computer-generated ultrasonic stimuli, have recently been initiated. We are especially excited by the opportunity to perform functional MRI at seven Tesla in alert awake animals which is provided by the use of *pteronotus parnellii*.

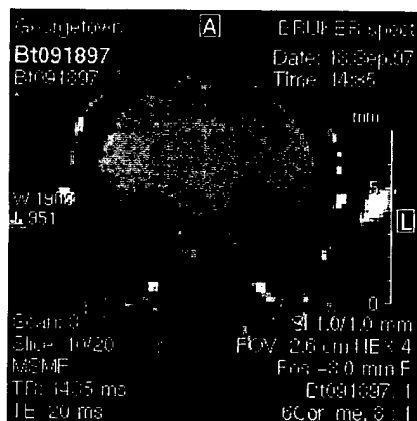


Figure 6. Coronal image of *pteronotus parnellii* (moustached bat).

Project 1c: Somatosensory Cortex

Our goals were: (1) To map the somatosensory cortex in rodents using functional magnetic resonance imaging; (2) to use the non-invasive functional MRI mapping to address a variety of neurobiological questions about auditory processing in the bat.

Figure 7 shows functional imaging data from rat brain obtained using an experimental protocol consisting of paw-stroking. The figure shows both an activation map (part A), and a timecourse (part B) of the MRI signal in a representative “activated” pixel. The imaging data were acquired using Echo Planar Imaging (and shows some geometric distortion, a characteristic of that fast imaging method).

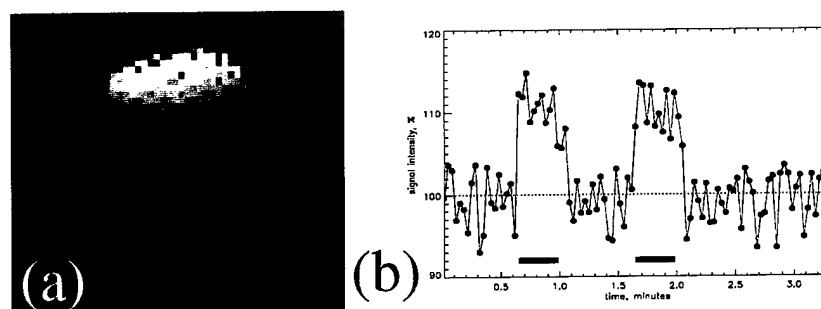


Figure 7. Functional MRI data from hind paw stroking. (a) Coronal image of rat brain, showing activated regions (in red) due to stroking of right hind paw (the geometric distortion is characteristic of Echo Planar Imaging). The coronal image is depicted using the radiological convention (the left side of the brain appears on the right side of the image). (b) Time course of a pixel in the activated region, showing stimulation periods (black bars) and corresponding intensity increases.

Project 2: Magnetic Resonance Outcome Measures in Rodent Models of Central Nervous System Injury

This area of our research activities uses multi-modal magnetic resonance imaging to perform “*in vivo* histology” by assessing changes in anatomy and physiology following injury. Our collaborators include Prof. Alan Faden and Drs. Gerard Fox and Susan Knoblach of his laboratory. The ability to exploit our minimally-invasive imaging methods to pursue serial studies in order to follow the course of secondary injury over time in individual subjects promises to give great insight into the mechanisms of neuroinjury, and to provide a window into mechanisms of neuroprotection.

Project 2a: Traumatic Brain Injury

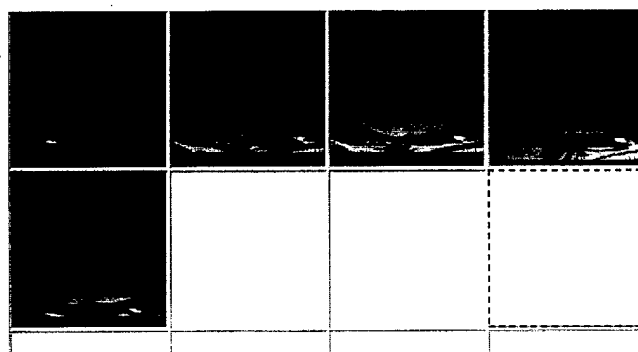
Our goals were: (1) To develop multi-modal magnetic resonance imaging outcome measures for rodent models of CNS injury; (2) to compare these MRI outcome measures with histological and behavioral outcome measures.

Some investigators working with animal models of brain injury have applied MRI for very specific applications such as the evaluation of collagenase-induced hemorrhage and fluid-percussion induced traumatic brain injury (TBI). Techniques involving standard MRI using T2 weighting have been shown to be fairly insensitive, however, to acute (within 90 mins. post - TBI) changes following experimental TBI. Therefore, investigators have utilized diffusion weighted imaging (DWI), which has been determined more sensitive for the early diagnosis of ischemia and for the early detection of pathological changes following TBI. Moreover, studies using DWI pulse sequences have demonstrated the ability to discriminate between traumatized and ischemic tissue.

The feasibility of diffusion MRI, however, to predict lesion extent and other lesion characteristics related to outcome at non-acute time points has not yet been studied. Furthermore, the verification and correlation of actual cell and tissue injury to diffusion or high resolution MRI scans has yet to be reported. The purpose of our study was, therefore, to evaluate for the first time in vivo the temporal evolution of MR signal changes using isotropic diffusion and high-resolution spin-echo pulse sequences at 7 Tesla in rats subjected to fluid-percussion induced TBI. Additionally, the study compares MR signal changes to histopathological sections obtained from TBI animals and neurological evaluations of functional deficit.

Scans obtained using spin-echo pulse sequences displayed remarkable high-resolution (74 μm) in control and TBI animals. Changes in MR signal were evident in these T2 weighted and proton density weighted scans as increases and decreases in pixel intensity. High resolution scans revealed regions of hyperintensity suggesting cytotoxic and vasogenic forms of edema while hypointense regions were thought due to hemorrhage and mechanical disruption of tissue. Regions displaying hyperintensities had maximal increases, at the 2 week time point (n= 6); see figure 8 for sample data showing the same coronal slice imaged over a two-week period. Regions exhibiting hypointensities appeared generally consistent in size over the two week period. Most injured areas were seen in the ipsilateral hemisphere and included cortex, hippocampus, thalamus, and striatum. Occasionally hyperintensities were seen in contralateral hippocampus and cortex. Injury was particularly prominent at the boundaries between the cortex, the hippocampal formation, and the white matter tracts. Hyperintensities were generally in the hippocampal formation at 24 hr while hemorrhage manifested itself primarily in cortex throughout the two week period. Injury was rarely seen at the actual site of the craniotomy. Total lesioned area (i.e., hyperintense plus hypointense areas) averaged $6 \pm 1.5\%$. Greatest region of injury seen in slices 2 and 3, i.e. at the level of the thalamus and at the level of the hippocampus. Qualitative inspection of MR scans revealed a number of neuroanatomical changes indicating injury in the TBI animals. Among these included cavitation and blood accumulation (hypointense regions) in tissue resulting in presumably what one might call an "exit wound" seen distal to the site of craniotomy. These sort of changes were especially evident in pilot horizontal images. The location of this injury is consistent with the expected site of injury based on previous histopathological data.

Figure 8. Coronal images of the brain of a rat which underwent a fluid-percussion model of traumatic brain injury. The five images were acquired (left to right, top to bottom): Before injury; 1-2 hours post injury; 3-4 hours post injury; 24 hours post injury; and 2 weeks post injury.



Animals showed a consistent improvement in neurological function over the two week period. At 24 hours animals were moderately to severely impaired (median composite score = 15). At one week animals showed recovery of function (median composite score = 20) that gradually improved even further by two weeks (median composite score = 26). The results of the neurological scoring at these time points is consistent with the moderate level of TBI injury that was induced as seen in other experiments using the same model.

JOSEF P. RAUSCHECKER, Ph.D., D.Sc.

Dr. Rauschecker's laboratory focuses on the understanding of higher auditory processing. While the ultimate goal is to reveal the mechanisms of human speech and language, it is important to pursue neurobiological studies in animal models, because studies in humans can with few exceptions only be performed noninvasively. The availability of modern imaging techniques has had an enormous impact on the design of such studies, because these techniques form a direct link between animal and human work. Finally, the enormous capacity of the cerebral cortex to reorganize itself after peripheral injury, deprivation, or during learning merits particular attention. This becomes especially relevant as we consider cortical plasticity in centrally deaf or blind patients, during tinnitus, or in patients with Alzheimer's disease or stroke.

Project 1: Cortical Mechanisms of Auditory Processing in Primates

Project 1A: Processing of Complex Sounds in Nonprimary Auditory Cortex

Dr. Rauschecker's group continues to explore the functional organization of nonprimary auditory cortex in macaque monkeys. The analysis of single unit responses to complex auditory stimuli in different cortical fields is the focus of these studies. In particular, monkey vocalizations were used for stimulation, as they resemble human speech sounds in great detail. The vocalizations were decomposed into their constituent elements, and temporal and/or spectral combination-sensitivity for these elements was tested. It was found that non-linear summation in the frequency and time domain is an important mechanism for response selectivity in higher areas, such as the lateral belt. By contrast, neurons in primary auditory cortex A1, if they respond selectively to a particular monkey call, do so simply on the basis of their frequency selectivity, i.e. they show linear summation (Fig. 1). As had been shown previously, reversing the temporal order of a call abolishes the response in many lateral belt neurons, whereas it does so less often in A1. Thus, auditory cortical areas are organized into a clear processing hierarchy. It can be inferred that the phonological decoding of speech sounds in humans is based on similar neural mechanisms as those in nonprimary auditory cortex of primates (Rauschecker, 1997).

Project 1B: Neuroanatomical Connectivity of Auditory Cortex

The processing hierarchies within primate auditory cortex were also investigated with neuroanatomical tracer studies. During the past year a major study was completed and published, in which the projections from auditory thalamus to the auditory cortical areas on the supratemporal plane were explored (Rauschecker et al., 1997). It was found that the principal relay nucleus of the auditory thalamus, the ventral part of the medial geniculate nucleus (MGv), projects in parallel to the primary auditory cortex (A1) as well as the rostral area (R). Lesions of A1 therefore do not disrupt the functioning of R, although they almost completely knock out responses in the caudomedial area.

In a similar approach, the laboratory (with the help of a Neuroscience graduate student, Sergei Zhenochin) now analyses the connections from thalamus to the lateral belt. Results of an injection into the middle part of the lateral belt, area ML, are shown in Fig. 2. Two major clusters of labeled cells are found, one in the MGv, another one in the supragenulate nucleus (SG). It appears, therefore, that MGv provides input to a third cortical area in addition to A1 and R. The projection from the SG is interesting too, because the SG had previously been considered mainly as a visual nucleus.

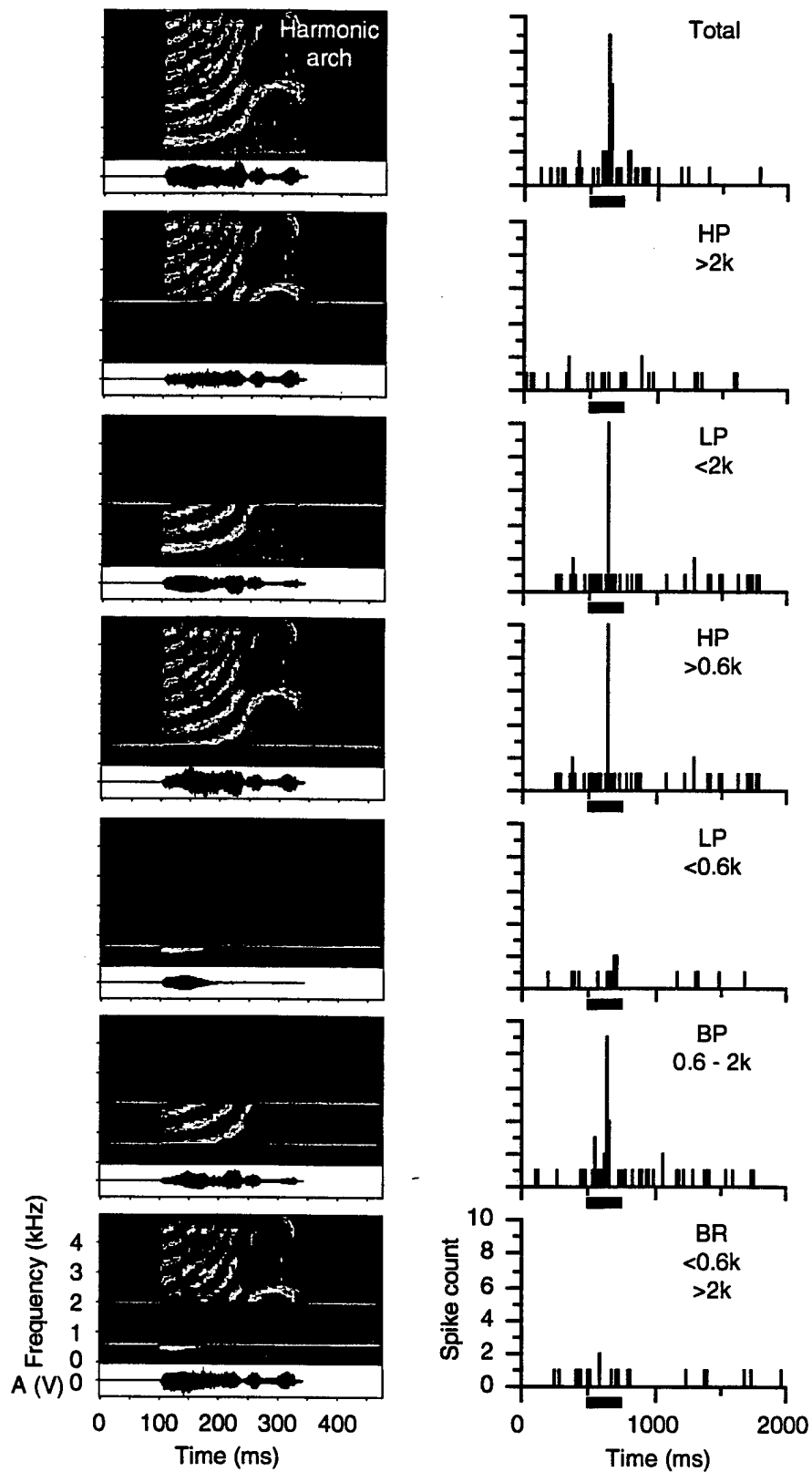
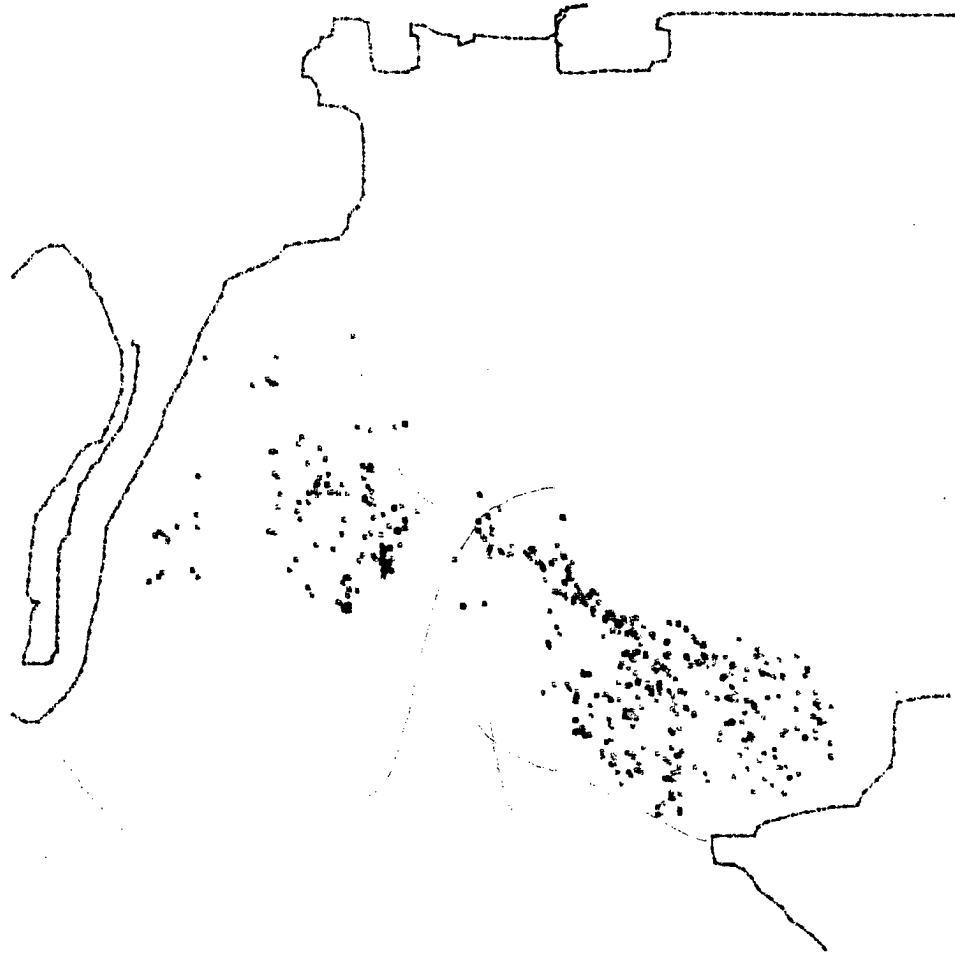


Fig.1: Spike activity of a single neuron in primary auditory cortex of a rhesus monkey in response to a monkey vocalization of a particular type ("harmonic arch") and filtered versions of that call. It can be shown that, in contrast to neurons in nonprimary auditory cortex, such as the lateral belt, selectivity of A1 neurons is solely based on frequency tuning. HP: high-pass; LP: low-pass filtering. Only a narrow segment of the frequency spectrum in the call contributes to the neuronal response, as shown by playing a bandpass filtered version of the call.

dustf239

total: 532 cells
FR : 0 c.
DY : 527 c.
FB : 5 c.



1 mm

Fig. 2: Retrogradely labeled cells in the auditory thalamus of a rhesus monkey after injection of the tracer diaminodino yellow (DY) into one of the lateral belt areas (ML). Two distinct clusters of labeled neurons are found, one in the MGv, another in the suprageniculate nucleus (see text).

Project 2: Neuroimaging of Auditory Cortex

Project 2A: Optical Imaging of Auditory Cortex in Cats

During the past year Dr. Tian has successfully completed the installation of the optical imaging system (Imager 2001, Optical Imaging Inc.) for use on cat auditory cortex. Intrinsic optical signal changes related to blood oxygenation are measured that reveal neuronal ensemble activity in the cortex at a scale of about 500 μm (Malonek and Grinvald, 1996). This gives insight into the organization of functional columns in the auditory cortex. Pilot experiments on visual cortex confirmed the known organization of orientation columns. By analogy, the organization of FM direction columns in auditory cortex is now the focus of investigation, in addition to studies using pure tones and bandpass noise by analogy to the monkey studies. All three modes of stimulation demonstrate the tonotopic organization of these auditory areas, but at the same time reveal interesting differences in the activation pattern (Fig. 3). Correlation with electrophysiological work will be needed to come to a conclusive interpretation of these results. Optical recording is also performed with the potential to extend this approach towards presurgical screening in humans as a collaboration with the Department of Neurosurgery.

Project 2B: Functional MRI of Auditory Cortex in Humans

Conceptually similar types of auditory stimuli, such as bandpass noise (BPN) pulses and frequency modulated (FM) glides, as in the animal studies on cats and monkeys, are used in human studies with functional magnetic resonance imaging (fMRI). In addition, human speech sounds ("phonemes") are used, which are composed of the same types of information-bearing elements as they are contained in subcomponents of monkey calls. Over the last year, Dr. Mark Wessinger has run a most successful program of fMRI of human auditory cortex on the new 1.5T Siemens Vision scanner at Georgetown. These results are so far probably the best data this new magnet has delivered among users of GICCS and the Dept. of Radiology. The results from BPN and FM stimuli show larger areas of activation from BPN than from pure tones. Use of phonemes ("consonant-vowel combinations") results in even larger activation that is mainly restricted to the left hemisphere (Fig. 4). The transition between non-speech and speech sounds can thus be identified in fine detail.

Project 3: Reorganization and Plasticity of Cortical Representations

Dr. Rauschecker's group is also testing the hypothesis that the central auditory system is organized into dual processing streams of a "where" and a "what" system, as in the visual and somatosensory systems. In monkeys, as stated above, electrophysiological and neuroanatomical approaches are combined, in order to test this idea (Rauschecker et al., 1997). In humans, neuroimaging techniques have been used to corroborate previous findings. In our continuing collaboration with the group of Dr. Mark Hallett at the National Institutes of Health, using positron emission tomography (PET), sound localization of "virtual auditory space" stimuli (generated by software developed at GICCS on customized hardware purchased off the DOD grant) identified a center in the right inferior parietal lobule (IPL) as specialized for auditory spatial processing. At the same time, the rostral portion of the superior temporal gyrus (STG) was deactivated, indicating involvement in auditory pattern processing (Weeks, et al., 1997) (Fig. 5).

The enormous plasticity of this system is demonstrated by the finding that the area of activation in the IP is significantly enlarged in congenitally blind people and extends far into normally visual areas (18 and 19) in the occipital lobe (Aziz-Sultan et al., 1997). In late blind individuals much less expansion is found. The recent PET data from blind humans tie in well with prior results from Dr. Rauschecker's lab on visually deprived cats (Rauschecker and Korte, 1993; Rauschecker, 1995), further bridging the gap between single unit recording in animals and brain imaging in humans.

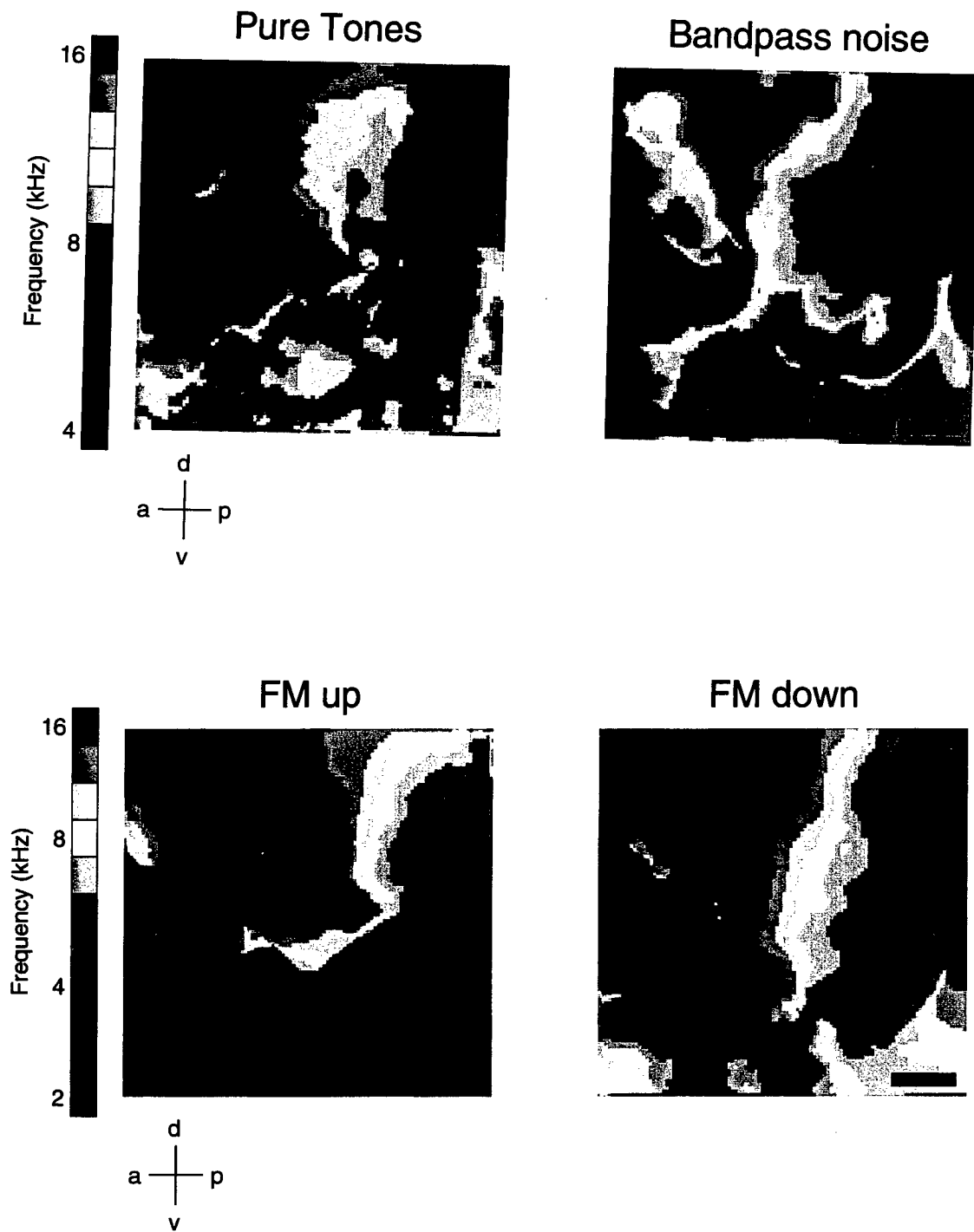
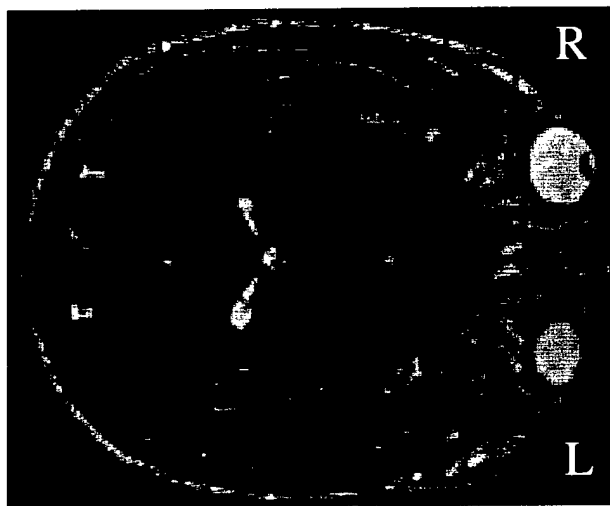
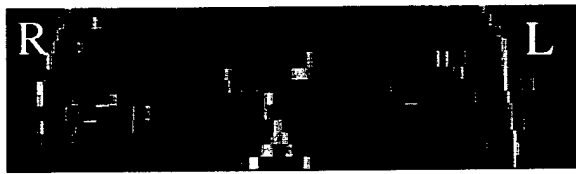
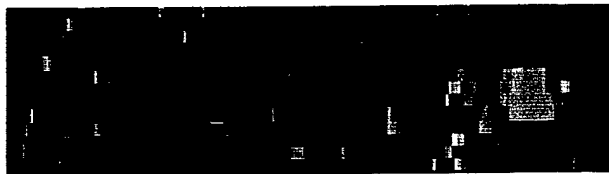


Fig. 3: Optical imaging of cat auditory cortex using different types of sound. Bandpass noise stimuli lead to more orderly activation than pure tones. FM sweeps in one direction elicit a different pattern than FM sweeps in the opposite direction. This is due to differential activation of various cortical areas (A1, A2, and AAF) by these stimuli.

Pure-Tone vs. Band-Passed Noise



- Pure-tone (PT) activation
- Band-passed noise (BPN) activation
- PT and BPN activation



Band-Passed Noise vs. Consonant-Vowel



- Band-passed noise (BPN) activation
- Consonant-vowel (CV) activation
- BPN and CV activation

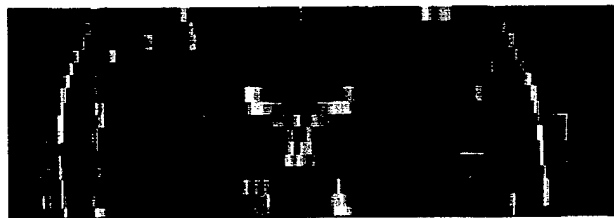
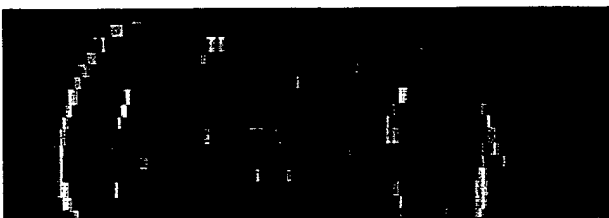


Fig. 3: Optical imaging of cat auditory cortex using different types of sound. Bandpass noise stimuli lead to more orderly activation than pure tones. FM sweeps in one direction elicit a different pattern than FM sweeps in the opposite direction. This is due to differential activation of various cortical areas (A1, A2, and AAF) by these stimuli.

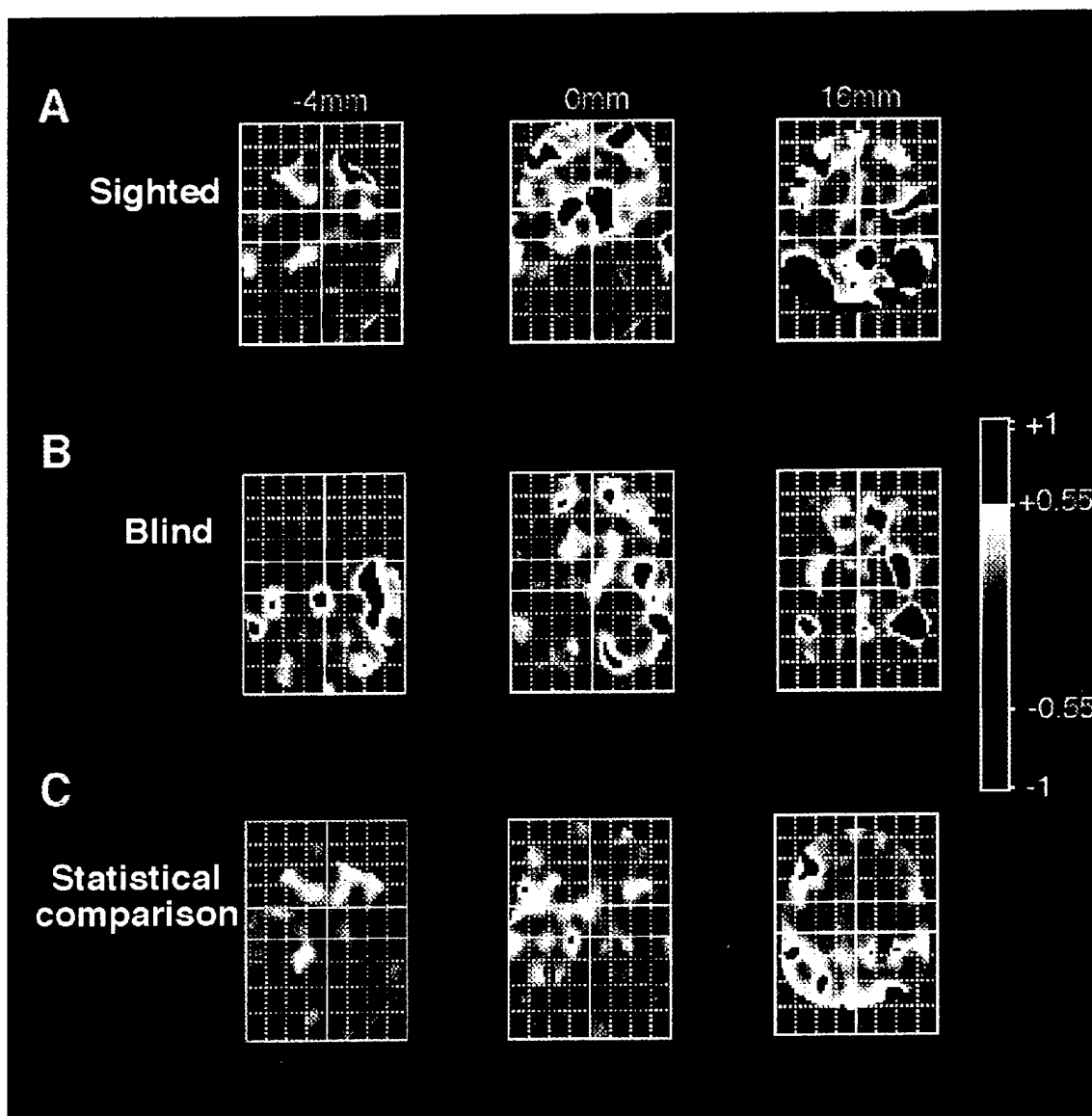


Fig. 5: Results of positron emission tomography (PET) in sighted and congenitally blind people during localization of a virtual auditory space stimulus.

The plasticity of auditory cortex is expected to prove a valuable tool for the study of other forms of plasticity important for functional recovery in patients with central deafness and blindness. Furthermore, it may lead to treatment of tinnitus. Finally, understanding of cortical plasticity is necessary for development of treatment of patients with stroke or Alzheimer's disease.

A comparative approach, in which parallel animal and human studies are planned and conducted together, is the most powerful approach towards understanding the human brain in health and disease. Collaborations between members of a team utilizing complementary techniques are needed for continued success along these lines.

References

- Rauschecker, J.P., Tian, B., Pons, T. and Mishkin, M. Serial and parallel processing in macaque auditory cortex. *J. Comp. Neurol.* 382: 89-103, 1997.
- Rauschecker, J.P. Processing of complex sounds in the auditory cortex of cat, monkey, and man. *Acta Otolaryngologica*, in press.
- Weeks, R.A., Tian, B., Wessinger, C.M., Cohen, L.G., Hallett, M. and Rauschecker, J.P. Identification of the inferior parietal lobule as the site of auditory space perception in man. *Neurology* 48, S30.003, 1997.
- Aziz-Sultan, A., Weeks, R.A., Tian, B., Cohen, L.G., Rauschecker, J.P. and Hallett, M. Auditory localisation demonstrates cross modal plasticity in congenitally blind subjects. *Neurology* 48, S30.004, 1997.
- Malonek, D., Rauschecker, J.P., Grinvald, A. and Jezzard, P. fMRI and optical intrinsic signals in cat visual cortex: differences in response dynamics. *Soc. Neurosci. Abstr.* 23, in press.
- Malonek, D. and Grinvald, A. Interactions between electrical activity and cortical microcirculation revealed by imaging spectroscopy: implications for functional brain mapping. *Science* 272(5261):551-4, 1996.
- Rauschecker, J.P. and Korte, M. Auditory compensation for early blindness in cat cerebral cortex. *J. Neurosci.* 13(10):4538-4548, 1993.
- Rauschecker, J.P. Compensatory plasticity and sensory substitution in the cerebral cortex. *Trends in Neurosci.* 18 (1):36-43, 1995.
- Rauschecker, J.P., Tian, B. and Hauser, M. Processing of complex sounds in the macaque nonprimary auditory cortex. *Science* 268:111-114, 1995.

JIAN-YOUNG WU, Ph.D.

The GICCS Optical Imaging Laboratory, studies the neuronal activity in neocortex. Neocortex is one of the last frontiers in neuroscience. One ultimate goal for system neurobiologists is to understand how complete and complex cognition develops from a simple and partial representation of individual neurons.

The research fits into an intermediate step between neurons and brain-- the role of dynamic neural assemblies which are subconscious functional units with complex internal representations.

The laboratory uses optical imaging to analyze the population neural events in neocortex. Voltage sensitive dye imaging directly reports the electrical activity of the neurons and can have a temporal resolution of 0.5 ms, enough to follow dynamic neural events. Currently we have two major projects in my laboratory. One is aimed at understanding the localized dynamic neural assemblies, and the other is aimed at understanding the initiation site (as a pathological neural assembly) of epileptiform activity.

Project 1: Localized Cortical Neural Assembly

The long-term objective of this project is to understand local cortical neural assembly for information processing and storage. Neural assemblies are dynamic ensembles of active neurons and can be instantly created or dissolved within a population of active neurons.

Here we present data supporting our hypothesis that dynamic neuronal ensembles exist in cortical slices. Most of the experiments have been reliably repeated and published in abstract forms (Wu et al 1996; 1997a). Some data is in preparation for publishing in full papers (Wu et al 1997b).

Neocortical slices (400 μ m, coronal section) from temporal cortex and other cortical areas from 20 to 30 day old SD rats were incubated for two hours in 95% O₂ / 5% CO₂ equilibrated artificial cerebral spinal fluid (ACSF). The slices were perfused in the oxygenized ACSF containing 0.02 mg/ml of voltage sensitive dye RH 479 for one hour. The stained preparation was then perfused with ACSF at 29 °C in a recording chamber mounted on the recording microscope.

Dye-related absorption signals (705 nm) were imaged by a 124-element diode array at a rate of 1,000 frames/second. The photo-current from each photodetector was individually converted to voltage, amplified and analog filtered at 400 Hz before digitizing. The signal was about 0.1 to 1 percent of the resting light intensity. The data was stored in a computer and analyzed by a program written and developed using IDL high-end programming language.

Project 1a: Optical images of 4 to 7 Hz Spontaneous Oscillations

Although oscillation in nervous system has been extensively studied, very little is known about the spatial distributions of active neurons during synchronized oscillations. The hypothesis of this proposal is that local neuronal ensembles develop during cortical oscillations. We have employed optical imaging to examine this. Our experimental model, the 4 to 7 Hz oscillations, has been previously described for neocortical slices. They occurred spontaneously in epochs (Figure 1, top) under low Mg²⁺ conditions. Cortical layer five is sufficient and necessary to generate this oscillation. The intrinsic bursting neurons, found in layer 5, were thought to be responsible for generating this oscillation. The same mechanism was also thought to generate the cortex-originated 4 to 7 Hz (theta rhythm) oscillations in awake animals.

The 4 to 7 Hz population oscillations could be recorded by field potential electrodes everywhere in the preparation (Figure 1b, top trace). Voltage sensitive dye imaging revealed that this oscillation was not homogeneously distributed. Instead, it appeared as a spatially confined "patch" of activation traveling along the cortex (Figure 1c). The patch covered a 0.1 to 0.5 mm wide cortical section (Figure 1c, 2), with an irregular shape perpendicular to cortical layers.

Evidence supporting the hypothesis that the "activity patches" are indeed neuronal activities in slices comes from three of our findings: **1.** The signal recorded by a field potential electrode correlates extremely well with the photo-signal simultaneously recorded from the same area. **2.** The optical signal was wavelength dependent, and had a maximum at 705 nm but disappeared at 670 nm. This is a major feature of voltage sensitive dye signal from the dye molecules bounded on the excitable membrane. **3.** The photo signals could change in sub-millisecond time course, as seen in the stimulus evoked activity (Figure 3) and during the traveling of the patches. This fast temporal response could not come from another source, such as activity related intrinsic optical signals.

During the oscillations, when an active patch passed through a local field potential (LFP) electrode, a depolarization was detected. When an LFP electrode (or an optical detector) repeatedly encountered the passing through of a series of these active patches, a periodical depolarization was recorded which appeared as oscillations (Figure 1b). With the imaging of this traveling activity, the signal recorded by the LFP electrode could no longer be accurately defined as population oscillations. Instead, this activity represented features of neural "attractor", appearing as a spatially cohesive ensemble (the activity did not spread while traveling) with self-sustained activity (about 50 to 200 ms). A recent model indicates that such modular activity can emerge dynamically through local interactions in an ordinary reciprocal neuronal network without novel circuitry. The patches of traveling activity have been seen in most of the slices tested ($n = 120$) from most neocortical areas, suggesting that the activity is organized by intrinsic network mechanisms existing in all neo-cortexes. In the following sections, I will give these active patches a working name-- **Dynamic Ensembles**. The proposal will further show whether our dynamic ensembles are the same as the activity predicted in the artificial network.

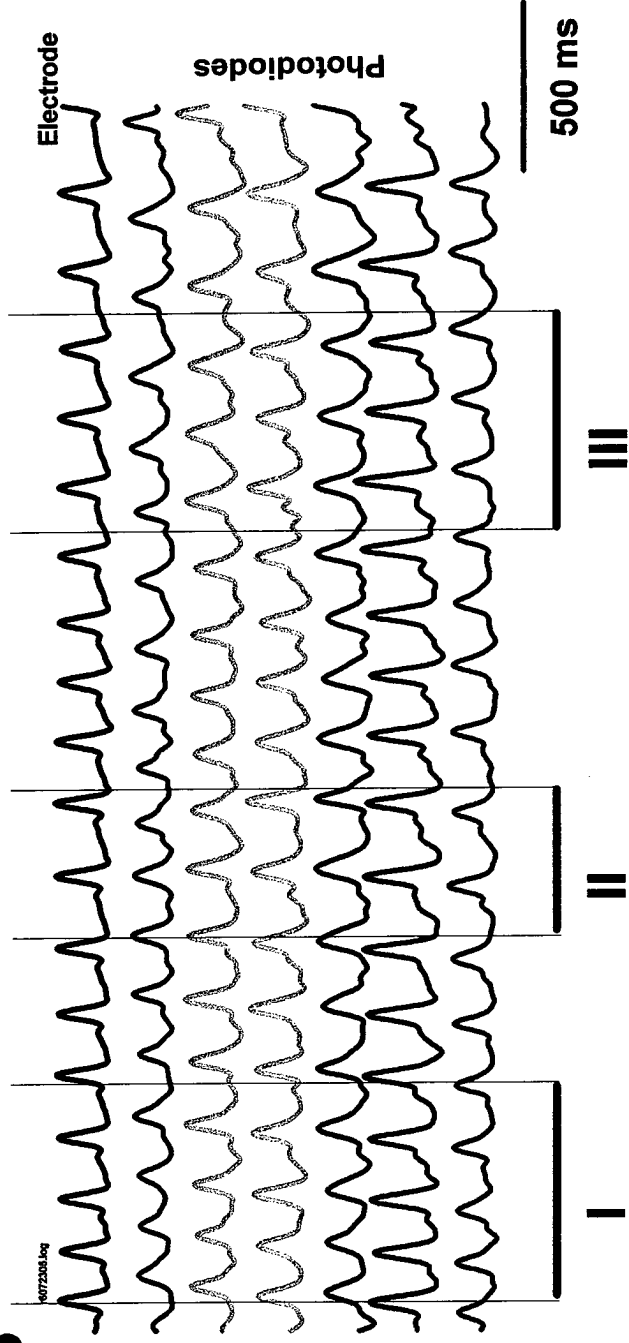
Project 1b: Traveling, Jumps and Collisions of the Dynamic Ensembles

The dynamic ensembles were observed travel a long range (5 mm). Since brain slices are virtually one-dimensional networks, only two traveling directions are possible. Most (97%, $n = 200$) of the ensembles kept the same traveling direction for their lifetime. However in a consecutive series of ensembles, individuals could travel in different directions (Figure 1, C I and III). Two ensembles could develop simultaneously at different locations and travel toward each other, resulting in collision and annihilation of the activity (Figure 1 C, II). Traveling is a continuous process in which neurons join and leave the ensemble dynamically. This rules out the possibility that the ensemble activity is associated with specific circuitry in a particular region.

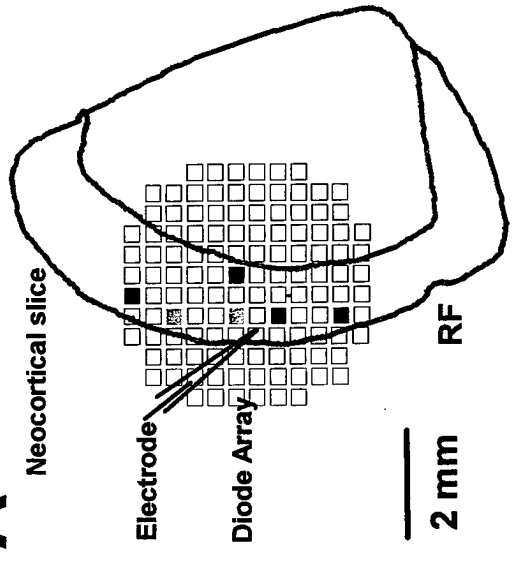
Using the fact that most of the ensembles are traveling instead of stationary, we can also strongly assert that the activity we see is related to the dynamic neuronal activity of the cortical network rather than caused by uneven damage to the preparation.

The traveling of the ensembles consisted of a slow-smooth motion of 6 ± 2 mm/sec and fast "jumps" at 150 mm/sec. The jumps appeared as rapid progression of the front edge of the activity within a few milliseconds, followed by rapid withdrawal of the back edge. This abrupt change in velocity suggests that some network components can only be activated as a whole unit and the traveling ensemble might consist of smaller network "units". When a unit is joining or leaving an ensemble, it appears as rapid progression or withdrawal of the boundaries. These units are unlikely to be based on the cortical columnar organizations since the jumping location varies when different ensembles pass through the same image field.

B



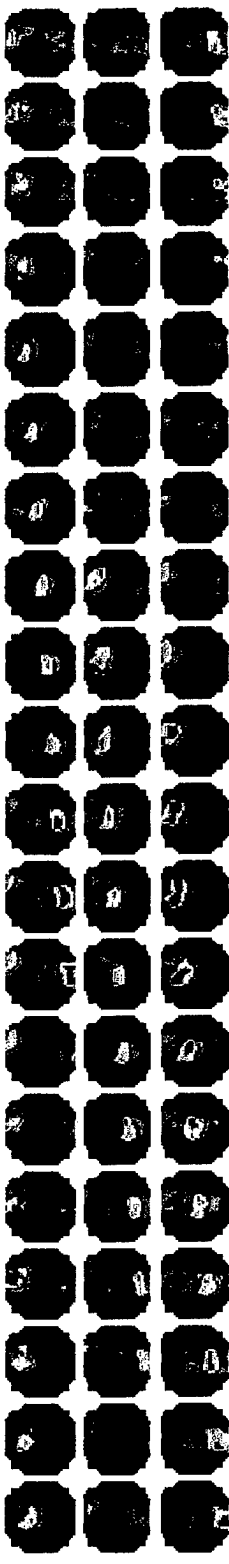
A



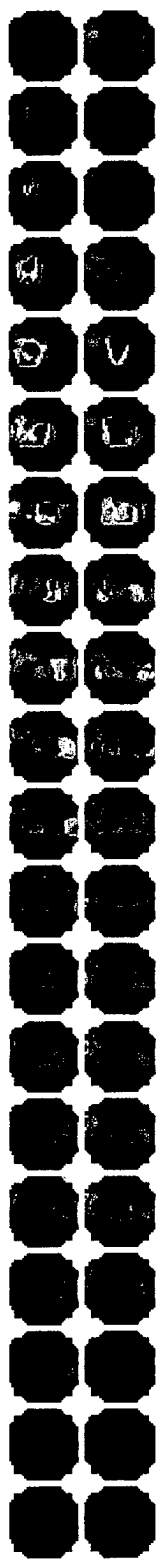
C

Activation →

I. Moving Up



II. Collisions



III. Moving Down

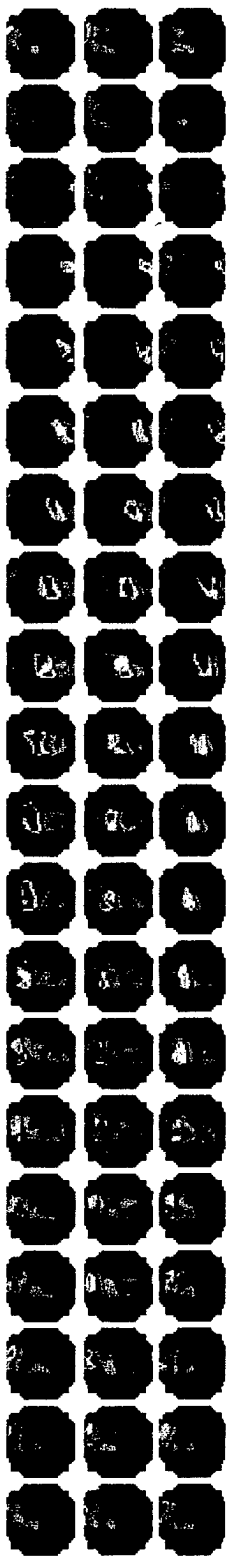


FIGURE 11 - LEGEND
TO FOLLOW

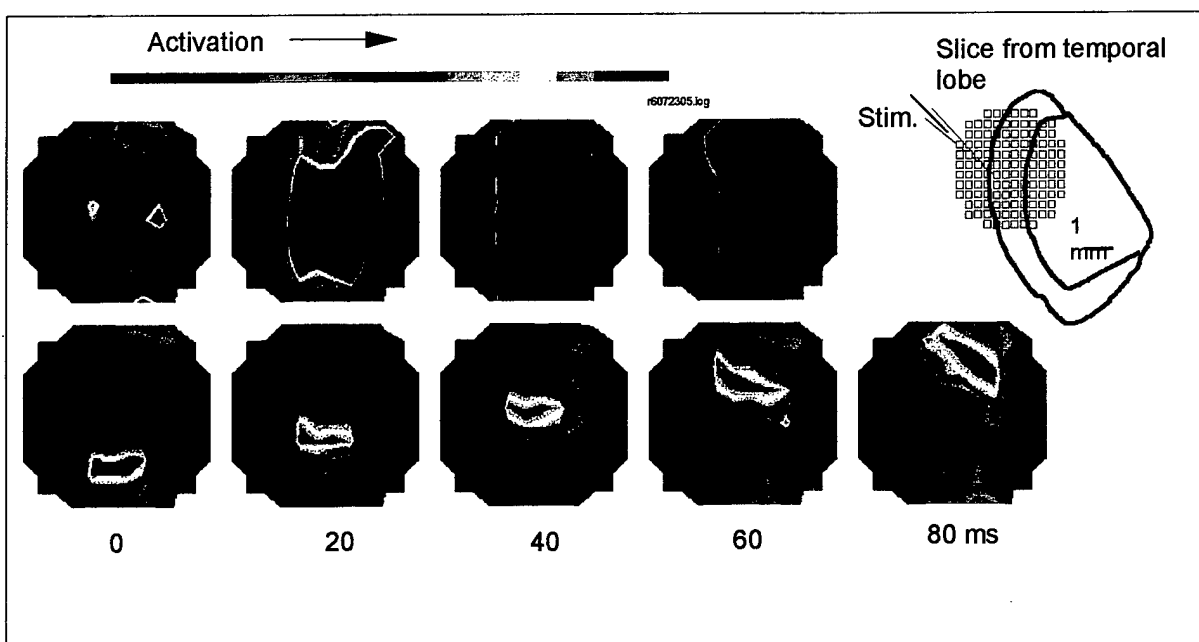


FIGURE 2 -SEE NEXT PAGE FOR LEGEND

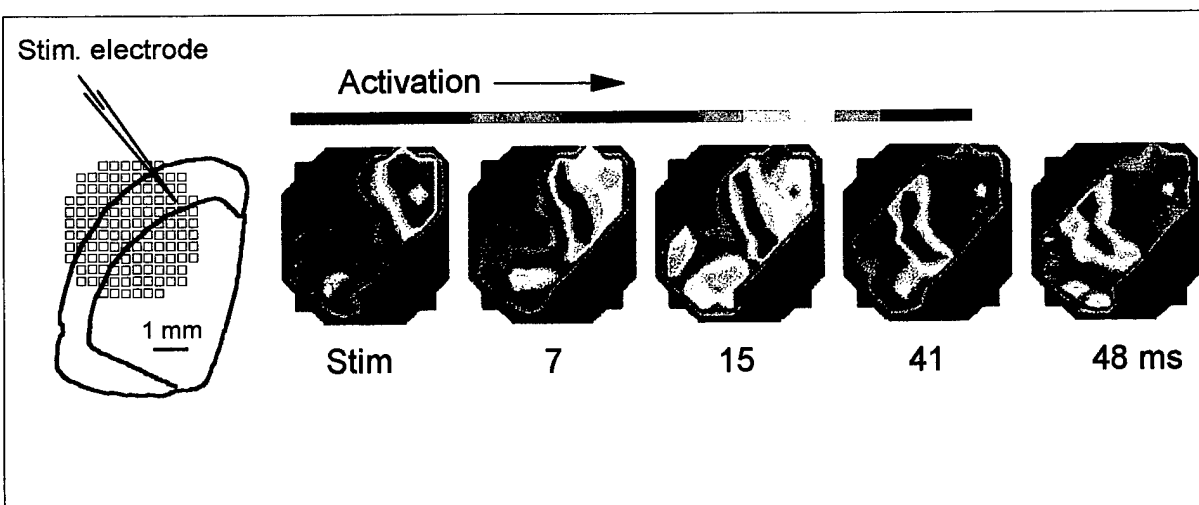


FIGURE 3 - SEE NEXT PAGE FOR LEGEND

Figure 1. Traveling activity patches during population oscillations.

A. Experimental arrangement for optical imaging and electrode recordings. A coronal section of a 400 μm slice from the temporal lobe (Bregma - 4.7 mm, from 27 days old rat) is imaged by an array of 124 photo-detectors (the open squares). A field potential electrode is placed at the center of the imaging field, in layer II of the cortex. The colored squares are selected optical detectors for which the recording traces are shown in B with corresponding colors. The image field is about 4.5 mm in diameter. Each array element covers $0.49 \times 0.49 \text{ mm}^2$ of the cortical section. All the active neurons through the thickness of the slice tissue (0.4 mm) contributed to the signal. Thus each detector could detect the population optical signal from a volume of $0.49 \times 0.49 \times 0.4 \text{ mm}^3$, containing about 10,000 cortical neurons (Douglas and Martin, 1991). The preparation was perfused in magnesium free ACSF.

B. Oscillations recorded simultaneously from field potential electrode and optical detectors. The data is captured from a 16-second optical recording trial during spontaneous oscillations. Electrical signals (top first trace, black) and optical signals (color traces) from different locations in the preparation show a phase difference of the oscillation. The color of the traces represents the location of the optical detectors (corresponding to the color squares in panel A). The field potential is roughly 0.2 mV and the optical signal is roughly 0.05 percent of the illumination intensity. Both electrical and optical signals are low-pass filtered at 300 Hz and the amplitude of the traces has been normalized to show the phase relations. Optical images from three sections (I, II, and III) of this recording trial were shown in C with higher temporal resolutions. Note the field potential oscillation (black trace) correlates well to the optical signals from the same location (green trace, from layer II and III; and red trace, from layer V and VI).

C. Dynamic ensembles travel during population oscillations. Image series selected from three sections I, II and III of the recording B and displayed at 10 ms per frame. The dynamic ensembles appeared as spatially cohesive patches of activity with an elevation of population firing rate. (The higher the firing rate the warmer the colors). Their traveling range was at least 4.5 mm across the entire field of view. Section I). Three ensembles emerged from temporal cortex (temporal cortex area 3) and moved up across the field of view to the occipital cortex. When each one moved across the field potential electrode, a cycle of oscillations was detected (black trace in B). Section II). 0.5 seconds after I, two ensembles simultaneously emerged from occipital and temporal areas (top and bottom of the field). They moved toward each other and collided in the center of the field of view. Two continuous collision events occurred during period II. Note that the activity was quickly annihilated after the collisions. After the collisions in period II the traveling direction of the ensembles was reversed. Section III). One second after the collisions in period II the all the ensembles were emerged from the occipital cortex and traveled to the temporal lobe areas.

Figure 2. Dynamic ensembles are different from epileptiform events.

The preparation was perfused in magnesium free ACSF. Images are displayed in 20 ms intervals. Top row: An epileptiform event induced by an electrical stimulus. The stimulus electrode was placed at the center of the field of view (see scheme at upper right). An epileptiform event was initiated at the time of the first image and expanded to the entire field of view in about 30 ms. In contrast, the dynamic ensembles emerged from the same cortical area (same field of view, 7 seconds later) stayed cohesive for at least 80 ms (bottom row). The top row are displayed in a lower pseudo-color scale in order to show the propagation of the epileptiform event.

Figure 3. Dynamic ensembles can be induced in normal magnesium ACSF.

Left panel: The arrangement for imaging and stimulation electrode. A stimulation electrode is placed in the deep layers, at the upper right corner of the image field. First imaging panel from the left: An electrical shock ($50\text{V} \times 0.05 \text{ ms}$) to the deep cortical layers induced an evoked activity. The slice was perfused in normal ACSF thus the activity was limited in the local area. (not an epileptiform event). Seven milliseconds later, a dynamic ensemble emerged in the active area but not from the stimulus point (2nd image from the left). The ensemble activity stayed cohesive for about 40 ms and traveled down in the image field.

In cortical slices the dynamic ensembles traveled ten times faster than the thalamus spindle oscillation waves although they have similar repeating frequencies. This means that within a certain spatial distance containing ten thalamic spindle waves, only one cortical ensemble could be contained. This makes thalamus spindle oscillations appear as traveling waves and cortical theta oscillations appear as discrete ensembles.

Project 1c: The Dynamic Ensembles are Different from Epileptiform Events

It is important to clarify that ensemble activity is different from typical epilepsy events. Our images showed that the traveling ensembles are different from the paroxysmal events in several ways (Figure 2). Paroxysmal events appeared in the optical imaging as unlimited spreading of an excitation wave that expanded from its initiation site to the entire preparation. In various epilepsy models the paroxysmal events share these common features. In contrast the ensemble activity remains cohesive for its lifetime and travels only in one direction (Figure 2). The dynamic features (self-sustainability and self regulation) of the ensemble activity will be further examined in the proposed experiments.

Project 2: Initiation And Spreading of Seizure-Like Activity in Cortical Slice Preparation

The long term objective of this research is to understand the development of organized epileptiform events from the interactions of local neuronal groups in neocortex. Epileptiform activity (EA) can be initiated from cortical structures in a number of epilepsy models, indicating that the initiation of EA can be intrinsic within the cortex. Examination of the spatial and temporal characteristics of EA using conventional electrophysiological techniques requires a cumbersome array of electrodes and careful current source analysis. It is best achieved by means of imaging techniques with high temporal resolution as the transient signal tends to be in the millisecond domain. We applied high speed (1 frame per msec) optical recordings using voltage-sensitive dyes to measure EA over a region of the cortex about $4.5 \times 1.5 \text{ mm}^2$ and so the initiation site can be imaged with few location adjustments. Here we present the imaging data showing the direct evidence where EA is spontaneously initiated in the cortical slice and how the epileptic foci are organized.

Project 2a: Spontaneous EA Initiation Sites Revealed by Optical Recordings

It is directly shown that the paroxysmal event started from the middle layer and propagated to superficial and deep layers as well as horizontally across the cortical slice (Figure 4). The onset of paroxysmal event started earliest in the trace recorded from the middle layer and was a few msec delayed in the other traces. The further the physical location was from the recording site, the more delayed the onset (Figure 4 upper panel). This is seen in the consecutive image display where a light spot representing activation of cortical neurons appeared in the middle layer and then expanded to the superficial and deep layers as well as adjacent areas. These results indicate that EA was initiated by the epileptic focus located in layer III or IV in the parietal cortical area (Figure 4 lower panel). The location of such a focus was quite stable; repeated optical recordings ($n=10$) from the same preparation revealed the same initiation and spreading scheme. Spontaneous EA could also be initiated in deep (probably layer V or VI) and superficial layers (probably layer I or II), as revealed by the imaging data (Figure 5). Optical recordings were repeated 4 to 10 trials on all the preparations, showing that each initiation site was very stable. Drifting of the initiation site was never found. All of the imaging data on the epileptic focus showed that the activation started from a small confined area less than $0.3 \times 0.3 \times 0.4$ or 0.04 mm^3 and spread smoothly from the initiation site to its adjacent cortical area. The initiation sites across the cortex varied randomly from preparation to preparation. None of the initiation sites were found close to the border of the cortex, suggesting that the formation of such an epileptic focus may not result from slicing or cutting

lesions. In all the experiments ($n=11$), the initiation sites were scattered over the cortical slice and were observed in occipital, parietal, temporal, and perirhinal areas. Among them, 5 were in deep layers, 2 in middle layers, and 4 in superficial layers, respectively.

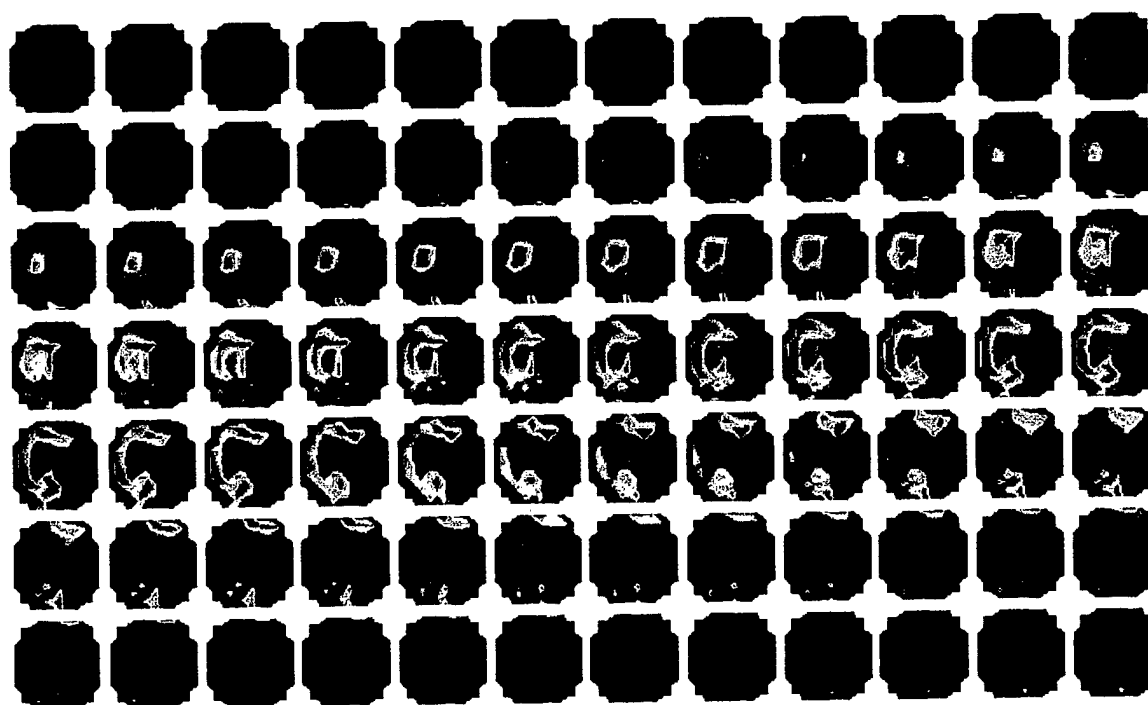
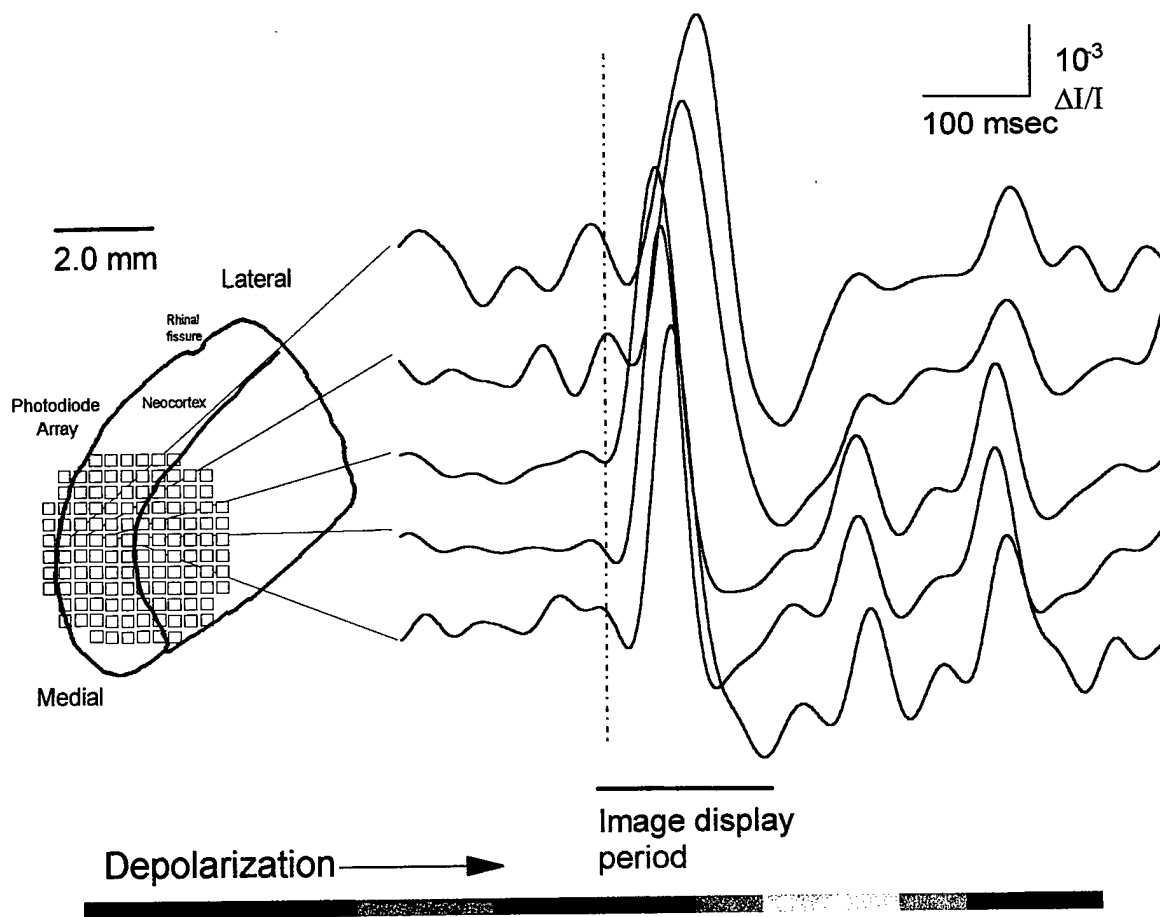
Project 2b: Electrically Evoked Paroxysmal Events in Various Layers

We have demonstrated that spontaneous paroxysmal events can be initiated in various cortical layers and so it seems that cortical neurons in various layers are capable of initiating EA. There might be a possibility that the initiation site in middle or superficial layers is controlled by layer V pyramidal neurons which start paroxysmal events before the activation in upper layers is detected. To verify this possibility, a glass microelectrode was applied to measure the ability of stimuli to initiate paroxysmal events in different layers. A single electrical pulse (10V 0.1 msec) was delivered at the electrode's tip which was less than 1 mm (usually about 0.1 mm) in diameter and placed in one of the six layers. Only a few neurons around the tip were affected by the stimulation. We found that paroxysmal events were reliably evoked in all cortical layers by the stimulation. The evoked paroxysmal events had the same characteristics as spontaneous paroxysmal events, and propagated vertically and horizontally. The initiation site depended only on the position of the stimulation electrode's tip (Figure 6). The images show clearly that activation first appeared at the stimulus electrode's tip with no delay and then spread smoothly to the neighboring areas. No saltatory activation from the stimulus electrode's tip to deep layers or other cortical areas was observed in any of the experiments ($n=8$). Various areas of the cortex including frontal occipital, parietal, temporal, perirhinal, and hippocampal cortices were tested; all the cortical structures were found to be capable of generating evoked paroxysmal events.

Discussion

In our experiments, imaging data from optical recording using voltage-sensitive dyes revealed that paroxysmal events could spontaneously be initiated in various cortical layers. Paroxysmal events could be evoked by electrical stimulation in any layer of the neocortex regardless of discharges from layer V pyramidal neurons. Therefore, it is possible that neurons in various layers may become initiation cells and trigger EA in zero Mg^{2+} epilepsy model, although layer V pyramidal neurons may provide background excitability for the neurons in other layers as suggested by the evidence that elimination of layer V abolishes the activity in superficial layers. It is likely that cortical neurons may initiate EA when they burst autonomously at a higher firing rate than other neurons, particularly when a number of neurons burst simultaneously. This implies that various cortical neurons in all layers are capable of initiating paroxysmal events once they are active, and such initiation processes do not rely on a specific type of neurons.

The epileptic focus revealed by imaging data was composed of a small confined area less than 0.04 mm^3 , indicating that relatively few cortical neurons were activated when paroxysmal events started. As this is the smallest area a photodiode can detect in our experiments, a real epileptic focus could be much smaller. We hypothesize that a neuron (pool) with repetitive discharge properties in the epileptic focus may synchronously activate its adjacent neurons and thus initiate EA. This is simulated by the electrical stimulation which generates synchronized activation of cortical neurons around the microelectrode tip. The majority of active neurons were excitatory or only had excitatory effect on adjacent cells even when inhibitory neurons could also be activated. This was not caused by dormancy of GABAergic neurons, since addition of inhibitory transmitter GABA (200 mM) in zero Mg^{2+} ACSF did not abolish the capacity of paroxysmal event initiation, suggesting that the inhibitory function in the cortex may not be effective during zero Mg^{2+} induced EA. In conclusion, our optical imaging studies on EA initiation have shown that spontaneous EA can start in various cortical layers, suggesting that the mechanism for forming the epileptic focus may exist in all cortical layers.



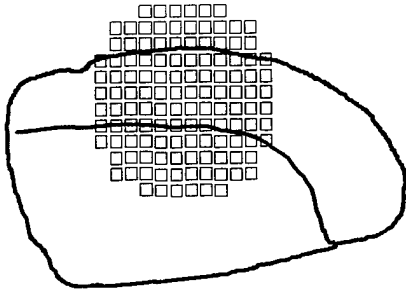
R7030609

Frame step: 2 msec

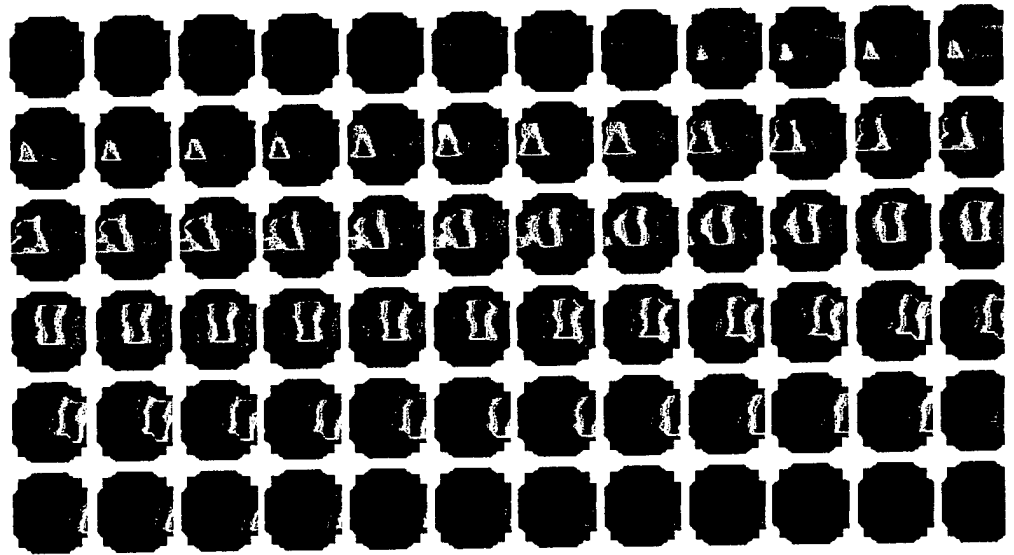
FIGURE 4-- LEGEND
TO FOLLOW

Depolarization →

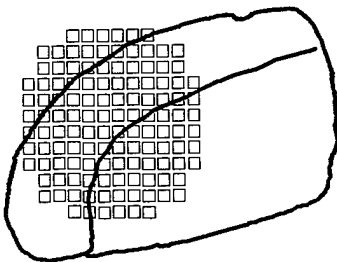
2.0 mm



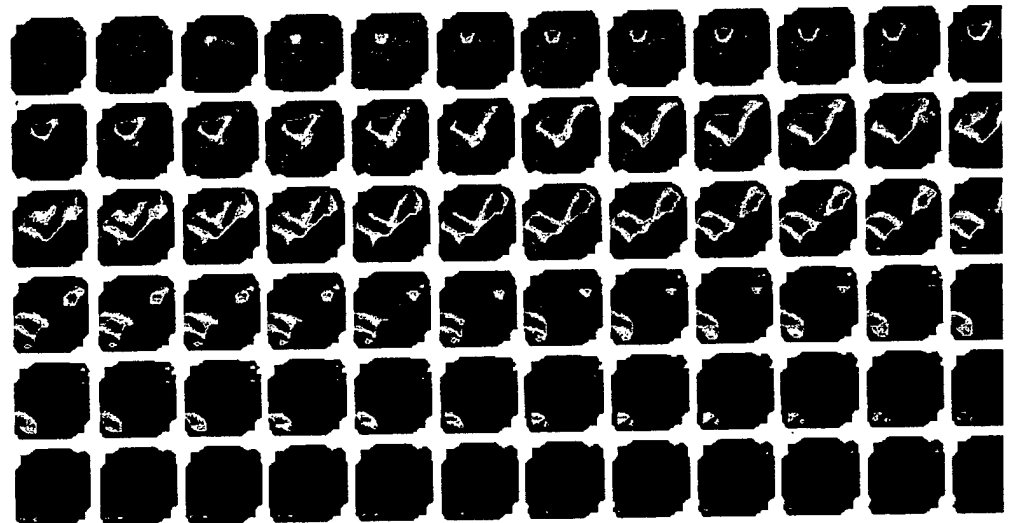
R7022401



2.0 mm



R7032701



Frame step: 2 msec

FIGURE 5 - LEGEND
TO FOLLOW

Depolarization →

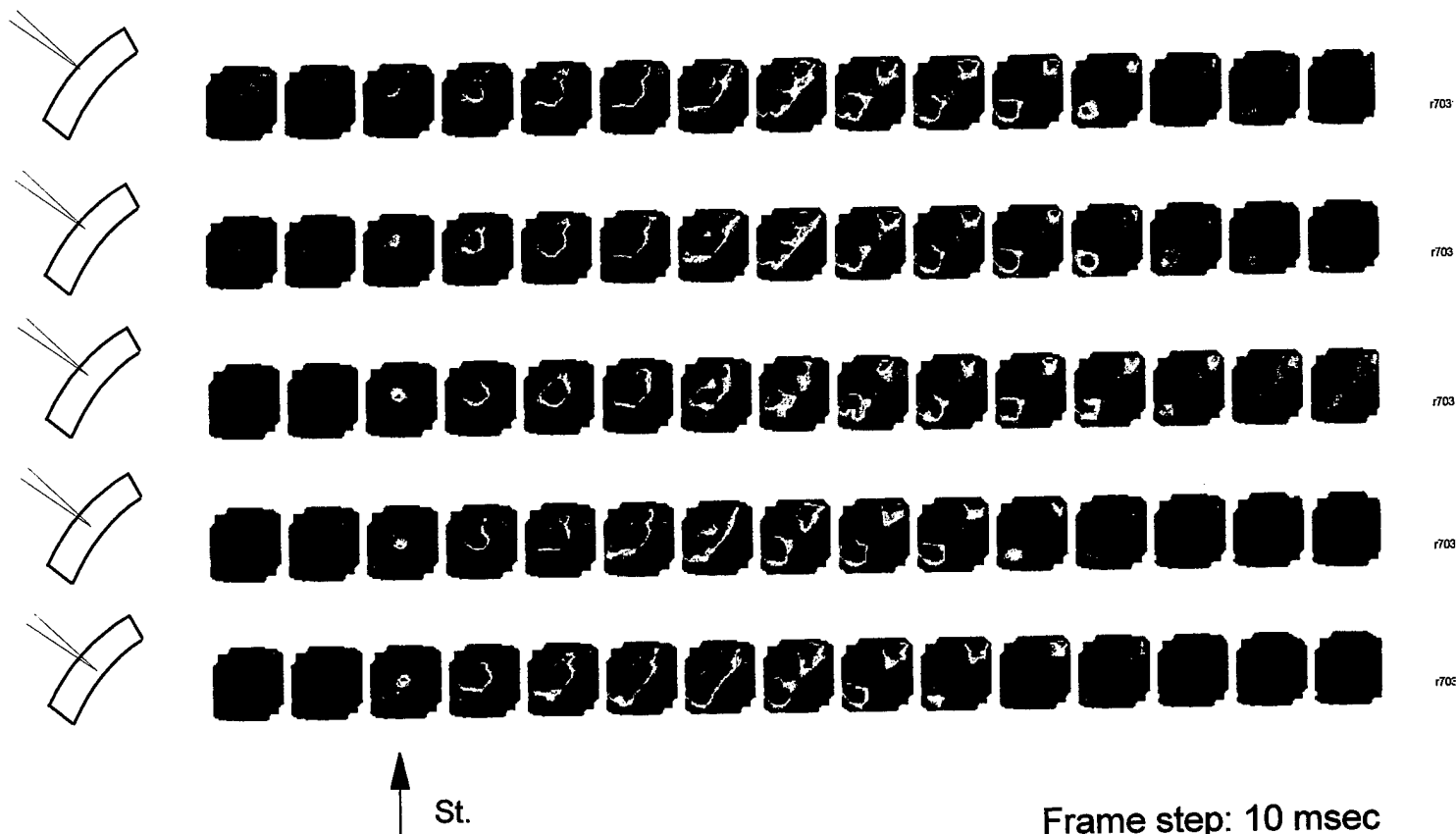


FIGURE 6 - LEGEND
TO FOLLOW

Figure 4. EA initiation site located in the middle layer of the cortex.

Upper panel: Schematic illustration of a 124 element photodiode array over the neocortical slice (left) shows the location of optical recordings of a paroxysmal event. The onset time of the paroxysmal event varied with position and the earliest onset was found at the diode location where the image of the middle layer (probably layer III or IV) in the occipital cortical area was projected (right). The dashed line indicates the earliest onset time. Only five traces of optical recordings from different cortical layers are displayed and their locations were pointed out by the fine lines. The onset from the other traces occurred a few msec later, with a similar wave form. Lower panel: Consecutive image display of the same optical data. Pseudocolor indicates the membrane potential changes with the red side indicates activation of the neuronal tissue. A light spot located at where the middle trace in Upper panel was recorded started first, and then the activation expanded to reach superficial and deep areas of cortical image as well as adjacent areas. The first activated area became inactivated first. The time step for each frame was set to 2 msec and 1 frame in between each two images was omitted here. The total display time was 168 msec.

Figure 5. Two optical recordings from different slices showing initiation sites in different layers.

Upper panel: Consecutive image display shows that a paroxysmal event was initiated in deep layer (probably layer V or VI) of the temporal cortical area. Lower panel: In another experiment, consecutive image display show that a paroxysmal event was initiated in the superficial layer (probably layer I or II) in the parietal cortical area. All the imaging results show that the activation spread from the initiation site to the adjacent areas. The areas activated first became inactivated first. The time step for each frame was set to 2 msec and 1 frame in between each two images was omitted here. The total display time for each experiment was 144 msec.

Figure 6. EA initiation in different layers by electrical stimulation via a microelectrode.

The location of the stimulation microelectrode's tip is shown by the schematic illustrations on the left. The location of the electrode tip was moved after one or two trials of optical recordings were acquired at one location. All optical recordings from the same preparation were acquired at the same location. The time step for consecutive image display was set to 10 msec and 9 frames in between each two images were omitted here. The numbers on the right indicate different trials. A brief stimulus (10V 0.1 msec) was given when no spontaneous activity was detected in the cortical slice in each trial. The arrow and sign St. indicate when stimulation started. The activation was observed immediately when stimuli were delivered at the tip of microelectrode and then spread to the adjacent areas.

References

- Tsau, Y., L. Guan, and J.-Y. Wu. Dynamic Change of organization in rat neocortical slice. Abstracts, Soc. for Neuroscience 22, 1057, 1996.
- Tsau, Y., L. Guan, and J.-Y. Wu. Initiation and propagation of spontaneous epileptiform activity in rat neocortical slice. Abstract, American Epilepsy Society, *Epilepsia*, 37:51, 1996.
- Wu, J.-Y., L. Guan, and Y. Tsau. Global traveling wave and localized oscillations in neocortical slice. Abstracts, Soc. for Neuroscience, 22, 1057, 1996.
- Hahm, J.-O. Y. Tsau, K.C. New, J.-Y. Wu, R.L. Martuza, and S.D. Rabkin. Gene transfer in human and rat cortical slices using defective herpes simplex virus (HSV) vectors. Abstracts, Soc. for Neuroscience, in press.
- Guan, L., Y. Tsau and J.-Y. Wu. Formation of Epileptic focus is suppressed by the activities from other initiation sites. Abstracts, Soc. for Neuroscience, in press.
- Tsau, Y., L. Guan, and J.-Y. Wu. Initiation and propagation of epileptiform activity in neocortical slices. Abstracts, Soc. for Neuroscience in press.
- Wu, J.-Y., L. Guan, and Y. Tsau. Optical imaging of dynamic neuron ensembles in neocortical slices. Abstracts, Soc. for Neuroscience, in press.
- Tsau, Y., L. Guan, and Jian-young Wu. Organization of the origin of paroxysmal synchronized activity in neocortex, in preparation.
- Tsau, Y., L. Guan, and Jian-young Wu. Spontaneous epileptiform activity can be initiated in various neocortical layers: an optical imaging study, in preparation.
- Wu, J.-Y., L. Guan, W. Chen, and Y. Tsau. Visualization of temporary neural assemblies in neocortical slices, in preparation.
- Tsau, Y., L. Guan, and Jian-young Wu. Spreading of epileptiform activity in neocortical slices, in preparation.

COMPUTATIONAL NEUROSCIENCE: Two faculty members work in this area. Dr. Goodhill models neuronal development, including the structure of cortical mappings and axonal guidance. Dr. Pouget uses mathematical analysis and computer simulations to study mechanisms of information processing in selected cortical regions.

GEOFFREY J. GOODHILL, Ph.D.

Dr Goodhill has two main research goals, both broadly relating to neural development. The first goal is to understand the theoretical principles governing the development and structure of cortical mappings. The second research goal is to understand quantitatively how gradients of chemotropic factors guide axons to appropriate targets in the developing brain.

Project 1: Development of Cortical maps

Two key questions for understanding sensory processing are, how is information about the world represented in the cortex, and how are these representations formed during development. The best studied cortical areas in this regard are V1 and V2, where features of the visual scene such as position, orientation, direction and disparity are represented in maps. Understanding how these maps and the relationships between them come about is an important step in answering the above questions. The relative importance of genetic versus epigenetic (particularly activity-dependent) mechanisms in determining cortical structure is still a subject of intense debate. This debate impacts directly on the design of effective therapies for treating the effects of early sensory visual experience.

Dr Goodhill has been testing the hypothesis that cortical map structure arises from activity-dependent learning rules that attempt to represent highly correlated input features close together, acting in conjunction with genetically determined constraints such as the shape of the target area. To do this he has been using the elastic net algorithm, a theoretical model of cortical development that is well suited to exploring questions of large-scale map structure. This has been applied to low dimensional feature spaces representing position, orientation, ocular dominance.

For the ocular dominance case, Dr Goodhill has identified several influences on overall column orientation (figure 1). For the orientation case, similar effects occur (figure 2). This work shows how patterned afferent activity in conjunction with genetically determined constraints could influence the structure of cortical maps, and generates novel predictions that can be tested experimentally to further probe mechanisms of cortical self-organization.

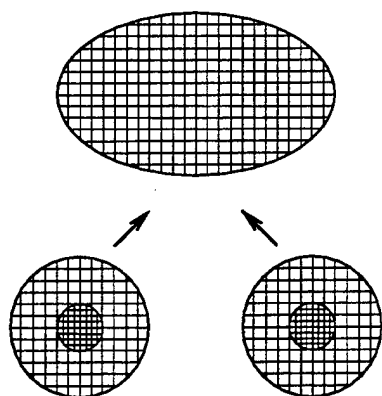
Project 2: Axon Guidance by Gradients

Axon guidance by gradients plays an important role in wiring up the developing nervous system. Growth cones seem to sense a concentration difference between their two ends, and convert this into a signal to move up or down a gradient. Dr Goodhill has been formulating a simple mathematical framework to understand when and where gradient detection can occur as a function of gradient shape. This framework has been applied to two examples: the guidance of axons by target-derived diffusible factors in vivo and in collagen gels, and to guidance by substrate-bound gradients of optimal shape, as might be relevant in the retinotectal system.

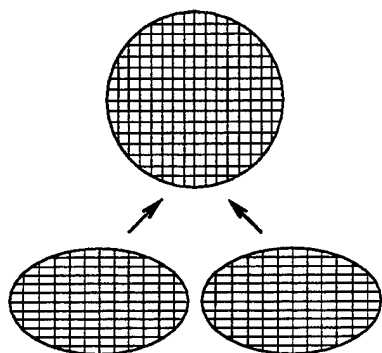
The mathematical framework is shown in figure 3. Target-derived diffusible factors have been implicated in the guidance of axons from the trigeminal ganglion to the maxillary process in the mouse, of commissural axons in the spinal cord to the floor plate, and of axons and axonal branches from the corticospinal tract to the basilar pons. In order to calculate the size of this change, and how it evolves with time, it is necessary to assume a particular model for the diffusion of factor in vivo and in vitro. Perhaps the simplest assumption (figure 3) is that a small target continuously produces factor at a constant rate into a large volume. The concentration of the factor as a function of distance r from the target after time t has elapsed from the start of factor production, $C(r, t)$, is then given by

$$C(r, t) = \frac{q}{4\pi Dr} \operatorname{erfc} \frac{r}{\sqrt{4Dt}} \quad (1)$$

A



B



C

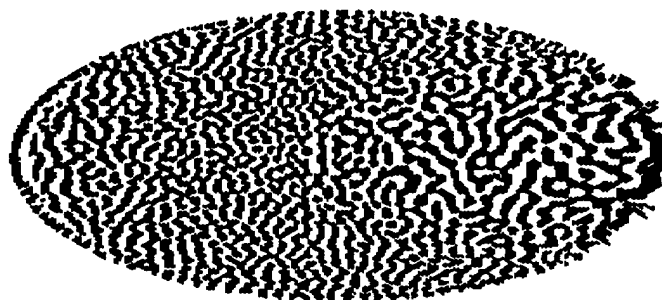
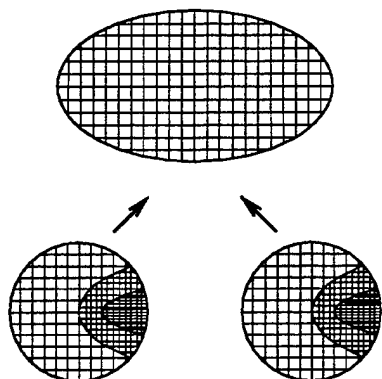


Figure 1: Influences on the overall pattern of ocular dominance columns. The left column shows a schematic representation of the mapping problem considered, and the right column shows the result of an elastic net simulation in each case. **A.** Effect of a foveal region of higher feature point density: columns are wider in the foveal representation. Note also the effect of target shape, causing columns to line up parallel to the short axis of the ellipse. **B.** Anisotropic correlations (feature points closer together along the y axis than the x axis): columns line up parallel to the direction of weaker correlations. Target shape is circular in this case to eliminate other biases to column direction. **C.** Combined effect of elliptical target, foveal region of increased density, and anisotropic correlations in the fovea. The number of columns was chosen to roughly match the number of columns in the macaque.

A



B



Figure 2: Orientation maps produced by the elastic net for a mapping from $(x, y, \cos(2\theta), \sin(2\theta))$ space to a two dimensional cortex. The boundary of the input spatial dimensions is circular. θ was regularly spaced in intervals of 30° . Each cortical cell is represented by a hexagon colored according to the orientation represented. Note that only 3 hexagons can join at a point, so pinwheels inevitably have some spatial extent in this representation. **A.** Cortical sheet with circular boundary. **B.** Cortical sheet with elliptical boundary. Note the bias in the overall direction of flow in the latter case, and the tendency in both cases for the stripes to intersect the border at right angles.

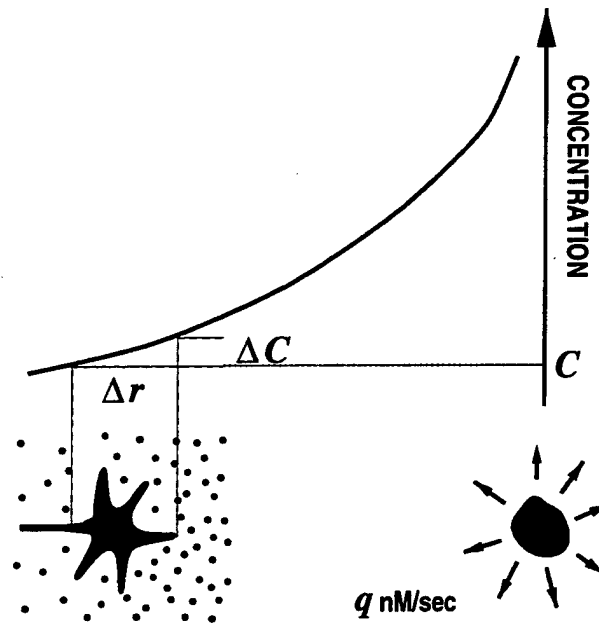


Figure 3: This shows a growth cone sitting in (or on) a gradient of increasing concentration of a chemoattractant. The spatial extent of the growth cone is Δr , and the concentrations at its two ends are C and $C + \Delta C$. For diffusible factors this gradient can be created by the release of factor from a target, shown here at a rate of q nM/sec. Gradients can also be set up in other ways, for instance by translation of morphogenetic gradients. The same picture applies for chemorepellent factors, except that now ΔC is converted into a growth signal in the opposite direction.

where D is the diffusion constant of the factor through the substrate, and q is the rate of factor production by the target. Using this equation and estimates for the parameters, it is possible to calculate when and where the constraints mentioned earlier are satisfied: that is, when and where guidance of a growth cone is possible. Results are shown in figure 4.

For substrate-bound gradients, constraints on gradient shape arise from constraints on how morphogenetic gradients can be translated into gradients of ligand expression. It is now possible to ask what is the *optimal* gradient shape, i.e. that which would guide growth cones over the maximum possible distance. Given similar assumptions about growth cone sensing to those used above for the diffusible factor calculations, the answer turns out to be straightforward (figure 5).

Two distinct spatial limits on guidance emerge from this work: 1 mm for a target-derived diffusible gradient, and 1 cm for a substrate-bound gradient. These values fit well with experimental data. Experimental predictions of this work are that (1) for diffusible factors, guidance over larger distances than 1mm may be possible if the start of production of factor is carefully matched to the time when guidance is required, and (2) for substrate-bound factors, the shape of the gradient in situ will predict the mechanism of gradient detection.

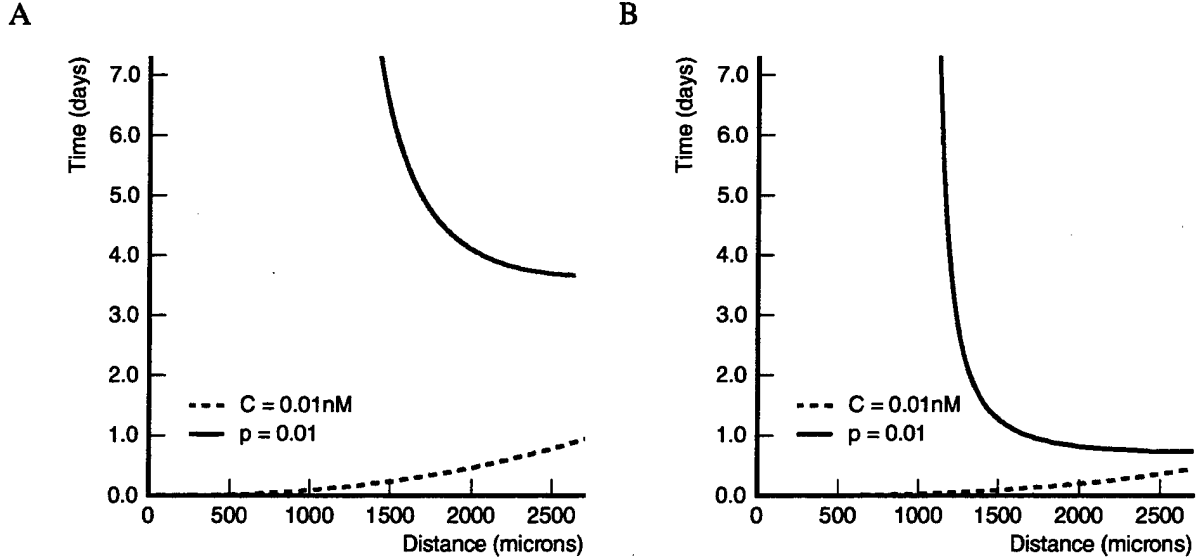


Figure 4: Interaction of constraints for guidance by a diffusible factor. **A** is for a large molecule with diffusion constant $D = 10^{-7} \text{ cm}^2/\text{sec}$. **B** is for a slightly smaller molecule with $D = 5 \times 10^{-7} \text{ cm}^2/\text{sec}$ (D is expected to scale roughly inversely with the cube root of the molecular weight). Each graph shows, at each distance, the time at which two constraints are satisfied: the low concentration limit, where not enough receptors are bound for a gradient signal to be detected (assumed to be $K_D/100$ with $K_D = 1 \text{ nM}$), and the fractional change constraint (assumed to be $\Delta C/C = 1\%$). The region between the two curves in each graph is where guidance is possible. In both cases the guidance limit imposed by the fractional change constraint once the gradient has stabilized is 1 mm. However, guidance range is extended at earlier times, when the fractional change constraint has yet to take full effect. This is particularly apparent for the slowly diffusing molecule ($D = 10^{-7} \text{ cm}^2/\text{sec}$).

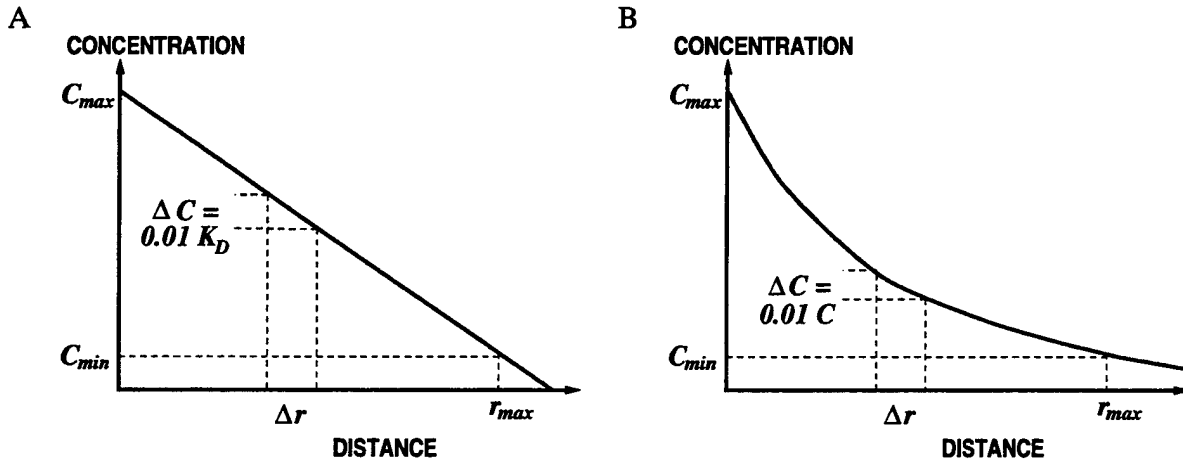


Figure 5: The shape of the gradient that gives guidance over the maximum possible distance is determined by the gradient reading mechanism. **A**. In the absolute change case, the optimal gradient is linear and the maximum guidance range is given by $r_{max} = \frac{\Delta C}{p} \frac{C_{high} - C_{low}}{k_d}$, where p is the minimum fractional change detectable by the growth cone (assumed to be 1%). **B**. In the fractional change case, the optimal gradient is exponential and the maximum guidance range is given by $r_{max} = \frac{\Delta C}{p} \log_e \frac{C_{high}}{C_{low}}$. For reasonable parameter values, r_{max} is about 1 cm in both cases.

ALEXANDRE POUGET, Ph.D.

The goal of Dr. Pouget's laboratory is to investigate the mechanisms of information processing in cortical circuitry. We use primarily a computational approach involving mathematical analysis and computer simulations. Our research focuses on how neurons encode sensory information through their firing rate and how these signals are being subsequently used to guide motor behaviors such as grasping or navigation.

This progress report provides a brief description of the three main projects currently developed in my laboratory. The first one is concerned with the role of cortical lateral connections in neural coding. We have found analytically that lateral connections can be used to performed optimal non-linear filtering of noise. The second project shows that this filtering property is consistent with the effect of sensory adaptation, one of the most widely used paradigm in human psychophysics. The third project is concerned with spatial perception and the neural structure of object-centered representations, a type of representation involved in object recognition and manipulation.

Project 1: Neural Coding: Lateral Connections and Noise Filtering

This work has been done in collaboration with Sophie Deneve, Peter Latham and K. Zhang.

There are many ways information processing systems can encode information. Computers, for example, encode signals with a binary code, i.e., strings of 0's and 1's. In the brain, neurons communicate by sending electrical pulses, or spikes, along their axon. These spikes trigger the release of neurotransmitter at the synapses which, in turn, changes the membrane potential of the post-synaptic neurons. Information is believed to be encoded through the firing rate – the number of impulses per second – and possibly the timing of the spikes. Post-synaptic neurons are faced with the problem of having to decode, or interpret, these responses, but little is known about how they perform this task. The difficulty in decoding neural signals comes largely from the presence of a large amount of noise in cortical circuitry. Thus, in response to a fixed stimulus, a neuron might fire 3 spikes on average over many trials but it can be 2 spikes or 6 spikes on any particular trial.

Last year, we had found that lateral connections—connections linking neurons at the same hierarchical level of processing—can be used to perform maximum likelihood estimations, a statistically optimum decoding method (Zhang *et al.*, 1996; Pouget & Zhang, 1997; Pouget *et al.*, 1997). Our model uses lateral connections (figure 1-A) to implement expectations about sensory signals in the form of bell-shaped stable states (figure 1-B). These expectations allow the system to filter out the noise non-linearly while preserving the maximum information about the signal.

These preliminary results were based on computer simulations of a recurrent network. This year we have been able to demonstrate analytically the equivalence between this network and maximum likelihood.

Let A be a noisy pattern of activity from the n input units in response to a sensory stimulus, θ_0 . Because the input units have a bell-shaped tuning to θ , A is a noiseless hill of activity centered on θ_0 corrupted by noise. The maximum likelihood method consists in finding out which noiseless hill of activity would be the most likely, given that you observe A . This operation is equivalent to projecting orthogonally the activity A onto the manifold, viz., the subspace, of all possible noiseless hills of activity.

If the manifold was just a hyperplane, the projection would be linear. This manifold is unfortunately non-linear, i.e., the set of all possibly stable hill follows a curved trajectory in activity space, making this projection operation particularly complicated. We have found, however, that our network computes an approximation to this projection (figure 2) which, in the limit of low noise, is as good as maximum likelihood (Pouget *et al.*, 1997).

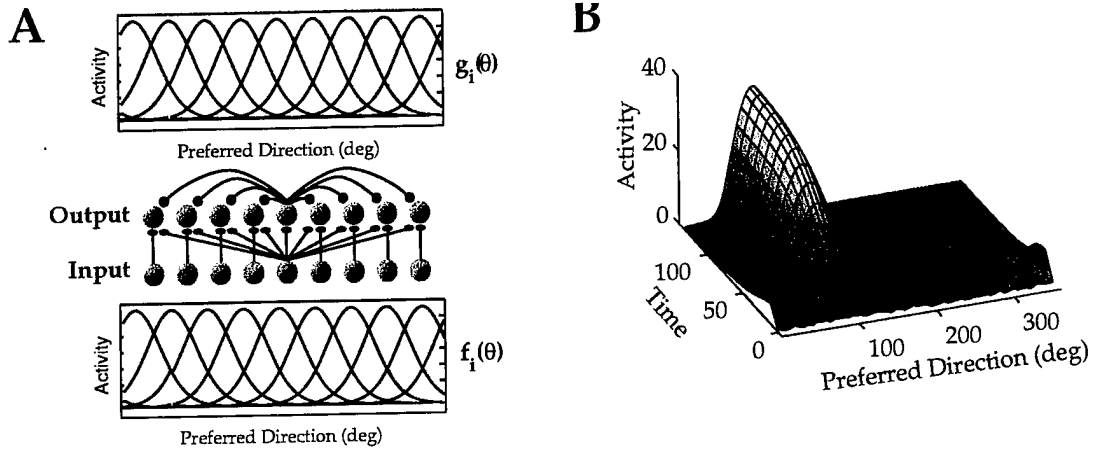


Figure 1: A- Two layer network for estimation using coarse code. The first layer generates the noisy activity pattern $\{a_i\}$ according to the bell-shaped tuning functions $\{f_i(\theta)\}$. B- Activity over time in the output layer in response to an initial small random pattern of activity. The activity of the units are plotted as a function of their preferred direction of motion. The weights were set in such a way that bell-shaped patterns of activity, consistent with the tuning functions $\{f_i(\theta)\}$, are stable states for the output layer

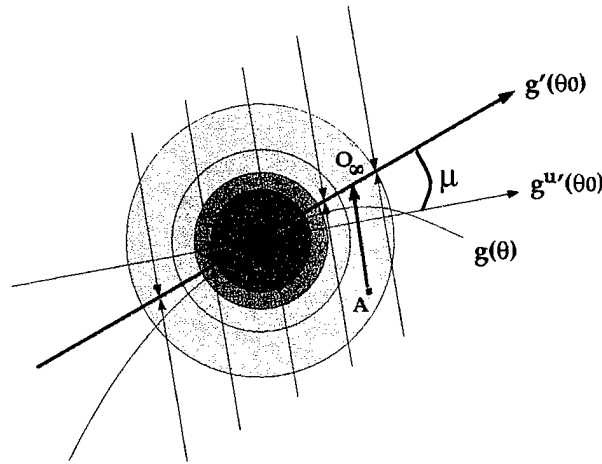


Figure 2: Our network projects the initial noisy activity A onto the tangent, $g'(\theta_0)$, of the manifold, $g(\theta)$, of all noiseless states along trajectories that are almost orthogonal to $g'(\theta_0)$. This is very close to a maximum likelihood estimation

In the coming years, we intend to extend this work to multisensory integration, the process by which information pertaining to the same object, but coming from different sensory modalities, such as the face and voice of a person, are merged in a unitary representation.

Project 2: Neural Coding: Adaptation

This work has been done in collaboration with Jean-Christophe Ducom.

When asked to discriminate orientation around the vertical, human subjects can typically distinguish gratings differing by as little as 2 degrees. Adaptation to vertical orientation prior to this task has the counterintuitive effect of decreasing this threshold. By contrast, adaptation ± 15 degrees away from the vertical raises the threshold and introduces a perceptual bias away from the adapted orientation (e.g., after adaptation at -15 degrees, 0 degrees is perceived as 5 degrees, see figure 3 for a demonstration). These findings have been interpreted as reflecting the statistical properties of the mechanisms responsible for reading out the cortical representation of orientation.

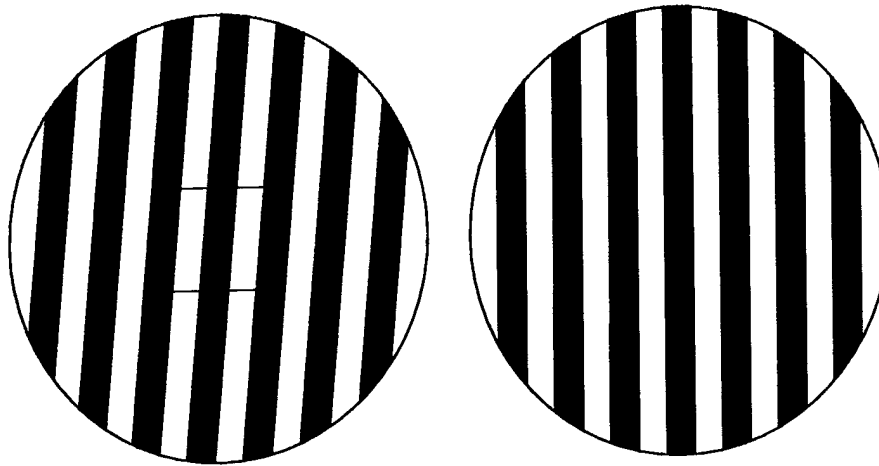


Figure 3: Demonstration of a perceptual bias introduced by sensory adaptation. Fixate the left grating for 30s or more keeping your gaze within the red square. Then switch to the right grating. Although it is vertical it should appear as slightly tilted counterclockwise.

We have found that this explanation is unlikely to be correct because none of the read out methods published in the literature can fully account for the effect of adaptation. We propose instead that these effects are the consequence of the mechanisms responsible for cleaning up noise in the cortical representation of orientation (Pouget *et al.*, 1997). We have simulated adaptation in the model described in the previous section and we have found that this circuit exhibits the same changes in threshold and bias as human subjects in a discrimination task after adaptation (Pouget97e). These results provide additional evidence that lateral connections play a critical role in noise reduction in the cortex.

Project 3: Object-centered Representations

This work has been done in collaboration with Sophie Deneve.

Several authors have argued that tasks such as object recognition (Hinton, 1990) and manipulation (Olson & Gettner 1995) are easier to perform if the object is represented in object-centered coordinates, a representation in which the subparts of the object are encoded with respect to a frame of reference centered on the object. Compelling evidence for the existence of such representations in the cortex comes from experiments on hemineglect--- a neurological syndrome resulting from unilateral lesions of the parietal cortex. A right lesion, for example, leads patients to ignore stimuli located on the left side of their egocentric space. Recently, Driver et al. (1994) showed that the deficit can also be object-centered. Hence, hemineglect patients can detect a gap in the upper edge of a triangle when this gap is associated with the right side of the object but not when it belongs to the left side (figure 4-A).

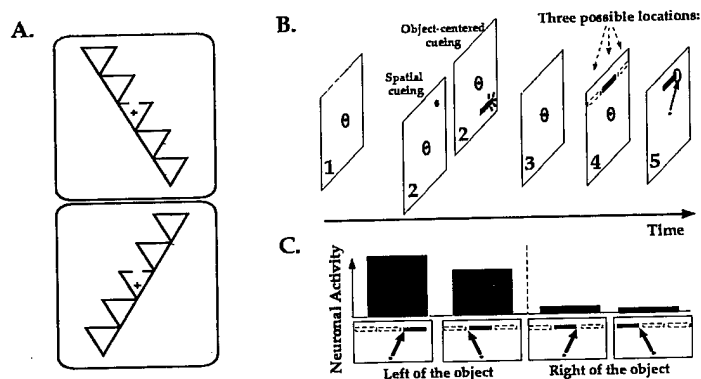


Figure 4: A- Driver et al. (1994) experiment demonstrating object-centered neglect. Subjects were asked to detect a gap in the upper part of the middle triangle, while fixating at the cross, when the overall figure is tilted clockwise (top) or counterclockwise (bottom). Patients perform worse for the clockwise condition, when the gap is perceived to be on the left of the overall figure. B- Sequence of screens presented on each trial in Olson and Gettner experiment (1995). C- Schematic response of an SEF neuron for 4 different conditions. Adapted from Olson and Gettner, 1995

What could be the neural basis of these object-centered representations? The simplest scheme would involve neurons with receptive fields defined in object-centered coordinates, i.e., the cells respond to a particular side of an object regardless of the position and orientation of the object. A recent experiment by Olson and Gettner (1995) supports this possibility. They recorded the activity of neurons in the supplementary eye field (SEF) while the monkey was performing object-directed saccades. The task consisted of making a saccade to the right or left side of a bar, independent of the position of the bar on the screen and according to the instruction provided by a visual cue. For instance, the cue corresponding to the instruction 'Go to the right side of the bar'

was provided by highlighting the right side of a small bar briefly flashed at the beginning of the trial (step 2 in figure 4-B).

By changing the position of the object on the screen, it is possible to compare the activity of a neuron for movements involving different saccade directions but directed to the same side of the object, and vice-versa, for movements involving the same saccade direction but directed to opposite sides of the object. Olson and Gettner found that many neurons responded more prior to saccades directed to a particular side of the bar, independently of the direction of the saccades. For example, some neurons responded more for an upward right saccade directed to the *left* side of the bar but not at all for the same upward right saccade directed to the *right* side of the bar (column 1 and 3, figure 4-C). This would suggest that these neurons have bar-centered receptive¹ fields, i.e., their receptive fields are centered on the bar and not on the retina. This would correspond to what we will call an *explicit* object-centered representation.

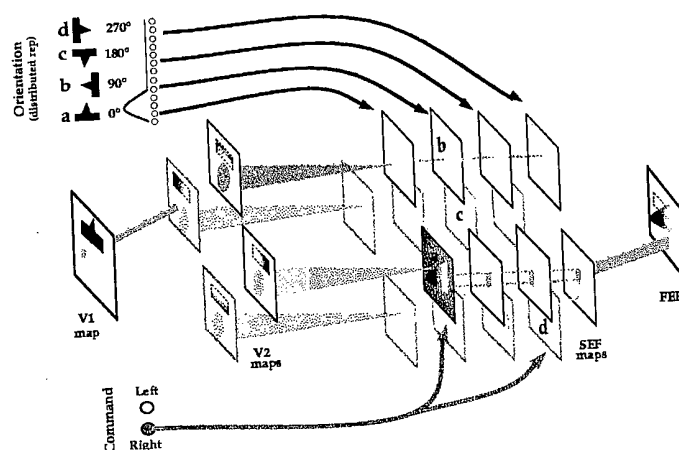


Figure 5: Schematic structure of the network with activity patterns in response to the horizontal bar shown in the V1 map and the command 'Go to the right'. Only one SEF map is active in this case, the one selective to the right edge of the bar (where right is defined in retinal coordinates), object orientation of 0° and the command 'Go to the right'

We believe that these data are compatible with a different type of representation which is more suitable for the task performed by the monkey. We have developed a neural network which can perform a saccade to the right, or left, boundary of an object, regardless of its orientation, position or size--- a generalization of the task used by Olson and Gettner. The network (shown in figure 5) performs a mapping from the image of the bar and the command (indicating the side of the object to which the saccade must be directed) to the appropriate motor command in oculocentric coordinates (the kind of command observed in the frontal eye field, FEF). We use a bar whose left and right sides are defined with respect to a triangle appearing on the top of the bar (see figure 5).

¹ we use the term receptive field in a general sense, meaning either receptive or motor field

Neurons in the intermediate maps in our network, called the SEF maps, have the following property: 1- they have an invariant tuning curve for the direction (and amplitude) of saccadic eye movements in oculocentric coordinates, just like neurons in the FEF or the SC, and 2- the gain of this tuning curve is modulated by the orientation of the object as well as the command (Deneve & Pouget, 1997, Deneve & Pouget, Submitted). Figure 6-A shows how the tuning curve for saccade direction of one particular unit varies as a function of these two variables. In this particular case, the cell responds best to a right-upward saccade directed to the left side of the object when the object is horizontal. Therefore, the SEF units in our model do not have an invariant receptive field in object-centered coordinates but, nevertheless, the gain modulation is sufficient to perform the object-centered saccade.

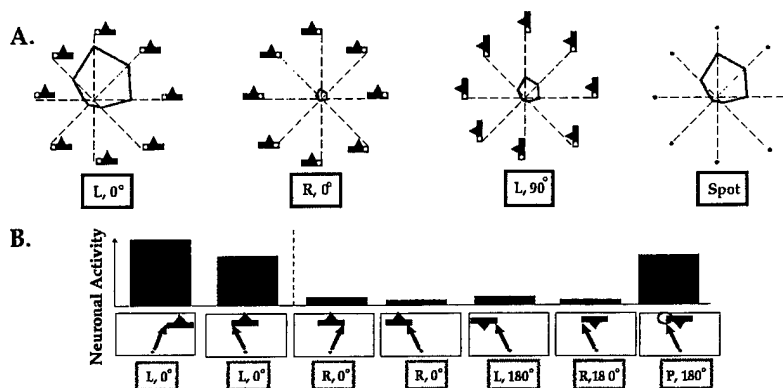


Figure 6: A- Polar plots showing the selectivity for saccade direction of a representative SEF units. The first three plots are for various combinations of command (L: left, R: right, P: spatial cueing) and object orientation. The left plot corresponds to saccades to a single dot. B- Data for the same unit but for a subset of the conditions. The first four columns can be directly compared to the experimental data plotted in figure ??-C from Olson and Gettner. The 5th and 6th columns show responses when the object is inverted. The seventh columns corresponds to spatial cueing.

The data published by Olson and Gettner (1995) and more recent experiments (Olson & Gettner, 1997) are consistent with the gain modulation hypothesis. First, all the SEF neurons had oculocentric receptive fields when tested on saccades to a single dot (personal communication), an observation which is difficult to reconcile with an explicit object-centered representation. Second, if we sample our data for the conditions used by Olson and Gettner, we find that our units behave like real SEF cells. The first four columns of figure 6-B show a unit with the same response properties as the cell represented in figure 4-C. Figure 6-B also shows the response of the same unit when the object is upside down and when we use a spatial cue. Note that this unit responds to the left side of the bar when the object is upright (1st column), but not when it is rotated by 180° (5th column), unless we use a spatial cue (7th column). Similar modulations by the orientation of the object have now been reported by Olson and colleagues (Olson & Gettner, 1997).

We have also found that lesions in the SEF map can lead to a syndrome similar to neglect and can therefore account for the Driver et al. (1994) experiment depicted in figure 4-A. These simulation are based on the assumption that each cortical hemisphere contains more units selective for the contralateral side of space (Deneve & Pouget, 1997, Deneve & Pouget, Submitted). Therefore, our model provides the first theory relating the behavior of hemineglect patients involved in an object-centered task with neurophysiologic data from single neurons in the supplementary eye field of a monkey.

References

- Deneve, S., & Pouget, A. Neuronal object-centered representations: map or gain modulation? In: Society For Neuroscience Abstracts, 1997.
- Deneve, S., & Pouget, A. Neural Basis of Object Centered Representations. In: Advances in Neural Information Processing Systems, vol. 11. Cambridge, MA: Morgan-Kaufmann, submitted.
- Driver, J., Baylis, G.C., Goodrich, S.J., & Rafal, R.D. Axis-based neglect of visual shapes. *Neuropsychologia*, **32(11)**, 1353-1365, 1994.
- Hinton, G.E. Mapping part-whole hierarchies into connectionist networks. *Artificial Intelligence*, **46(1)**, 47-76, 1990.
- Olson, C.R., & Gettner, S.N. Object-centered direction selectivity in the macaque supplementary eye. *Science*, **269**, 985-988, 1995.
- Olson, C.R., & Gettner, S.N. Object-centered direction selectivity in macaque supplementary eye field is expressed with respect to multiple axes. In: Society For Neuroscience Abstracts, 1997.
- Pouget, A., & Ducom, J.C. Noise reduction, discrimination and adaptation in cortical circuits. In: Society For Neuroscience Abstracts, vol. 23, 1997.
- Pouget, A., & Zhang, K. Statistically efficient estimation using cortical lateral connections. In: Mozer, M.C.; Jordan, M.I., & Petsche, T. (eds), *Advances in Neural Information Processing Systems*, vol. 9. Cambridge, MA: MIT Press, 1997.
- Pouget, A., Zhang, K., Deneve, S., & Latham, P.E. Statistically efficient estimation using population coding. *Neural Computation*, in press.
- Zhang, K., Pouget, A., & Dayan, P. Using lateral connections for population coding. In: Society For Neuroscience Abstracts, vol. 22, 1996.

DRUG DISCOVERY AND DESIGN: There are currently two faculty members in this area. Dr. Kozikowski's work relates to the design and synthesis of new pharmacological research tools for understanding brain mechanisms, including cognitive drug development. Dr. Wang utilizes molecular modeling techniques as part of drug development.

ALAN P. KOZIKOWSKI, Ph.D.

Development of novel drugs and pharmacological tools for probing the mechanisms of cognitive dysfunction and cellular signaling.

Dr. Kozikowski's group is actively involved in the design and synthesis of new molecular entities for use in probing various aspects of brain function. Such work demands a multidisciplinary setting, in which modern day methods of organic synthesis are coupled with state-of-the-art molecular modeling capabilities, and with cutting edge biology. While details of the various projects are delineated below, we note here that one of the most exciting projects relates to huperzine A. Venture moneys are now being raised to advance huperzine A and one of its more potent analogues to the clinic for the treatment of Alzheimer's disease.

Development of the Laboratory

During the past year a drug discovery group has been assembled within GICCS. A total of eight postdoctoral fellows trained in the art of organic synthesis are presently working in the Kozikowski laboratories. The laboratory has been outfitted with chemical hoods in order to accommodate this chemical synthesis/drug design activity. Moreover, a state-of-the-art high field NMR is now in place which is essential to adequately characterizing all new compounds synthesized in our laboratories. Other spectroscopic tools available for our work include FT-IR, low resolution GC-MS, and polarimeter.

Furthermore, the drug design program has been strengthened through the recruitment of Dr. Shaomeng Wang, an Assistant Professor skilled in the art of computer modeling. Dr. Wang's expertise makes it possible for us to view the target proteins on the computer, especially in the cases where x-ray structural information is available, and to carry out systematic docking of small molecules to the macromolecular targets. Such docking studies allow for the more rational design of small molecules likely to exhibit the desired pharmacological properties. Computer modeling protocols are now being used to design ligands for the dopamine transporter, acetylcholinesterase, and caspase 3.

Project 1: Metabotropic Glutamate Analogues

In a project relating to our interest in elucidating the role of metabotropic glutamate receptor (mGluR) subtypes in normal and pathophysiological states, we have undertaken the design, synthesis and biological assay of compounds that may exhibit selectivity for the individual mGluRs. To date we have discovered that derivatization of quisqualic acid leads to a mGluR2 specific antagonist, and that the N-benylation of the aza analogue of ACPD leads to an mGluR6 selective agonist. The latter compound was found to be neuroprotective in cellular assays of brain injury. Recently, we have now identified a novel bicyclic analog (aminobicyclohexanedicarboxylic acid or ABH₆D) of the prototypical mGluR ligand ACPD that is several fold more potent than ACPD (Scheme 1). Data for four possible isomers of ABH₆D at six of the mGluR subtypes are provided in Table 1. As expected, one of the four isomers is more active than ACPD, while the other three are less active, thus enabling us to define the preferred conformation of ACPD at the mGluRs. It is our intention to further pursue chemical alterations in this lead structure so as to identify ligands of improved subtype selectivity. Using the various lead structures that are now available to us, we will further expand the present efforts using molecular modeling techniques so as to acquire a better understanding of the topography, both steric and electronic, of the individual mGluRs, thus aiding the design of compounds of altered subtype selectivity, potency, and degrees

of agonism or antagonism. This research is likely to find application in the discovery of ligands for clinical use in the treatment of Alzheimer's disease, stroke, spinal cord injury, and Parkinson's disease. Recent reports demonstrate, for example, that mGluR receptor agonists increase the release of soluble amyloid precursor protein derivatives from rat brain cortical and hippocampal slices, thus suggesting mGluR ligands as possible therapeutic agents for Alzheimer's disease.

Scheme 1

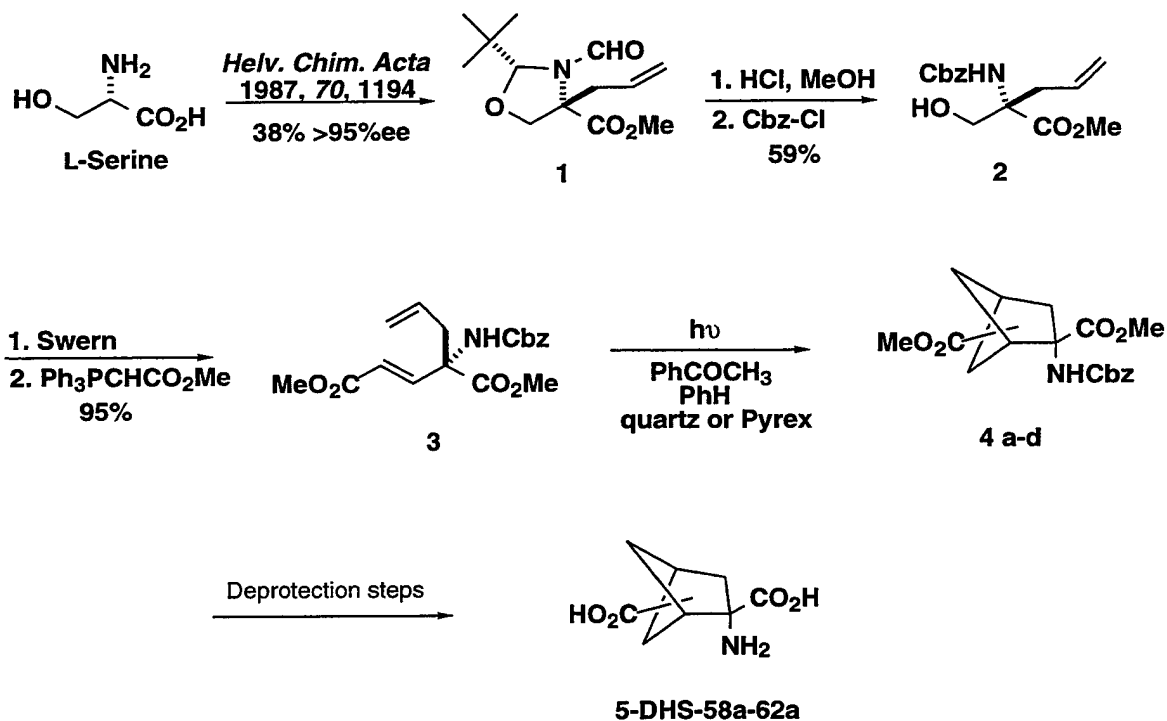


Table 1. EC₅₀ values obtained for the ABH₆D's at six of the mGluR subtypes.

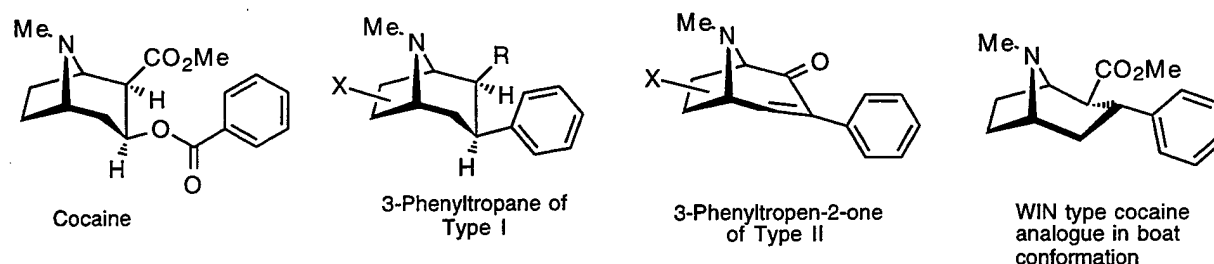
Compound Tested	Group I mGluRs (EC ₅₀ values, μM)	
	mGluR1a	mGluR5a
Glutamate	4.9 \pm 0.2	3.1 \pm 0.2
ACPD	15.0 \pm 2.2	23.0 \pm 2.6
AP4	NE	NE
5-DHS-58a	121 \pm 10	57 \pm 6
5-DHS-59a	1000	1000
5-DHS-61a	232 \pm 23	91 \pm 11
5-DHS-62a	1.6 \pm 0.14	0.72 \pm 0.11

Compound Tested	Group II mGluRs (EC ₅₀ values, μM)	
	mGluR2	mGluR3/1
Glutamate	0.29 \pm 0.07	1.9 \pm 0.31
ACPD	2.0 \pm 0.3	40.0 \pm 5.8
AP4	NE	NE
5-DHS-58a	54 \pm 9	185 \pm 87
5-DHS-59a	1000	1000
5-DHS-61a	38 \pm 10	255 \pm 84
5-DHS-62a	0.33 \pm 0.06	2.2 \pm 1.5

Compound Tested	Group III mGluRs (EC_{50} values, μ M)	
	mGluR4a	mGluR6
Glutamate	9.8 ± 0.8	4.9 ± 0.4
ACPD	~ 800	82 ± 6
AP4	0.33 ± 0.09	0.28 ± 0.02
5-DHS-58a	~ 1000	~ 800
5-DHS-59a	1000	1000
5-DHS-61a	1000	1000
5-DHS-62a	23 ± 7	5.3 ± 0.9

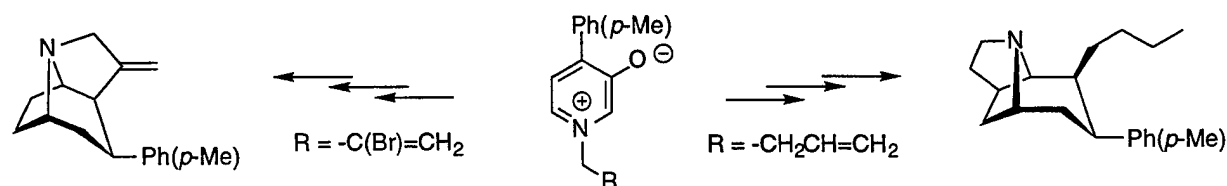
Project 2: Cocaine Medications

We have now worked out methods for gaining access to a wide variety of analogues of cocaine using a dipolar cycloaddition approach of oxidopyridinium salt with dipolarophile. This novel approach allows access to a wide variety of cocaine analogues of Type I bearing diverse functionality at positions 1, 2, 3, 6, and 7 by way of the troponone of Type II. Previously, we had found that methoxylation of cocaine's 6-position led to a compound that acts as a weak cocaine antagonist. The present chemistry thus permits us to expand upon the past work, and to now



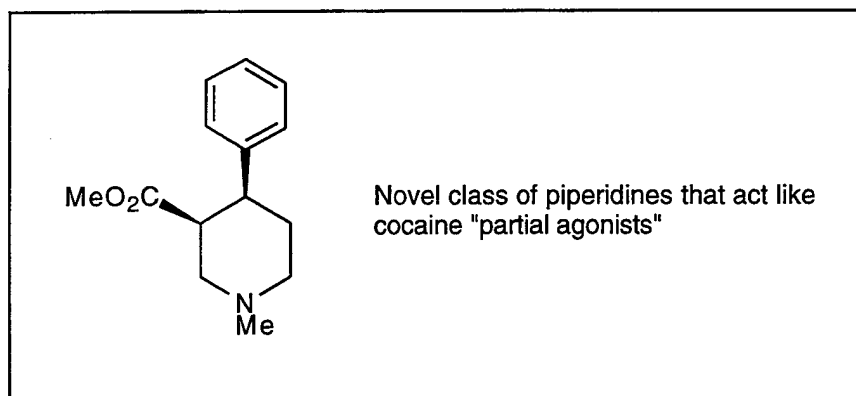
explore whether it is possible to retain such "antagonistic" activity while at the same time increasing compound potency. We have found recently that cocaine analogues in which the tropane ring assumes the boat conformation still retain high affinity for the dopamine transporter (DAT), thus defining further structural aspects of the cocaine recognition site associated with the dopamine transporter. To further define the spatial requirements of cocaine's lone electron pair on nitrogen in its affinity for DAT, we have recently completed the synthesis (Scheme 2) of several rigidified analogues, in which the bridge nitrogen is linked to either the C-2 or C-6 positions of the tropane ring. These compounds are presently in biological testing.

Scheme 2. Cocaine analogues with a fixed nitrogen lone pair.



The identification of a cocaine antagonist or cocaine partial agonist may possibly be useful as a medication in the treatment of cocaine abuse. Recently, we have identified a novel class of piperidine structures that appear to act as partial agonists in rodent models of drug discrimination. This exciting breakthrough is being followed up through further animal studies, in a combination of locomotor assays, cocaine self-administration studies, and drug discrimination paradigms. Examples of data obtained for the trans (+)-piperidine in the locomotor assay and in the

methamphetamine drug discrimination paradigm are shown in the accompanying graphs. Pursuant to this class of structures, other analogues of these piperidines are being synthesized that may possess a longer lasting duration of action.



Project 3: TRH Analogues for Traumatic Brain Injury and Stroke

We have synthesized a number of novel structural analogues of thyrotropin-releasing hormone (TRH) that may find use in traumatic brain injury. A variety of TRH analogues in which its histidine moiety has been replaced by functionality believed to enhance its neuroprotective activity have now been assembled in our laboratories, as discussed in the last report to the DOD. Moreover, we have identified recently certain dipeptide mimics of TRH that can be rapidly synthesized in the laboratory, and which have proven to be very effective in animal models of traumatic brain injury. These new analogues are now under active study in the laboratories of Dr. Faden. Currently, a patent is being prepared on these new structures, and further efforts will be made to examine these compounds in animal models of stroke. Since we are in the process of preparing this patent application, we are not at liberty to disclose the structure of these new mimics.

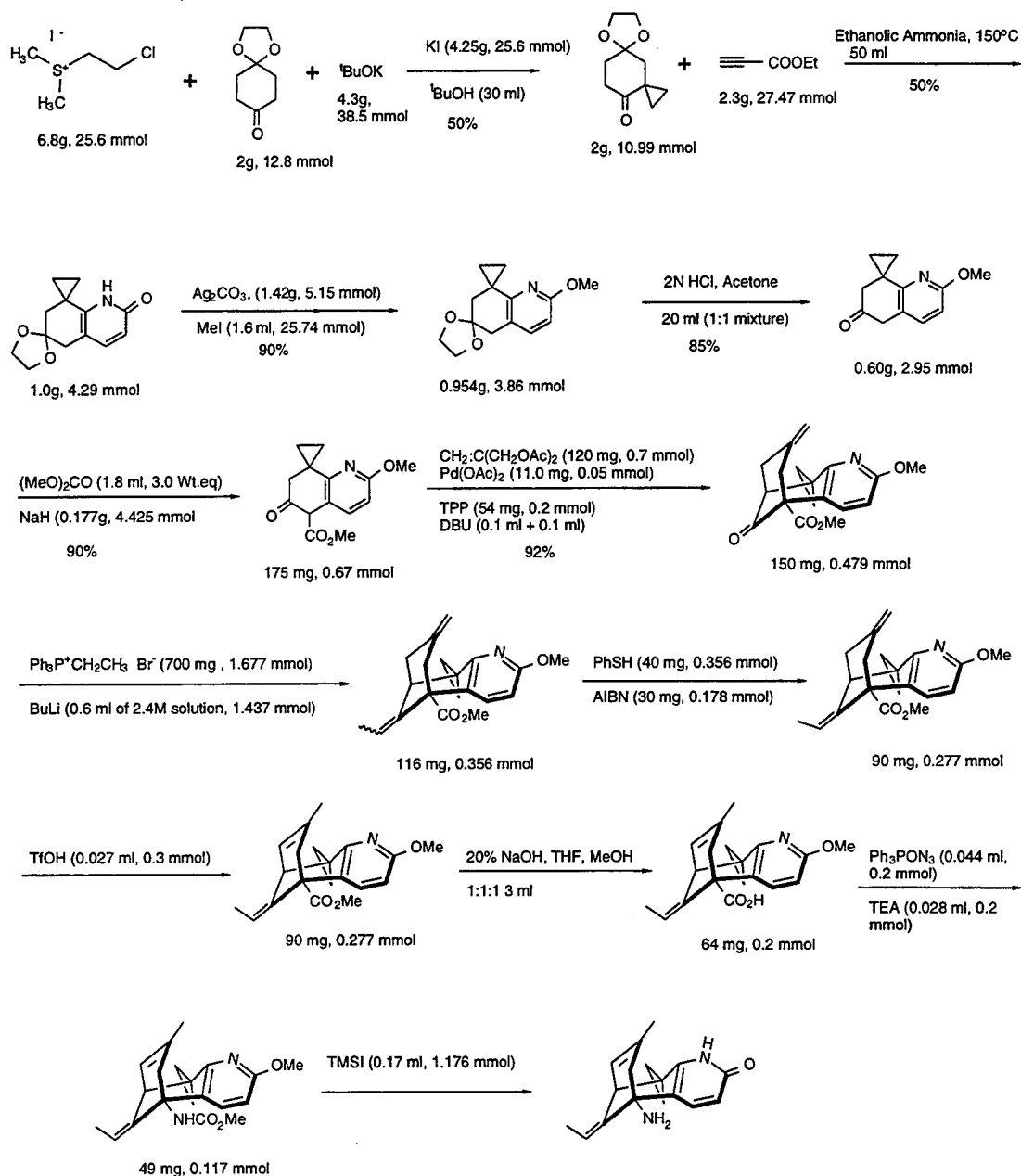
Project 4: Huperzine A and Analogues for Alzheimer's Disease

We have conducted extensive modeling studies on huperzine A, a naturally occurring alkaloid that has shown promise in the treatment of Alzheimer's disease. Through the modeling studies we have now identified compounds that may have an increased potency for inhibiting acetylcholinesterase. The modeling studies make use of a co-crystal x-ray structure of HA in complex with AChE. By placing analogues into the same site as that occupied by HA in the crystal, and performing dynamics simulations, we are able to estimate whether the new analogues are likely to serve as improved inhibitors of the enzyme. For example, using the modeling techniques, we have been able to explain why the location of a methyl group at HA's C-10 position leads to a compound exhibiting 8-fold improved potency, whereas introduction of a C-10 equatorial methyl leads to a compound possessing a higher K_i . In the former case the methyl group points into a hydrophobic region, whereas in the latter, the methyl group points into a more polar pocket. As the size of the C-10 substituent is increased from methyl to ethyl and propyl, activity drops off dramatically, possibly indicating a serious steric interaction of this substituent with the "walls" of the active site gorge. Clearly, while some additional steric volume is available in the region of the AChE binding site occupied by the C-10 axial substituent of HA, the available space is small, with the methyl analogue serving as the optimal structure.

Using such modeling studies, we have now selected additional compounds for synthesis that are likely to show improved activity. By identifying compounds that show altered AChE inhibitory potency, lipophilicity, improved duration of action, etc. it is likely we will be able to identify superior AChE inhibitors for the treatment of Alzheimer's disease. In this direction, we have recently completed the synthesis of the C-10 cyclopropyl analogue of huperzine A (see accompanying scheme). Since the 10,10-dimethyl analogue is slightly more potent than huperzine A, we anticipate that by tying the two methyl groups together, as in the cyclopropyl analogue, we

should obtain an even more potent compound that may exhibit a slower off-rate from the enzyme. This change in enzyme off-rate may in turn confer an enhanced therapeutic advantage to the compound, since a smaller amount of drug would be needed to inhibit the enzyme. Additionally, this more lipophilic compound may more readily penetrate the blood brain barrier. The synthesis of the new analogue is detailed in Scheme 3, and the compound is presently in testing by Doctor Doctor's group at Walter Reed Army Institute of Research for its AChE inhibitory activity.

Scheme 3. Synthesis of the 10-Cyclopropyl Derivative of Huperzine A.

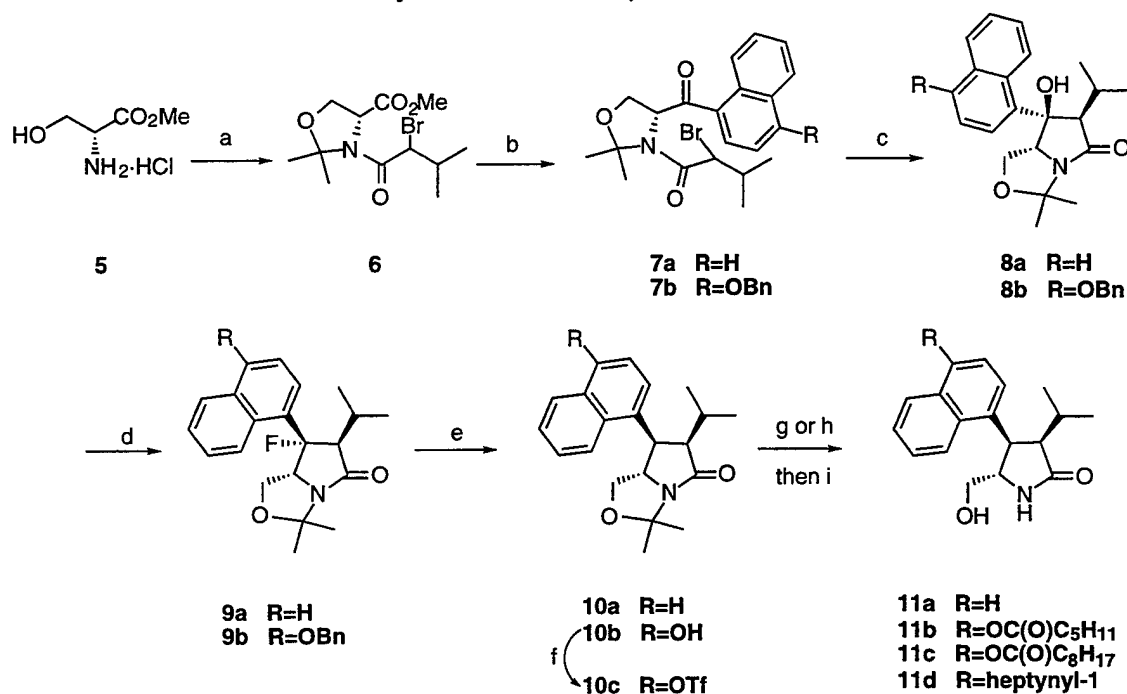


Project 5: PKC Activators as Anti-cancer Agents

We have succeeded to synthesize a new protein kinase C (PKC) activator based upon the natural product lead structure, indolactam V (ILV). PKC plays an instrumental role in a variety of intracellular signaling processes, controlling diverse processes such as memory formation and cellular growth. In order to better elucidate the involvement of PKC in cellular signaling, it is mandatory to identify PKC ligands that show enhanced levels of isozyme selectivity, since at

present at least 11 isoforms of PKC have been characterized. Based upon extensive modeling studies using the crystal structure information obtained for the cys2 activator binding domain of PKC δ , we have designed and synthesized a new series of PKC ligands, the γ -lactams, that are distantly related to ILV. The search for a simpler structural template that retains PKC activating properties was driven largely by our desire to work with a compound that was readily amenable to modification, so that we could more rapidly define those features relevant to the discovery of isozyme selective activators. We have to date been able to achieve the discovery of ligands possessing a potency of 200 nM at PKC α . After several more cycles of modeling, synthesis, and biological testing have been undertaken, it is likely that we may be able to identify ligands of subnanomolar potency. These compounds will then be tested in cellular models as anticancer agents, and if potent as antiproliferative agents, will then be taken into in vivo animal models for the treatment of breast cancer. To date, we have found that certain benzolactam analogs of ILV are active in retarding the progression of tumor development in rodent studies. We anticipate that our recent discovery that these γ -lactams retain significant PKC activating properties will accelerate our search for new anticancer agents.

Scheme 4. Synthesis of novel γ -lactams as activators of PKC.



a. 1) α -bromo-isovaleryl chloride, Et₃N (2 equiv.), CHCl₃, 23°C 2) DMOP, p-TsOH (cat.), Benzene, reflux b. 1) DIBAL, CH₂Cl₂, -70°C 2) Grignard Reagent (2 equiv.), THF, -78°-0°C 3) NMO, TPAP(cat.), 4Å M.S., CH₂Cl₂, 23°C c. SmI₂, THF-HMPA, FeCl₃(cat.), 23°C d. DAST(2equiv.), CH₂Cl₂, -78°C-23°C e. H₂, 5% Pd/C, MeOH f. Tf₂O, 2,6-lutidine, CH₂Cl₂ g. acyl chloride, pyridine, 23°C h. 1-heptyne, 10%mol PdCl₂(PPh₃)₂, CuI(cat.), Et₃N, DMF, 60°C i. 1,2-ethanedithiol (10equiv.), BF₃·Et₂O (2equiv.), CH₂Cl₂, 23°C

Project 6: Design of Inhibitors of CPP32

Apoptosis derives from a Greek word that means to fall off, as leaves from a tree. It is a process in which the cell shrinks, and eventually the apoptotic cell bodies that are produced are phagocytosed. Apoptosis is characterized by preservation of membrane integrity, cytoplasmic and nuclear condensation, reduction in cellular volume, plasma membrane bleb formation, and nuclear fragmentation. During apoptosis the morphological changes are often accompanied by internucleosomal cleavage of genomic DNA; the breakdown of the DNA occurs in discrete fragments of 180-200 base pairs, which appear as a DNA ladder in agarose gel electrophoresis.

Apoptosis differs from necrosis in that the latter involves cell death that is accompanied by inflammatory processes. Thus in apoptosis cells can die one at a time, among a group of healthy cells, whereas in necrosis a whole group of cells may die at the same time. Death by necrosis is generally associated with a traumatic injury, ischemia, chemical exposure, and the like. Apoptosis is often confused or mixed up with programmed cell death (PCD). The latter term originated to describe cell death occurring at normal stages of the developmental program and that is initiated by some physiological trigger. In some cases PCD of cells shares morphological changes that are similar to those of apoptosis, but this is not always so.

While a complete pathway for cell death has not been defined, it is very clear from a number of studies that the CED-3/ICE family of proteases plays an essential role in apoptosis. The CED-3 homologue, CPP32, also known as apopain, plays a definitive role in cell death, for it is involved in the destruction of certain key homeostatic and repair enzymes at the onset of apoptosis. CPP32 degrades proteins by effecting cleavage of functional domains comprised of the $(P_4)Asp-X-X-Asp(P_1)$ motifs. Targets for cleavage by CPP32 include poly(ADP-ribose) polymerase (PARP, which is an enzyme involved in DNA repair), the 460,000 M_r catalytic subunit of the DNA-dependent kinase essential for double-strand break repair, the 70000 M_r small nuclear ribonucleoprotein necessary for mRNA splicing, and other enzymes including protein kinase C delta. Studies have revealed that levels of CPP32 mRNA and activity are elevated in association with apoptosis, and that its inhibition can lead to a reduction in apoptosis *in vitro* and *in vivo*.

Of particular interest to our own research is the structural work that has been done on apopain. Researchers at the Merck Research Laboratories have recently been able to determine the three-dimensional structure of apopain in complex with the tetrapeptide aldehyde inhibitor, Ac-DEVD-CHO. This inhibitor has been shown to have a 49-fold preference for CPP32 versus ICE (interleukin-1 β converting enzyme, which belongs to a second phylogenic subfamily of proteases, and whose role in apoptosis is less secure). In contrast, the tetrapeptide aldehyde Ac-YVAD-CHO is far more selective for ICE ($K_i = 0.76$ nM) than for CPP32 ($K_i = 10,000$ nM).

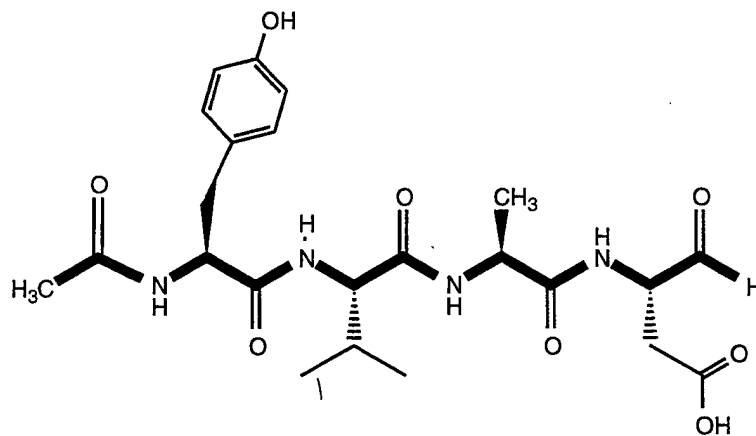


Figure 1. Ac-YVAD-CHO, selective inhibitor of ICE

The x-ray work reveals that the tertiary and quaternary structure of these cysteine proteases are similar. In both proteases two heterodimers associate to form a tetramer, a four-chain assembly with two-fold rotational symmetry. A diagram of the tetrapeptide aldehyde inhibitor bound to CPP32 is provided below. As is clear from this diagram, Cys 285 engages in thiohemiacetal

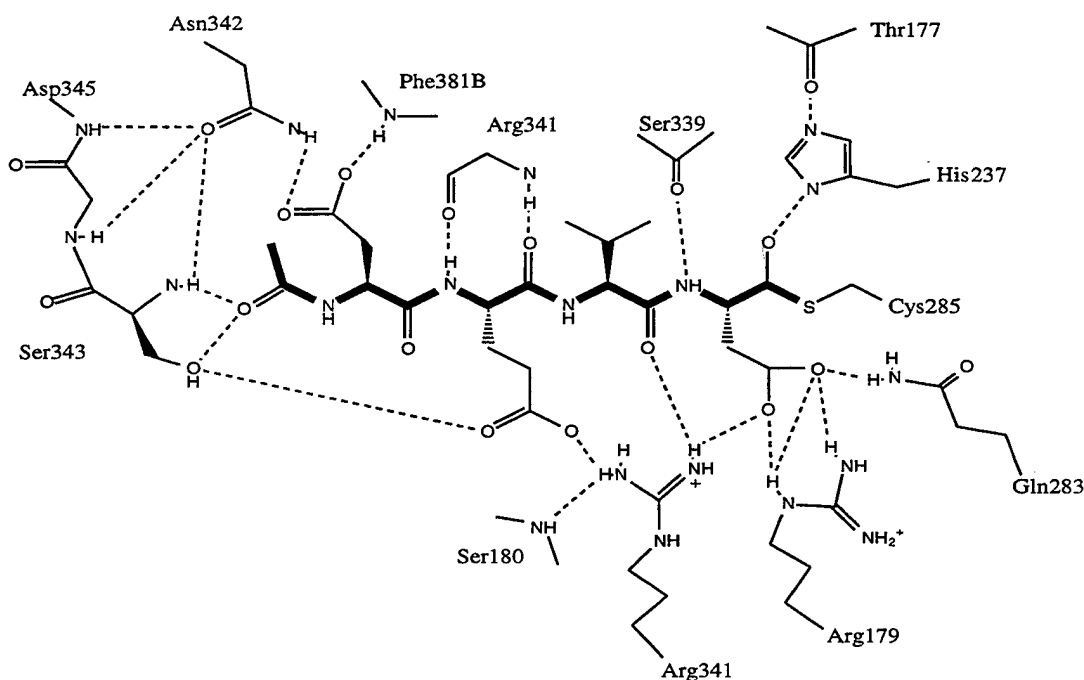


Figure 2. Hydrogen bonds and other polar interactions between the bound tetrapeptide aldehyde inhibitor and CPP32/apopain.

with the aldehyde group, thus mimicking the transition state for amide bond hydrolysis. The binding pockets of ICE and apopain are similar, with the exception particularly of the S_4 subsite which appears to be responsible for the differences in substrate specificities. As expected from the preference for a P_4 Tyr in the ICE inhibitors, the corresponding subsite in the ICE enzyme corresponds to a large, shallow hydrophobic depression, while the P_4 site in apopain is narrow and intimately engulfs the P_4 aspartate residue side chain. Time dependent irreversible inhibitors of ICE have been designed that are acyloxymethylketones, and which react by displacement of the carboxylate group by the active site cysteine 285.

In order to discover compounds that may serve as cell permeable and selective inhibitors of these cysteine proteases, and in particular CPP32, we have chosen to investigate approaches based upon database screening methods in which a pharmacophore query is set up employing various elements of the x-ray structural information of the tetrapeptide inhibitor Ac-DEVD-CHO in complex with CPP32. Using this information, several weak lead compounds were identified by Dr. Wang, and currently this information is being used in conjunction with rational drug design concepts to devise new inhibitors of CPP32. Several likely candidates have been designed, and the chemistry group is now in the process of synthesizing these molecules for biological assay. This project represents a significant new area of our research program, and one which we believe holds tremendous promise in the search for new therapeutics in the treatment of major brain disorders including stroke and Alzheimer's disease.

Conclusion

A number of useful chemical entities have been discovered that may serve as novel pharmacological tools for further elucidating important aspects of cellular communication. Additionally, compounds have been identified that may actually serve as clinical candidates for the treatment of specific disease processes such as Alzheimer's disease, stroke, and cancer. It is our plan to continue to work in the promising areas described above in the coming year, with the intention to further refine the activities of these novel agents. Considerable effort will be spent in the coming year to identify novel inhibitors of the enzymes involved in the cell death cascade, or apoptosis.

SHAOMENG WANG, Ph.D.

Dr. Wang's laboratory is interested in computational structural biology (protein folding, drug and receptor interactions), design and discovery of novel therapeutic agents. He joined the GICCS in July 1996.

Project 1: Design And Discovery Of Cocaine Antagonists For The Treatment Of Cocaine Abuse

Cocaine abuse is one of the greatest concerns of the American public today. It is believed that cocaine produces its "reinforcing" effects through the inhibition of the reuptake of dopamine (DA) by the dopamine transporter (DAT) on dopaminergic terminals. Therefore, a compound that can inhibit the binding of cocaine at the DAT but does not inhibit (pure cocaine antagonist) or only weakly inhibit ("partial agonist") the reuptake of DA could be useful to counter some of the adverse effects of cocaine in cases of cocaine overdose. Such a compound may also be used for maintaining patients in cocaine treatment programs. However, despite intense research efforts directed toward the development of cocaine antagonists, compounds with significant cocaine antagonist activity have not been reported. In the past, due to the lack of cocaine antagonists as lead compounds, most of the chemistry efforts have been devoted toward modifications of known DAT inhibitors, such as cocaine itself. We believe that the discovery of novel lead cocaine antagonists is critical in this stage. Toward this goal, we propose to use a novel approach, termed "3D-database pharmacophore searching" to discover such compounds, which has been found to be effective in discovering novel lead compounds.

In this approach, crucial structural features and their 3D geometrical relationships that are important for compounds inhibiting cocaine binding will be elucidated through molecular modeling studies of known DAT inhibitors. From this information, 3D-pharmacophore models, including both structural and geometric requirements, will be developed. These pharmacophore models will then be used to search a large 3D-database of small molecules to identify compounds that meet the 3D-pharmacophore requirements. Samples of selected compounds will be acquired and evaluated in both [^3H]mazindol binding and [^3H]DA reuptake assays. Compounds that show high potency in the [^3H]mazindol binding assay and little potency in the [^3H]DA reuptake assay will be considered as potential lead cocaine antagonists. These compounds will be further evaluated in assays of cocaine antagonism. For compounds showing significant cocaine antagonist activity, they will be subjected to extensive chemical modifications, with the aid of molecular modeling, to further improve their potency and selectivity.

In this project, we will undertake the following: (1) Molecular modeling of cocaine analogues and other classes of DAT inhibitors to identify crucial structural features and their 3D geometric relationships that are important for cocaine binding activity; (2) Development of 3D-pharmacophore models and search of the National Cancer Institute (NCI) 3D database of 206,876 compounds to identify compounds ("hits") that meet pharmacophore requirements; (3) Biological evaluation of selected "hits" in the [^3H]mazindol binding and [^3H]DA uptake assays. Compounds that show more than 5-fold selectivity between the [^3H]DA uptake and [^3H]mazindol binding assays will be considered as potential lead compounds and will be evaluated further in assays of cocaine antagonism; (4) Molecular modeling studies of cocaine antagonist lead compounds discovered through steps (1) to (3) and development of new pharmacophore models, and repetition of steps (2) and (3); (5) Molecular modeling-assisted design and chemical modifications on these lead compounds, aimed at the further improvement of their potency and selectivity.

A pharmacophore model has been proposed based upon our molecular modeling studies. We have conducted the 3D-database pharmacophore search based upon the pharmacophore model on the National Cancer Institute 3D-database of 200,000 compounds and identified 385 candidate compounds for biological evaluations. The first 70 compounds out of the 385 selected candidates have been tested in the [^3H]mazindol binding assay. Thirteen compounds displayed more than 50%

inhibition at 10 mM in the [^3H]mazindol binding assay. In addition, 23 compounds showed an inhibitory activity of 30% to 50% at 10 mM, 8 compounds showed an inhibitory activity of 20% to 30% at 10 mM in the [^3H]mazindol binding assay. Overall, more than 60% of 70 compounds showed significant activity at 10 mM in the [^3H]mazindol assay. These results clearly demonstrate that the pharmacophore model used in the 3D pharmacophore search is very effective in identifying compounds with diverse chemical structures that can effectively compete with [^3H]mazindol binding to the cocaine site on the DAT.

The most potent compound is capable of inhibiting more than 90% of [^3H]mazindol binding to the DAT at 10 mM and its estimated IC_{50} value is somewhat similar to that of cocaine. This compound, however, shows very little selectivity, since at the same concentration, it also inhibits 86.7% of [^3H]DA reuptake. Therefore, this compound may be a promising lead as a DAT inhibitor, but it may not a good lead compound for the development of cocaine antagonists or of "partial agonists". Nevertheless, since highly potent, lipophilic, long lasting DAT inhibitors may be useful as potential therapies for the treatment of cocaine dependence, we will test such compounds in the NIDA's behavioral screening program.

On the other hand, two other compounds not only showed fairly good potency in the [^3H]mazindol binding but also displayed some selectivity versus [^3H]DA reuptake, thus representing potential promising lead cocaine antagonists. One compound was further tested to determine its K_i values in both the [^3H]mazindol binding and [^3H]DA reuptake assays. By assuming a competitive mechanism, its K_i values were determined to be 2.93 ± 0.03 mM in the [^3H]mazindol binding assay and 22.1 ± 1.5 mM in the [^3H]DA reuptake assay, respectively, in three separate experiments. Its uptake-binding ratio is thus 7.5-fold. This compound is currently being evaluated in a number of cocaine antagonism assays as described in biological evaluation section. This compound may represent a potential promising cocaine "partial agonist" lead compound if its cocaine antagonist activity is confirmed.

Our results clearly show that using a 3D pharmacophore searching approach, we can identify large number, structurally diverse compounds that can potentially compete with cocaine binding to the DAT. Among these large number, structurally diverse compounds, some compounds may display differential activities at the cocaine and DA binding sites.

Future Directions

The discovery of potential cocaine antagonist lead compounds will have significant impact in at least two aspects. (1) Based upon these lead compounds, new pharmacophore models, which incorporate these new information, can be designed. 3D-database pharmacophore searching using these new pharmacophore models based upon cocaine antagonist lead compounds will undoubtedly allow us to discover even better cocaine antagonist leads. (2) Extensive chemical modifications will be made based upon these leads to further improve their potency at the [^3H]mazindol binding and selectivity versus [^3H]DA reuptake. Our ultimate goal is to further develop these lead compounds, through extensive chemical modifications, to arrive at potential clinical candidates for the treatment of cocaine dependence.

Project 2: Design and Discovery of Caspase-3 Specific Inhibitors

Apoptosis, or programmed cell death (PCD), is triggered by a number PCD factors. Inappropriate apoptosis is now believed to contribute to the pathology of several human diseases, including neurological diseases such as Alzheimer's disease and Parkinson's disease, and solid tumors. A number of genes have been identified to play key roles in apoptosis. In *C. elegans*, these genes include CED-9, CED-4, CED-3. In addition, two additional factors, cytochrome C (also designated as Apaf-2, apoptotic protease activation factor 2) and dATP play crucial roles in the activation of CED-3. It has been shown that CED-9, which functions upstream of CED-3 and CED-4, negatively regulates the apoptotic program by preventing the activation of CED-3 and

CED-4, probably through blocking the release of cytochrome C, a key activation factor for CED-3, from mitochondria. CED-4 is required for the activation of CED-3, in addition to cytochrome C.

The apoptotic program delineated in *C. elegans* is conserved in mammalian cells. The corresponding homologues to CED-9, CED-4 and CED-3 are Bcl-2, Apaf-1, and caspase-3. Bcl-2 can block the release of cytochrome C from mitochondria, which prevents the activation of caspase-3 (caspase was derived from cysteine caspase for these cysteine proteases always cleave a site with aspartate residue on the C-terminal). In the presence of cytochrome C and dATP, Apaf-1 binds to cytochrome C and activates caspase-3, although the precise mechanism of this activation is not known. The activated caspase-3 is capable of autocatalysis as well as cleaving and activating other members of the caspase family, leading to rapid and irreversible apoptosis. Activated caspase-3 will cleave and activate the DNA fragmentation factor, DFF, which in turn leads to the degradation of DNA into nucleosomal fragments, a hallmark of apoptosis. Deletion of caspase-3 from the mouse genome through homologous recombination results in excessive accumulation of neuronal cells, owing to a lack of apoptosis in the brain. Addition of active caspase-3 to normal cytosol activates the apoptotic program. A specific, high affinity ($K_i < 1$ nM) caspase-3-specific tetrapeptide inhibitor, Ac-DEVD-CHO, can abolish the ability of cytosol from apoptotic cells to induce apoptosis in normal nuclei and block the initiation of the cellular apoptotic program in response to apoptotic stimuli. These data clearly suggest that caspase-3 is both necessary and sufficient to trigger apoptosis. Although a tetra-peptide inhibitor, Ac-DEVD-CHO, is of high specificity and of high affinity and has served a useful role in defining the enzymology and function of some members of caspase-3 protease family, it is of limited utility for advanced drug development. Clearly, a high affinity, non-peptide, specific caspase-3 inhibitor is of great value to study the functions of caspase-3 in vivo systems. Unfortunately, non-peptide caspase-3 inhibitors have not been reported.

We are well poised for the structure-based discovery and design of non-peptide caspase-3 inhibitors since the X-ray structure of the tetra-peptide inhibitor Ac-DEVD-CHO in complex with caspase-3 has been determined. Based upon the X-ray structure, the cysteine 285 sulfur reacts with the aldehyde group on the tetra-peptide inhibitor and forms a thiohemiacetal, which is stabilized by His 237 through a hydrogen bond formed between the hydroxyl of the thiohemiacetal group and the nitrogen at the d1 position on the His 237 ring. The carboxylic group of the aspartic residue at P1 position plays an important role by forming a number of hydrogen bonds with Arg 179, Gln 283 and Arg 341. The hydrophobic side chain of valine residue at P2 position in the inhibitor interacts with a number of hydrophobic residues, including Tyr 338, Trp 340, and Phe 381. The glutamate residue at P3 position forms a number of hydrogen bonds with the side chain of Arg 341 and Ser 343. The aspartic acid at P4 position forms two hydrogen bonds between its carboxylic group and the side chain of Asn 342, and with the backbone NH group of Phe 381. The carbonyl group of the acetyl group forms a strong hydrogen bond with the backbone NH group of Ser 343.

Discussion

Based upon the X-ray structure of caspase-3 in complex with the tetra-peptide Ac-DEVD-CHO, the aldehyde group is essential for the inhibitor to react with the sulfur group of Cys 285. In addition, the carboxylic group of the aspartate residue at the P1 position on the inhibitor plays a crucial role through interacting with a highly charged positive pocket in the receptor binding site. The isopropyl side chain of the valine residue at the P2 position on the inhibitor appears to be of importance since it interacts with a number of hydrophobic residues in the receptor. As mentioned above, the glutamate residue at the P3 position and the aspartate residue at the P4 position may be important for both binding affinity and specificity. Attempts to identify compounds that will mimic all these important interactions were not successful. Thus, we turned our efforts to identify compounds that will mimic the crucial interactions at the P1 and P2 positions.

We have therefore constructed a pharmacophore model that consists of the aldehyde group and the carboxylic group on aspartate residue. The geometric parameters between these two groups, as revealed by the X-ray structure, were incorporated into the pharmacophore model since these parameters are probably important for the effective interactions between the inhibitor and the receptor. A 3D-database search of the National Cancer Institute 3D-database of 216,000 compounds retrieved a number of compounds that meet the requirements of the pharmacophore model. The samples of these compounds were obtained and these compounds were then evaluated for their ability to block the caspase-3-like activity in cellular extract in collaboration with Dr. Alan Faden.

One compound with molecular weight less than 300, displays significant activity (we estimated that it's activity is about 500-fold less potent than the extremely potent tetra-peptide inhibitor, Ac-DEVD-CHO). Based upon this compound, we have designed new compounds that can mimic all the essential moieties in the tetra-peptide inhibitor.

Future Directions

These newly designed compounds will be synthesized in collaboration with Dr. Alan Kozikowski. Then these new compounds will be tested for their ability to inhibit the caspase-3 activity in collaboration with Dr. Alan Faden. It is expected that potent, non-peptide, highly selective caspase-3 will be yielded from this project.

Project 3: Computational Structural Biology

3a. Protein folding-A new and powerful free energy biased, computer simulation method

Three-dimensional structures of enzymes ultimately determine their biological properties. As genome science rapidly evolves and develops, it is increasingly important to have the ability to predict the three-dimensional structures of enzymes of interest since experimental determination of the 3D-structures of enzymes of interest using either X-ray diffraction or multi-dimensional NMR techniques is painstaking and slow. Toward this end, we have developed a novel and powerful computational method termed "free energy biased molecular dynamics simulation approach" for the studies of the kinetic process of protein folding and the prediction of protein structure.

Among many prediction and search approaches, molecular simulation method displays a number of promising prospects. It takes atomic interaction details into account and directly incorporates both enthalpy and entropy effects. However, molecular simulation of a large system such as enzymes with thousand atoms is very time consuming and the time scale it can access is very limited (often limited to nano-seconds). Many important biological processes such as protein folding and drug-receptor binding takes place in a time scale of from micro- to milliseconds and there are beyond the reach of current computer power with conventional simulation techniques. Therefore, in order to study these biological processes using simulation methods, we have to either simplify the systems of interest or to improve the simulation efficiency dramatically.

We have developed a new algorithm called "free energy biased molecular dynamics simulation approach" because this algorithm efficiently directs a system moves toward a lower free energy state. Although conventional simulation methods also direct a system toward lower free energy states, a system need to overcome many local energy barriers before it reaches the lowest free energy state. This is especially true in dense phase. For instance, a peptide in aqueous solution can hardly change its conformation in hundreds of pico-seconds, and to fold a peptide in explicit water with conventional simulation methods is still not possible at the present time.

The efficiency of this algorithm can be easily seen by comparing simulations of substance P, a important neuro-peptide of 11 amino acids, in explicit water with conventional simulation and with our new algorithm. With our new algorithm and within 200 pico-seconds, the peptide folded to a partial helix conformation, which agrees well with NMR result [1]. While with the

conventional MD simulation of the same time period, the peptide only fluctuated around the starting extended conformation (Fig. 1).

With this algorithm we also studied the folding of several other peptides. A synthetic 16-residue peptide Ac-AAQAAAQAAAQAAY-NH₂ was observed to fold into a two-segment helix conformation. Experiment measurement found this peptide forms about 50% helix in water [2]. Four b-hairpin sequences[3,4], I. RGITVNGKTYGR; II.YQNPDGSQA; III. IYSNPDGTWT; IV. IYSNSDGTWT, were simulated in water and certain percent of b-sheet conformations were observed (Fig. 2).

To extend this algorithm to protein folding studies, we implemented a solvent accessible area solvation model[5]. We have applied this algorithm to a 23-residue designed sequence which is so far the shortest peptide that has a well defined tertiary structure in water without disulfide bonds [6]. It has a b-sheet near the N-terminal and a helix segment near C-terminal, and the two structures arranged to form a tertiary structure. Within 1000 pico-second simulation, we observed the folding process and transformation between different conformations (Fig. 3). It was also found that the final dominant conformation of this peptide resembles the experimentally observed structure.

Future Directions

Since this new algorithm improve the simulation efficiency in an order of 100- to 1000-fold in comparison with convention simulation methods, we will be able to apply this efficient and novel new algorithm to fold peptides with up to 50 amino acids to investigate the detailed protein folding kinetics such as b-amyloid, which has important implication in Alzheimer's disease. We will also be interested to utilize our new method in protein structure prediction. In addition, we will investigate the detailed kinetic process of a drug molecule binding to its enzyme using this efficient computer simulation technique.

Project 3b. Drug-receptor interactions: A new monte carlo docking method

It has been well recognized that a drug molecule excises its biological effects through its specific binding to its receptors. Therefore, the ability to be able to predict the precise manner a drug molecule binds to its target is of paramount importance to the understanding of the mechanism of a drug and to the structure-based drug design. Docking is the operation to place a ligand or a drug molecule into the receptor active site with the most energetic stable binding mode. Our docking philosophy is to try to find global minimum in terms of total system potential energy. Obviously, this is a non-trivial problem since multiple dimensionality is involved in the global minimum searching. Toward this goal, we have developed a new Monte Carlo simulation docking method and this is coded into a MCDOCK computer program.

In the MCDOCK, receptor and ligand 3D structures are used as the input data. Often the 3D-structure of the receptor (enzyme) is obtained through X-ray diffraction or NMR techniques, or computer predictions. The structure of the ligand can be generated from computer programs such as CORINA. Then, ligand is placed into the binding pocket of receptor by comparing the relative orientation of them. This step is called geometry-based docking, which serves as a pre-docking. This step is quick but not very accurate. Although in some cases, it can predict the binding-mode of a ligand quite well. After the pre-docking step, energy-based MCDOCK is performed to search potential energy minimums by combining different Markov chains and different sampling techniques. There are two kinds of Markov Chains employed in the energy based docking, single main chain and multiple side chains. Each point along these chains represents a random sampled configuration. We split the searching task into non-localized and localized searching, which are performed in the main chain and side chains respectively. The main chain searching is assigned with a higher temperature in the canonical sampling. This is a non-localized searching and the probability to overcome certain energy barrier is increased with increasing temperature. Larger step

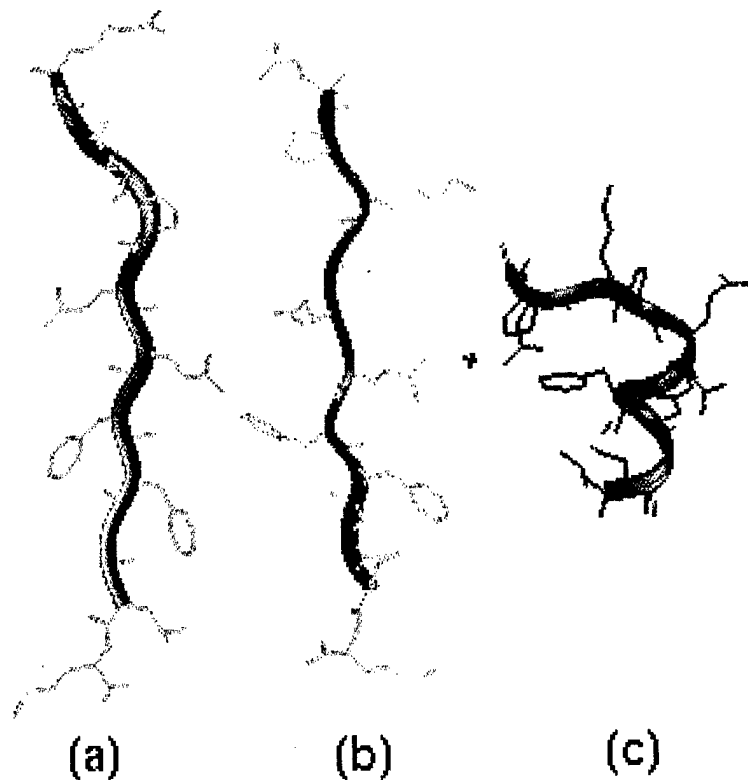


Fig.1 The conformations of substance P in water. (a) Starting conformation; (b) After 200 ps simulation with conventional MD method; (c) After 200 ps simulation with our FBMD method.

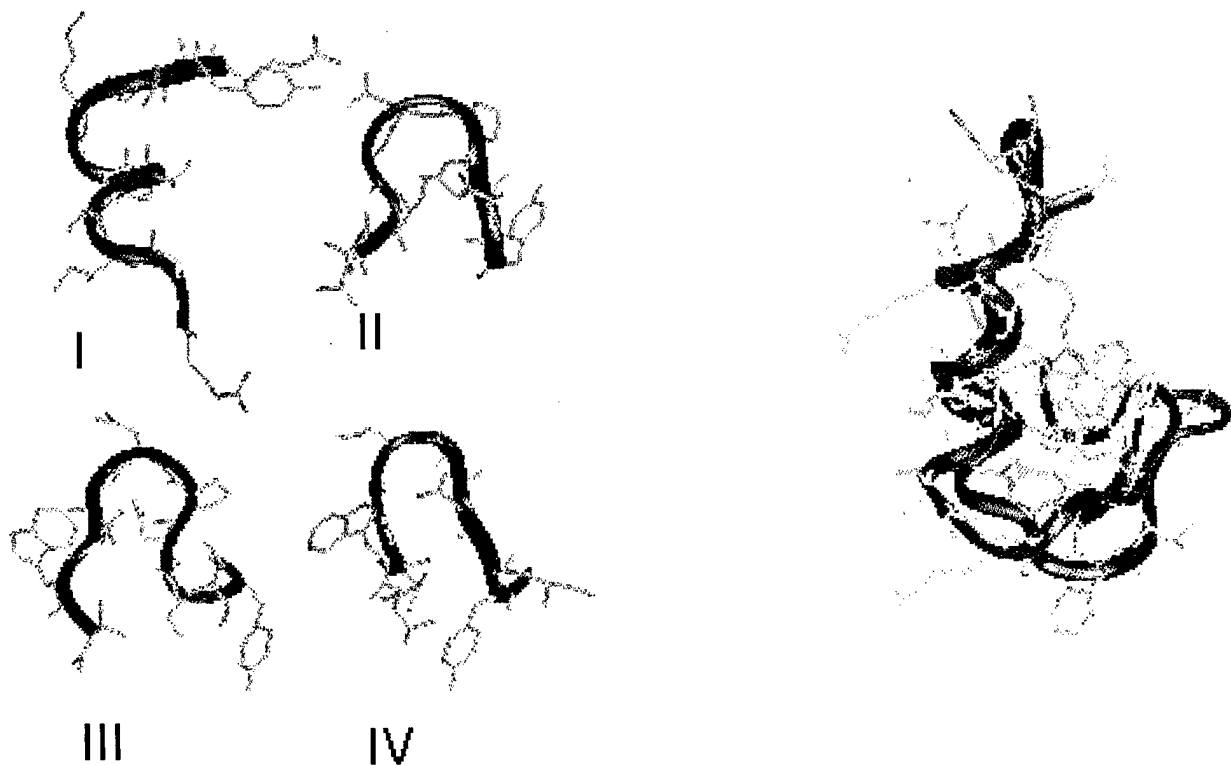


Fig.2 Solution conformations of four designed Peptides from the FBMD simulations.

Fig.3 The tertiary structure of the 23-residue peptide obtained by our FBMD simulation (red) and from NMR experiment (green).

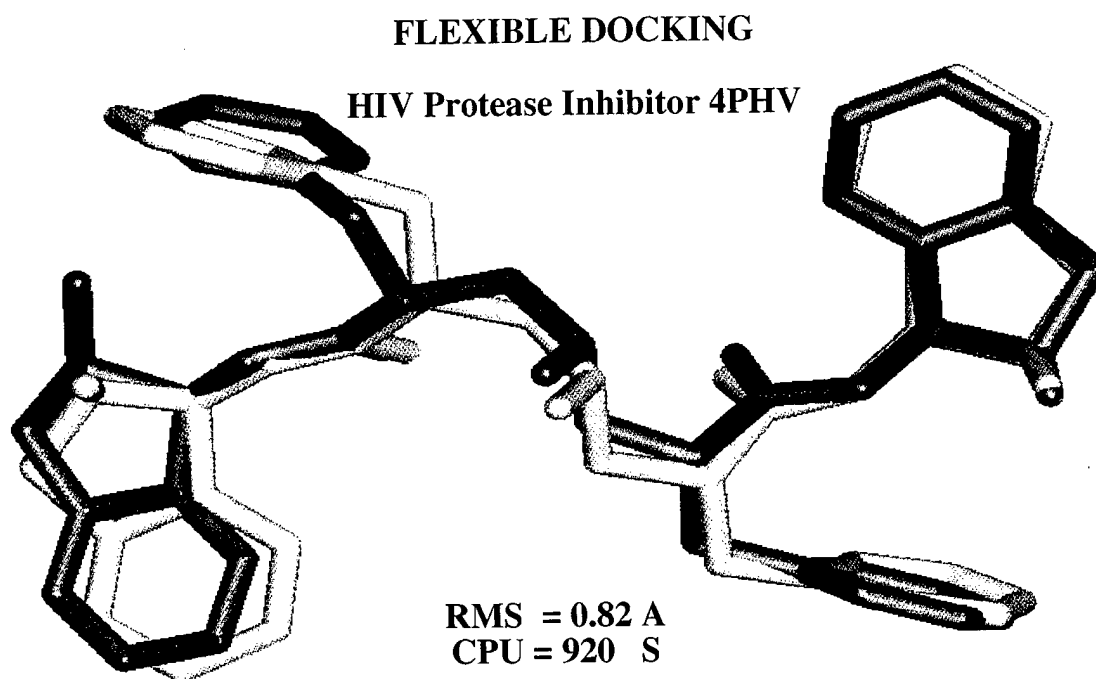
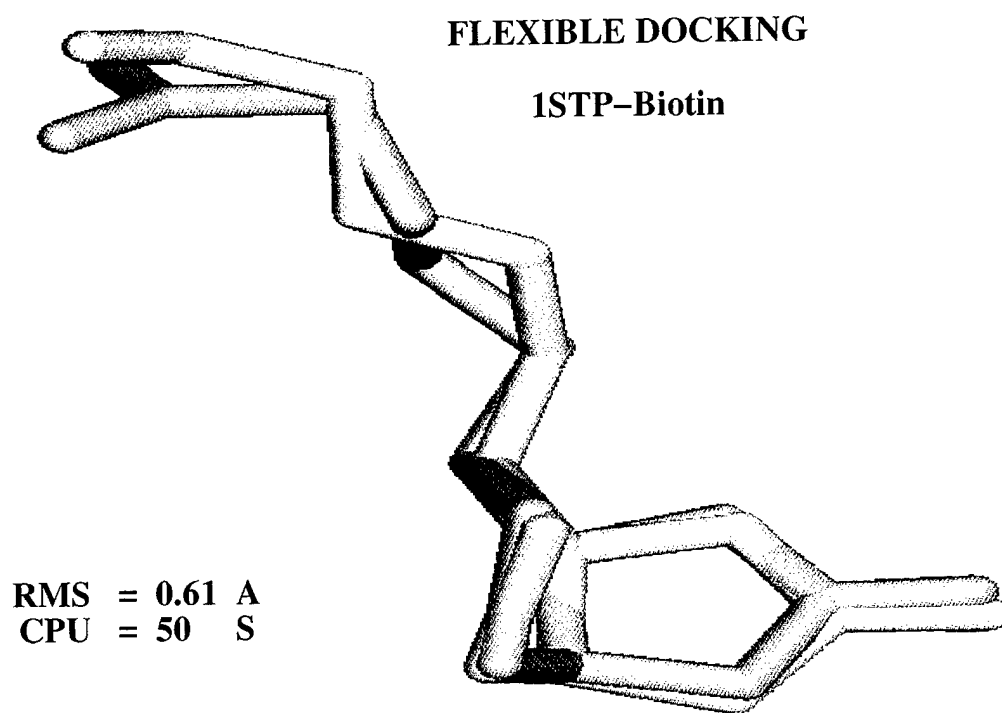


Figure 4. Docking studies of ligands binding to their receptors.

lengths are employed in the main chain searching. Consequently, it is less precise to locate the accurate local minimum in the potential surface. This main chain is divided into several segments and the configuration with the lowest energy within each segment is recorded. Those side chains are propagated from these recorded configurations in main chain by a simulated annealing method, which is to gradually reduce the temperature in the MC simulation and more precisely locate local minimum. The step lengths in the side chain simulations are normally set to be about 10 to 50% of that in the main chain simulations. The side chain searching is a localized searching. The main purpose of the side chain simulations is to more precisely locate the local minimum. The lowest energy configuration from these side chains is then further refined by increasing interaction cut-off value. We also implemented different sampling schemes to optimize the probability to overcome different energy barrier, such as global sampling of three overall Euler's angles and all torsion angles of ligand as well as Markov chain sampling of all variables. To enhance the searching efficiency, there is one importance sampling distribution developed in our Monte Carlo searching using a effective temperature.

We have tested 29 complexes which their binding modes are known from X-ray diffraction. For the rigid body docking, an average RMS (root of mean square) value of 0.5 D was obtained for all-non hydrogen atoms for the ligand between the predicted and the X-ray determined binding modes. For flexible ligand docking, RMS of 1 D was obtained. In addition, our method is very fast. Two examples of such predictions are shown in Figure 4. On average, it takes about 60 seconds for rigid body docking and less than 900 seconds for flexible ligand docking. Therefore, this new method will be a powerful tool for the studies of drug-receptor interactions and for structure-based drug design and discovery.

Future Directions

We plan to take the flexibility of the receptor into account in our MCDOCK program. We will investigate the role of X-ray crystallographic water molecules in drug-receptor interactions. We plan to utilize this new and efficient docking algorithm in a number of drug design and discovery projects.

MOLECULAR NEUROBIOLOGY AND PLASTICITY: There are three faculty in this research area. Dr. Etcheberrigaray evaluates molecular mechanisms of Alzheimer's disease with particular reference to a novel potassium channel and a novel G- protein. Dr. Faden's group evaluates the molecular and cellular correlates of secondary neuronal injury following trauma, including apoptosis. Dr. Swope's research relates to the actions of novel receptor protein kinases.

RENÉ ETCHEBERRIGARAY, M.D.

The principal aim of the research program is to study molecular alterations in Alzheimer's disease. The research focuses on ion channels (potassium channels, IP_3 calcium release channel), second messengers (intracellular calcium, inositol cascades), and phosphorylating enzymes such as protein kinase C. These molecules (and associated cellular processes) have been implicated in mechanisms of memory storage and also in cell toxicity events. Thus, their alterations may be of particular relevance in AD pathophysiology. Fibroblasts are the principal cellular model for these studies. We have initiated projects to study in parallel some such alterations in brains from AD patients. Additional projects in early stages of development include: the study of the influence of presenilin-1 mutations in calcium regulation and ion channel activity, possible link between the - amyloid fragment C100 on IP_3 -mediated calcium release, and regulation of soluble APP secretion by various novel PKC activators.

Project 1: Restoration of K^+ Function in AD Fibroblasts by Novel Activators of PKC

Recent research has identified consistent molecular alterations in fibroblasts from AD patients as compared to controls including young, age-matched, and individuals suffering from other neurological and psychiatric conditions. Briefly, we have identified a dysfunctional K^+ channel and an enhanced IP_3 mediated calcium release in fibroblasts from AD patients. In addition, the K^+ channel defect was induced by -amyloid treatment (10 nM) in otherwise normal fibroblasts. These studies have provided the bases for potential diagnostic methods using combined molecular changes as well as new venues on understanding the pathophysiology of AD. In addition to the above mentioned changes, alterations in protein kinase C have been found in fibroblasts and brains of AD patients. Studies have found reduced levels of PKC in brains and in fibroblasts of AD patients. Immunoblotting analyses revealed that only the α isoform was significantly reduced. PKC may also play a role in APP processing since it contains phosphorylation sites and PKC activators influence the type of secreted APP products. It has been shown that PKC activation can increase the rate of the non-amyloidogenic processing in cellular models. Therefore, the general finding of reduced PKC amounts and/or activity in AD (brain and fibroblasts) is consistent with the apparently normal regulatory role of PKC favoring non-amyloidogenic processing of APP. My principal goal is to understand the potential involvement of protein kinase C in the context of the above mentioned K^+ channel alterations and to provide a pathophysiological important link between these alterations. Electrophysiological and calcium imaging techniques have been employed to conduct this project.

A. Calcium Imaging. Human fibroblasts from AD patients were obtained from the Coriel Cell Repositories (Camden, NJ) and cultured as described (9, 11). In brief, cells were seeded in 25 mm glass cover slips that were placed in 35 mm Nunc dishes with Dulbecco's modified Eagle's culture medium (DMEM) supplemented with 10% fetal calf serum. Cells were used 3 to 5 days after seeding at uniform subconfluent density levels (ca. 180 cells per mm^2). Culture medium was removed just before experiments. Of the familial AD cases that were studied, five cell lines belonged to the chromosome 14-linked Canadian family 964, whose affected individuals were recently demonstrated to carry presenilin 1 mutations. Additional eight to ten cell lines from other AD kindreds carrying different mutations and five cell lines from sporadic cases were also studied. Five cell lines from age-matched controls were tested as well. Many of these cell lines have been

extensively characterized for K⁺ channel function in previous studies. Calcium measurements were performed as follows: culture medium was removed and cells were washed at least three times with BSS (in mM: NaCl 140, KCl 5, CaCl₂ 2.5, MgCl₂ 1.5, HEPES 10, Glucose 5, pH=7.4). The fluorescent probe was loaded by incubating the cells in 1 M (in BSS) fura 2-AM (Molecular Probes) for 60 min at room temperature. After loading, cells were washed thoroughly with BSS or BSS-0 Ca²⁺ (in mM: NaCl 140, KCl 5, CaCl₂ 0.1, MgCl₂ 1.5, EGTA 1, HEPES 10, Glucose 5, pH= 7.4). After washes, 1 ml of fresh solution was added for intracellular Ca²⁺ baseline measurements. Cells were treated with the novel, isozyme-selective PKC activators, benzolactam and LQ2. These compounds are analogs of the natural product indolactam and they can be modified to achieve enhanced isozyme selectivity. As per preliminary results, 1 and 15 min incubation with 50 nM benzolactam were used to test all cell lines. In addition, well known PKC activators such as phorbol-12-13 dibutyrate (PDBu) and the inactive control phorbol 4 were also used within the same concentration range as for benzolactam. Dimethyl sulfoxide(DMSO) was used to make up stock solutions of all compounds, maintaining final concentration of DMSO between 0.4% to 0.6%. The TEA (Sigma) challenge was performed by adding to the dish 3 ml of TEA-modified BSS (TEA-MBSS) solution (in mM: TEA 133.3, NaCl 6.7, KCl 5, CaCl₂ 2.5, MgCl₂ 1.5, HEPES 10, Glucose 5, pH= 7.4). This solution was adjusted to prevent osmolarity changes. The 334 /380 nm ratios was acquired at a rate of 1/sec. for about 300 sec, with a Zeiss-Attofluor system. A 40x Zeiss Fluor (oil immersion) objective lens was used. At least five dishes of a given cell line were used for each experimental condition. The number of cells measured per cell line and condition was > 50. In a given cell, an elevation of at least 100% from baseline was considered a "response". Experiments for each cell line was repeated on at least one separate occasion (minimum one week interval).

B. Electrophysiology. Cell culture procedures were performed as for imaging experiments, except that cells were seeded in 35 mm Nunc petri dishes. Ion channels were measured in cell cultures at the same stage as for the imaging experiments. Patch clamp experiments were performed at room temperature (21-23 C) following established procedures. Culture medium was removed just before the experiments. After rinsing, 1 ml of bath recording solution (in mM: NaCl 140, KCl 5, CaCl₂ 2, MgCl₂ 1, HEPES 10 NaOH), pH= 7.4) was added. Pipettes were made with a Mecnex PC, pipette puller from blue tip capillary tubes (I.D. 1.1-1.2). They will be filled with the following solution (in mM): KCl 140, CaCl₂ 2, MgCl₂ 1, HEPES 10(NaOH), pH= 7.4. Microelectrode resistance was 6-8 M . Pipettes were driven by a Burleigh piezoelectric micromanipulator. Cells were visualized under an inverted Zeiss 105 microscope. Recordings were obtained with an Axopatch 1D amplifier, digitized and acquired with a PC based system (Digidata 1200, Axon Instruments). The recordings were also stored on tape (PCM/VCR) for later analyses. Data acquisition and analyses were performed with Pclamp 6 and Axoscope software packages (Axon Instruments). Most of the experiments were conducted in the cell-attached mode because the basic initial characterization was conducted with this modality. Furthermore, the cell attached mode more closely parallels the fluorescent imaging experiments and the cells' integrity is preserved. Additional experiments using the whole-cell were performed in a subsample to determine if other K⁺ currents, in addition to the 113 pS channel, are affected in AD and/or involved in the TEA response. It will be interesting to explore if a K_A type of current is affected (and perhaps restored) since this type was found to be highly sensitive to β -amyloid treatment. Treatments with the same compounds listed above will be conducted after obtaining base line recordings. Experimental conditions will be kept as identical as possible to those employed in the imaging experiments.

C. PKC Assays. Standard immunoblotting techniques was used to directly quantify the isozymes α , δ , ϵ , ζ , and in response to treatments with PKC activators. These isoforms are known to be expressed in fibroblasts. Particular attention was devoted to the isoform since it has been consistently implicated in AD. The same cell lines from AD and control donors tested by fluorescent imaging and patch clamp were used here. The treatments with PKC activators were conducted in a similar manner (incubation times, concentrations) as done for imaging and

electrophysiological experiments. Cell culture conditions were as described for the previous experiments but the cells were grown to confluency in T-75 culture flasks. Culture medium was removed, the cells rinsed with cold PBS and then scraped in PBS. The cell pellet was collected by low speed centrifugation (800 rpm, 10 min). The pellet was resuspended in 2 ml of the following homogenization buffer (in mM unless otherwise noted): Tris-HCl 20, EGTA 2, EDTA 2, DTT 5, sucrose 320, phenylmethanesulfonylfluoride 2, aprotinin 25 µg/ml, leupeptin 20 µg/ml, pH=7.5. Homogenization was achieved by sonication. Ultracentrifugation was used to separate particulate and soluble fractions. The resultant pellet was resuspended in the same buffer plus Triton X-100 (1.0%), sonicated, and incubated on ice for 45 min. Protein determination was carried out using the Pierce kit BCA Protein Assay Reagent following the manufacturer's directions. Samples were diluted with running buffer (1:1)(Novex), boiled for 5 min and loaded (15 µg of protein per lane) on a 12% precasted SDS-PAGE gel and later electrophoretically transferred onto nitrocellulose membranes. Nonspecific binding was blocked (1h) with Blotto (PIERCE). Monoclonal primary antibodies (anti-PKC, Transduction Laboratories) was added (1:250) and incubated overnight at 4 C. After thorough washes and a 1 h incubation with secondary antibodies (alkaline phosphatase anti-mouse IgG, Vector Laboratories) the blots were developed with an alkaline phosphatase kit (Vector Laboratories) following the manufacturer's instructions. Densitometric analyses were performed using NIH image version 1.6. PKC activity were determined by using non-radioactive methods. A commercially available kit (PIERCE) was employed for this purpose.

The different tissue distribution, apparently distinctive roles of different isozymes, and the differential involvement in pathology makes important to use pharmacological tools that are capable of preferentially target specific isozymes. Recent research in the medicinal chemistry field has resulted in the development of non-tumor promoter PKC activators that target with greater specificity the α and β isoforms. The compound to be used here- (2S,5S)-8-(1-Decynyl) benzolactam V (benzolactam)-is a derivative of the natural product indolactam. Indolactam was first isolated from the mycelia of *Streptomyces mediodicidicus* and is a member of the teleocidins family. The specificity to particular isozymes appears to derive from the maximum energy interaction between aromatic rings of benzolactam and four residues (different for different isozymes) within the regulatory domain of the protein. Conformational aspects also seem to play a role in conferring isozyme specificity. LQ2, a related compound, will also be used. These compounds, like phorbols, compete for the regulatory domain of PKC.

TEA induced calcium responses. Calcium levels were measured in several cells simultaneously using fluorescent imaging techniques. Typical images of basal and elevated calcium levels in fibroblasts are depicted in Fig. 1.

Baseline TEA responses (measured as % of cells responding) have been documented to be minimal, in general below 10%, in cell lines from AD patients. This finding was confirmed for the cell lines examined here. Familial Alzheimer's disease cell lines (FAD) AG06848, AG08170, AG04401, and AG07872 also exhibited minimal responses to TEA as depicted in bar graphs. The same held true for three sporadic AD cases: AG06263, AG07375 and AG07377. There was, however, a significant increase in the % of cells responding to TEA in cells from FAD and SAD cases treated for 1 min with 50 nM of the novel, isozyme()-selective PKC activator, benzolactam, compared to the control group ($p < 0.005$, Mann Whitney). The well known, non-selective PKC activator PDBu was also used. After PDBu incubation for 45 min, the % of cells responding to the TEA application was not significantly different from the control group. Shorter incubation time was also without effect in both cell lines. The control group included untreated cells and cells treated with DMSO alone and the inactive compound 4- β -phorbol for each cell line. The number of cell lines tested per cell line and per condition was >100 (=6,000 total number of cells tested).

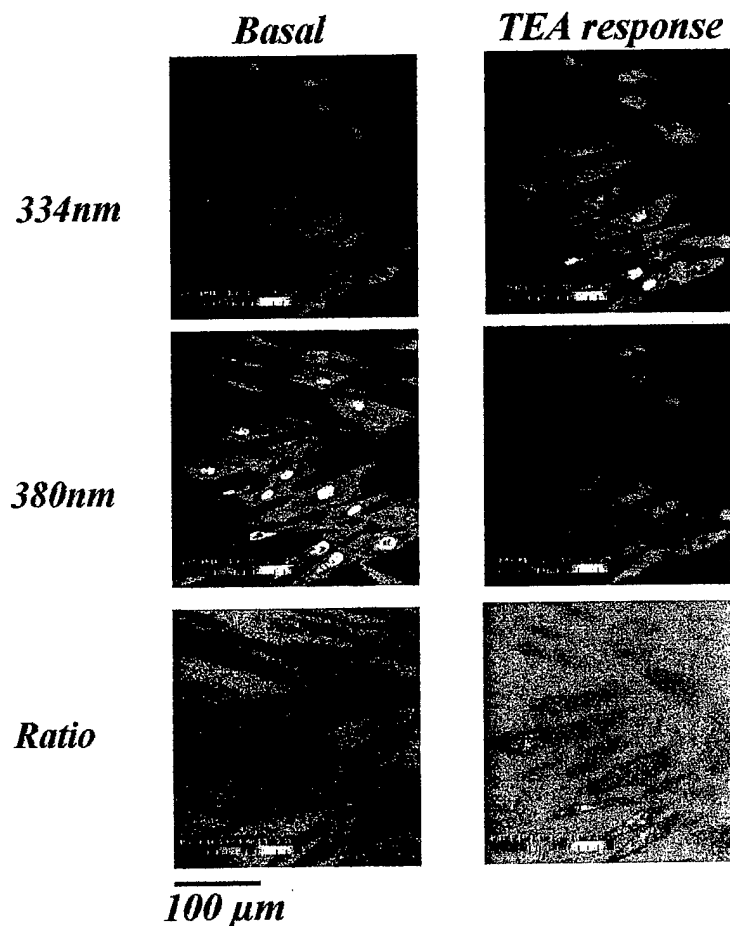


Fig. 1. Human Fibroblasts. Fluorescent images of human fibroblasts in culture at subconfluent levels. Pseudo color images represent calcium levels before and after TEA application as seen when cells are excited by 334nm (numerator), 380nm (denominator) UV light. The 334/380 nm ratio is represented in the bottom set of ratio images.

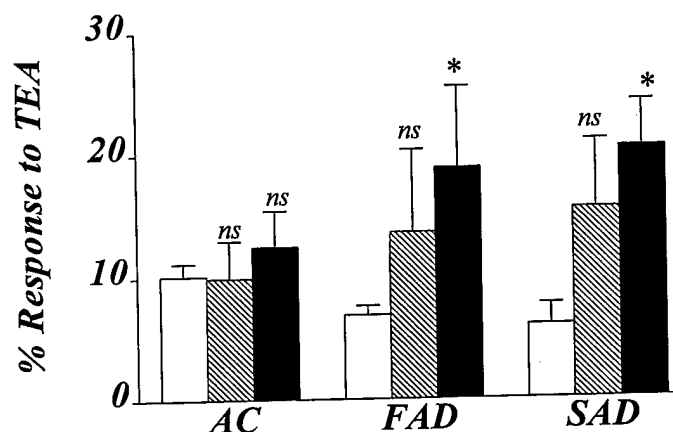


Fig. 2. TEA Responses. Calcium elevations in response to TEA (as % of responding cells). Response to TEA is pooled across cell lines for each group - age-matched control (AC), Familial Alzheimer disease (FAD) and Sporadic Alzheimer disease (SAD). Open bars represent response in untreated, DMSO-treated cells and 4- β -phorbol-treated cells while hatched and solid bars indicate response in cells treated with PDBu and BL, respectively. Benzolactam treatment significantly increased the response to TEA in FAD and in SAD but not in AC cell lines compared to control group. In contrast, there was no effect of the non-selective PKC activator, PDBu in any of the cell lines.

Examples of typical time courses of calcium responses are depicted in Fig. 3. The left panel illustrates the normally observed lack of effect of TEA in AD cell lines. The right panel shows that pretreatment of the same cells with benzolactam "restores" the TEA response.

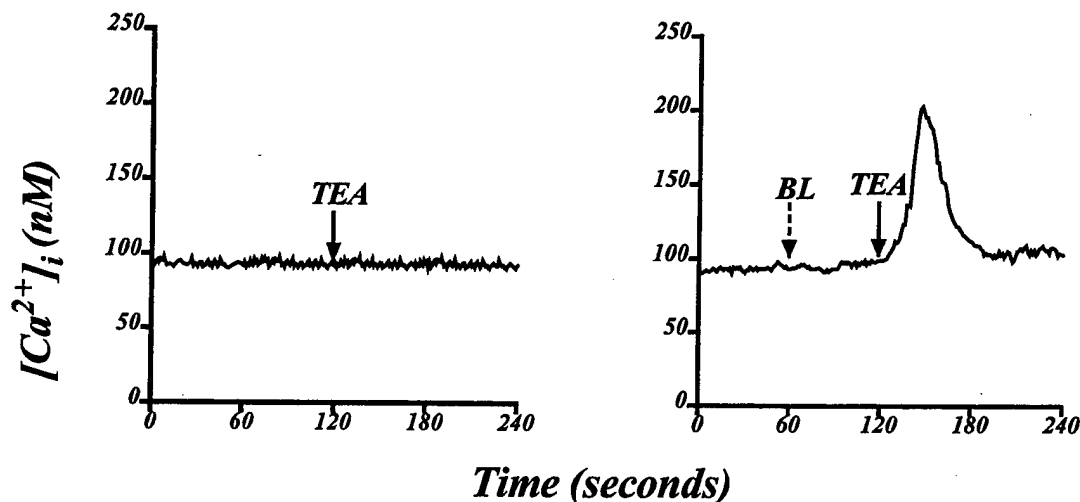


Fig.3 Time-Course of Calcium Responses. The left panel illustrates lack of effect of TEA in AD cells. The situation changes markedly when benzolactam(at 60 s) is added prior to TEA application (at 180 s, right panel). Ordinate in seconds.

Protein kinase C assessment. Conventional immunoblot techniques were employed to assess PKC since this isozyme seems to be predominantly affected in AD fibroblasts. Fig. 4a depicts a representative Western blot of soluble and particulate PKC in controls, FAD and SAD cell lines. In agreement with other studies, basal level of PKC is higher in the untreated group in the 2 AC cell lines as compared to the 3 FAD cell lines ($t=-8.886$; $p<0.005$). It was also higher for 2 SAD but failed to reach statistical significance cell lines ($t=-2.79$, ns). Treatment of FAD and SAD with BL for 1 min revealed a pronounced redistribution of the isoform of the enzyme from cytosol to membrane compared to AC (Fig. 4b, solid and open bars). On the other hand, there were no significant differences in PKC redistribution between AC, FAD and SAD cell lines after treatment with BL for 15 min (Fig. 4b, hatched bars).

These preliminary results indicate that the benzolactam effect can be observed in both FAD and SAD cell lines, with a slightly higher potency in FAD lines. Interestingly, the non-selective PKC activator PDBu had only a minor(not significant) effect in the SAD cell lines. This result, at least in part, can be attributed to the much lower affinity of PDBu to PKC as compared to benzolactam. The two compounds were used at equimolar concentrations. Perhaps it is also an important factor that benzolactam exhibits a much higher affinity and selectivity for the α and β isozymes. This is particularly relevant since the γ isozyme has been consistently reported to be defective in AD fibroblasts and has been primarily implicated in brain studies. The immunoblot assay provides solid evidence for the direct effect of benzolactam on PKC. In summary, these results are consistent with a significant role for PKC in restoring the TEA-induced calcium responses in AD fibroblasts. These results also suggest that the α isoform may play a predominant role.

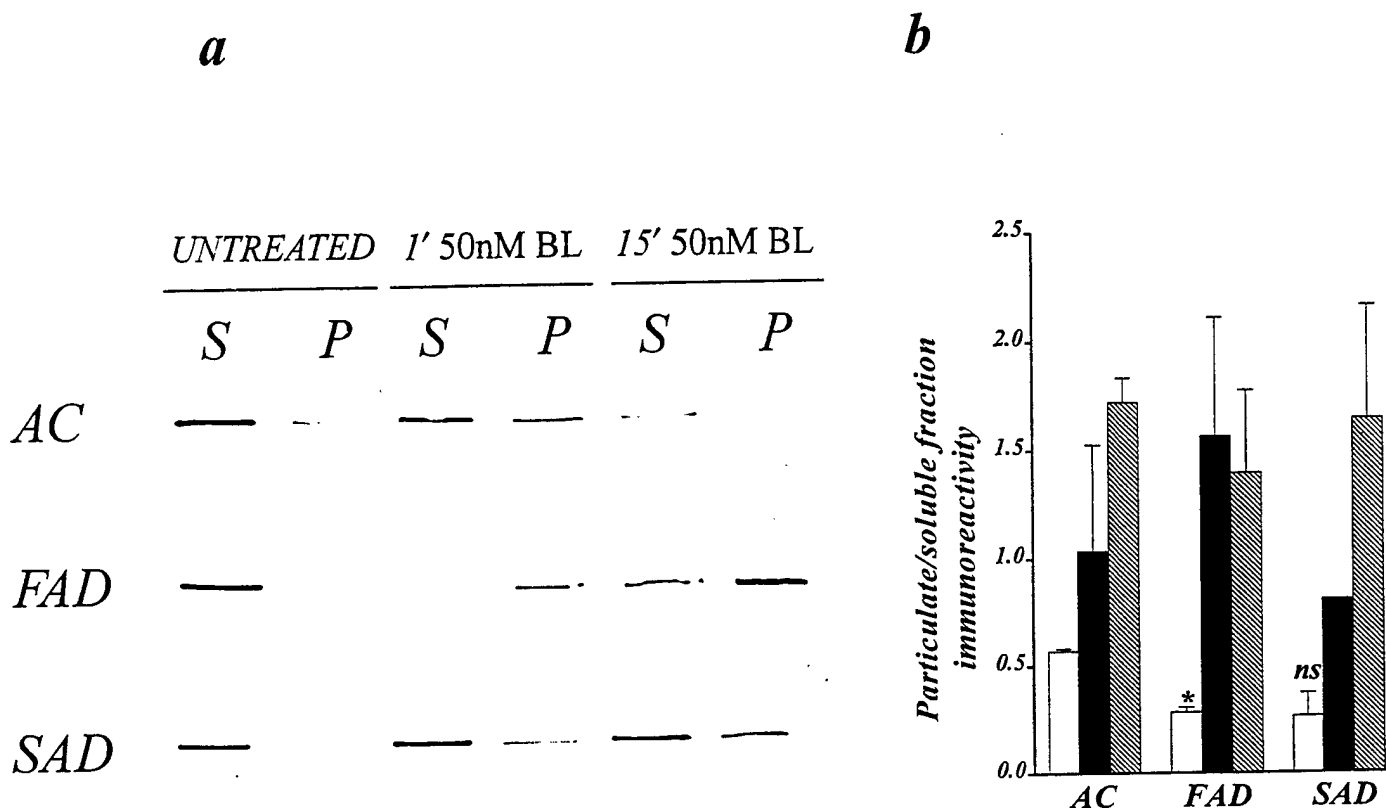


Figure 4. Translocation of PKC induced by benzolactam. **a.** Representative immunoblots from three cell lines. **b.** PKC redistribution from cytosol (soluble fraction) to membrane (particulate fraction) expressed as ratio of particulate to soluble fraction immunoreactivity measured by densitometric analyses. Ratio values for the 3 treatment groups - untreated, 1 and 15 min treatment with BL are represented by open, black and hatched bars, respectively. Basal levels of the enzyme are significantly higher in the AC group compared to the FAD and SAD groups. Vertical bars indicate standard error of means. Asterisks indicate significant differences in basal levels as compared to controls (* $p < 0.005$, two-tailed t -test).

Project 2: Potassium Channels in Human Brain Synaptosomes

Despite the advances in identifying relevant molecular changes in peripheral tissues, it remains important to determine whether or not similar changes take place in the central nervous system, the primary site of AD pathology. Nevertheless, studying ion channels (and IP3 receptors) in human brain cells, specially from post-mortem material, constitutes a major technical challenge. Acute cell dissociation, although theoretically possible, may not give enough viable cells to make it a practical approach. There is, however, an alternative procedure that has the potential to circumvent most of these obstacles to study ion channels in a cell free system, from a variety of protein sources including purified protein channel, channels from intracellular and extracellular vesicles and or membranes, and from synaptosomes. In addition, viable synaptosomes have been successfully obtained from human brain autopsy material. Thus, synaptosomal membranes from AD brains can be incorporated in lipid bilayers to study ion channels. As a preliminary and preparatory step, we used synaptosomal membranes from experimental animals (gerbils) and successfully and routinely incorporated ion channels into the lipid bilayers. We have now obtained access to the University of Michigan Alzheimer's Disease Brain Bank (P50-AG08671) and initiated studies in human tissues.

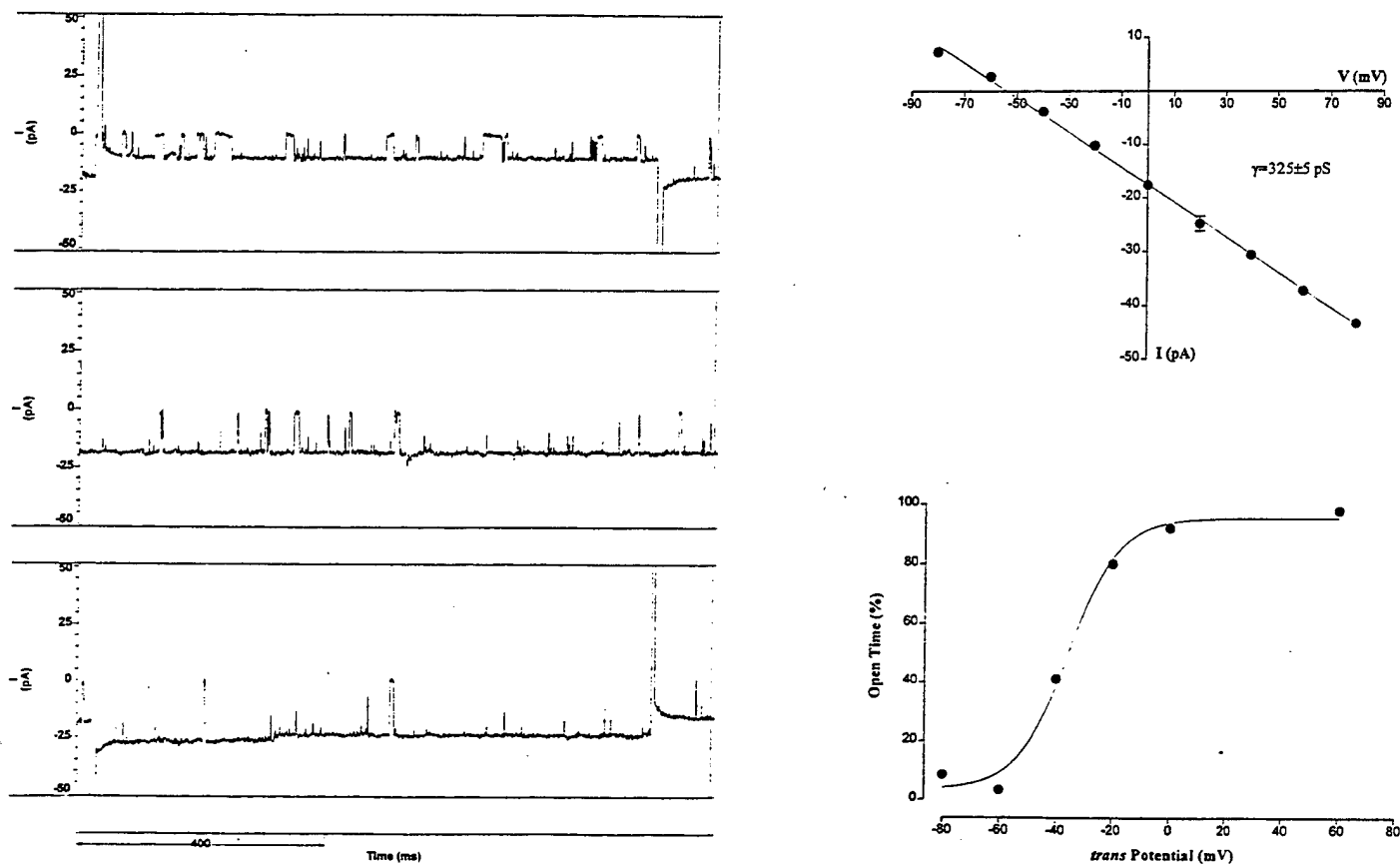


Fig. 5. K⁺ channels in human brains. Representative traces, I/V curves and kinetics of the large conductance K⁺ channel from human synaptosomes incorporated into artificial lipid bilayers.

Synaptosomes were prepared following conventional procedures. The tissue was manually homogenized and later subjected to a sucrose density gradient ultracentrifugation. The experimental chamber consisted of two compartments separated by a thin Teflon film. The chambers were filled with a Kasp solution; 50 mM in the *cis* chamber and 500 mM in *trans*. The bilayers were formed by applying a mixture of palmitoylcholinephosphatidylethanolamine and phosphatidylserine (1:1, 50 mg/ml) onto a 100 μ m diameter hole present in the teflon film. When a stable bilayer was formed, 5 to 10 of the synaptosome suspension is added to the *cis* chamber. Ion channels were detected using a patch clamp amplifier (Axopatch -1D, Axon Instruments) equipped with a CV-4B bilayer head stage. Data were simultaneously acquired by computer (Digital 1200, Axon Instruments) and recorded on video tape with a pulse code modulation/VCR digital recorder (Venter) and directly. Data was analyzed with the Pclamp and Axoscope suit of programs (Axon Instruments).

Preliminary data indicates that functional ion channels can, indeed, be detected in synaptosomes prepared from autopsy material. We have observed at least two types of K⁺ channels in human brain synaptosomes. Initial characterization revealed a channel of large conductance (335 pS) that exhibited marked voltage dependence, increasing its open probability from negative to positive *trans* potentials in a *s*-shaped manner. A second channel of intermediate conductance (190 pS) was also found. Figure 5 depicts representative traces of the large conductance channel. Voltage/ current relationship and open probability curve are shown on the right panel. Ongoing studies continue to characterize these and other channels from the biophysical and pharmacological perspectives. More importantly, a full comparison of the properties of the channels in AD vs. control brains will be conducted.

Project 3: Regulation of Amyloid Precursor Protein Secretion by PKC

Protein kinase C, known to be defective in AD, influences the type of APP secreted products. PKC activation appears to favor secretion of soluble, non amyloidogenic products. This project, in the early experimental stages, will provide further support for the hypothesis implicating PKC as a major player in AD pathophysiology (Project 1). Fibroblasts from AD patients (including those carrying PS1 mutations) and PC12 cells were treated with novel, non tumor promoter PKC activators. Preliminary results indicate that basal secretion of soluble APP is lower in AD fibroblasts as compared to controls. Benzolactam is capable of significantly increasing the secretion of the soluble product in AD fibroblasts. Fig. 6 shows the immunoblot analysis used to measure secreted APP under basal and after PKC activation. Ongoing experiments involve the testing of cell lines from different familial and sporadic AD cases and the testing of other metabolic products of the APP protein.

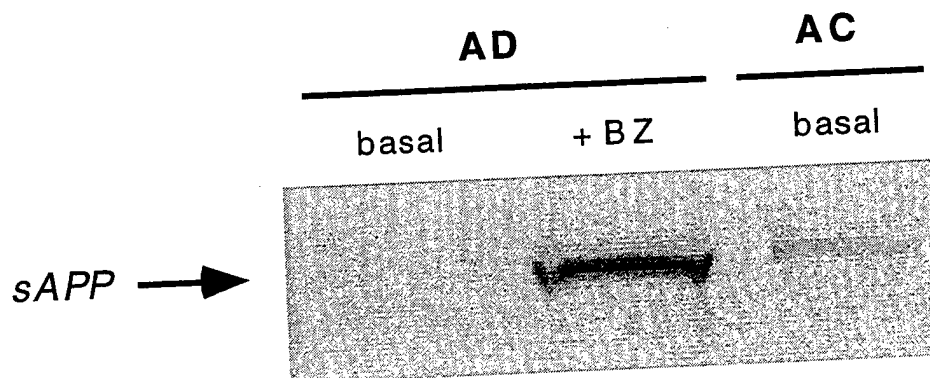


Fig. 6. Soluble APP secretion. Representative immunoblot of sAPP secretion induced by PKC activations.

Project 4: Neuroprotective Effects of Dantrolene in Global Ischemia

A number of cellular models have indicated that Dantrolene, used to treat malignant hyperthermia, interferes with calcium release from intracellular stores. It has been shown as cytoprotective to insults that elevate intracellular calcium. In some cases, a direct link to blockade

of calcium release has been demonstrated. We extended these studies to animal models subjected to ischemic insult.

Global ischemia was induced in Mongolian gerbils by 5 min bilateral carotid artery occlusion. Animals were treated with dantrolene (10 mg./kg) or vehicle alone (DMSO) at 0, 30, 60 or 120 min post-ischemia intravenously. EEG recovery time was significantly shorter in the dantrolene treated group (0 min). No behavioral differences were observed among groups as measured by the paper shed test. Four days after surgery hippocampal CA1 cell were counted. Dantrolene significantly increased the number of normal CA1 cell from 0 to 60 min post-ischemia (fig. 7). These results indicate that Dantrolene might be useful as a neuroprotectant in preventing ischemic damage.

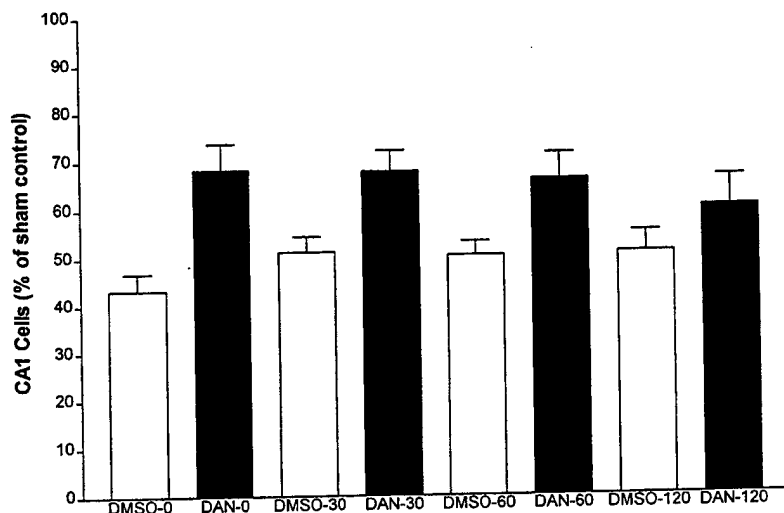


Fig. 7. CA1 cells survival in Dantrolene-treated and control gerbils.

Projects 5 and 6: Influence of the C-100 Fragment and PS1 Mutations on Ion Channels and Calcium Regulation.

The C-100 fragment, a subproduct of the amyloid precursor protein, and PS1 mutations play a significant, although not well understood role in AD pathophysiology. Our objective will be to examine ion channels and calcium regulation in cells transfected to express these native and mutated products. These projects, although related, are independent collaborations established with Drs. Macphie and Neve (Harvard University) for the C-100 studies and with Dr. Kosik (Harvard University) for the PS1 studies. Both projects are in the planning and preliminary experimental stages.

Conclusions and Future Directions

Significant amount of data have already been collected. Preliminary results strongly suggests that PKC might play a major role in AD. We have also completed the preliminary work that will allow the study of ion channels in AD brains. Completion of these two projects constitutes two of the main goals for the next year. Studies on APP secretion and transfected cells will be developed to advance stages.

ALAN I. FADEN, M.D.

Dr. Faden's research focuses on the chemical pathobiology of secondary tissue damage following central nervous system (CNS) trauma and utilizes multidisciplinary approaches including molecular and cellular neurobiology, neuropharmacology, behavioral evaluation (including cognitive) and magnetic resonance techniques. Four parallel but independent lines of investigation are supported in part by the Institute. These are detailed below:

Project 1: Development and Refinement of Injury Models

Project 1a: *In Vitro* Models

A series of cell culture models of secondary neuronal injury have been developed. These include rat cerebellar granule cells subjected to combined serum and potassium deprivation, considered a relatively classical model of apoptotic cell death; and two models of traumatic neuronal injury using combined neuronal/glia cultures derived from rats. Over time we have refined these cell culture systems so that they can be performed in 96-well plates, thereby markedly enhancing the efficiency of our studies and better permitting automated analysis of biochemical changes. The purpose of these *in vitro* model systems are to complement our *in vivo* models of CNS injury and permit more critical assessment of injury mechanisms, particularly at the molecular and cellular level.

Apoptosis of Cerebellar Granule Cells

Detailed methods were provided in last year's annual report and can be found in a recently published paper (Eldadah et al., 1997). Combined serum/potassium deprivation leads to an apoptotic cell death involving approximately 50% of cells after 12 hours deprivation and more than 80% with 48 hours deprivation. This model has been used primarily to examine the role of selected caspases in programmed cell death (vide infra). It has also been utilized in preliminary studies to evaluate the neurotoxic effects of β -amyloid, which has been implicated as an important physiological factor in Alzheimer's Disease.

Trauma Models

Glial cell cultures are prepared from 1 to 3 day old Sprague-Dawley rats and neuronal cells are prepared from the cortexes of 18-day embryonic Sprague-Dawley rats. The composition of the cultures was assessed using immunocytochemistry, including antibodies to GFAP (for glia) or to SMI33, SMI34, and MAP-2 (neuronal markers). Cell death was examined using a variety of techniques, including LDH release, ethidium homodimer-1 assay, or trypan blue staining. Injury was produced employing one of two devices. One device, developed for use in 24-well plates, produces concentric circular cuts (numbering from 1 to 6) by needles that are rotated through the cultures by an electrical driver. The second model, developed for use in 96-well plates, employs 18 parallel blades with injury controlled using an electromagnet. The advantage of the first model is that cell death can be varied from approximately 10% to nearly 90% according to the number of concentric circular cuts used (Mukhin et al., 1997a). Both models show high correlation among the various methods to assess cell death. In each case, the cultures are washed thoroughly 30 minutes after trauma in order to separate primary from secondary injury effects. Our studies demonstrate that glial cells are far more resistant to traumatic injury than are neurons and show little if any spread of injury (secondary injury); in contrast, neuronal cell death spreads from the sites of injury outward to involve progressively additional neurons over a 24 hour period following trauma (Figure 1). Each trauma model has been utilized to examine mechanisms of secondary neuronal injury as well as the response to pharmacological treatments. In both models, secondary injury has been found to be highly sensitive to modulation of NMDA receptor mediated events. They have also proved highly useful for studying the role of metabotropic glutamate receptors in secondary injury (vide infra).

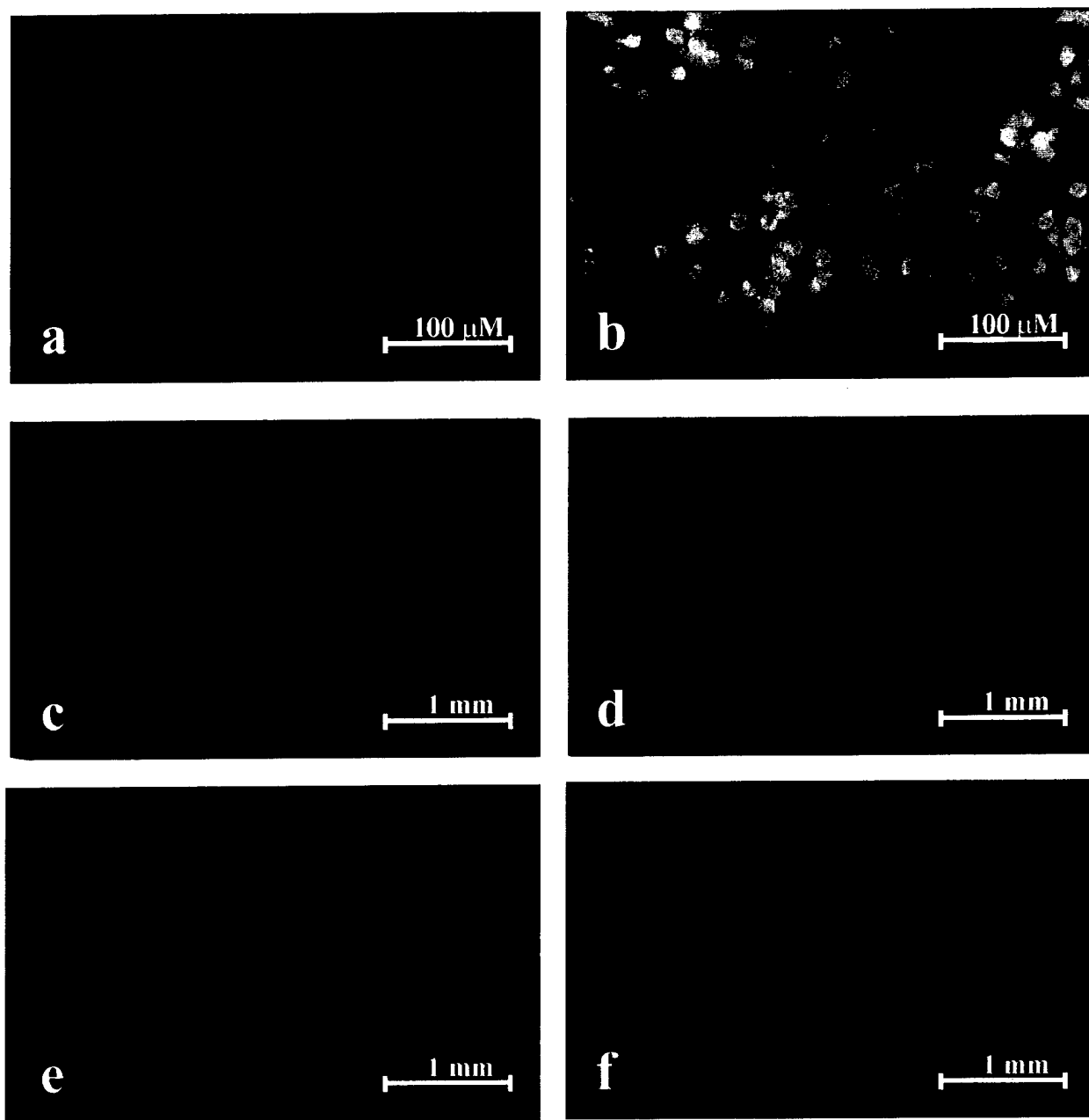


Figure 1. Cytological analysis of neuronal/glial and glial cultures. **a:** MAP-2 staining of fixed neuronal/glial cultures at 16-18 DIV demonstrated numerous positive cells with neuronal morphology including a dense network of processes. **b:** Same field was stained for 5 min with 10 μ M EthD-1 to obtain a total cell count. Approximately 50% of total cells are stained by MAP-2 antibodies. **c:** Thirty minutes after injury to neuronal/glial cultures, EthD-1 staining is pronounced at the site of initial injury. **d:** Between 16-18 h after injury, propagation of neuronal injury is detected by increased EthD-1 staining further removed from the punch site. **e:** Glial cultures stained with EthD-1 30 min after injury demonstrate less primary cell death than neuronal/glial cultures. **f:** EthD-1 staining remains localized to the punch site in glial cultures 16-18 h after injury.

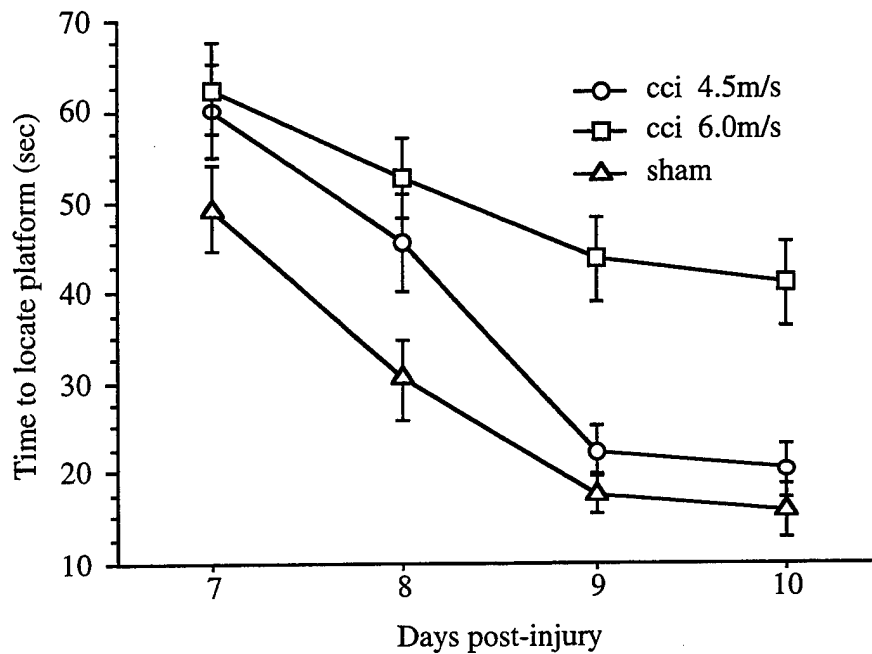
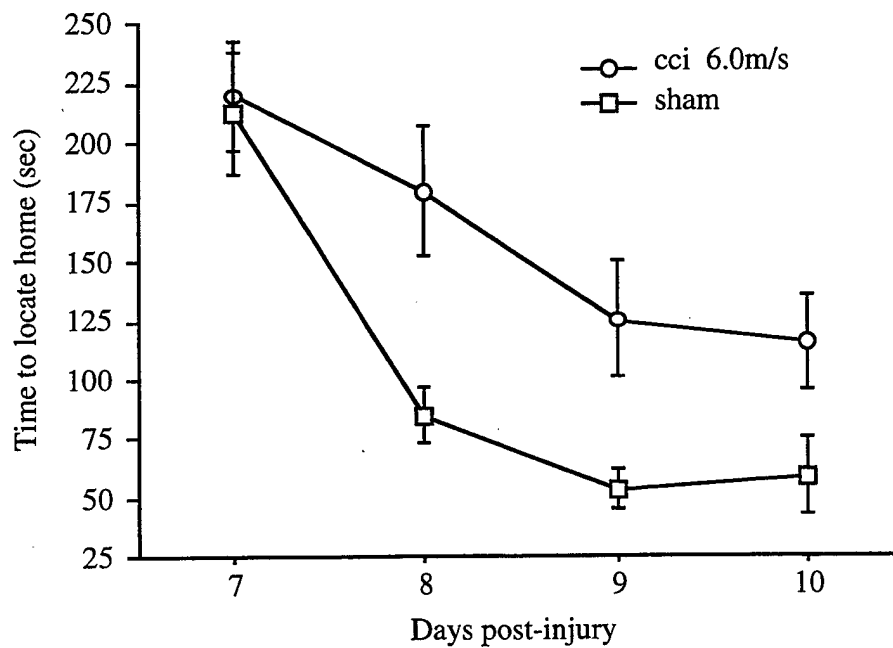
A**B**

Figure 2: (A) Effect of mild (4.5m/s) and moderate (6.0m/s) controlled cortical impact injury on spatial learning behavior in the Morris water maze. Sham-operated animals rapidly acquire this task, whereas moderately-injured mice show little improvement over the four days of testing. Mice receiving a mild injury eventually acquire the task after the third and fourth day of training. (B) Effect of moderate injury on learning in the Barnes maze, an additional spatial learning task. Sham-operated mice out-perform injured animals on days 8, 9 and 10 post-injury.

Project 1b: Controlled Cortical Impact Injury in Mice

A model has been developed in mice in which controlled cortical impact is induced using a device that regulates both the velocity of injury and the amount of tissue deformation. Injury is produced over the lateral parietal cortex through a burr hole by a pneumatically driven impactor. This model has been used to examine post-traumatic changes in cognitive function, including use of Morris water maze, Barnes maze, and Y maze methods. Injured animals show sustained cognitive deficits during the first one to three weeks following trauma (Figure 2). They also demonstrate sustained motor dysfunction utilizing a beam walking test. The model more recently has been used to examine the neuroprotective effects of various drugs (*vide infra*) as well as to study a specific gene defect on recovery of function.

Project 2: Role of Caspases in Neuronal Apoptosis

A group of proteases known as caspases has been implicated as potential mediators of the apoptotic cascade. These proteases are the mammalian homologues of the *C. elegans* Ced-3 pro-apoptotic gene product and can be divided into two classes of enzymes: the ICE-like proteases and the CPP32-like proteases. The CPP32-like proteases, which included CPP32, ICH-1, MCH-1, and a growing list of others, can cleave several functionally important proteins, such as poly (ADP-ribosyl) polymerase (PARP), an enzyme involved in DNA repair, and lamin B, a cytoskeletal element associated with the nuclear membrane. The cleavage of these two substrates may contribute to the appearance of DNA fragmentation and to the changes in nuclear morphology during apoptosis, respectively. Both of these proteins contain the sequence Asp-Glu-Val-Asp (DEVD), which is recognized specifically by CPP32-like proteases and cleaved adjacent to the C-terminal aspartate. Caspases, particularly CPP32 (Caspase-3) have been implicated as important factors contributing to apoptotic cell death in a number of model cell systems. We have evaluated their role in neuronal apoptosis, using both our cerebellar granule cell model and fluid percussion induced traumatic brain injury.

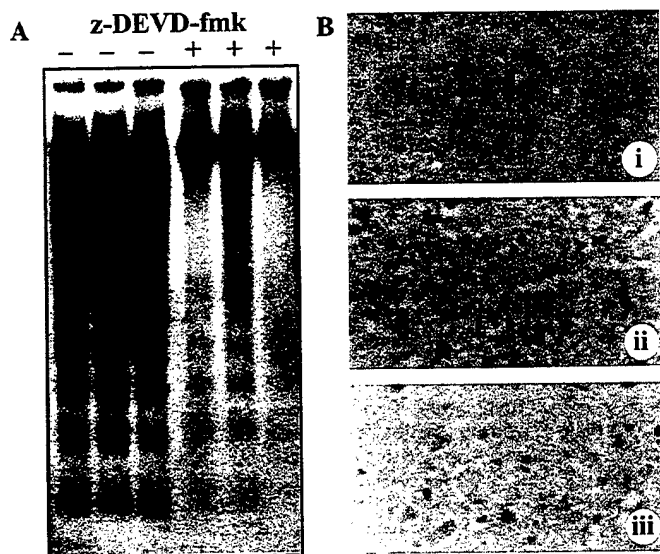
Project 2a: Role of Caspases in Apoptosis Caused by Serum/Potassium Deprivation in Cerebellar Granule Cells

We have previously reported that combined serum/potassium deprivation causes significant apoptosis at 12 or 48 hours associated with a significant upregulation in caspase-3 mRNA levels and caspase-3 activity as reflected, by either PARP cleavage assay or a fluorometric assay (Eldadah et al., 1997). Of note was the lack of ability to detect caspase-1 mRNA levels or caspase activity. Treatment with a selective caspase-3 inhibitor (z-DEVD-fmk) produced significant neuroprotection in these cultures. Together these observations strongly support a significant role for caspase-3, but not caspase-1, in neuronal apoptosis caused by combined serum/potassium deprivation in cerebellar granule cells. Ongoing studies are examining potential mechanisms of caspase-3 induced apoptosis by examining certain of downstream signalling pathways.

Project 2b: Role of Caspases in Apoptosis Associated with Traumatic Brain Injury

We have utilized a lateral fluid percussion traumatic brain injury model in rats to examine the degree to which apoptotic cell death contributes to the function deficits after traumatic brain injury as well as the potential role of caspases in this secondary injury process. We have demonstrated using both TUNEL staining and DNA fragmentation assays that apoptosis was an important feature of fluid percussion induced traumatic brain injury in rats. Using double staining and immunocytochemical techniques, we further demonstrated that apoptosis involved predominantly neurons (Yakovlev et al., 1997). TBI is associated with a significant upregulation in mRNA levels for caspase-3, and to a lesser extent caspase-1, as well as significant increase in caspase-3 activity. Intracerebroventricular treatment with z-DEVD-fmk, a selective caspase-3 inhibitor, resulted in a marked reduction in post-traumatic apoptosis and a significant improvement in motor recovery (Figures 3 and 4). Together these findings demonstrate that apoptosis contributes significantly to the neurological deficits found in traumatic brain injury and that

caspase-3 is critically involved in this response. These findings suggest an entirely new conceptual framework for the treatment of traumatic CNS injuries and indicate that inhibitors of factors involved in both apoptosis and necrosis may be necessary to achieve optimal therapeutic results.



Figur. Effect of z-DEVD-fmk administration *in vivo* on internucleosomal DNA fragmentation in rat cortex after TBI. Five microliters of DMSO vehicle (–) or z-DEVD-fmk (160 ng in 5 μ l of DMSO) were administered 30 min before and 6 and 24 hr after TBI. *A*, Genomic DNA from injured cortex of treated with vehicle (–) or z-DEVD-fmk (+) rats was isolated 3 d after TBI. One microgram of DNA from each sample was *Taq*-labeled with [α^{32} P] dATP and analyzed in a 1.5% agarose gel. The autoradiograph demonstrates DNA fragmentation patterns from three rats treated either with DMSO (–) or z-DEVD-fmk (+). *B*, TUNEL staining of corresponding sections from parietal cortex of a sham-operated control animal (*i*) and traumatized brains from animals treated with DMSO vehicle (*ii*) or z-DEVD-fmk (*iii*). Cryosections fixed in formalin were stained for TUNEL, using the TACS2 TdT kit (Trevigen), and visualized by HRP/TACS blue (Trevigen). TUNEL-positive nuclei appear dark gray or black, whereas nonapoptotic nuclei appear light gray.

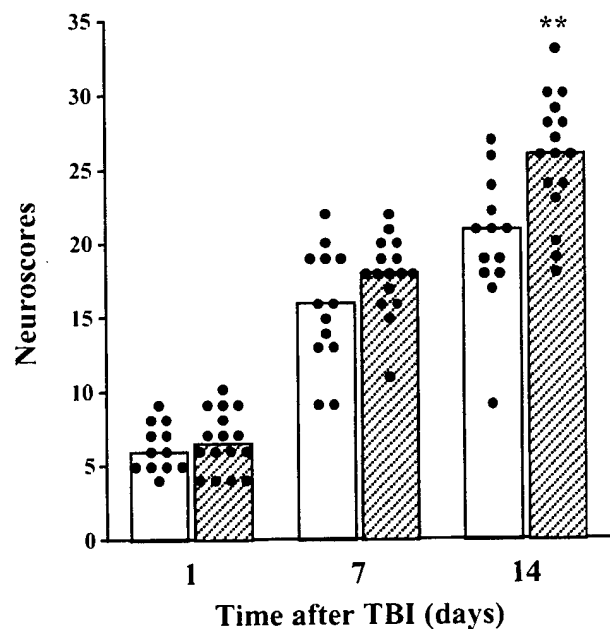


Figure 4 Effect of intracerebroventricular administration of zDEVD-fmk on neurological recovery after lateral fluid percussion-induced TBI. The histogram represents median scores at indicated times after trauma. Each filled circle represents an individual animal's cumulative neuroscore, reflecting performance on a battery of motor tests. Open bars, Vehicle-treated injury, $n = 13$; filled bars, zDEVD-fmk-treated injury, $n = 16$. ** $p < 0.01$ versus vehicle-treated injury, using the Mann-Whitney U test after Kruskal-Wallis nonparametric ANOVA.

Project 3: Role of Metabotropic Glutamate Receptors (mGluR) in Traumatic Neuronal Injury

Our laboratory was the first to demonstrate a role for the NMDA class of ionotropic glutamate receptors in CNS trauma. More recently, we have been examining the role of non-ionotropic glutamate receptors mGluR in secondary injury. mGluR have been divided into three groups based on sequence homology, second messenger pathways, and pharmacological sensitivity. Based on these profiles, we have proposed that group I mGluR contribute to secondary neuronal death in part by modulating NMDA receptors and that groups II and III mGluR are neuroprotective, through mechanisms that involve either modulation of adenylyl cyclase activity and/or reduction of presynaptic glutamate release.

We have utilized both *in vivo* and *in vitro* model systems to examine the role of mGluR in secondary injury. Using the *in vitro* model system, we have demonstrated activation of group I mGluR exacerbates traumatic injury and that antagonists to group I mGluR are neuroprotective; utilizing antisense deoxynucleotides, we demonstrated that mGluR1, but not mGluR5, is involved in this process (Mukhin et al., 1996). Employing the fluid percussion TBI model, we showed that treatment with an mGluR antagonist that is more active in mGluR1 than mGluR5 provides significant neuroprotection when administered icv prior to trauma (Mukhin et al., 1996). In follow-up studies, we have demonstrated that modulation of group of mGluR is partially but not completely involved in this process (Mukhin et al., 1997b).

In more recent work, we have shown that group III agonists are neuroprotective in an *in vitro* trauma model system and that antagonists to group III mGluR exacerbate injury (Figure 5 and 6). We believe that modulation of cyclic AMP is likely to be involved as administration of a cyclic AMP analog, at concentrations that do not by themselves affect injury, attenuate the neuroprotective effects of group III mGluR agonists. Taken together these findings clearly demonstrate a pathophysiological role for group I mGluR and a neuroprotective role for group III mGluR in traumatic neuronal injury. Of potential importance is our observation that administration of either group I mGluR antagonists or group III mGluR agonists have additive neuroprotective effects to those of an NMDA antagonist. These observations have important implications for the treatment of traumatic injury and suggest that modulation of mGluR be considered as a potentially important adjunct to treatment directed at ionotropic glutamate receptors.

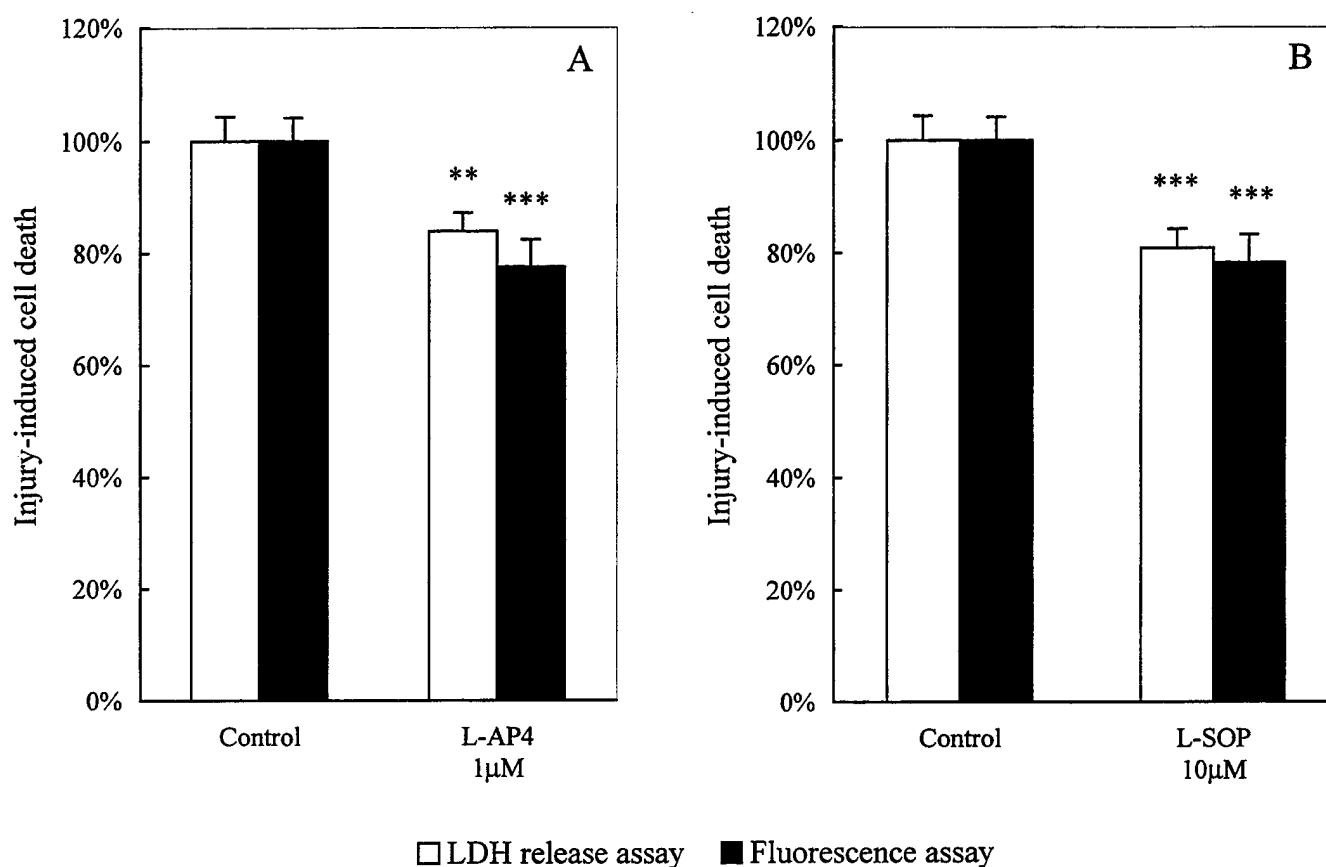


Figure 5. Neuroprotective effect of (A) L-AP4 and (B) L-SOP on injury-induced cell death evaluated by LDH release assay and fluorescent assay with EthD-1. Cultures were incubated in presence of L-AP4 (1 μ M) or L-SOP (10 μ M) 30 min before and 16-18 hr after injury. LDH activity was measured 16-18 hr after injury. Fluorescence was measured as described in Methods. Data expressed as a percentage of injury-induced LDH release or fluorescence increase in absence of agonists. Values represent mean \pm s.e.m., n = 32 - 64 per condition. ** p < 0.01, *** p < 0.001 versus control, unpaired Student's t-test.

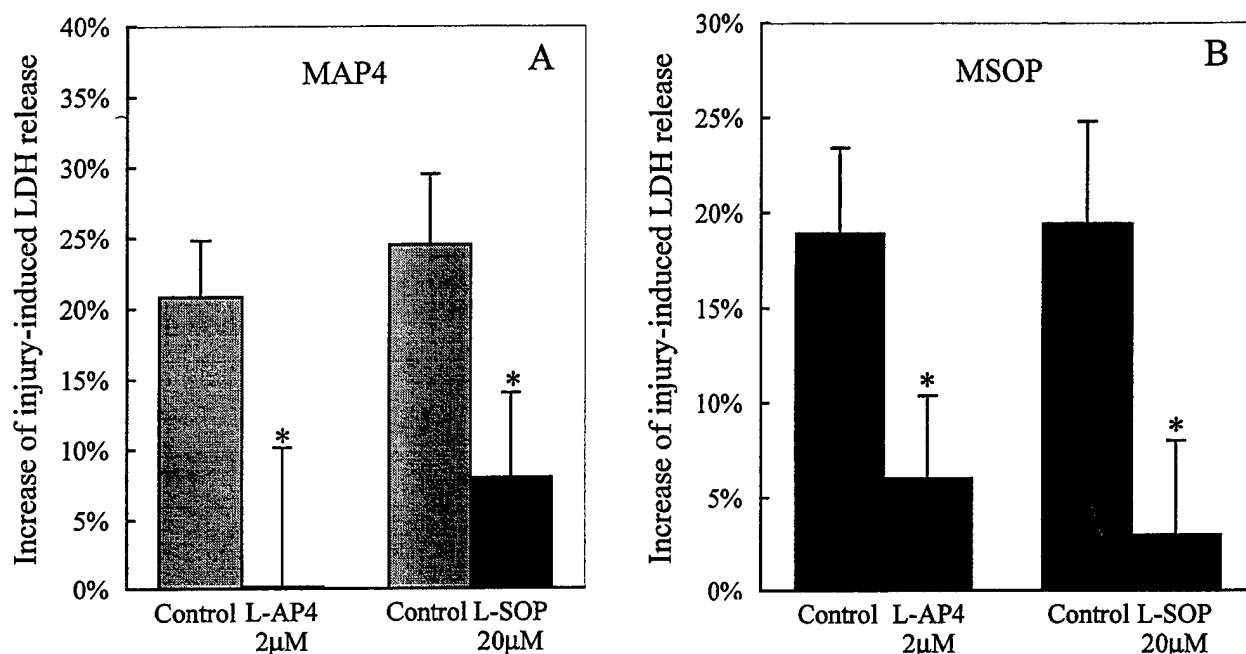


Figure 6. Exacerbation of injury-induced neuronal cell death by group III antagonists (A) MAP4 and (B) MSOP is reduced by group III mGluR agonists. Cultures were incubated in presence of MAP4 (1500 μ M) or MSOP (1500 μ M) alone (control) and in combination with L-AP4 (2 μ M) or L-SOP (20 μ M) for 30 min before and 16-18 hr after injury. LDH activity was measured 16-18 hr after injury. Data expressed as a percentage of injury-induced LDH release in absence of agonists and antagonists. Values represent mean \pm s.e.m., $n = 32 - 64$ per each condition. * $p < 0.05$ versus control MAP4 or MSOP, using Student's t-test.

Project 4: Drug Design: Developing novel neuroprotective agents for CNS injury

There is an active collaboration between my laboratory and those of Drs. Kozikowski and Wang, the goal of which is to develop novel neuroprotective agents to treat central nervous system injury. The focus to date has been to develop novel thyrotropic (TRH) analogs and selective caspase inhibitors. Development strategies are described in detail in the sections describing the work of Drs. Kozikowski and Wang. The TRH work has led to the development of a series of compounds that show striking neuroprotective effects with regard to either motor recovery or cognitive recovery after trauma. These compounds, modified at both the N-terminus and imidazole ring, are intended to have high CNS activity, to be resistant to enzymatic degradation by endopeptidases and show less endocrine and/or autonomic effects as compared to TRH.

We have studied the effects of various TRH analogs on outcome following fluid percussion induced TBI in rats or controlled cortical impact in mice. Three new analogs showed beneficial effects on motor recovery in the rat TBI model. Treatment with several analogs also resulted in markedly improved motor and cognitive recovery in the mouse TBI model (Figures 7 and 8). Ongoing studies are evaluating the dose-response characteristics, therapeutic window, and other physiological actions (autonomic, endocrine, analeptic effects) of these compounds.

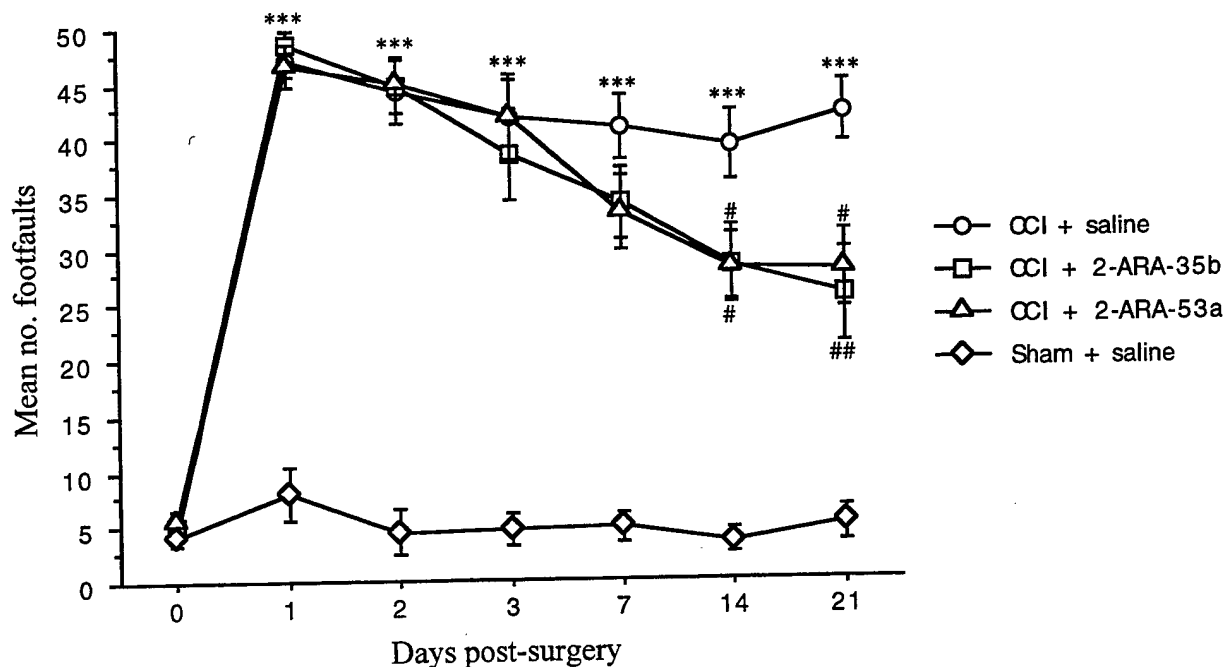


Figure 7: Performance of sham-operated and controlled cortical impact (CCI)-injured mice in a beam walking task measuring fine motor coordination. Results are expressed as daily mean \pm SEM number of right hindlimb footfaults (maximum 50) per treatment group. # $p < 0.05$, ## $p < 0.01$ with respect to CCI + saline; *** $p < 0.001$ with respect to Sham + saline.

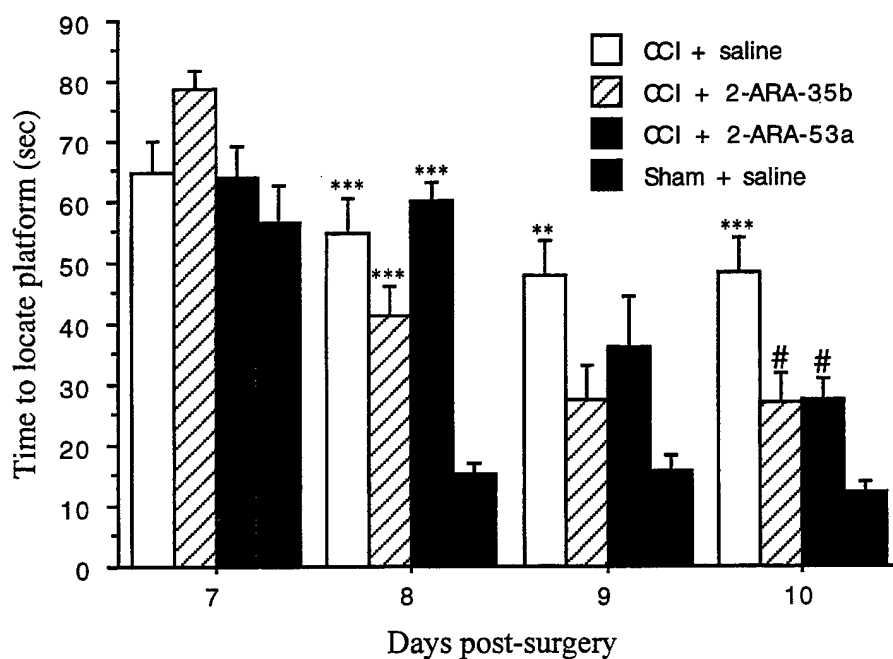


Figure 8: Latency to find the hidden platform in a version of the Morris watermaze. Results are expressed as daily means \pm SEM for each group over 4 trials. * $p < 0.05$, ** $p < 0.01$, *** $p < 0.001$ with respect to Sham + saline; # $p < 0.01$ with respect to CCI + saline.

References

- Mukhin A, Fan L, and Faden A.I. Activation of metabotropic glutamate receptor subtype mGluR1 contributes to posttraumatic neuronal injury. *J Neurosci* 16(19):6012-6020, 1996.
- Eldadah, B., Yakovlev, A.G., and Faden, A.I. The role of CED-3-related cysteine proteases in apoptosis of cerebellar granule cell. *J Neurosci* 17(16):6105-6113, 1997.
- Mukhin AG, SA Ivanova, SM Knoblach, and AI Faden. New *in vitro* model of traumatic neuronal injury: Evaluation of secondary injury and glutamate receptor mediated neurotoxicity. *J Neurotrauma* 14:651-663, 1997a.
- Yakovlev, A.G., Knoblach, S.M., Fan, L., Fox, G.B., Goodnight, R., and Faden, A.I. Activation of CPP32-like caspases contributes to neuronal apoptosis and neurological dysfunction after traumatic brain injury. *J Neurosci* 17(19): 7415-7424, 1997.
- Mukhin AG, Ivanova SA, and AI Faden. mGluR modulation of post-traumatic neuronal death: Role of NMDA receptors. *Neuroreport* 8:2561-2566, 1997b.

SHERIDAN L. SWOPE, Ph.D.

Neurotransmitter receptors are of primary importance in synaptic transmission and are targets for regulation. Modulation of the function, expression, or density of receptors has a profound effect on synaptic efficacy and thus may mediate plasticity. Accumulating evidence supports a role for phosphorylation in the regulation of synaptic transmission (Swope et al., 1992; 1997). Protein tyrosine kinases are a unique class of kinases initially found to mediate cell transformation and proliferation. However, protein tyrosine kinases are also involved in

differentiated cell function. In fact, many protein tyrosine kinases are most highly expressed in the brain, being present both pre- and postsynaptically, suggesting their importance in the regulation of synaptic activity. Our long-term goal is to study the role of protein tyrosine kinases in synapse formation and function.

Much of the current understanding of synapses originates from studies of the neuromuscular junction (NMJ). The nicotinic acetylcholine receptor (AChR) is the ligand gated ion channel that mediates rapid postsynaptic depolarization at the NMJ. Because of its abundance in the electric organs of *Torpedo californica*, the AChR is the best characterized neurotransmitter receptor and has served as a model to elucidate the structure, function, and modulation of neurotransmitter receptors and ion channels. The AChR is phosphorylated on tyrosine residues both *in vitro* and *in vivo*, and this tyrosine phosphorylation is correlated with a modulation of the rate of receptor desensitization. In addition, tyrosine phosphorylation of the AChR and/or other postsynaptic components is involved in the nerve induced clustering of the AChR during synaptogenesis at the NMJ. Furthermore, protein tyrosine phosphorylation mediates the effect of acetylcholine receptor inducing activity (ARIA) to increase AChR transcription by nuclei underlying the synapse. Our interest has been to identify protein tyrosine kinases that are expressed postsynaptically at the NMJ which function to regulate the AChR.

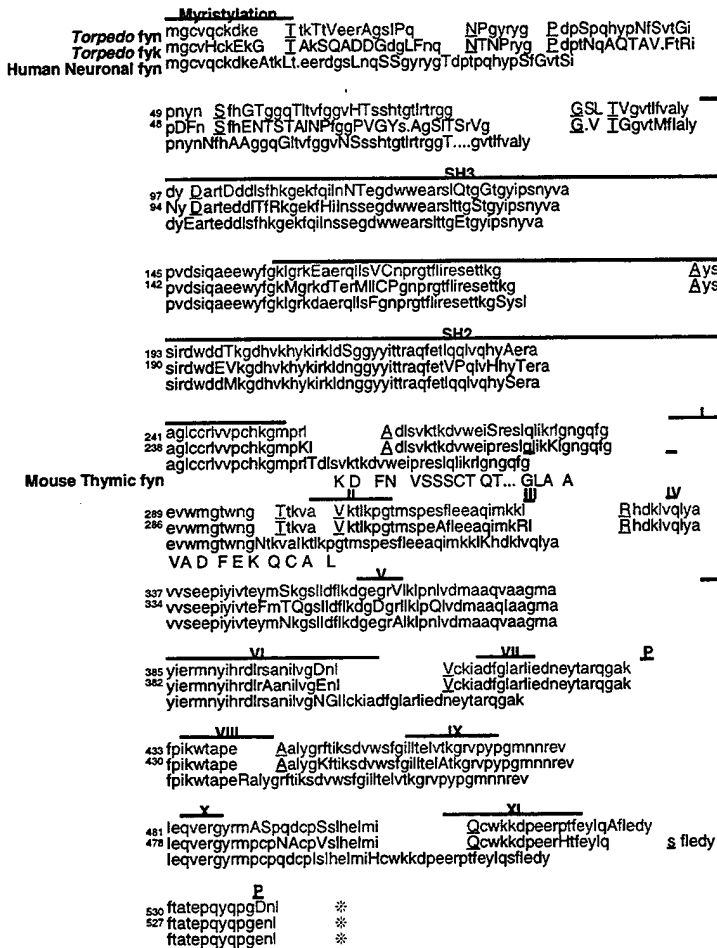


Fig 1. Complete amino acid sequences of Fyn and Fyk. The deduced amino acid sequences of Fyn and Fyk are indicated. For each clone, amino acid identities with human neuronal Fyn are indicated by shading. Amino acids of nonidentity with neuronal Fyn but identity between Fyn and Fyk are indicated by underlining. The divergence between the neuronal and the alternatively spliced thymic form of Fyn is shown. Conserved protein tyrosine kinase subdomains are indicated by horizontal bars: SH3 and SH2, src homology domains 3 and 2; P, putative phosphorylation sites; I-XI, conserved subdomains. The amino acid positions in the sequence of each clone are indicated on the left.

Torpedo mDEYqSGeet Tfl vdevsGi lkeS ieTaiggnayq
 Mouse EDFqAS eetAf VvdevsS iVke AieS aiggnayq

PsR vnqwtSSV VeLC IsqltklgKpfkyivt Svimgkng
 HsK vnqwtTNV LeQT IsqltklgRpfkyivt Cvimgkng

aglhT asscYwd NNAdgsctvrwenkmycivsV fglsi *
 aglhSassc FwdSST dgsctvrwenkmycivsTfglsi *

Fig 2. Complete amino acid sequences and homology between Torpedo and Mouse Tctex. Using the yeast-two hybrid system with the unique domain to Fyn as a probe, a positive clone was identified and dideoxysequenced. The deduced translation product of the Torpedo clone and its homology to mouse Tctex is shown. Amino acid identities are indicated by shading.

In addition, Fyn and Fyk phosphorylate the receptor *in vitro* (Swope and Haganir, 1993). These initial studies suggest that Fyn and Fyk are important regulators of synaptic function at the NMJ and in the central nervous system.

Laboratory Development

Over the last year, Dr. Ali Mohamed, a postdoctoral fellow with biochemical and molecular biological experience in the area of protein phosphorylation and Mr. Tao Mou, MS a research assistant with a masters degree in Biochemistry and extensive molecular biological experience have continued to be members of the laboratory. In addition, Ms Patricia Clutton, a Ph.D. student and Ms. Bina Christy, a research assistant have joined the our group. The efforts of these researchers will enable our laboratory to attain its research goals. Extramural funding from the National Institutes of Health, National Institute of Neurological Disorders and Stroke in the form of an R29 or First Award has been successfully extended via a noncompetitive renewal. Furthermore, an application for additional funding through the Muscular Dystrophy Association is pending.

As a new laboratory at the Georgetown Institute of Cognitive and Computation Sciences, the aim of our current research is to continue to test the hypothesis that Fyn and Fyk are involved in synapse formation and function at the NMJ by regulating the AChR. Furthermore, the molecular mechanisms by which these two kinases act to regulate synaptic transmission are being investigated.

We have identified two Src like kinases, Fyn and Fyk, that together comprise the predominant protein tyrosine kinase activity in the AChR enriched postsynaptic membrane of *Torpedo* electric organ (Fig 1; and Swope and Haganir, 1993). Fyn and Fyk are also present in skeletal muscle and brain. These two kinases associate with the AChR via a binding of their src homology 2 (SH2) domains to the tyrosine phosphorylated δ subunit of the receptor (Swope and Haganir, 1994).

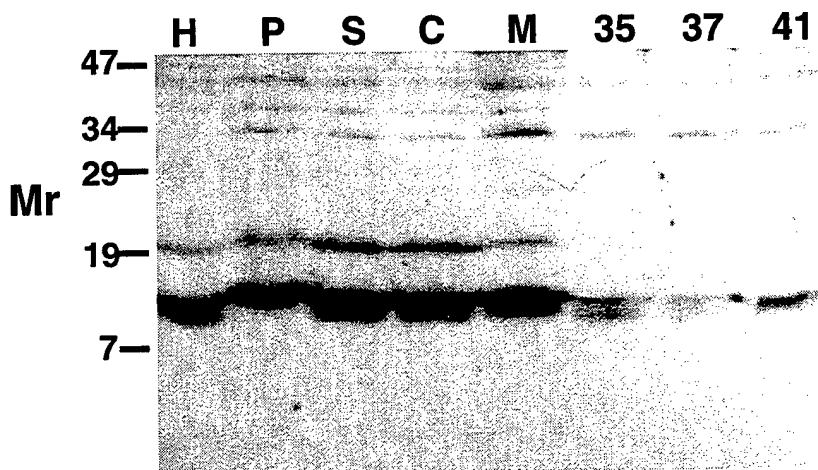


Fig. 3 Subcellular distribution of Tctex protein in *Torpedo* electric organ. *Torpedo* electric organ tissue was fractionated by sucrose density centrifugation. Aliquots of the indicated fractions representing 25ug (H) or 75ug (P, S, C, M, 35, 37, 41) were resolved by 15% SDS-PAGE and analyzed by Western blotting with affinity purified α Tctex antibody. Fractions analyzed were total homogenate (H), low speed pellet (P), low speed supernatant (S), cytosol (C), total membranes (M), nonpostsynaptic membranes (35), mixed membranes (37), and postsynaptic membranes (41). Molecular weights are as indicated at the left.

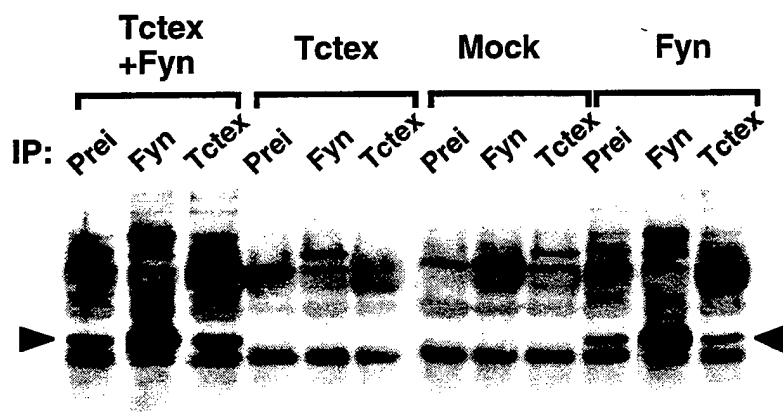


Fig 4. **Tctex and Fyn Coimmunoprecipitation.** QT6 cells were transfected with Tctex+Fyn, Tctex, pBK-CMV (Mock), or Fyn. The cellular proteins were solubilized and immunoprecipitated with preimmune, anti-Fyn, or anti-Tctex serum. The precipitated proteins were analyzed by Western blot using an anti-phosphotyrosine antibody. The position of Fyn is indicated by an arrow head.

We are using this antiserum to test for an association of MuSK with Fyn and Fyk using coimmunoprecipitation and affinity chromatography experiments.

Project 2: Clarification of the Signal Transduction Cascade Involving Fyn and Fyk

We are also in the process of characterizing the signal transduction pathway(s) by which Fyn and Fyk act to regulate synapse formation and function by asking: what are the identities of cellular components that interact directly with Fyn and Fyk? These ongoing studies will be performed using coimmunoprecipitation techniques, fusion protein affinity chromatography, and the yeast two-hybrid system. The yeast two-hybrid method is excellent for discovering functional interactions between two proteins. The yeast GAL4 protein is a transcriptional activator consisting of a DNA binding domain and a transcriptional activation domain. This system uses two different vectors each containing one of the GAL4 domains. Neither domain alone has the ability to activate transcription. However, if the two domains are brought together, for example via protein-protein interaction, transcriptional activation is restored. By fusing a known protein such as a fragment of Fyn and Fyk to the binding domain, proteins that interact with that region of the kinase can be identified from a cDNA library fused to the activating domain. This method has become generally applicable for the cloning of target proteins based on

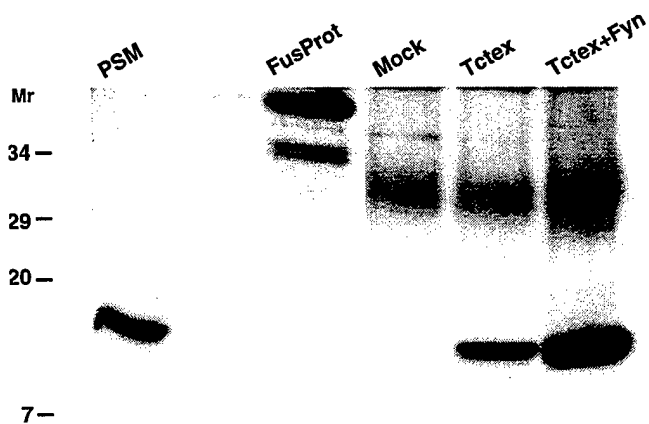


Fig 5. **Effect of Fyn on Tctex Expression.** QT6 cells were transfected with pBK-CMV empty plasmid, Tctex, or Tctex and Fyn pBK-CMV expression constructs. The cellular proteins, 10ug of Torpedo electric organ postsynaptic membrane proteins (PSM), and an aliquot of Tctex GST fusion protein (Fus Prot) were analyzed by Western blot using an anti-Tctex antibody. Molecular weights are as indicated.

protein-protein interaction including protein kinase substrates.

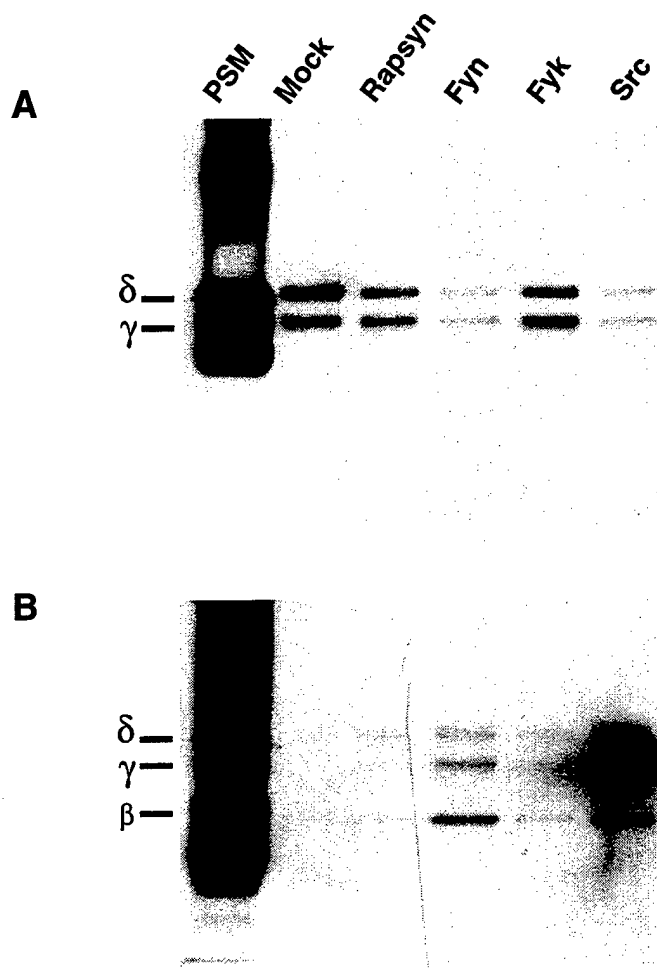


Fig 6. AChR Phosphorylation. Q-F18 cells were transfected with pBK-CMV (Mock), rapsyn alone, or rapsyn with Fyn, Fyk, or Src. The cells were solubilized and the AChR purified using acetylcholine affinity resin. The purified AChR was analyzed by Western blot using an anti-AChR (A) or anti-phosphotyrosine antibody (B). AChR subunit location are as indicated.

function of Tctex. For example, coexpression of Fyn dramatically upregulated the expression of Tctex (Fig 5). In addition, the sequence of *Torpedo* Tctex indicated a putative tyrosine phosphorylation site at Tyr4 (Fig 2). In fact, a Tctex fusion protein could be phosphorylated on tyrosine residue(s) *in vitro* by immunoprecipitated Fyn (unpublished results). These results demonstrate that Fyn regulated the expression of Tctex, that Tctex and Fyn formed a complex, and suggest that Tctex may be a substrate for Fyn at the NMJ. Anchoring of postsynaptic components at the NMJ by cytoskeletal elements is now believed to involve tyrosine phosphorylation of postsynaptic components. Thus, Fyn may regulate AChR aggregation via an effect on the Tctex cytoskeletal element. In fact, Tctex is complexed with the AChR in *Torpedo* electric organ (unpublished results). Determining the function of Tctex at the NMJ will be a focus of ongoing experiments in our laboratory.

Project 3: Determination of the Physiological Roles of Fyn and Fyk

To determine the physiological role of Fyn and Fyk in synapse formation and function, a strategy involving expression of recombinant kinases in a heterologous cell line that expresses the AChR has been developed. Fyn and Fyk were efficiently expressed when the Q-F18 quail

Using the yeast two-hybrid system, we identified a molecular component of *Torpedo* electric organ that interacts with the unique domain of Fyn. This 13kDa component was homologous to a previously identified mouse sterility factor, Tctex-1 (Fig 2) that is a light chain of the cytoplasmic microtubule protein dynein. *Torpedo* Tctex-1 (Tctex) was detected in the cytosolic and membrane fractions, including the postsynaptic membranes, of electric organ using antiserum generated to a fusion protein derived from the *Torpedo* clone (Fig 3). In addition to the association in yeast, Tctex and Fyn formed a complex, as demonstrated by coimmunoprecipitation, when coexpressed in a heterologous cell system (Fig 4). In this experiment, the expressed Fyn was the predominant phosphotyrosine containing protein and thus demonstrated significant nonspecific precipitation with the control preimmune serum. However, the enrichment of Fyn in the Tctex immunoprecipitation from cotransfected cells was six fold over coprecipitation with the preimmune serum as demonstrated by quantitative densitometry scanning. In addition, coprecipitation was dependent on expression of both Tctex and Fyn. Thus, the cytoskeletal protein Tctex did form a complex *in vivo* with the protein tyrosine kinase.

Our results also suggested that Fyn may regulate the expression and

fibroblast cell line was transfected with kinase constructs as demonstrated by the immune complex kinase assay (unpublished results). In addition, Fyn and Fyk appeared to be active as the total cellular protein tyrosine phosphorylation was increased by expression of the kinases as shown by Western analysis of cellular lysates with an anti-phosphotyrosine antibody (unpublished results).

Recent experiments support the hypothesis that Src kinases mediate the phosphorylation of the AChR *in vivo*. Coexpression of Fyn, Fyk, or Src and the AChR specific cytoskeletal protein rapsyn in the Q-F18 cells increased tyrosine phosphorylation of the AChR as demonstrated by phosphorylation state specific antibodies (Fig 6). AChR purified from Q-F18 cells transfected with the kinases and rapsyn were analyzed in parallel for AChR content (Fig 6A) and AChR tyrosine phosphorylation (Fig 6B). When the ratios of AChR phosphorylation to expression were compared, it was determined that AChR phosphorylation was increased 1.8 fold by rapsyn, 20 fold by rapsyn plus Fyn, 1.7 fold by rapsyn plus Fyk, and 50 fold by rapsyn plus Src. Thus, Fyn and Src dramatically increased AChR phosphorylation. These data provide strong evidence that Src kinases are important regulators of the AChR. Experiments are in progress to determine the molecular mechanism by which Fyn, Fyk, and Src modulate synaptic transmission at the NMJ via a direct regulation of the AChR. These investigations include examining the regulation of AChR clustering during synaptogenesis and receptor channel properties at the adult synapse.

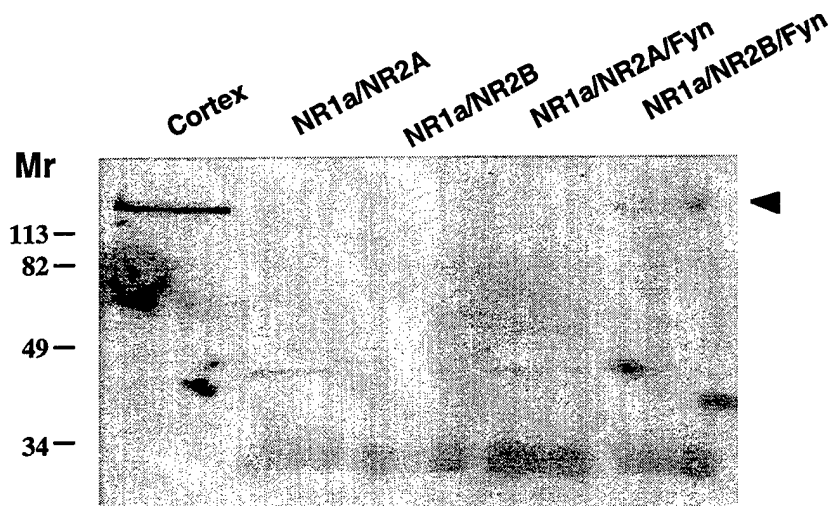


Fig 7. NMDA-R 2B subunit Phosphorylation. HEK293 cells were transfected with NR1a/NR2A, NR1a/NR2B, NR1a/NR2A/Fyn, or NR1a/NR2B/Fyn pBK-CMV expression constructs. The cells were solubilized and subjected to immunoprecipitation with anti-NR1a, anti-NR2A, and/or anti-NR2B antibody. The immunoprecipitates and 20ug of rat brain cortex were analyzed by Western blot using an antiphosphotyrosine antibody. Molecular weights are as indicated. The position of the NMDA-R 2B subunit is indicated by an arrow.

Project 4: Determination of the Physiological Roles of Fyn at Central Synapses

Src class protein tyrosine kinases including Fyn are very highly expressed in neurons of the brain suggesting their importance in synaptic transmission within the central nervous system. Fyn has been implicated as an important mediator of learning and memory since Fyn knock out mice show impaired spatial learning and long term potentiation (LTP) within the hippocampus. The N-methyl-D-aspartate (NMDA) glutamate receptor is thought to be critical for LTP, a molecular model for learning and memory. In

addition, NMDA receptor subunits NR2A and NR2B are tyrosine phosphorylated. Thus, we have begun to investigate the role of Fyn in regulating the NMDA receptor. Recent experiments demonstrated that the NR2B but not the NR2A was tyrosine phosphorylated when coexpressed with Fyn in a heterologous expression system (Fig 7). These data further support the importance of Fyn in the molecular basis of learning and memory via a direct regulation of the NMDA receptor. Future studies will investigate whether Fyn mediated phosphorylation of the NMDA receptor regulates channel properties of this important ligand gated ion channel of the central nervous system.

In summary we have made significant progress in demonstrating that Src class protein tyrosine kinases are involved in the regulation of ligand gated ion channels both in the peripheral and central nervous system. Clarification of these basic molecular processes are relevant to an

understanding of synaptic transmission in healthy people as well as those afflicted with neurological and neuromuscular diseases.

References

- Swope, S.L., Moss, S.J., Blackstone, C. and Huganir, R.L. Phosphorylation of ligand-gated ion channels: a possible mode of synaptic plasticity. *FASEB J.*, 6:2514-2523, 1992..
- Swope, S.L. and Huganir, R.L. Molecular cloning of two abundant protein tyrosine kinases in *Torpedo* electric organ that associate with the acetylcholine receptor. *J. Biol. Chem.*, 268:25152-25161, 1993.
- Swope, S.L. and Huganir, R.L. Binding of the nicotinic acetylcholine receptor to SH2 domains of fyn and fyn protein tyrosine kinases. *J. Biol. Chem.*, 269:29817-29824, 1994.
- Swope, S. L. Qu. Z. and Huganir, R. L. Phosphorylation of the nicotinic acetylcholine receptor by protein tyrosine kinases. *Ann. N.Y. Acad. Sci.* 757: 197-214, 1995.
- Swope, S. L., Moss, S.J., Raymond, L., and Huganir, R. L. Phosphorylation of Ligand-Gated Ion Channels. In: D. Armstrong and S. Rossie (Eds.) *Advances in Second Messengers and Phosphoproteins*, in press.
- Mou, T., Fung, E., and Swope, S. L. Identification of a *Torpedo* electric organ component that interacts with the Fyn protein tyrosine kinase. Abstract, 27th Annual Meeting, Society for Neuroscience, No. xxx.x pxxxx, in press.
- Mou, T., Fung, E., and Swope, S. L. Identification of a *Torpedo* electric organ component that interacts with the Fyn protein tyrosine kinase, in preparation.

OTHER GICCS SPONSORED RESEARCH

ROBERT S. LEDLEY, D.D.S.

"Texture Analysis for Scene Segmentation" Phase II

Project Overview

During Phase I of this funded investigation on image texture analysis we hypothesized that the DCT would be useful for texture identification. The manuscript which we submitted with the Phase I final progress report on June 8, 1995, outlined the development of shift-insensitive texture measurements derived from DCT coefficients, also known as DCT derived shift-insensitive texture measurements (DCTDSITM). During Phase II of this project we identified that using the maximum function as a secondary image filter could also be used to produce shift-insensitive texture measurements. In that study the maximum function was used in conjunction with the Derivative of Gaussian functions. The DCTDSITMs were only tested on small images which contained only four textures. In order to expand the practical use of DCT coefficients and validate our earlier study additional studies were performed.

DCT Coefficients, DCTDSITM and the Maximum Function

In our previous report we compared texture categorization using DCT coefficients and the DCTDSITM developed within the report of an image with four textures. In order to confirm our previous result and further study the utility of the maximum function in shift-insensitive texture analysis, we tested the ability of (a) DCT coefficients alone, (b) DCTDSITMs and (c) the maximum function applied to both DCT coefficients and DCTDSITMs to categorize the textures in a new image composed of four Brodatz textures.

Figure 1 shows the newly developed image in the upper right corner and the texture mask in the upper left corner. The classification results for all texture classification methods are shown in Table 1. Like our previous results the DCT coefficients did a poor job of classifying four textures, whereas the DCTDSITMs performed rather adequately. The middle left image shows the results from using the DCT coefficients alone to classify the four textures. As can be seen from this image and Table 1, the DCT coefficients classify only 35% of the image texture correctly whereas the DCTDSITMs (also called DCT Texture) classify 91% of the image texture correctly.

Using the maximum function provides impressive results. Using the maximum function with DCT coefficients as input provides a correct classification of 94% of the image texture whereas the maximum function in combination with the DCTDSITMs provides marginal improvement in texture classification.

Overall it appears that using the maximum function in combination with DCT coefficients provides the most accurate classification of texture. However, the calculation of the maximum function over the DCT area requires more calculations than calculating the DCTDSITMs. In addition, once the DCTDSITMs are calculated, the number of texture measurement values that are used is reduced from 340 to 68. This reduced the process of calculating the discriminant function for classification tremendously.

Classifying an Image with Many More Textures

Figure 2 shows that the same performance pattern when an image with sixteen textures is used, however the differences in the three high-performance methods is broadened. This study shows that using the maximum function on the DCT texture values substantially enhances their performance and that the maximum function applied to the DCT coefficients allows texture classification which is substantially better than using the texture coefficients, even when they are used in combination with the maximum function.

Although the DCT coefficients used in conjunction with the maximum function outperform the DCTDSITMs used in conjunction with the maximum function overall, this performance is not universal for all textures. For example, Table 2b shows that Textures 4, 7, and 12 are classified equally well by the two methods, and Textures 10, 14, and 15 are classified better using DCTDSITMs used in conjunction with the maximum function.

Expanding the Area of Texture Measurements

So far the area over which the maximum function is applied is regulated by the DCT coefficient area processed to provide the DCT coefficient values. However, a problem arises for textures which contain subtextures which are larger than the size of the area processed by the DCT. Although one solution would be to use larger areas to calculate the DCT, this requires an enormous amount of calculations and would produce an enormous number of DCT coefficients which requires an enormous amount of storage and analysis. A solution to this problem might be to use the characteristics derived from a small area to characterize a larger area. For example, textures 6 and 11 contain subtexture which are very large. The influence of the size of these subtextures are evidenced by the fact that large areas of them are classified incorrectly when the DCTDSITMs, combined with or without the maximum function, are used to classify the texture image. Interestingly, the misclassified regions are shaped like part of the subtexture.

The maximum function was applied to the DCT coefficients and DCTDSITMs over 16 x 16, 32 x 32 and 64 x 64 areas. The classification performance using the maximum functions with these areas were then evaluated. Figure 3 shows the resulting classification images and Tables 2c, 2d, and 2e show the detailed classification matrix for these images. In order to further analyze the influence for these different methods, the correct classification for each texture using these three fixed area maximum functions and the original variable area maximum function were analyzed in Table 3. Along the bottom of each column is a symbol indicating the method which provided the best classification performance. As can be seen from Table 3, different textures require different maximum functions for optimal classification accuracy.

Conclusion

This study confirms our early results on the use of the DCT for texture classification. We have extended our work in order to identify a new shift-insensitive texture transformation -- the maximum function. The maximum function appears to be very useful in improving the performance of texture classification based on DCT coefficients and DCTDSITMs. Furthermore, our analysis on various sized maximum functions suggest that a method should be developed which chooses the appropriate area of maximum function transformation in order to provide optimal texture classification.

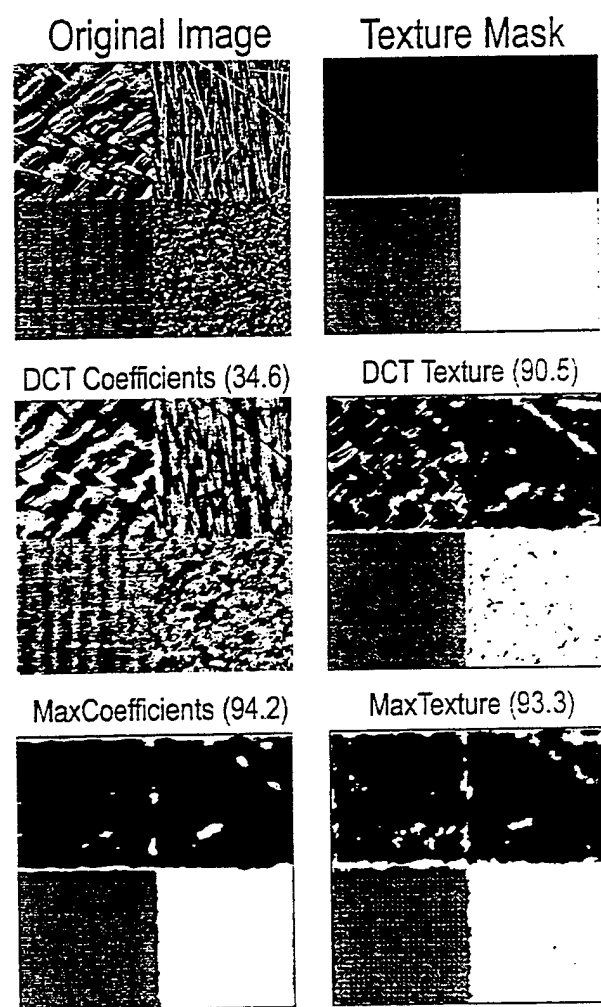


FIGURE 1

Table 1

DCT Coefficients (35%)

46 10 14 29
32 22 19 26
21 15 34 30
24 17 23 35

Maximal DCT Coefficients (94%)

88 03 03 06
00 91 00 09
00 00 100 00
00 00 03 97

DCT Texture (91%)

80 02 00 18
03 86 00 11
00 00 99 01
02 00 01 97

Maximal DCT Texture (93%)

86 03 01 11
00 91 00 09
00 00 97 03
00 00 01 99

Original Image

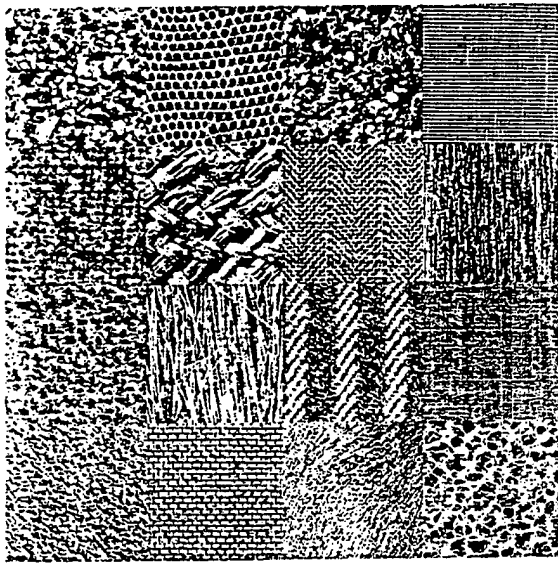
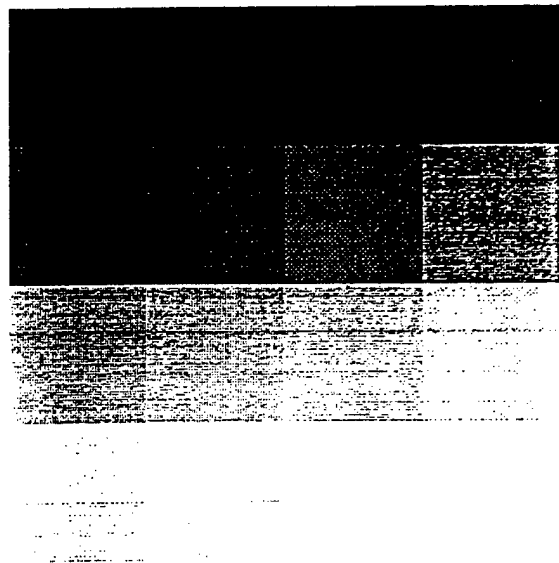
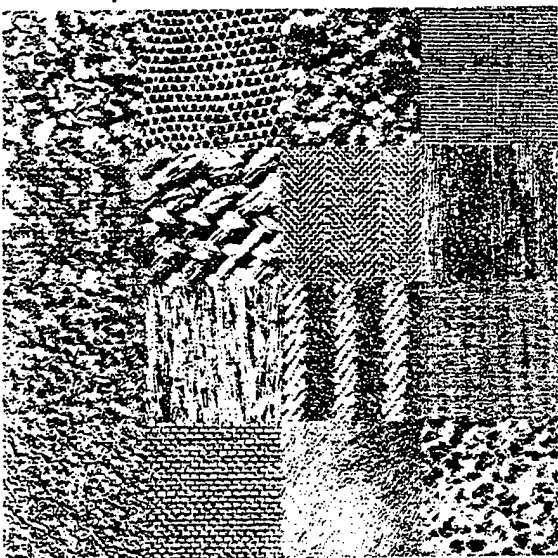


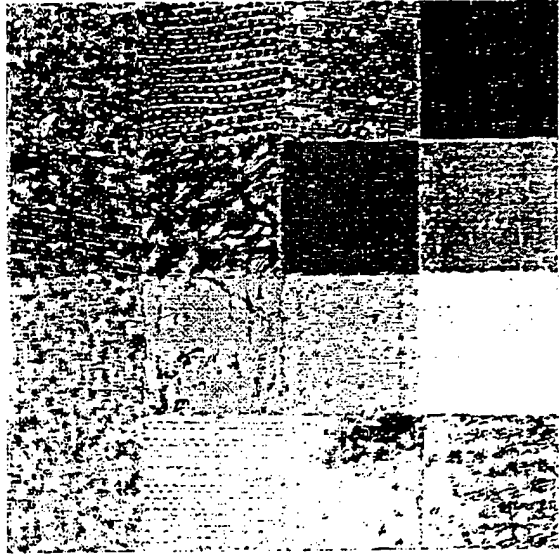
Image Mask



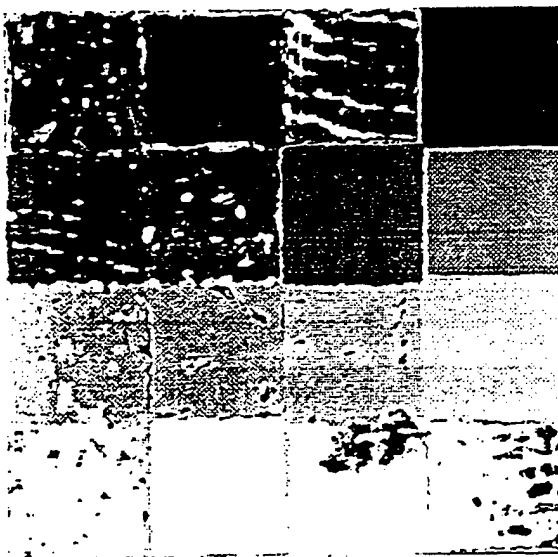
DCT Coefficients (11%)



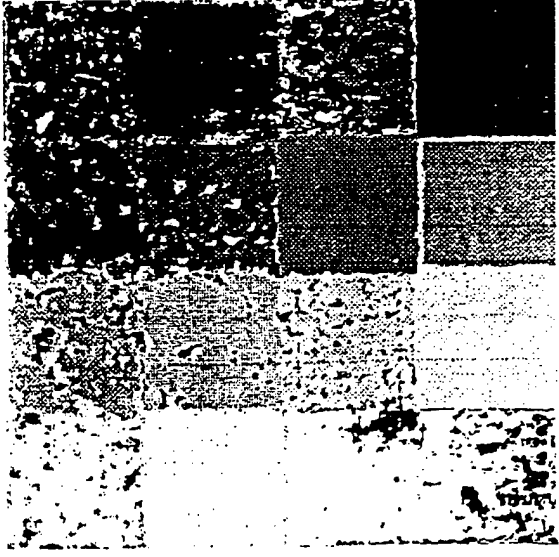
Texture Coefficients (66%)



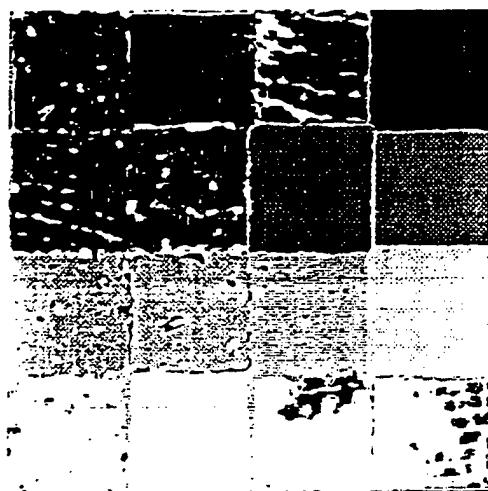
DCT MaxCoefficients (85%)



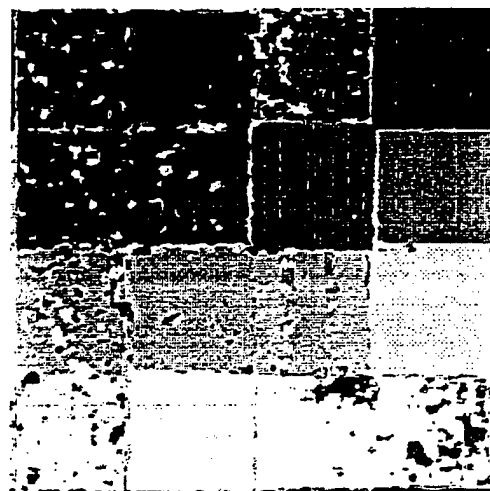
Texture MaxCoefficients (78%)



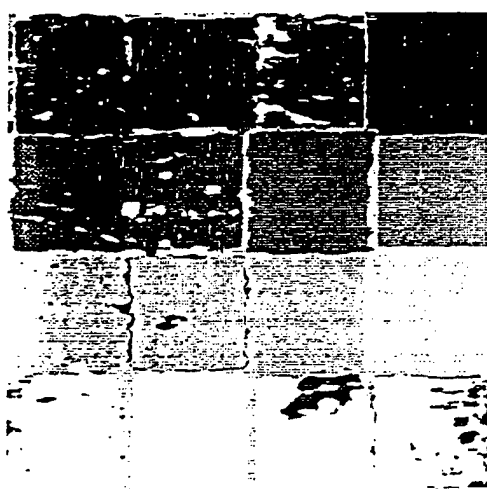
Maxium DCT Fixed 16 (86%)



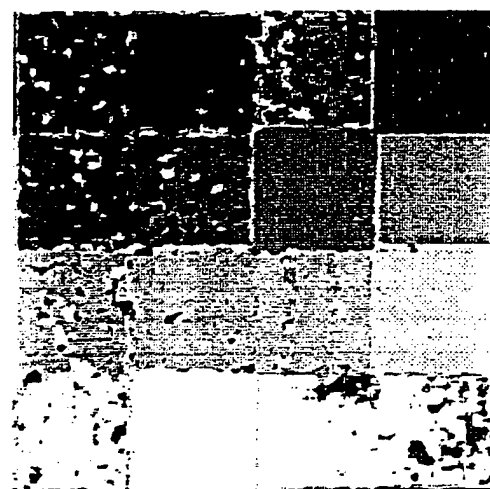
Maxium Texture Fixed 16 (80%)



Maxium DCT Fixed 32 (85%)



Maxium Texture Fixed 32 (80%)



Maxium DCT Fixed 64 (84%)



Maxium Texture Fixed 64 (78%)

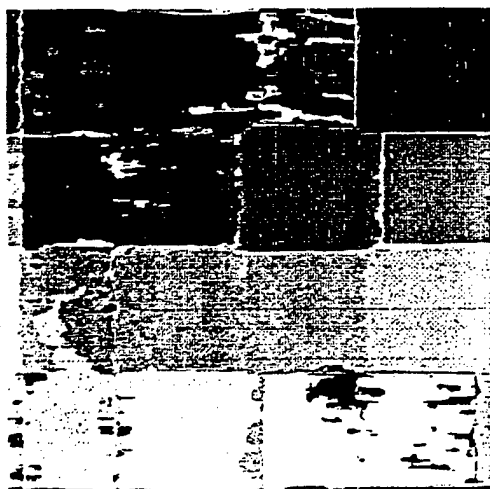


Table 2a

DCT Coefficient Values (11,3)														
1.8	2.1	2.1	5.1	1.2	1.4	3.7	3.5	1.1	17.7	2.4	3.9	1.9	2.7	1.4
1.4	2.3	3.9	8.0	1.0	1.5	4.1	33.6	1.2	16.5	2.7	4.8	2.0	2.6	1.9
1.8	2.6	3.3	5.3	1.6	1.3	3.7	36.7	2.0	12.9	2.9	5.6	2.2	4.1	1.9
1.9	1.5	1.5	17.8	1.8	2.1	8.9	23.7	1.4	9.6	2.8	8.0	3.2	6.0	1.2
2.7	3.1	4.5	6.9	2.9	2.4	5.9	30.1	2.6	9.4	3.6	7.5	2.9	5.3	2.1
1.8	1.4	2.2	3.5	0.8	1.4	3.0	3.3	1.3	18.4	2.5	4.3	1.9	2.9	1.8
2.3	2.4	2.7	10.3	1.2	1.6	7.6	17.1	1.4	20.6	2.5	5.0	2.4	3.3	1.6
4.4	2.6	4.1	7.9	2.6	2.3	3.3	40.1	2.1	5.5	2.4	6.7	3.3	5.8	1.4
2.9	3.2	4.0	7.7	1.8	1.9	5.9	24.8	3.0	13.0	3.0	8.0	3.2	4.8	2.0
0.9	3.6	1.9	4.9	0.7	1.2	5.1	8.5	0.8	31.7	4.5	3.1	1.6	2.8	2.2
1.7	2.5	2.5	7.0	1.5	1.2	3.7	28.7	1.8	15.6	3.9	5.9	2.4	3.1	1.0
3.2	2.9	3.3	11.2	1.0	1.7	7.2	14.0	3.2	9.5	4.3	18.7	4.1	4.9	1.7
3.4	3.2	3.2	9.2	1.9	2.1	7.4	21.1	2.3	13.8	4.0	8.0	3.4	4.4	2.0
4.0	2.4	3.3	10.0	1.4	2.7	7.0	15.5	2.7	11.5	4.7	8.7	4.1	8.5	2.8
1.9	1.9	1.6	4.4	0.6	1.6	5.7	5.6	2.2	28.1	3.1	6.1	1.2	3.1	2.2
2.5	3.0	2.6	4.4	1.0	1.7	5.7	19.7	2.1	19.7	3.9	5.0	2.5	3.9	3.2
DCT Texture Values (65,9)														
40.0	9.4	8.2	0.5	3.2	10.0	3.7	0.0	3.7	0.8	7.3	0.0	8.7	0.5	4.5
3.8	62.9	5.9	0.0	0.5	0.0	5.6	0.0	0.6	2.0	3.5	0.0	11.2	0.5	3.3
9.6	3.9	26.5	0.0	21.3	12.2	0.5	0.1	3.7	0.8	1.8	0.0	2.7	0.2	1.2
0.0	0.0	0.0	93.7	0.0	0.0	0.9	0.0	0.0	0.0	0.3	3.1	0.0	1.7	0.0
1.7	0.1	7.9	0.0	60.6	8.7	0.0	1.9	2.0	0.4	1.2	0.0	0.6	0.0	9.7
16.0	2.5	11.6	0.0	15.9	28.8	1.0	0.0	5.0	0.2	5.9	0.0	3.9	0.1	5.0
0.3	0.3	0.0	0.0	0.0	0.0	96.4	0.0	0.0	0.0	0.7	0.0	1.1	1.1	0.0
0.0	0.0	0.0	0.5	0.7	0.0	0.3	92.9	0.0	0.3	0.8	0.3	0.0	3.5	0.0
4.6	2.9	7.1	0.0	5.9	2.0	1.9	0.0	43.8	0.0	12.5	0.7	12.5	2.0	0.6
0.5	2.1	1.3	0.0	2.8	0.2	0.2	1.4	0.0	85.1	3.3	0.0	1.2	0.2	0.5
3.4	0.7	0.0	0.0	0.1	3.1	2.1	0.0	9.0	0.8	61.1	0.7	5.9	8.7	4.1
0.0	0.0	0.0	0.0	0.0	0.0	0.1	0.0	0.0	0.0	0.0	99.6	0.0	0.2	0.0
6.9	7.1	1.9	0.0	0.6	1.7	2.0	0.0	13.3	0.2	11.2	0.1	48.4	1.7	0.9
0.1	0.0	0.0	0.0	0.0	0.0	1.3	0.1	0.5	0.0	5.0	0.6	0.3	91.2	0.0
0.3	0.0	0.1	0.0	12.9	0.6	0.3	0.0	2.8	0.6	5.2	0.0	1.4	1.0	0.4
2.9	1.2	11.6	0.0	15.7	7.0	0.2	0.2	2.5	1.5	1.0	0.5	1.5	0.7	51.9

Table 2b

Regional Maximal DCT Coefficient Values (84.8)												
82.5	0.6	0.7	0.6	0.3	3.7	1.8	0.0	0.2	0.1	1.6	0.0	6.1
0.6	92.1	0.4	0.0	0.0	0.0	2.9	0.0	0.0	0.0	1.6	0.0	4.8
1.7	1.2	53.9	0.4	16.0	1.6	0.9	0.0	2.2	0.2	2.2	0.0	1.7
0.0	0.0	0.0	99.8	0.0	0.0	0.2	0.0	0.0	0.0	0.0	0.0	0.0
1.1	0.0	6.1	0.0	82.2	2.6	0.0	1.3	1.7	0.2	0.5	0.0	0.2
6.1	0.1	2.4	0.0	11.1	66.9	0.7	0.1	2.4	0.2	4.1	0.0	1.0
0.0	0.0	0.0	0.0	0.0	0.0	99.7	0.0	0.0	0.0	0.3	0.0	0.0
0.0	0.0	0.0	2.0	0.0	0.0	0.2	88.4	0.0	0.0	5.2	1.8	0.0
0.0	0.2	1.3	0.0	0.2	0.2	0.0	0.0	77.2	0.0	8.9	2.3	8.6
0.4	1.8	2.3	0.0	0.4	0.2	0.0	0.0	0.2	88.4	1.6	0.0	2.1
0.9	0.0	0.0	0.0	0.0	0.8	1.7	0.0	1.5	0.0	91.5	2.6	0.6
0.0	0.0	0.0	0.0	0.0	0.0	0.0	0.0	0.0	0.0	0.0	100.0	0.0
2.2	1.6	0.3	0.0	0.0	0.0	0.0	0.0	2.5	0.0	3.5	0.0	89.7
0.0	0.0	0.0	0.0	0.0	0.0	0.3	0.0	0.0	0.0	3.9	0.0	0.0
0.1	0.0	0.1	0.0	3.9	7.5	0.2	0.0	7.0	0.0	3.8	0.3	0.0
0.5	0.5	4.1	1.3	9.5	1.1	0.0	0.0	2.5	0.4	0.9	1.6	1.4
Regional Maximal DCT Texture Value (77.6)												
67.5	4.5	8.1	1.0	0.4	4.0	3.0	0.0	2.1	0.1	1.6	0.0	3.5
4.7	88.7	0.5	0.0	0.0	0.0	1.4	0.0	0.3	0.2	0.6	0.0	2.7
11.1	1.4	31.0	0.7	18.8	17.7	1.6	0.0	4.2	0.4	1.7	0.0	2.3
0.0	0.0	0.0	99.9	0.0	0.0	0.1	0.0	0.0	0.0	0.0	0.0	0.0
0.8	0.0	5.6	0.0	76.2	6.1	0.1	1.7	1.3	1.0	1.2	0.0	0.3
12.1	0.4	11.8	0.0	16.0	46.9	1.1	0.0	4.4	0.2	2.6	0.0	0.6
0.1	0.0	0.0	0.0	0.0	0.0	99.6	0.0	0.0	0.0	0.1	0.0	0.2
0.0	0.0	0.0	1.6	0.0	0.0	1.5	86.9	0.0	0.7	3.2	0.7	0.0
3.4	0.3	4.6	0.0	1.6	1.3	0.1	0.0	66.1	0.0	9.8	1.3	8.0
0.2	2.8	0.5	0.0	0.3	0.0	0.3	1.0	0.1	90.1	3.4	0.0	0.7
4.8	0.2	0.2	0.0	0.3	1.6	1.3	0.0	8.7	0.5	71.6	2.3	1.6
0.0	0.0	0.0	0.0	0.0	0.0	0.0	0.0	0.0	0.0	0.0	99.4	0.0
3.7	4.1	0.7	0.0	0.1	0.0	1.1	0.0	4.3	0.3	3.6	0.0	78.8
0.0	0.0	0.0	0.0	0.0	0.0	0.2	0.0	0.7	0.0	1.8	0.0	0.0
0.2	0.0	0.3	0.0	8.4	0.2	0.1	0.0	3.4	0.4	3.4	0.0	1.9
2.9	0.6	5.3	0.5	15.5	2.2	0.8	0.0	3.0	1.5	1.6	0.7	1.8
											1.1	61.5

Table 2c

Maximal DCCT Coefficient Values in Fixed 16 x 16 Area (85.6)

	0.8	0.2	1.2	0.6	1.6	1.7	0.0	0.2	0.1	1.4	0.0	3.5	0.0	0.0	1.3
87.5	0.8	0.2	1.2	0.6	1.6	1.7	0.0	0.2	0.1	1.4	0.0	3.5	0.0	0.0	1.3
0.6	91.9	0.4	0.0	0.0	0.0	0.2	0.0	0.1	0.0	2.2	0.0	4.5	0.0	0.0	0.0
0.8	1.6	51.0	1.1	16.5	2.9	1.2	0.0	1.9	0.3	2.0	0.0	2.0	0.0	1.0	17.6
0.0	0.0	0.0	99.8	0.0	0.0	0.1	0.0	0.0	0.0	0.0	0.0	0.0	0.0	0.0	0.0
1.2	0.0	7.6	0.0	77.8	4.4	0.0	1.6	1.6	0.4	0.5	0.0	0.2	0.0	1.0	3.7
4.6	0.0	1.3	0.0	10.2	70.8	0.6	0.2	1.7	0.1	4.4	0.0	1.3	0.3	2.3	2.1
0.0	0.0	0.0	0.0	0.0	0.0	99.7	0.0	0.0	0.0	0.3	0.0	0.0	0.0	0.0	0.0
0.0	0.0	0.0	2.6	0.0	0.0	0.6	88.4	0.0	0.0	3.3	3.4	0.0	1.6	0.0	0.0
0.1	0.4	0.8	0.0	0.2	0.6	0.0	0.0	83.2	0.0	7.4	3.3	3.4	0.0	0.0	0.7
0.9	2.5	1.0	0.0	0.2	0.0	0.0	0.0	0.2	88.3	1.0	0.0	2.8	1.6	0.6	0.9
0.5	0.1	0.0	0.0	0.0	0.1	1.3	0.0	0.7	0.0	93.3	3.7	0.3	0.0	0.2	0.0
0.0	0.0	0.0	0.0	0.0	0.0	0.0	0.0	0.0	0.0	0.0	100.0	0.0	0.0	0.0	0.0
1.2	1.1	0.2	0.0	0.0	0.1	0.0	0.0	1.6	0.1	3.3	0.1	92.3	0.0	0.0	0.1
0.0	0.0	0.0	0.0	0.0	0.0	0.1	0.0	0.0	0.0	3.3	0.0	0.0	96.5	0.0	0.0
0.2	0.0	0.0	0.0	4.3	6.6	0.0	0.0	6.3	0.1	5.4	0.2	0.2	0.6	75.2	1.1
0.2	1.1	4.8	2.2	7.8	0.7	0.1	0.0	1.3	0.9	0.8	2.5	1.5	0.0	2.8	73.5

Maximal DCCT Texture Values in Fixed 16 x 16 Area (79.7)

	4.8	3.0	2.7	0.0	3.4	2.0	0.0	0.8	0.0	0.5	0.0	2.4	0.1	0.0	2.0
78.6	4.8	3.0	2.7	0.0	3.4	2.0	0.0	0.8	0.0	0.5	0.0	2.4	0.1	0.0	2.0
2.8	91.4	0.2	0.0	0.0	0.0	3.4	0.0	0.0	0.1	0.7	0.0	0.9	0.5	0.0	0.0
8.4	1.5	35.8	1.6	17.0	17.0	2.8	0.1	2.7	0.4	1.8	0.0	2.7	0.4	0.3	7.5
0.0	0.0	0.0	99.9	0.0	0.0	0.1	0.0	0.0	0.0	0.0	0.0	0.0	0.0	0.0	0.0
1.0	0.0	7.4	0.1	74.5	3.8	0.0	2.1	2.3	2.3	0.5	0.0	0.2	0.1	1.7	3.8
9.4	0.5	9.5	0.0	13.7	53.8	1.3	0.0	3.3	0.5	5.3	0.0	0.6	0.1	0.7	1.3
0.0	0.0	0.0	0.1	0.0	0.0	99.5	0.0	0.0	0.0	0.2	0.0	0.1	0.2	0.0	0.0
0.0	0.0	0.0	3.4	0.1	0.0	2.0	86.2	0.0	1.5	0.5	0.9	0.0	5.4	0.0	0.0
1.7	0.2	3.6	0.0	1.1	0.5	0.4	0.0	71.5	0.1	8.5	1.7	7.1	2.0	0.7	1.1
0.0	1.6	0.1	0.0	0.0	0.0	2.0	0.9	0.0	90.4	3.5	0.0	0.4	1.1	0.0	0.0
0.4	0.1	0.0	0.0	0.0	0.0	2.3	0.0	9.6	1.0	75.2	2.0	3.6	2.7	3.0	0.0
0.0	0.0	0.0	0.3	0.0	0.0	0.0	0.0	0.0	0.0	0.0	99.1	0.0	0.5	0.0	0.0
3.1	3.4	0.6	0.0	0.1	0.0	2.0	0.0	5.1	0.2	3.5	0.1	78.6	2.7	0.5	0.3
0.0	0.0	0.0	0.0	0.0	0.0	0.8	0.0	0.0	0.0	0.4	0.0	0.0	98.8	0.0	0.0
0.1	0.0	0.4	0.0	8.5	0.1	0.0	0.0	2.9	0.4	4.5	0.0	1.1	2.9	78.8	0.3
1.4	0.2	3.2	2.5	14.1	1.8	0.5	0.1	1.8	1.3	3.5	2.2	1.6	1.3	1.2	63.5

Table 2d

Maximal DC T Coefficient Values in Fixed 32 x 32 Area (85.4)

88.0	0.6	0.4	1.7	0.0	1.0	4.2	0.0	0.0	0.2	0.9	0.0	2.4	0.0	0.0	0.6
1.0	90.7	0.6	0.0	0.0	0.0	0.3	0.0	0.0	0.0	2.6	0.0	4.9	0.0	0.0	0.0
0.5	2.1	58.0	3.4	15.0	1.6	1.3	0.0	2.7	0.4	2.3	0.0	0.1	0.0	0.6	11.1
0.0	0.0	0.0	99.1	0.0	0.0	0.9	0.0	0.0	0.0	0.0	0.0	0.0	0.0	0.0	0.0
1.2	0.0	5.1	0.0	80.8	3.9	0.0	4.2	2.2	0.1	0.5	0.0	0.0	0.1	0.5	1.6
3.1	0.0	1.5	0.0	9.4	70.3	1.2	0.1	3.0	0.1	7.5	0.0	0.4	0.1	2.4	1.0
0.0	0.0	0.0	0.0	0.0	0.0	98.8	0.0	0.0	0.0	1.2	0.0	0.0	0.0	0.0	0.0
0.0	0.0	0.0	2.7	0.0	0.0	1.0	86.9	0.0	0.0	4.9	3.0	0.0	1.5	0.1	0.0
0.0	0.3	0.7	0.0	0.0	0.6	0.0	0.0	81.6	0.0	5.0	5.6	5.8	0.0	0.0	0.3
0.8	2.9	2.5	0.0	0.0	0.3	0.0	0.0	0.5	85.3	4.4	0.0	1.5	1.3	0.4	0.2
0.0	0.0	0.0	0.0	0.0	0.0	1.6	0.0	0.7	0.0	92.6	4.9	0.0	0.0	0.0	0.0
0.0	0.0	0.0	0.0	0.0	0.0	0.0	0.0	0.0	0.0	0.0	100.0	0.0	0.0	0.0	0.0
0.6	2.2	0.4	0.0	0.0	0.0	0.2	0.0	1.0	0.0	5.3	0.1	90.2	0.0	0.0	0.0
0.0	0.0	0.0	0.0	0.0	0.0	0.0	0.0	0.0	0.0	6.7	0.1	0.0	93.1	0.0	0.0
0.0	0.0	0.0	0.0	4.2	8.0	0.0	0.0	3.0	0.0	6.7	0.5	0.2	0.5	75.9	0.9
0.4	1.0	3.1	2.2	6.7	0.9	0.0	0.0	1.8	0.8	0.3	2.8	2.0	0.0	3.1	74.8

Maximal DC T Texture Values in Fixed 32 x 32 Area (80.2)

79.8	3.2	3.2	4.8	0.0	1.4	2.3	0.0	0.2	0.0	1.0	0.0	2.3	0.0	0.0	1.7
2.5	91.1	0.1	0.0	0.0	0.0	3.0	0.0	0.0	0.3	0.3	0.0	1.8	0.8	0.0	0.0
6.7	1.2	38.1	4.4	15.0	15.1	2.8	0.0	1.7	0.6	1.3	0.0	2.8	0.4	0.6	9.2
0.0	0.0	0.0	100.0	0.0	0.0	0.0	0.0	0.0	0.0	0.0	0.0	0.0	0.0	0.0	0.0
0.6	0.0	7.7	0.1	74.8	3.2	0.0	5.7	1.8	1.2	0.7	0.0	0.5	0.0	1.4	2.2
5.9	0.2	6.0	0.0	14.9	58.3	2.8	0.0	3.1	0.5	6.0	0.0	0.7	0.0	0.5	0.9
0.0	0.0	0.0	0.2	0.0	0.0	99.3	0.0	0.0	0.0	0.3	0.0	0.0	0.2	0.0	0.0
0.0	0.0	0.0	3.1	0.0	0.0	2.3	84.6	0.0	0.5	3.1	0.4	0.0	6.0	0.0	0.0
0.7	0.0	1.7	0.0	0.2	0.1	0.0	0.0	73.0	0.3	6.1	4.5	10.5	2.0	0.9	0.1
0.0	1.2	0.0	0.0	0.0	0.0	0.5	0.5	0.0	90.6	7.0	0.0	0.0	0.2	0.0	0.0
0.4	0.0	0.0	0.0	0.0	0.0	1.8	0.0	11.2	1.3	75.1	3.5	1.0	4.2	1.5	0.0
0.0	0.0	0.0	0.0	0.0	0.0	0.0	0.0	0.0	0.0	0.0	99.1	0.0	0.1	0.0	0.0
1.6	2.5	0.3	0.0	0.0	0.0	2.8	0.0	3.3	0.2	6.5	0.1	80.4	2.0	0.1	0.2
0.0	0.0	0.0	0.0	0.0	0.0	0.7	0.0	0.0	0.0	1.5	0.0	0.0	97.8	0.0	0.0
0.6	0.0	2.4	0.1	8.7	0.1	0.1	0.0	3.7	0.0	5.4	0.0	0.3	3.2	74.5	1.0
1.5	0.0	2.3	2.2	11.2	0.7	0.1	0.0	1.9	1.8	5.6	2.9	0.6	0.6	1.9	66.8

Table 2e

Maximal DCCT Coefficient Values in Fixed 64 x 64 Area (83.8)													
85.8	1.0	0.0	0.2	0.0	0.0	11.4	0.0	0.0	0.4	0.0	1.2	0.0	0.0
2.2	87.5	1.0	0.0	0.0	0.0	0.4	0.0	0.1	0.0	0.0	6.4	0.1	0.0
0.1	3.1	58.4	7.6	10.7	0.5	2.1	0.0	2.1	0.4	0.0	2.4	0.0	9.3
0.0	0.0	0.0	95.5	0.0	0.0	4.5	0.0	0.0	0.0	0.0	0.0	0.0	0.0
1.8	0.0	2.1	0.1	78.1	5.7	0.0	7.8	2.2	0.1	0.2	0.1	0.3	0.3
1.2	0.0	0.1	0.0	3.2	76.9	2.6	0.0	2.3	0.0	11.1	0.6	0.2	1.5
0.0	0.0	0.0	0.0	0.0	0.0	99.6	0.0	0.0	0.0	0.4	0.0	0.0	0.0
0.0	0.0	0.0	2.4	0.0	0.0	5.3	81.2	0.0	0.0	4.4	0.1	3.2	0.1
0.0	0.5	0.9	0.0	0.0	0.1	0.0	0.0	81.0	0.4	3.3	10.6	0.0	0.0
0.1	2.2	3.2	0.0	0.0	0.0	0.0	0.0	1.4	80.6	8.1	0.0	1.3	0.4
0.0	0.0	0.1	0.0	0.0	0.0	0.1	0.0	0.2	0.0	94.6	4.2	0.1	0.0
0.0	0.0	0.0	0.0	0.0	0.0	0.1	0.0	0.0	0.0	99.9	0.0	0.0	0.0
0.5	1.3	0.2	0.0	0.0	0.0	0.0	0.0	1.3	0.0	6.8	0.1	89.1	0.5
0.0	0.0	0.0	0.0	0.0	0.0	0.1	0.0	0.0	0.0	8.9	2.1	0.7	88.3
0.0	0.0	0.2	0.0	7.9	5.6	0.1	0.0	2.0	0.0	11.3	2.2	0.3	68.8
0.3	1.2	1.7	1.7	1.7	0.1	0.6	0.0	1.2	0.9	0.8	3.0	0.0	6.2
													75.5
Maximal DCCT Texture Values in Fixed 64 x 64 Area (77.8)													
77.0	1.1	0.3	10.0	0.0	7.7	3.1	0.0	0.1	0.0	0.7	0.0	0.0	0.1
6.6	83.7	2.4	0.0	0.0	0.0	2.6	0.0	0.0	0.1	0.1	0.0	3.5	0.0
2.8	2.4	28.6	10.5	8.5	26.8	2.5	0.0	1.6	1.0	1.1	0.0	2.0	11.9
0.0	0.0	0.0	100.0	0.0	0.0	0.0	0.0	0.0	0.0	0.0	0.0	0.0	0.0
1.0	0.0	2.0	0.3	71.6	4.2	0.0	7.3	1.3	5.3	0.2	0.0	0.2	5.7
5.9	0.2	2.3	0.0	11.3	65.5	7.8	0.0	0.8	0.3	4.1	0.0	0.6	1.2
0.0	0.0	0.0	0.3	0.0	0.0	99.8	0.0	0.0	0.0	0.0	0.0	0.0	0.0
0.0	0.0	0.0	3.8	0.0	0.0	8.0	79.9	0.0	1.0	0.5	0.1	6.8	0.0
0.0	0.1	3.0	0.0	0.0	0.4	0.3	0.0	62.5	0.5	9.0	6.2	4.8	0.3
0.0	0.1	0.0	0.0	0.0	0.0	0.1	0.0	0.0	84.0	16.1	0.0	0.1	0.0
0.5	0.0	0.1	0.0	0.0	0.0	2.0	0.0	0.5	0.3	93.0	2.9	0.1	0.0
0.0	0.0	0.0	0.1	0.0	0.0	0.0	0.0	0.0	0.0	0.0	98.6	1.3	0.0
1.8	2.9	0.3	0.0	0.0	0.0	5.4	0.0	2.1	0.0	8.2	0.0	73.0	0.2
0.0	0.0	0.0	0.0	0.0	0.0	0.5	0.0	0.0	0.0	3.4	0.0	96.1	0.0
0.9	0.0	0.6	0.2	11.9	0.3	0.0	0.0	2.8	0.0	8.8	0.0	4.4	66.4
0.8	0.0	1.0	2.5	9.2	0.3	0.4	0.0	2.9	2.6	8.7	1.7	1.4	3.0
													65.2

Table 3

Texture Number		1	2	3	4	5	6	7	8	9	10	11	12	13	14	15	16
DCT Coefficient Values		82.5	92.1	53.9	99.8	82.2	66.9	99.7	88.4	77.2	88.4	91.5	100.0	89.7	95.7	75.1	73.3
		87.5	91.9	51.0	99.8	77.8	70.8	99.7	88.4	83.2	88.3	93.3	100.0	92.3	96.5	75.2	73.5
		88.0	90.7	58.0	99.1	80.8	70.3	98.8	86.9	81.6	85.3	92.6	100.0	90.2	93.1	75.9	74.8
		85.8	87.5	58.4	95.5	78.1	76.9	99.6	81.2	81.0	80.6	94.6	99.9	89.1	88.3	68.8	75.5
32		V	V	64	V	V	64	U	V	16	V	64	V	16	16	U	64
DCT Texture Values		67.5	88.7	31.0	99.9	76.2	46.9	99.6	86.9	66.1	90.1	71.6	99.4	78.8	97.2	79.9	61.5
		78.6	91.4	35.8	99.9	74.5	53.8	99.5	86.2	71.5	90.4	75.2	99.1	78.6	98.8	78.8	63.5
		79.8	91.1	38.1	100.0	74.8	58.3	99.3	84.6	73.0	90.6	75.1	99.1	80.4	97.8	74.5	66.8
		77.0	83.7	28.6	100.0	71.6	65.5	99.8	79.9	62.5	84.0	93.0	98.6	73.0	96.1	66.4	65.2
32		16	32	U	U	V	64	U	V	32	U	64	V	32	16	V	32

STUDY OF EARLY EXPERIMENTAL ALLERGIC ENCEPHALOMYELITIS

John R. Richert, M.D.

SUMMARY

At the time of last year's progress report, mice of the EAE-susceptible strain B10R-III and the standard transgenic mouse strain FVB had been ordered. They were back-ordered from the supplier due to heavy demand, so we had to take them when they were available. These arrived several weeks after submitting the progress report. The small bore 7-Tesla magnet was not available for use at that time (due to use by other investigators), so the preliminary MRI studies on healthy mice could not be pursued. Because we had not previously induced EAE in B10R-III mice (our previous experience had been in the SJL strain which was no longer available due to a more than 6-month back-order), and because no one had previously tried to induce EAE in the FVB strain, we proceeded to try to induce EAE in both strains using 400 µg of MBP as antigen emulsified in complete Freund's adjuvant, and three different doses of pertussis toxin (which helps damage the blood brain barrier): 100 ng, 200 ng, and 400 ng.

Six of B10R-III mice and 5 of 6 FVB mice developed EAE as in Table 1.

Table 1. Numbers of mice with EAE in each group sensitized with MBP and 100 ng, 200 ng, or 400 ng of pertussis toxin.

B10R 100 ng 2 of 2	B10R 200 ng 2 of 2	B10R 400 ng 2 of 2	FVB 100 ng 3 of 3	FVB 200 ng 1 of 2	FVB 400 ng 1 of 1
-----------------------	-----------------------	-----------------------	----------------------	----------------------	----------------------

Various clinical characteristics of the mice are shown in Table 2. One FVB mouse in the 200 ng group displayed mild initial signs of EAE and subsequently underwent a spontaneous relapse on day 45. Histologic analyses are in progress.

Table 2.

Strain	Incidence	Day of Onset	Severity*	Duration (days)
B10.R III	1.00	95 ± 1.1	3.8 ± 1.1	Chronic
FVB	0.83	12.8 ± 4.1	2.6 ± 1.2	8.3 ± 1.1

*Severity measured on a 7-point scale

These results show that FVB mice are EAE-susceptible under standard sensitization conditions. This is an important finding because it eliminates the need to eventually breed transgenic mice that express the human TCR (in our case) or other genes (in the case of other investigators studying various aspects of EAE) into other EAE-susceptible strains.

Unfortunately, the MRI scanner was still not available to us at the time that these experiments were being carried out. It was being used by other investigators within GICCS who, like us, wished to perform their experiments prior to the machine being shipped to Germany for repairs. We simply could not postpone the EAE studies for the several month period during which the MRI machine was to be under repair. Ironically, two days before the machine was to be shipped and one day after we sacrificed our last mouse for histologic evaluations, the MRI machine unexpectedly became available for one day. Unfortunately, we had no mice remaining from this group on which to perform the MRI studies. Nevertheless, the FVB model of EAE will be very useful for the MRI studies that will be performed in future experiments, including those with the TCR transgenic mice.

We have proceeded with the generation of TCR transgenic FVB mice. Using the TCR transgene constructed by Dr. Baker in our group, we have successfully produced FVB mice that have integrated the gene for the human TCR β chain that we have been studying and that is used in the human recognition of myeline basic protein (MBP) peptide 83-97. These mice are currently being bred to homozygosity. The generation of TCR α chain transgenic mice is still in process. Once homozygous α and β chain transgenic mice are established, they will be evaluated for tissue expression of the transgene product and then bred together to produce mice that are homozygous for the $\alpha\beta$ heterodimer. These mice will then be evaluated for their susceptibility to the development of EAE and the use of the human $\alpha\beta$ TCR in the production of disease. The 7 Tesla MRI scanner will be used in these studies. As a prelude to these studies, we will proceed with preliminary MRI evaluations of EAE in FVB mice when the scanner is available to us.

PUBLICATIONS

Baker AM, Grekova MC, Richert JR: EAE-susceptibility of FVB mice. In preparation.

REAL-TIME VISUALIZATION OF GENE EXPRESSION IN CEREBRAL CORTEX: OPTICAL RECORDING OF NEURAL CIRCUITS FOLLOWING VIRAL VECTOR GENE DELIVERY

Samuel D. Rabkin, Ph.D.

SUMMARY

In collaboration with Dr. Jian-young Wu of GICCS, we have begun a project in which gene expression is visualized in real time by optical recording following delivery of transgenes to the CNS. The long term goal of this collaborative project is to examine the functional consequences on cortical circuitry of genetically altering the neurotransmitter balance at excitatory synapses in adult primary sensory cortex. The sophisticated technical expertise in the two collaborating laboratories endows this project with unique capabilities. This collaborative research grant has provided us with the support to establish the methodologies necessary to pursue this project. We have worked out many of the technical difficulties in preparing slices, infecting cells in the slice in a localized fashion, maintaining the infected slices in a viable condition for sufficient time to obtain detectable expression of the delivered transgene, performing injections *in vivo* with minimal damage and developed conditions for histo- and immunohisto-chemical detection of transgene expressing cells. The fruitful nature of this collaboration has encouraged Dr. Wu and myself to continue these studies in earnest. The preliminary data that has been obtained will be used as part of a NIH RO1 submission.

Cortical slices *in vitro*

The initial stages of this project involved setting up a facility to work with acute slices in my laboratory and developing conditions to infect cells at discrete locations in the slice with defective HSV vectors. In these initial experiments, HSV vectors expressing lacZ, either from the defective vector genome or the helper virus genome, were used. Expression of the reporter gene lacZ is easy to detect using X-gal histochemistry. Cells in the slices were infected after injection of the defective vectors, then fixed and processed for X-gal histochemistry.

Brains were obtained from 3-week-old Sprague-Dawley rats. Coronal slices of cerebral cortex, 400 μ m thick, were cut on a vibratome and placed in a slice chamber, continuously perfused with oxygenated (95% O₂) artificial cerebrospinal fluid. A number of different methods for viral vector delivery were tried to optimize the number of cells expressing the transgene and the localization of the expressing cells within the slice. We found that the optimal method of delivery was to make numerous injections of small volumes of virus (25 nl aliquots, totaling 200-400 nl) in a relatively short period of time (~ 5 minutes), using an infusion pump to push virus out of a fine-tipped glass micropipettes. Glass micropipettes were pulled on a vertical puller (Kopf), and the tips broken against a glass slide to enlarge the tip diameter. Injections were concentrated in cortical layers 2, 3, and 4, as these regions were shown in optical imaging studies to be most active after a stimulatory pulse. Injected slices were then incubated at 31°C in oxygenated artificial cerebrospinal fluid for various times (8-18 hours). Slices were then fixed and processed by X-gal histochemistry for detection of lacZ expressing cells. Positive staining was obtained in six slices injected with vector bearing the reporter gene lacZ.

Human cortical slices *in vitro*

Cortical tissue was obtained from surgical resections of temporal lobe excised for the therapeutic alleviation of epilepsy. The tissue was obtained directly from the neurosurgeon and placed in ice-cold artificial cerebrospinal fluid. The tissue was trimmed to a 5-10 mm block in the

laboratory and cut on a vibratome. Slices were cut orthogonal to the sulcal boundaries of the gyrus. Volumes of virus ranging from 400-1000 nl were injected into various sites within cortical layers 2, 3, and 4. As with the rat cortical slices, after 16-18 hours of incubation to permit gene expression, the slices were fixed and processed for β -galactosidase histochemistry for detection of lacZ expression. Preliminary findings have shown transgene expression in two slices from separate patients. We found that greater amounts of virus were necessary to obtain gene expression in the human tissue compared to the rat tissue. This is likely due to cell death occurring in the slice during the more prolonged preparation phase of the human slices. Optimization of the preparation of human slices is ongoing, involving greater coordination with the attending neurosurgeon and the set-up of space and equipment within the OR.

Cerebral cortex *in vivo*

The ultimate goal of these studies is to examine the effects of gene expression *in vivo*. The localization of defective vector infected cells in the cortex *in vivo* was determined using dvGPT1/G207. This vector contains the reporter gene human placental alkaline phosphatase (PLAP) on the defective genome and the reporter gene lacZ on the helper virus. Rats were injected with dvGPT1/G207 into the primary somatosensory cortex (Bregma: L +5, A-P -1). After survival periods ranging from 2-7 days, the animals were sacrificed and the brains processed for lacZ or PLAP histochemistry. We found that transgene expression was detected in cells of neuronal and non-neuronal morphology at the primary injection site, most pronounced at days 2 and 3 post-injection. In addition, PLAP staining cells (defective vector infected) were detected at secondary sites in the brain, presumably via retrograde transport. These sites included the locus coeruleus, bilateral, and the ipsilateral cortex (Figure 1).

Optical recording of slices *in vitro*

Dr. Jian-young Wu has set up the appropriate equipment for optical recording from defective HSV vector infected slices. Experiments are currently underway using defective HSV vectors expressing glutamatic acid decarboxylase (GAD) and optical imaging of dvGAD infected slices.

SIGNIFICANCE

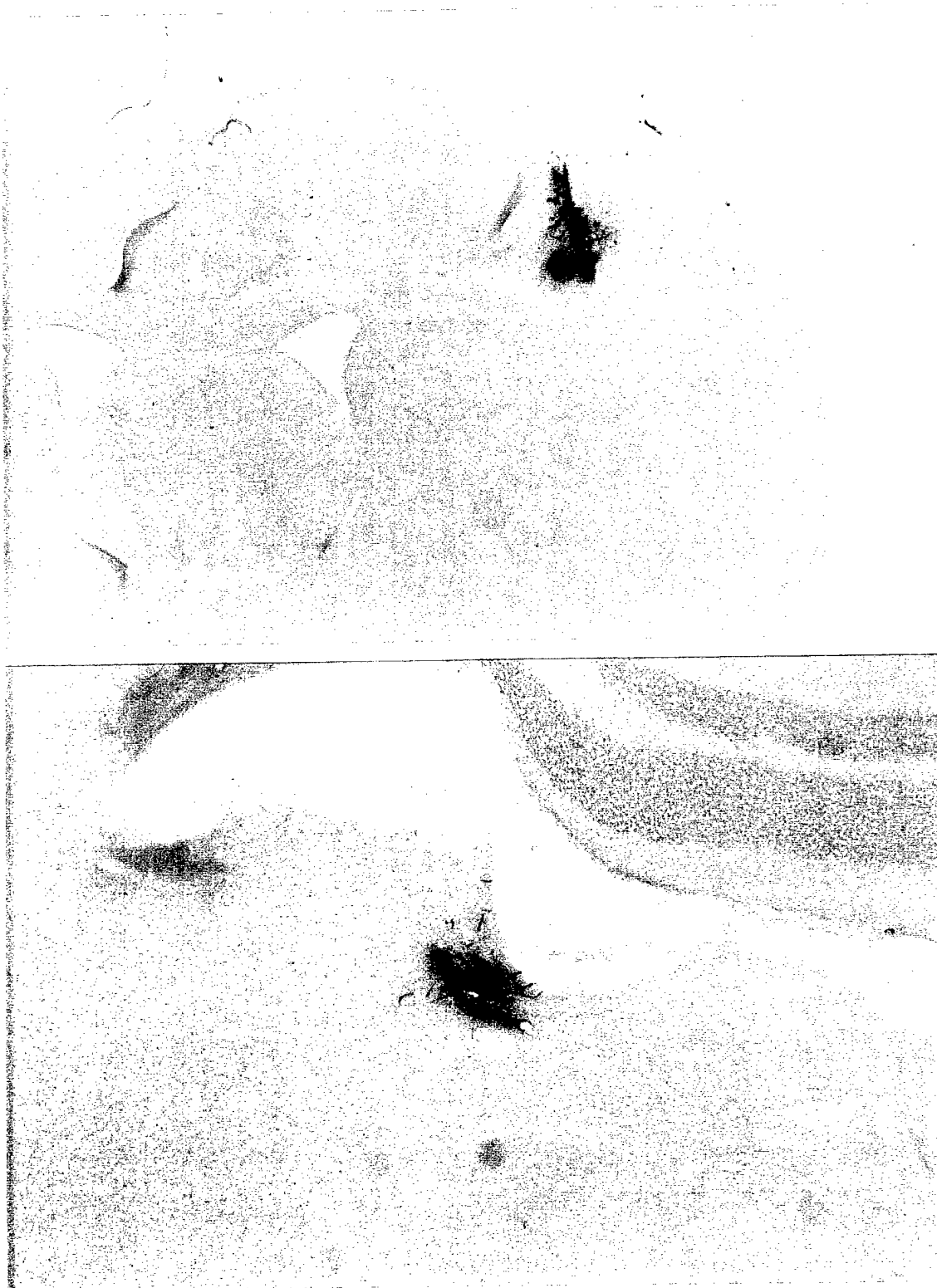
Neurotransmitter imbalance is a concern of great importance in many disease states, as well as being essential to the understanding of normal synaptic function. Currently, there is an enormous amount of interest in gene delivery to the CNS to ameliorate or alleviate conditions brought on by transmitter imbalance. With this project, we plan to determine the viability of using defective HSV vectors to manipulate neurotransmitter levels in the brain and thereby alter neural physiology.

PUBLICATIONS

Hahm, J.-O., New, K. C., Martuza, R. L. and Rabkin, S. D. Differential localization of defective particle and helper virus gene expression following injection of defective herpes simplex virus (HSV) vectors in the brain. *Abs. Soc. Neurosci.* 22: 378.2 (1996)

Figure 1

Primary Injection Site



PLAP Positive Cells in Ipsilateral Locus Coeruleus

PUBLICATIONS FROM THE GICCS FACULTY IN THE LAST YEAR (including abstracts)

Dr. Bavelier

- Neville, H. & Bavelier, D. (1996) L'extension des aires visuelles chez les sourds. *La Recherche*, 289, 90-93. [Visual areas development in deaf Individuals].
- Neville, H. & Bavelier, D. (1996) Aumento de las areas visuales en los sordos: Los cortex visual y auditivo no son tan distintos como se cree. *Mundo Cientifico*, 172, 854-857.
- Deruelle, C. & Bavelier, D. (1996). Coding of visual information within and between objects. *Perception*, 25, 93.
- Bavelier, D., Corina, D., Jezzard, P., Clark, V. P., Padmanabhan, S., Karni, A., Rauschecker, J., Turner, R. & Neville, H. (1997). Sentences Reading: An fMRI Study at 4T. *Brain and Cognition*, 32 (2), 165-167.
- Neville, H.J., & Bavelier, D. (1997) Variability of developmental plasticity within sensory and language systems: Behavioral, ERP and fMRI studies. D. Hann, L. Huffman, I.I. Lederhendler, & D. Meinecke (Eds.) *Proceedings of the Conference for Advancing Research on Developmental Plasticity*.
- Bavelier, D., Corina, D., Jezzard, P., Padmanabhan, S., Clark, V. P., Karni, A., Prinster, A., Braun, A., Lalwani, A., Rauschecker, J., Turner, R. & Neville, H. (1997). Sentences Reading: a functional MRI study at 4T. *Journal of Cognitive Neuroscience*, 9 (5), 664-686.
- Corina, D., Bavelier, D., Jezzard, P., Clark, V.P., Padmanabhan, S., Rauschecker, J., Braun, A., Turner, R. & Neville, H. (November 1996). Cortical Organization for Language in Native Deaf and Hearing Signers. Part I: American Sign Language. *26th Annual Meeting of the Neuroscience Society*, Washington, DC.
- Bavelier, D., Corina, D., Jezzard, P., Clark, V.P., Karni, A., Padmanabhan, S., Rauschecker, J., Turner, R. & Neville, H. (November 1996). Cortical Organization for Language in Native Deaf and Hearing Signers. Part II: Written English. *26th Annual Meeting of the Neuroscience Society*, Washington, DC.
- Newman, A., Corina, C., Tomann, A., Bavelier, D., Braun, A., Clark, V.C., Jezzard, P. & Neville, H. (October 1997). Effects of Age of Acquisition on Cortical Organization for American Sign Language: A Functional Magnetic Resonance (fMRI) Imaging Study. *27th Annual Meeting of the Neuroscience Society*, New Orleans, LA.
- Bavelier, D., Deruelle, C., Klineberg, E. & Proksch, J. (November 1997). Positive and Negative Similarity Effects. *38th Annual Meeting of the Psychonomic Society*, Philadelphia, PA.

Dr. Eden

- Eden, G.F., VanMeter, J.W., Rumsey, J.W., Maisog, J. and Zeffiro, T.A. (1996). Abnormal processing of visual motion in dyslexia revealed by functional brain imaging. *Nature*, 348, 66-69.
- Eden, G.F. and Zeffiro, T.A. (1996). Looking beyond the reading problems in developmental dyslexia: Visualizing the visual processing deficits. *NIH Research*, 8, 31-35.
- Eden, G.F., VanMeter, J.W., Rumsey, J.M., and Zeffiro, T.A. (1996). The visual deficit theory of developmental dyslexia. *NeuroImage*, 4, S108-S117.
- Eden, G.F. (1996). Verbal and visual problems in reading disabled and normal children - a response to Dr. Cherkas-Julkowski. *Journal of Learning Disabilities*, 29(1), 8.
- Eden, G.F., Stein, J.F., Wood, H.M., and Wood, F.B. (1996). Visuospatial judgment in reading disabled and normal children. *Perceptual and Motor Skills*, 82, 155-177.
- Eden, G.F. and Zeffiro, T.A. (1996). Sensitivity of PET and fMRI in the detection of task related brain activity: implications for the study of brain development. In: G. R. Lyon, J. Rumsey, N. Krasnegor, and R. W. Thatcher (Eds.), *Developmental Neuroimaging: Mapping the Development of Brain and Behavior*, San Diego: Academic Press, Inc.
- Hilton, M., Ogden, T., Hattery, D., Eden, G., and Jawerth, B. (1996) Wavelet Denoising of Functional MRI Data. In: A. Aldroubi and M. Unser (Eds.), *Wavelets in Biology and Medicine*, CRC Press.

- Rumsey, J.M. and Eden, G.F. (1997) Functional Neuroimaging of Developmental Dyslexia: Regional Cerebral Blood Flow in Dyslexic Men. In: B. Shapiro, M.D. Timonium (Eds), Specific Reading Disability: A View of the Spectrum. York Press: Parkton, MD.
- Zeffiro, T.A., Eden, G.F., Woods, R.P. and VanMeter, J.W. (1997). Intersubject analysis of fMRI data using spatial normalization. Advances in Experimental Medicine and Biology, 413, 235-240.
- Eden, G.F., Stein, J.F., Wood, H.M., and Wood, F.B. (under review). Clock drawing in reading disabled children. Brain and Cognition.

Dr. Etcheberrigaray

- Araki, T., Taniwaki, T., Becerra, S.P., Chader, G.J., Hirashima, N., Etcheberrigaray, R. and Schwartz, J.P. "Pigmented epithelium-derived factor (PEDF) protects cerebellar granule cells against glutamate toxicity." (1996) *J. Neurochemistry* 66:S13C.
- Etcheberrigaray, R., Hirashima, N., Prince, J. and Alkon, D.L. "Altered calcium responses in fibroblasts from asymptomatic members of Alzheimer's Disease families." (1996) 26TH Annual Meeting Society for Neuroscience, 22:257a,
- Etcheberrigaray, R., Payne, J.L. and Alkon, D.L. " β -amyloid induces Alzheimer's disease features in human fibroblasts and in neuronal tissues." (1996) *Life Sciences*, 59:491-498.
- Hirashima, N., Etcheberrigaray, R., Bergamaschi, S., Racchi, M., Battaini, F., Binetti, G., Govoni, S. and Alkon, D.L. "Calcium responses in human fibroblasts: a diagnostic molecular profile for Alzheimer's disease fibroblasts." (1996) *Neurobiology of Aging*, 17:549-555.
- Taniwaki, T., Hirashima, N., Becerra, S.P., Chader, G.J., Etcheberrigaray, R. and Schwartz, J.P. "Pigment epithelium-derived factor (PEDF) protects cultured cerebellar granule cells against glutamate-induced neurotoxicity." (1996) *J. Neurochemistry*, in press.

Dr. Faden

- A.I. Faden. Pharmacological treatment of central nervous system trauma. *Pharmacology and Toxicology* 78:12-17, 1996.
- D.M. Basso, M.S. Beattie, J.C. Bresnahan, D.K. Anderson, A.I. Faden, J.A. Gruner, T.R. Holford, C.Y. Hsu, L.J. Noble, R. Nockels, P.L. Perot, S.K. Salzman, and W. Young. MASCIS evaluation of open field locomotor scores: effects of experience and teamwork on reliability. *J Neurotrauma* 13(7):343-359, 1996.
- Mukhin A, Fan L, and Faden A.I. Activation of metabotropic glutamate receptor subtype mGluR1 contributes to posttraumatic neuronal injury. *J Neurosci* 16(19):6012-6020, 1996.
- B.A. Eldadah, A.G. Yakovlev, and A.I. Faden. A new approach for the electrophoretic detection of apoptosis. *Nucleic Acids Res* 24(20):4092-4093, 1996.
- A.I. Faden. Pharmacologic treatment of acute traumatic brain injury. *JAMA* 276(7): 569-570, 1996.
- A.I. Faden. Neurotoxic versus neuroprotective actions of endogenous opioid peptides: implications for treatment of CNS injury. In : NIDA Research Monograph, NIDA Conference 163:318-330, 1996.
- Mukhin AG, Ivanova SA, and AI Faden. mGluR modulation of post-traumatic neuronal death: Role of NMDA receptors. *Neuroreport* 8:2561-2566, 1997.
- Mukhin AG, SA Ivanova, SM Knoblach, and AI Faden. New *in vitro* model of traumatic neuronal injury: Evaluation of secondary injury and glutamate receptor mediated neurotoxicity. *J Neurotrauma* 14:651-663, 1997.
- Yakovlev, A.G., Knoblach, S.M., Fan, L., Fox, G.B., Goodnight, R., and Faden, A.I. Activation of CPP32-like caspases contributes to neuronal apoptosis and neurological dysfunction after traumatic brain injury. *J Neurosci* 17(19): 7415-7424, 1997.
- Eldadah BA, Yakovlev AG, and Faden AI. The role of Ced-3-related cysteine proteases in apoptosis of cerebellar granule cells. *J Neurosci* 17(16):6105-6113, 1997.

- Faden, A.I., Ivanova, S.A., Yakovlev, A.G., and Mukhin, A.G. Neuroprotective effects of group III mGluR in traumatic neuronal injury. *J Neurotrauma*, in press.
- A.I. Faden. Pharmacotherapeutic treatment approaches for brain and spinal cord trauma. *In: Neurotrauma: A Comprehensive Textbook on Head and Spinal Injury* (R. Narayan, J. Wilberger, and J. Povlishock, eds.). McGraw-Hill: New York, 11:1479-1490, 1996.
- A.I. Faden. Therapeutic approaches to spinal cord injury. *In: Seil, F.J. (Ed.), Advances in Neurology: Neuronal Regeneration, Reorganization, and Repair*. Lippincott-Raven Publishers: Philadelphia, Vol. 72; Ch. 35, pp. 377-386, 1997.
- R. Vink, T.K. McIntosh and A.I. FADEN. Brain injury: metabolic aspects using magnetic resonance. *In: Encyclopedia of Neuroscience on CD ROM*, 2nd ed.(G. Adelman and B. Smith, eds.). Elsevier: New York, 1997.
- A.I. Faden, B.A. Eldadah, L. Fan and A.G. Yakovlev. Role of Ced-3 related cysteine proteases (caspases) in neuronal apoptosis and traumatic brain injury. Abstract, 8th International Symposium on Stroke, Neurotrauma, and other Neurological Disorders (LSUMC, New Orleans - July 1997).
- A.I. Faden, B. Eldadah, and A.G. Yakovlev. Gene responses associated with traumatic neuronal injury: molecular mechanisms of post-traumatic apoptosis. Abstract, 4th International Neurotrauma Symposium (Seoul, Korea - August, 1997).
- A.I. Faden, S. Ivanova, A. Yakovlev, and A. Mukhin. Agonists of group III metabotropic glutamate receptors (mGluR) reduce post-traumatic neuronal loss *in vitro* whereas antagonists exacerbate injury. Abstract, Society for Neuroscience 27th Annual Meeting (New Orleans, October, 1997).
- A.G. Yakovlev, S.M. Knoblach, L. Fan, and A.I. Faden. Activation of CPP32-like caspases contribute to neuronal apoptosis and neurological dysfunction after traumatic brain injury. Abstract, Society for Neuroscience 27th Annual Meeting (New Orleans, October, 1997).
- A.G. Mukhin, S.A. Ivanova, and A.I. Faden. Potential interaction between group I metabotropic glutamate receptors and NMDA receptors in mechanisms of post-traumatic neuronal death. Abstract, Society for Neuroscience 27th Annual Meeting (New Orleans, October, 1997).
- B.A. Eldadah, A.G. Yakovlev, and A.I. Faden. CPP32-like caspases play an important role in cerebellar granule cell apoptosis. Abstract, Society for Neuroscience 27th Annual Meeting (New Orleans, October, 1997).
- G.B. Fox, L. Fan, and A.I. Faden. Delayed motor and cognitive impairment following controlled cortical impact in a mutant mouse strain known to exhibit delayed Wallerian degeneration. Abstract, Society for Neuroscience 27th Annual Meeting (New Orleans, October, 1997).
- L. Fan, G.B. Fox, and A.I. Faden. Characterization of a controlled cortical impact model in the mouse: sustained motor deficits and pronounced cognitive impairment. Abstract, Society for Neuroscience 27th Annual Meeting (New Orleans, October, 1997).
- J.W. Allen, B.A. Eldadah, and A.I. Faden. Toxic effects of β -amyloid (1-42) on cerebellar granule cells. Abstract, Society for Neuroscience 27th Annual Meeting (New Orleans, October, 1997).
- S.M. Knoblach, and A.I. Faden. Interleukin-10 improves outcome and suppresses proinflammatory cytokine expression after traumatic brain injury. Abstract, Society for Neuroscience 27th Annual Meeting (New Orleans, October, 1997).
- B.C. Albeni, S.M. Knoblach, B.G.M. Chew, A.I. Faden, and J.J. Pekar. Temporal evaluation of *in vivo* traumatic brain injury (TBI) using multi-modal MRI. Abstract, Society for Neuroscience 27th Annual Meeting (New Orleans, October, 1997).
- S.A. Ivanova, A.G. Mukhin, J.W. Allen, and A.I. Faden. New *in vitro* model of traumatic brain injury: evaluation of secondary injury and NMDA receptor mediated neurotoxicity. Abstract, Fifteenth Annual National Neurotrauma Symposium (New Orleans, October, 1997).

Dr. Friedman

Friedman, R. B. Phonological text alexia: Poor pseudoword reading plus difficulty reading functors and affixes in text. *Cognitive Neuropsychology*, 1996, 13, 869-885.

- Glosser, G., Grugan, P., and Friedman, R.B. Semantic memory impairment does not impact on phonological and orthographic processing in a case of developmental hyperlexia. *Brain and Language*, 1997, 56, 234-247.
- Glosser, G., Friedman, R.B., Kohn, S.E., Sands, L., and Grugan, P. Repetition of single words and nonwords in Alzheimer's Disease. *Cortex*, in press.
- Glosser, G., Friedman, R.B., Grugan, P., Lee, J.H., and Grossman, M. Lexical semantic and associative priming in Alzheimer's disease. *Neuropsychology*, in press.
- Friedman, R. B. and Glosser, G. Aphasia, alexia, and agraphia. In H.S. Friedman (Ed.) *Encyclopedia of Mental Health*. San Diego: Academic Press, in press.
- Friedman, R.B. and Lott, S.N. Phonologic treatment for deep dyslexia using bigraphs instead of graphemes. *Brain & Language*, 1996, 55, 116-118.
- Glosser, G., Friedman, R.B., Kohn, S.E., and Grugan, P. Mechanisms for reading and repeating nonwords: Evidence from Alzheimer's Disease. *Brain & Language*, 1996, 55, 71-73.
- Lott, S.N. and Friedman, R.B. A speeded letter-by-letter reading treatment for pure alexia. *Brain & Language*, 1996, 55, 20-22.
- Friedman, R.B. and Lott, S. N. Treatment for pure alexia employing two distinct reading mechanisms. *Brain & Language*, in press.
- Glosser, G., Friedman, R. B., Kohn, S.L., and Sands, L. Nonword spelling in patients with probable Alzheimer's disease. *Brain and Language*, in press.
- Friedman, R. B., and Lott, S.N. Using models of memory to predict generalization effects in treatment for alexia. Submitted.
- Glosser, G., Grugan, P.K., & Friedman, R.B. A comparison of reading and spelling in patients with Alzheimer's disease. Submitted.

Dr. Goodhill

- Goodhill, G.J. & Baier, H. (1997). Axon guidance: stretching gradients to the limit. *Neural Computation*, in press.
- Goodhill, G.J. (1997). Stimulating issues in cortical map development. *Trends in Neurosciences*, 20, 375-376.
- Goodhill, G.J. & Sejnowski, T.J. (1997). A unifying objective function for topographic mappings. *Neural Computation*, 9, 1291-1304.
- Goodhill, G.J. (1997). Diffusion in axon guidance. *European Journal of Neuroscience*, 9, 1414-1421.
- Goodhill, G.J., Bates, K.R. & Montague, P.R. (1997). Influences on the global structure of cortical maps. *Proceedings of the Royal Society, Series B*, 264, 649-655.
- Goodhill, G.J. & Sejnowski, T.J. (1997). Objective functions for topography: a comparison of optimal maps. In *Proceedings of the Fourth Neural Computation and Psychology Workshop: Connectionist*.
- Representations, eds. John A. Bullinaria, David G. Glasspool & George Houghton (1997). London: Springer-Verlag.
- Goodhill, G.J. (1997). A mathematical model of axon guidance by diffusible factors. To be presented at the Neural Information Processing Systems conference, Denver, December 1997.
- Goodhill, G.J. (1997). Gradients for retinotectal mapping. To be presented at the Neural Information Processing Systems conference, Denver, December 1997.
- Goodhill, G.J. (1997). Axon guidance by diffusible factors: mathematical constraints. *Brain Research Association abstracts*, 14, 44.
- Goodhill, G.J. (1997). Theoretical analysis of axon guidance by a target-derived diffusible factor. *Society for Neuroscience abstracts*, 22, in press.

Dr. Kanwal

- Condon, C.J., Esser, K.-H., Kanwal, J.S., and Suga, N. Responses of FM-FM neurons to composite communication calls provide evidence for syntax processing in the auditory

- cortex of the mustached bat. Midwinter Meeting of the Association for Research in Otolaryngology, (1996) 19: 456
- Condon, C.J., Kanwal, J.S., and Suga, N. Responses of neurons in the ventroposterior auditory cortex of the mustached bat to communication calls. Midwinter Meeting of the Association for Research in Otolaryngology, (1997) 20: in press.
- Esser, K.-H., Condon, C.J., Kanwal, J.S. & Suga, N. Playback of composite communication calls reveals syntax processing in the FM-FM area of the mustached bat's auditory cortex. In: Goettingen Neurobiology Report, Proceedings of the 24th Goettingen Neurobiology Conference, Vol. II. Elsner, N., Schnitzler, H.-Ü., eds. Georg Thieme Verlag, Stuttgart New York, (1996) , 239.
- Esser, K.-H., and Kanwal, J.S. Auditory responses from neurons in the frontal cortex of the mustached bat. Midwinter Meeting of the Association for Research in Otolaryngology, (1996) 19: 447.
- Kanwal, J.S. Interhemispheric interactions suppress responses to communication call but not tonal stimuli in the primary auditory cortex of the mustached bat. Midwinter Meeting of the Association for Research in Otolaryngology, (1996) 19: 624.
- Ohlemiller, K.K., Kanwal, J.S., and Suga, N. Temporal facilitation for call processing in the FM-FM and CF/CF areas of the auditory cortex of the mustached bat. Neuroreport (1996) in press.
- Kanwal, J.S., and Suga, N. Excitatory, facilitatory and inhibitory frequency tuning of combination-sensitive neurons in the auditory cortex of the mustached bat. J. Neurophysiol. (1997) in press.

Dr. Kozikowski

- Mia Raves, M. Harel, Y.-P. Pang, I. Silman, A. P. Kozikowski, and J. L. Sussman, "3D Structure of Acetylcholinesterase Complexed with the Nootropic Alkaloid (-)-Huperzine A." *Nature Structure Biology.*, 4, 57-63 (1997).
- A. P. Kozikowski, D. Simoni, S. Manfredini, M. Roberti, and J. Stoelwinder, "Synthesis of the 6- and 7-Hydroxylated Cocaines and Pseudococaines," *Tetrahedron Lett.*, 37, 5333-5336 (1996).
- A. P. Kozikowski, Y. Liao, W. Tückmantel, S. Pshenichkin, A. Surin, C. Thomsen, P. Suzdak, and J. T. Wroblewski, "Synthesis and Biology of the Rigidified Glutamate Analogue, trans-2-Carboxyazetidine-3-acetic Acid (t-CAA)," *Bioorg. Med. Chem. Lett.*, 21, 2559-2564 (1996).
- W. Tückmantel, A. P. Kozikowski, S. Pshenichkin, and J. T. Wroblewski, "Synthesis and Biology of the 1-Benzyl Derivative of APDC - An Apparent mGluR6 Selective Ligand," *Bioorg. Med. Chem. Lett.*, 7, 601-606 (1997).
- D. Ma, H. Tian, H. Sun, A. P. Kozikowski, S. Pshenichkin, and J. T. Wroblewski, "Synthesis and Biological Activity of Cyclic Analogues of MPPG and MCPG as Metabotropic Receptor Antagonists," *Bioorg. Med. Chem. Lett.*, 7, 1195-1198 (1997).
- A. P. Kozikowski, L. Araldi, and R. G. Ball, "Dipolar Cycloaddition Route to Diverse Analouges of Cocaine, the 6- and 7-Substituted 3-Phenyltropanes," *J. Org. Chem.*, 62, 503-509 (1997).
- D. J. Hart, J. Li, W.-L. Wu, and A. P. Kozikowski, "Applications of Organosulfur Chemistry to Organic Synthesis: Total Synthesis of (+)-Himbeline and (+)-Himbacine," *J. Org. Chem.*, 62, 5023-5033 (1997).
- A. P. Kozikowski, S. Wang, D. Ma, J. Yao, S. Ahmad, R. I. Glazer, K. Bogi, P. Acs, S. Modarres, N. E. Lewin, and P. M. Blumberg, "Modeling, Chemistry, and Biology of the Benzolactam Analogues of ILV. 2. Identification of the Binding Site of the Benzolactams in the CDRD2 Activator-Binding Domain of PKC δ and Discovery of an ILV Analogue of Improved Isozyme Selectivity," *J. Med. Chem.*, 40, 1316-1326 (1997).
- A. H. Fauq, J. H. Zaidi, R. A. Wilcox, C. Varvel, S. R. Nahorski, A. P. Kozikowski, and C. Erneux, "Synthesis of Novel Metabolically Stable Analogues of D-myo-Inositol 1,4,5-Trisphosphate," *Tetrahedron Lett.*, 37, 1917-1920 (1996).

- R. A. Wilcox, A. Fauq, A. P. Kozikowski, and S. R. Nahorski, "Defining the Minimal Structural Requirements for Partial Agonism at the Type I myo-Inositol 1,4,5-Trisphosphate Receptor," *FEBS Lett.*, 402, 241-245 (1997).
- A. P. Kozikowski, M. Kotoula, D. Ma, N. Boujrad, W. Tückmantel, and V. Papadopoulos, "Synthesis and Biology of a 7-Nitro-2,1,3-benzoxadiazol-4-yl (NBD) Derivative of 2-Phenylindole-3-acetamide: A Fluorescent Probe for the Peripheral-type Benzodiazepine Receptor", *J. Med. Chem.* in press (1997).
- M. McKinney and A. P. Kozikowski, "Pharmacologic Studies of Himbacine and Huperzine A: Potential Use in Cholinergic Replacement Therapy," in *Herbal Medicines for Neuropsychiatric Diseases* (1997).
- Gian Luca Araldi, K. R. C. Prakash, Clifford George, and Alan P. Kozikowski, "An enantioselective synthesis of 2-alkyl-3-phenyltropanes by an asymmetric 1,3-dipolar cycloaddition reaction", *J. Chem. Soc., Chem. Commun.*, in press.

Dr. Pekar

- J. Pekar, P. Jezzard, D. A. Roberts, J.S. Leigh, Jr., J.A. Frank, and A.C. McLaughlin. "Perfusion Imaging with Magnetization Transfer Frequency Offset Compensation," *Magnetic Resonance in Medicine* 35:70-79 (1996).
- F.Q. Ye, J. Pekar, P. Jezzard, J. Duyn, J.A. Frank, and A.C. McLaughlin. "Perfusion Imaging of the Human Brain at 1.5 T Using Single-Shot EPI Spin-Tagging Approaches," *Magnetic Resonance in Medicine* 36:219-224 (1996).
- V.S. Mattay, J.A. Frank, A.K.S. Santha, J. Pekar, J.H. Duyn, A.C. McLaughlin, and D.R. Weinberger. "Whole Brain Functional Mapping with MRI." *Radiology* 201:399-404 (1996).
- A.C. McLaughlin, J. Pekar, A.K.S. Santha, and J.A. Frank. "Effect of Magnetization Transfer on The Measurement of Cerebral Blood Flow using Arterial Spin Tagging Approaches. " *Magnetic Resonance in Medicine* 37:501-510 (1997).
- F.Q. Ye, V.S. Mattay, P. Jezzard, J. Pekar, J.A. Frank, and A.C. McLaughlin. "Correction for Vascular Artifacts in Arterial Spin Tagging Techniques," *Proceedings of the meeting of the Society of Magnetic Resonance*, (New York, 1996), p. 11.
- V.S. Mattay, J.A. Frank, A.K.S. Santha, J. Pekar, A.C. McLaughlin, and D.R. Weinberger. "Reproducibility of Whole Brain fMRI Maps Acquired with Multi-Slice Isotropic Echo Planar Imaging" *Proceedings of the meeting of the Society of Magnetic Resonance*, (New York, 1996), p. 1893.
- B.G.M. Chew, B.C. Albensi, M.O. Mattingly, and J.J. Pekar, "High Resolution in vivo Brain MRI with Minimally Invasive Techniques." *Proceedings 38th Annual Experimental NMR Conference*, (Orlando, Florida, 1997), p. 67.
- C.M. Wessinger, B. Tian, K.C. Japikse, S. Ghosh, J.W. VanMeter, R.C. Platenberg, J. Pekar, and J.P. Rauschecker. "Processing of Complex Sounds in Human Auditory Cortex." *Association for Research in Otolaryngology*, 20:27 (1997).
- B.G.M. Chew, B.C. Albensi, M.O. Mattingly, and J.J. Pekar, "High Resolution in vivo Brain MRI with Minimally Invasive Techniques." *In Vivo NMR Research Center 10th Anniversary Symposium*, National Institutes of Health, Bethesda, Maryland, October 1997.
- B.C. Albensi, S.M. Knoblach, B.G.M. Chew, A.I. Faden, and J.J. Pekar. "Temporal evaluation of in vivo traumatic brain injury (TBI) using multi-modal MRI." *Abstracts, Society for Neuroscience 27th Annual Meeting* (New Orleans, October, 1997).
- C.M. Wessinger, B. Tian, J.W. VanMeter, R.C. Platenberg, J. Pekar, J.P. Rauschecker. "Hierarchical Processing within Human Auditory Cortex Examined with fMRI." *Abstracts, Society for Neuroscience 27th Annual Meeting* (New Orleans, October, 1997).

Dr. Pouget

- Pouget, A., and Sejnowski, T.J. Spatial transformations in the parietal cortex using basis functions. *Journal of Cognitive Neuroscience*. 9(2):222-237. 1997.

- Cai, R.H., Pouget, A., Schlag-Rey, M. and Schlag, J. Perceived geometrical relationships affected by eye movement signals. *Nature*. 386:601-603. 1997.
- Schlag, J., Pouget, A., Schlag-Rey, M. and Saderghpour, S. Interaction between natural and electrically evoked saccades. III. Is the compensation by collicular stimulation due to a feedback integrator not yet reset? *Journal of Neurophysiology*. In Press.
- Pouget, A., Zhang, K., Deneve, S. and Latham, P.E. Statistically efficient estimation using population code. *Neural Computation*. In Press.
- Bremmer, F., Pouget, A., Lappe, M. and Hoffmann, K. Eye position effects in monkey cortex. III. Representation of gaze direction at the population level. *European Journal of Neuroscience*. In Press.
- Gray, M.S., Pouget, A., Zemel, R.S., Nowlan, S.J., and Sejnowski, T.J. Reliable disparity estimation through selective integration. *Visual Neuroscience*. In Press.
- Zemel, R.S., Dayan, P., and Pouget, A. Probabilistic interpretation of population code. *Neural Computation*. In Press.
- Pouget, A. and Sejnowski, T.J. Lesion in a Basis Function Model of Spatial Representations: Comparison with Hemineglect. In "Parietal lobe contribution in orientation in 3D space". Thier, P. and Karnath, H.O. (eds). Springer Verlag. 1997.
- Pouget, A. and Sejnowski, T.J. A New View of Hemineglect Based on the Response Properties of Parietal Neurons. *Philosophical Transactions of the Royal Society: Series B* 352. In Press.
- Pouget, A. and Sejnowski, T.J. A New View of Hemineglect Based on the Response Properties of Parietal Neurons. *Philosophical Transactions: Biological Sciences*. In "Spatial Functions of the Hippocampal Formation and the Parietal Cortex". Neil Burgess, Kathryn Jeffery and John O'Keefe (eds). Oxford University Press. In Press.
- Pouget, A. and Driver, J. Visual Neglect. In "MIT Encyclopedia of Cognitive Sciences". Wilson, R. and Keil, F. (eds). MIT Press. In Press.
- Deneve, S. and Pouget, A. Neural Basis of Object-Centered Representations. *Advances in Neural Information Processing Systems*. 10. MIT Press, Cambridge MA. In Press.
- Deneve, S. and Pouget, A. Neuronal object-centered representations: map or gain modulation? *Society for Neuroscience Abstracts*. New Orleans. 1997.
- Pouget, A. and Ducom, J.C. Noise reduction, discrimination and adaptation in cortical circuits. *Society for Neuroscience Abstracts*. New Orleans. 1997.

Dr. Rauschecker

- Rauschecker, J.P., Tian, B., Pons, T. and Mishkin, M. (1997) Serial and parallel processing in macaque auditory cortex. *J. Comp. Neurol.* 382: 89-103.
- Rauschecker, J.P. (1997) Mechanisms of compensatory plasticity in the cerebral cortex. *Advances in Neurology* 73, 137-146
- Rauschecker, J.P. (1997) Processing of complex sounds in the auditory cortex of cat, monkey, and man. *Acta Otolaryngologica* (in press).
- Bavelier, D., Corina, D., Clark, V.P., Dale, A., Jezzard, P., Prinster, A., Karni, A., Lalwani, A., Rauschecker, J., Turner, R. and Neville, H. (1997) Sentence reading: a 4T fMRI study of cortical regions active during an English reading task. *Journal of Cognitive Neuroscience* (in press)
- Tian, B. and Rauschecker, J.P. (1997) Processing of frequency-modulated sounds in the cat's posterior auditory field. *J. Neurophysiol.* (in press)
- Grady, C.L., VanMeter, J.W., Maisog, J.M., Pietrini, P., Krasuski, J. and Rauschecker, J.P. (1997) Attention-related modulation of activity in primary and secondary auditory cortex. *Neuroreport* (in press)
- Jezzard, P., Rauschecker, J.P. and Malonek, D. (1997) An in-vivo model for functional MRI in cat visual cortex. *Magnetic Resonance in Medicine* (in press)
- Neville, H.J., Bavelier, D., Corina, D., Rauschecker, J.P., Karni, A., Lalwani, A., Braun, A., Clark, V., Jezzard, P., Turner, R. (1997) Cerebral organization for language in deaf and hearing subjects: Biological constraints and effects of experience. *Proc. Natl. Acad. Sci. USA* (in press)

- Rauschecker, J.P. (1998) Central auditory physiology. Invited contribution, MIT Encyclopedia of Cognitive Science (in press)
- Wessinger, C.M., Tian, B., Japikse, K.C., Ghosh, S., VanMeter, J.W., Platenberg, R.C., Pekar, J., Rauschecker, J.P. (1997) Processing of complex sounds in human auditory cortex. *Assoc. Res. Otolaryngol. Abstr.* 20, 105
- Tian, B., Fritz, J., Mishkin, M., Rauschecker, J.P. (1997) Neuronal responses to complex sounds in the lateral belt areas of rhesus monkey auditory cortex. *Assoc. Res. Otolaryngol. Abstr.* 20, 106
- Weeks, R.A., Tian, B., Wessinger, C.M., Cohen, L.G., Hallett, M. and Rauschecker, J.P. (1997) Identification of the inferior parietal lobule as the site of auditory space perception in man. *Neurology* 48, S30.003
- Aziz-Sultan, A., Weeks, R.A., Tian, B., Cohen, L.G., Rauschecker, J.P. and Hallett, M. (1997) Auditory localisation demonstrates cross modal plasticity in congenitally blind subjects. *Neurology* 48, S30.004
- Rauschecker, J.P. (1997) Parallel processing of complex sounds in primate auditory cortex. *Proc. Int. Union of Physiol. Sci.* 33, L081.04
- Middlebrooks, J.C., Kaas, J.H., Rauschecker, J.P. and Schreiner, C.E. (1997) Symposium: Auditory cortex - common cortical themes and specialization for hearing. *Soc. Neurosci. Abstr.* 23 (in press)
- Tian, B., Fritz, J., Ojima, H., Mishkin, M. and Rauschecker, J.P. (1997) Hierarchical processing of monkey calls within different areas of auditory cortex in the macaque. *Soc. Neurosci. Abstr.* 23 (in press)
- Wessinger, C.M., Tian, B., VanMeter, J.W., Platenberg, R.C., Pekar, J. and Rauschecker, J.P. (1997) Hierarchical processing within human auditory cortex examined with fMRI. *Soc. Neurosci. Abstr.* 23 (in press)
- Romanski, L.M., Goldman-Rakic, P.S., Tian, B., Fritz, J., Ojima, H. and Rauschecker, J. P. (1997) Projections from physiologically defined regions of the auditory association belt and parabelt cortical regions of the superior temporal gyrus target specific prefrontal regions in the primate. *Soc. Neurosci. Abstr.* 23 (in press)
- Malonek, D., Rauschecker, J.P., Grinvald, A. and Jezzard, P. (1997) FMRI and optical intrinsic signals in cat visual cortex: differences in response dynamics. *Soc. Neurosci. Abstr.* 23 (in press)

Dr. Swope

- Mou, T., Fung, E., and Swope, S. L. Identification of a Torpedo electric organ component that interacts with the Fyn protein tyrosine kinase. Abstract, 27th Annual Meeting, Society for Neuroscience, 1997.
- Swope, S. L., Moss, S.J., Raymond, L., and Huganir, R. L. Phosphorylation of Ligand-Gated Ion Channels. In: D. Armstrong and S. Rossie (Eds.) *Advances in Second Messengers and Phosphoproteins* (In press).

Dr. Ullman

- Michael Ullman, Suzanne Corkin, Marie Coppola, Gregory Hickok, John H. Growdon, Walter J. Koroshetz, Steven Pinker. A neural dissociation within language: Lexicon a part of declarative memory, grammar processed by procedural system. *Journal of Cognitive Neuroscience*, vol 9, number 2. Paper selected for special press release by the *Society for Neuroscience*. Discussed in *Nature* (News and Views), June 1997.
- Michael Ullman. Evidence that lexical memory is part of the temporal lobe declarative memory, and that grammatical rules are processed by the frontal/basal-ganglia procedural system. *Brain and Language*, in press.
- Michael Ullman and Myrna Gopnik. Inflectional morphology in hereditary specific language impairment. *Applied Psycholinguistics*, in press.

- Heather van der Lely and Michael Ullman. Past tense morphology in specifically language impaired and normally developing children. Submitted to *Language and Cognitive Processes*.
- Michael Ullman. Acceptability ratings of regular and irregular past tense forms: Evidence from word frequency and phonological similarity effects for a dual-system model of language. Submitted to *Language and Cognitive Processes*.
- Michael Ullman. The role of declarative and procedural memory in language.. *Brain and Cognition*. (abstract), in press.
- Michael Ullman and Suzanne Corkin. Lexical memory is part of declarative memory: H.M. is worse at irregular than regular past tense and plural formation. Paper to be presented 27th Annual Meeting of the Society for Neuroscience, New Orleans. *Society for Neuroscience Abstracts* (abstract). One of 200 abstracts from Meeting selected for press report by the *Society for Neuroscience*, 1997.
- Michael Ullman, Ruth Bergida, and Kathleen O'Craven. Distinct fMRI activation patterns for regular and irregular past tense. Poster presented at the Third Annual Conference on Functional Mapping of the Human Brain, Copenhagen. *NeuroImage*. Academic Press. (abstract), 1997.
- Michael Ullman and Eiling Yee. Sex differences in language: Evidence that men and women rely on different brain systems for past tense production. Poster presented at the Fourth Annual Meeting of the Cognitive Neuroscience Society, Boston. (abstract), 1997.
- Michael Ullman and Heather van der Lely. Can a "single mechanism" account for the representation of past tense morphology in grammatical SLI children? Poster presented at the Seventh International Congress for the Study of Child Language, Istanbul, Turkey. (abstract), 1996.

Dr. Wang

- Wang, S., Blumberg, P.M., Milne, G.W.A., and Kozikowski, A.P. Does a common pharmacophore really exist? A lesson learned from the studies of protein kinase C system. The National American Chemical Society Meeting, San Francisco, (1997).
- Kozikowski, A.P., Campiani, G., Sun, L.-Q., Wang, S., Saxena, A., and Doctor, B.P. Identification of a more potent analogue of the naturally occurring alkaloid huperzine A. Predictive molecular modeling of its interaction with AChE. *Journal of the American Chemical Society*, (1996) in press.
- Kozikowski, A.P., Wang, S., Ma, D., Jiangchao, Ahmad, S., Glazer, R.I., Bogi, K., Acs, P., Modarres, S., and Blumberg, P.M. Modeling, Chemistry and Biology of the benzolactam analogues of ILV. Identification of the binding site of the benzolactam in the CRD2 activator-binding domain of PKC δ and discovery of an ILV analogue of improved isozy selectivity. *Journal of the American Chemical Society*, (1996) submitted.
- Kozikowski, A.P., Tuckmantel, W., Pshenichkin, S., Wang, S., Surin, A., Thomsen, C., and Wroblewski, J.T. Synthesis and biology of the rigidified glutamate analogue, trans-2-carboxyazetidine-3-acetic acid (t-CAA). *Bioorg. Med. Chem. Lett.*, (1996) in press.
- Oligino, L., Sastry, L., Lung, T., Bihelow, J., Cao, T., Burke, T., Wang, S., Kragg, D., Roller, P., and King, C.R. Identification of a non-phosphorylated small peptide ligand of the Grb2 SH2 domain. *Science*, (1996) submitted.

Dr. Wu

- Guan, L., Tsau Y. and Wu J.-Y. Habituation studied using an Aplysia preparation with two sets of independent sensory inputs Abstracts, Soc. for Neuroscience, (1996) 22:694.
- Tsau, Y., Guan, L. and Wu J.-Y. Initiation and propagation of spontaneous epileptiform activity in rat neocortical slice. Abstract, American Epilepsy Society, (1996) in press.
- Tsau, Y., Guan, L. and Wu J.-Y. Dynamic Change of organization in rat neocortical slice. Abstracts, Soc. for Neuroscience, (1996) 22:1057.
- Wu, J.-Y., Guan, L. and Tsau Y. Global traveling wave and localized oscillations in neocortical slice neocortical slice Abstracts, Soc. for Neuroscience, (1996) 22:1057.

- Hoepp, H.P., Falk, C.X., Cohen, L.B. and Wu, J-Y. Effect of feedback from peripheral movements on the neuron activity in the Aplysia abdominal ganglion during the gill-withdrawal reflex. J. European Neuroscience (1996) in press.
- Wu, J.-Y., Lam, Y., Cohen, L. B., Fang, J., Loew, L. and Tsau, Y. Voltage-Sensitive Dyes for Monitoring Multi-Neuronal Activity in the Intact CNS. Histochemical Journal. (1996) in press.